UNIVERSITY of CALABRIA
Faculty of Engineering
Department of Mechanical Engineering

Ph. D. Thesis

XXIV Cycle (2008-2011)

Scuola di Dottorato "Pitagora" in Scienze Ingegneristiche

SSD: ING-IND/16 – Tecnologie e Sistemi di Lavorazione

Mechanisms and Modeling of White and Dark Layers Formation in Hard Machining of AISI 52100 Steels

Coordinator

Prof. Sergio Rizzuti

Supervisor

Dr. Domenico Umbrello

Candidate

Serafino Caruso

Dissertation Submitted to Obtain the Degree of Doctor in Mechanical Engineering

Accademic Year 2010/2011

UNIVERSITÀ della CALABRIA
Facoltà di Ingegneria
Dipartimento di Meccanica

Dottorato di Ricerca in Ingegneria Meccanica

XXIV Ciclo (2008-2011)

Scuola di Dottorato "Pitagora" in Scienze Ingegneristiche

SSD: ING-IND/16 – Tecnologie e Sistemi di Lavorazione

Dissertazione finale sottomessa per il conseguimento il titolo di Dottore di Ricerca in Ingegneria Meccanica

Mechanisms and Modeling of White and Dark Layers Formation in Hard Machining of AISI 52100 Steels

Coordinatore
Prof. Sergio Rizzuti

Supervisore
Ing. Domenico Umbrello

Candidato
Ing. Serafino Caruso

Anno Accademico 2010/2011

DEDICA

TABLES OF CONTENTS

CHAPTER PAGES

INTRODUCTION..... 1

CHAPTER 1

HARD TURNING PROCESS

1.1 INDUSTRIAL APPLICATIONS AND LIMITATIONS..... 3
1.2 TOOL WEAR..... 5
1.3 METALLURGICAL ASPECTS..... 7
1.4 CUTTING FORCES..... 8
1.5 CUTTING TEMPERATURES..... 10
1.6 CUTTING MATERIALS..... 13
1.7 MACHINE TOOL..... 15
1.8 SURFACE INTEGRITY..... 17
1.9 ACCURACY OF THE PROCESS..... 23
1.10 COST..... 24
1.11 RESIDUAL STRESSES INFLUENCE..... 25
1.12 FINITE ELEMENT MODELING..... 27
1.13 MOTIVATION OF THE PRESENT WORK..... 32
1.14 OBJECTIVES AND CONTRIBUTIONS..... 34
1.15 ORGANIZATION..... 35

CHAPTER 2

WHITE LAYER IN HARD MACHINING

2.1	WHITE LAYER FORMATION	36
2.1.1	EFFECT OF MATERIAL CHARACTERISTICS ON WHITE LAYER FORMATION	40
2.2	INFLUENCE OF THE CUTTING PARAMETERS	41
2.2.1	INFLUENCE OF THE CUTTING SPEED	41
2.2.2	INFLUENCE OF THE FEED RATE	47
2.2.3	INFLUENCE OF THE INITIAL WORKPIECE HARDNESS	49
2.2.4	INFLUENCE OF THE TOOL GEOMETRY	51
2.2.5	INFLUENCE OF THE TOOL MATERIAL	55
2.2.6	INFLUENCE OF THE COOLING CONDITIONS	55
2.2.6.A	WET CONDITION	56
2.2.6.B	MINIMUM QUANTITY LUBRICATION (MQL) CONDITION	57
2.2.6.C	CRYOGENIC COOLING	59
2.3	INFLUENCE OF THE WHITE LAYER ON FATIGUE LIFE	61
2.4	SUMMARY	64

CHAPTER 3

EXPERIMENTAL PROCEDURE FOR INVESTIGATING THE SURFACE INTEGRITY

3.1	EXPERIMENTAL PROCEDURE	67
3.2	CUTTING TOOL MATERIAL PROPERTIES	68
3.3	WORKPIECE MATERIAL PROPERTIES	71
3.4	EXPERIMENTAL SET- UP FOR HARD MACHINING OPERATION	76
3.5	CUTTING CONDITIONS	78
3.6	EXPERIMENTAL SET-UP FOR MICROSTRUCTURAL CHANGES ANALYSIS	79

3.7 EXPERIMENTAL PROCEDURE AND SET-UP FOR RESIDUAL STRESS ANALYSIS: X-RAY DIFFRACTION TECHNIQUE..... 83
3.8 EXPERIMENTAL PROCEDURE AND SET-UP FOR THERMAL ANALYSIS..... 91
3.9 SUMMARY..... 93

CHAPTER 4

EXPERIMENTAL RESULTS AND ANALYSIS

4.1 CUTTING FORCES..... 96
4.2 CUTTING TEMPERATURES 99
4.3 WHITE AND DARK LAYERS THICKNESS..... 102
4.4 WHITE AND DARK LAYERS HARDNESS..... 108
4.5 WHITE AND DARK LAYERS EDS ANALYSIS..... 112
4.6 X-RAY DIFFRACTION FOR PHASE ANALYSIS..... 115
4.7 RESIDUAL STRESS ANALYSIS..... 123
4.7.1 INFLUENCE OF THE CUTTING SPEED..... 125
4.7.2 INFLUENCE OF THE FEED RATE..... 126
4.7.3 INFLUENCE OF THE INITIAL WORKPIECE HARDNESS..... 127
4.7.4 INFLUENCE OF THE TOOL GEOMETRY..... 128
4.7.5 INFLUENCE OF THE MICROSTRUCTURAL CHANGES (WHITE AND DARK LAYERS)..... 128
4.8 SUMMARY..... 130

CHAPTER 5

FINITE ELEMENT MODELING FOR WHITE AND DARK LAYERS FORMATION AND RESIDUAL STRESSES ANALYSIS

5.1 APPLICATION OF ANALYTICAL AND NUMERICAL APPROACHES FOR PREDICTING THE WHITE LAYER..... 133

5.2 NUMERICAL MODELING..... 134

5.2.1 ADVANCED EMPIRICAL MODELS FOR PREDICTING WHITE AND DARK LAYERS FORMATIONS..... 135

5.2.2 PROPOSED NUMERICAL PROCEDURE..... 142

5.3 RESIDUAL STRESS ANALYSIS..... 144

5.4 SUMMARY..... 146

CHAPTER 6

NUMERICAL AND EXPERIMENTAL COMPARISON

6.1 FE CALIBRATION..... 148

6.2 FE VALIDATION..... 157

6.3 FE ANALYSIS..... 165

6.4 FE RESIDUAL STRESS PREDICTION..... 167

6.5 SUMMARY..... 171

CONCLUSION..... 172

ACKNOWLEDGEMENT..... 175

REFERENCES..... 177

INTRODUCTION

Hard turning, or turning of hardened steels (HRC > 45), is an attractive alternative to the other costly and yet environmentally harmful machining processes. Especially today, in which the economic crisis is interesting all over the world, hard turning is becoming more attractive for the good price/quality ratio. In fact, the potential process benefits as the higher process flexibility, the reduced setup time and the higher material removal rates are making hard turning the best choice in the surface finishing processes than grinding. However, the presence of the microstructural changes and their formation mechanisms, the influence of the cutting parameters and the tool geometry on the above mentioned microstructural changes and, lastly, the effects of these alterations on the surface integrity (roughness, residual stresses, etc.) have not been fully understood.

Although it is commonly believed that microstructual change (often called white layer) in hard turning is produced by thermally-induced phase transformation, there is limited understanding of the exact thermo-mechanical conditions present during its formation. Specifically, it is well known that white layer is the result of the combination of thermal effect (rapid heating and quenching which result in phase transformation) and mechanical effect (severe plastic deformation) but it is not well studied if thermal or mechanical effect is the main dominant cause of the phase transformation during hard machining.

For these lacks in scientific knowledge on microstructural phase transformations during hard turning, a wide experimental campaign was carried out with the aim to study and determine the influence of cutting tool geometry (honed and chamfered edges)

and process parameters (feed rate, cutting speed and workpiece initial hardness) on the machined surface in terms of residual stresses, microhardness modification, white and dark layers formation, etc.

Also, it was possible to investigate the metallurgical causes of the microstructural alterations. In particular, by EDS and X-Ray Diffraction analysis of the machined surface it was showed that white layer formation results in a martensitic structure, with the presence of retained austenite, for the phase transformation during hard turning. In addition, measurements of workpiece surface temperatures by thermo-camera suggest that phase transformations occur below the nominal austenite-start temperature due to high dislocation density associated with large strain.

Furthermore, no adequate numerical models are actually available in literature for predicting the phase transformations during turning of hardened steels. Therefore, a new FE strategy based on two advanced-empirical equations for white and dark layers prediction were developed and implemented by user subroutine in a commercial numerical software. Based on the comparison with experimental results it was verified the capability of the developed numerical strategy in predicting white and dark layers formation, hardness modification, cutting forces and temperatures, residual stress and the effect of white and dark layers on residual stress when orthogonal hard turning of AISI 52100 steel (54, 56.5 and 61 HRC) is carried out.

Finally, it is important to highlight that parts of the PhD activities were carried out in cooperation with research institutes in USA (Institute for Sustainable Manufacturing (ISM), University of Kentucky, Lexington, KY) and in Portugal (CEMDRX, laboratory for X-Ray Analysis of the Department of Physics of the University of Coimbra).

CHAPTER I

HARD TURNING PROCESS

The aim of this chapter is to provide a general review on the several physical and thermo-mechanical aspects that characterize the hard turning processes. Metallurgical fundamentals, mechanism of chip formation, machine tool, cutting materials, cutting forces and stress distribution, energy, temperature, geometric accuracy and potential in hard machining are deeply discussed. A detailed description concerning the microstructural changes and phase transformations on the machined surface (affected layer) are also analyzed; furthermore, the influence of the residual stresses on the machined parts are reported. Finally, a consideration on the several Finite Element codes and their techniques, developed to simulate the hard turning processes, is showed.

1.1 – INDUSTRIAL APPLICATIONS AND LIMITATIONS

Hard turning or cutting of hardened steel is performed on materials with hardness within the 45–68 Rockwell range using a variety of cutting inserts, preferably CBN. This is a topic of high interest for today's industrial production and scientific research [1-10]. Tests and first introductory steps have been made in automotive, gear, bearing, tool and die making industry. In research institutes and universities, basic

experimentally as well as theoretically investigations have been made since more than 25 years.

Mechanical components consisting of hardened steel are high performance components which are often loaded near their physical limits. Their functional behavior is principally influenced by the finishing processes which represent the last step in the process chain and are represented by cutting and grinding. For this reason finishing processes are defined as an important step and their results have to satisfy customer high quality requirements.

The product specific issues and demands also meet general trends in cutting such as flexibility, ecology, cost effectiveness, time to market and process agility. New machine tools as well as process technology focus on cutting hardened steel and rapidly lead to a highly raised industrial relevance of hard cutting. In fact, hard cutting is considered today as the main alternative to grinding operations under certain circumstances.

However, a simple comparison between hard cutting and grinding is difficult [11-18] due to variability of workpiece geometry and required quality; therefore their very different process characteristics make process selection a great challenge in industrial application. Fundamental process knowledge is the key for process selection and design.

The different geometrical features of cutting edges and grains used in hard turning and grinding create different surface structures. For example, a turned surface shows much wider and more regular feed marks than those of a ground one. Grinding can achieve very smooth surfaces of less than 0.05 μm Ra. Hard turning may achieve equivalent or better 2D surface roughness under certain cutting conditions. The peaks and valleys of the turned and ground surfaces also differ in depth and occurrence. Both surface types show negative skewness which gives good lubricant retention capability. With the tool and grinding wheel wear, surface structure will be significantly changed and a 3D surface map will be necessary to evaluate its effect on component performance.

Studies have shown that using the right combination of insert nose radius, feed rate or the new insert technology, hard turning can produce better surface finish than grinding. Multiple hard turning operations may be performed in a single setup rather than multiple grinding setups. This also contributes to high accuracy achieved by hard turning

With respect to grinding, industry demands an increased process flexibility, higher material removal rates and the possibility to use Minimum Quantity of Lubricant (MQL, mist or aerosol with very small quantity of oil-based lubricant) or even dry machining. Innovative concepts within the last years in the area of tool and process design were responsible for higher applicable material removal rates and an increased process flexibility (high speed grinding and high performance external peel grinding). However, coolant lubrication in grinding is still necessary. In Figure 1.1 a qualitative comparison of the processes hard cutting and grinding is given.

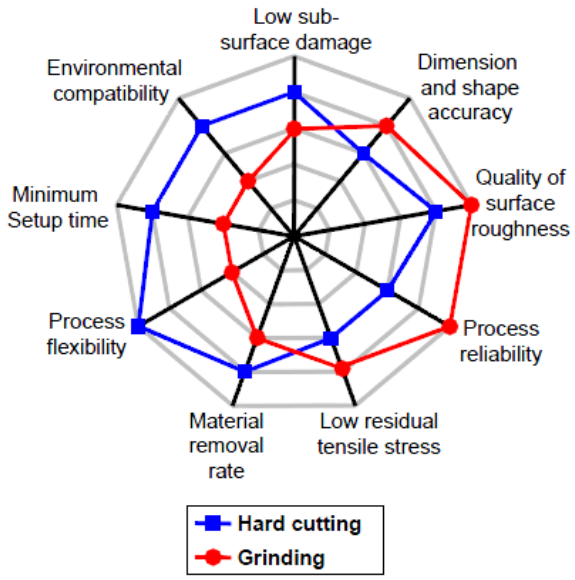

Figure 1.1 Qualitative overview of the capability of hard turning and grinding [11]

1.2 – TOOL WEAR

In hard turning, tool wear is a fundamental issue. Low surface roughness, minimal microstructural alterations and high dimensional accuracy are possible with unworn cutting tools on stiff and accurate machine tools. Production economics, however, requires a maximum tool life to justify tool cost. The process may be considered viable only if component quality can be ensured throughout the required tool life. Mechanisms of cutting tool wear and tool wear rates have been and still are the subject of various

research activities. The main objective is to achieve a maximum efficiency while maintaining a demanded process reliability when machining a workpiece with a given specification in surface, form and shape.

Over the years many researchers have contributed in this area, to state and to establish the modes of tool wear and the tool life in hard turning.

In [19-20] it was found that during hard machining by titanium tool, the main wear mechanisms is due to abrasion and adhesion.

During hard turning of AISI 4340 (63HRC) steel using Al_2O_3 and TiCN mixed ceramic tool, a decrease of the tool wear rate with increasing the cutting speed was showed [21], this is probably due to the thermal softening of the material for the high reached cutting temperatures, while during hard turning of AISI5140 steel with ceramic tool [22] a transfer layer formation on insert and the notch wear was observed along with the fracture on chamfer.

For their wide range of properties CBN cutting tools have been the most popular option in hard turning of various types of steels [23, 24], while in hard turning of AISI 4340 steels by CBN–TiN coated carbide inserts and PCBN compact inserts, it was found that flank wear is due to abrasive actions of the martensite present in the hardened AISI 4340 alloy [25]. Furthermore the crater wear of the CBN-TiN coated inserts was found to be less than that of the PCBN inserts. In machining Inconel with CBN tool, the binder was observed to play a major role in defining tool life due to diffusion phenomenon at high cutting temperatures [24]. Inconel diffused in the tool, making compound with less resistance to abrasion. This new layer was pulled off during machining, taking with it some of the elements of insert (binder and grains).

In machining AISI 52100 (100Cr6) steel with CBN tools, researchers showed that tool wear depends also on hardness value and the microstructural changes of workpiece material [26]. They also observed that the thrust force was increased as penetration of tool was difficult due to flank wear and suggested that it is better to monitor flank wear in terms of thrust force. The correlation of the CBN tool wear with cutting parameters, forces and surface finish have been established by various researchers [28], in machining 100Cr6 steel with CBN [28] it was found that the passive force could also be an effective measure for on-line tool condition monitoring. In some works a comparison of the performance of various tool materials during hard turning is reported [29]. While

comparing the tool life of ceramics and CBN tools when machining hardened steels, results showed that cutting velocity is predominant factor for tool wear followed by tool hardness and feed rate [29]. Although the CBN tools are the best choice for hard turning of steels, these tools were found to be the bad performers when machining Ti–6Al–4V alloy [30] principally due to abrasion and diffusion.

1.3 – METALLURGICAL ASPECTS

As far as the metallurgical aspects are concerned the mechanical properties of hardened steel can be adjusted in a wide range and consequently they influence the cutting process. In function of the alloys and the heat treatment, the hardness of hardened steels ranges between 45 and 68 HRC: higher hardness can be obtained by phase changes, due to the thermo-mechanical effects during machining, that lead to martensitic transformation and/or by carbide precipitation.

Depending on cooling rate pearlite, bainite and martensite is formed, in this case it is helpful the time temperature-transformation curve (TTT curve) that indicates the composition of the texture.

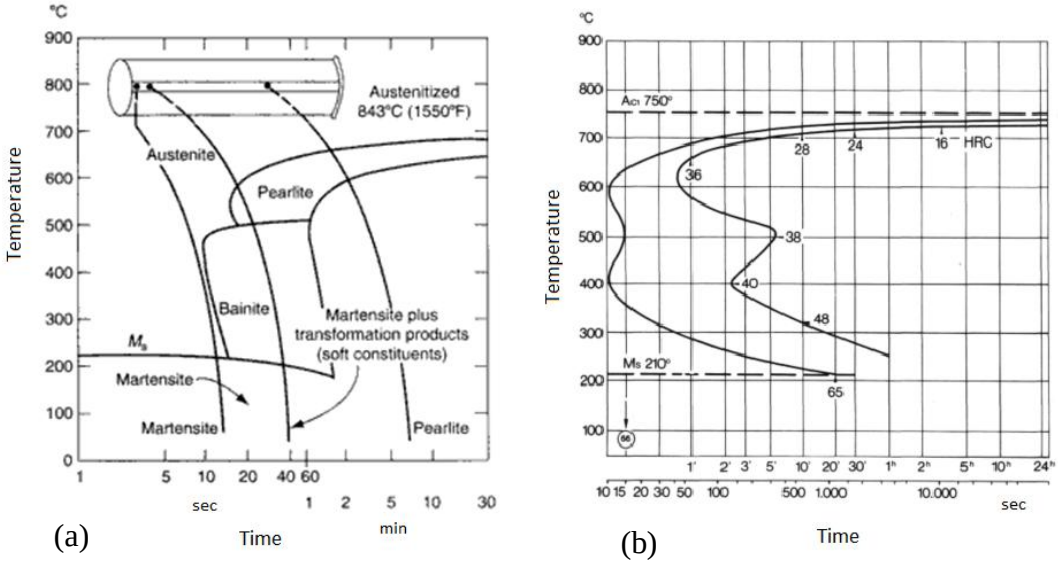

Figure 1.2 (a) CCT diagram and (b) TTT curve for 100Cr6 (AISI 52100)

Observing Figure 1.2 it is evident that the composition of the produced workpiece material is strictly related to the cooling speed: increasing the cooling rate the time for diffusion processes is low resulting in a reduced displacement of carbon atoms; this aspect proves that the heat treatments have an important role when the wear resistance and fatigue strength are taken into account.

In order to design mechanical parts and machines with optimal economical and technical properties, possible origins of failures need to be identified. In machines components in contact with moving parts are subject to the so called wear corrosion or frictional corrosion, that represents the main origin of friction fatigue fracture and has to be taken into account in machine part design. For this reasons steel components and cutting tools exposed to high mechanical loads are often heat treated. Hardening, quenching and tempering of ferrous materials lead to an improvement of mechanical properties of the workpieces not only in terms of strength and hardness, but also the fatigue strength is considerably increased. Heat treatments which aim to increase the hardness of components or of work surfaces lead to the improvement of wear resistance. Finally, also the subsurface hardness and structure constituents are of high importance in increasing the resistance against wear.

1.4 – CUTTING FORCES

Other important aspect in hard turning processes is the analysis of the forces and stresses that interest the process. Cutting forces may provide a better understanding of the machining process as they relate directly to the cutting conditions and tool condition during machining.

During hard machining processes, resultant forces and stress distributions in the contact area are substantially influenced by the process parameters.

Usually as the depth of cut is lesser than the nose radius radial component of tool forces is found most dominant [23, 31, 32], but with variable hone edge radius, the tangential force becomes more than radial force thus increasing the efficiency of cut

[33]. However, in hard turning of AISI 52100 (100Cr6) steel with CBN 7020 insert radial force component was found to be predominant [23], this result lead to not neglect, the radial force especially in characterizing static and dynamic behaviours of such machining system.

It was observed that during hard turning the cutting forces were higher at low cutting speeds and reduced when cutting speed increased [4, 34]. This is due to the fact that at high cutting speeds the cutting temperature is very high that results in thermal softening of the workpiece material thereby reducing cutting forces required for machining, while at low cutting speeds the presence of built up edge (BUE) and low cutting temperatures give higher cutting forces.

Finally, depending on the hardness of the workpiece material, two types of cutting mechanisms can be observed:

- With workpiece hardness ranging between 30 and 40 HRC: continuous chip appears (Figure 1.3) and, with the increase of the hardness, a decrease in the cutting forces. This can be explained by using the chip/tool interface temperature effect: with the increase of the workpiece steel hardness an increase in the tool/chip interface temperature is registered, so the steel being cut softens and the shear force on the rake face is reduced. Furthermore, the chip thickness decreases and the tool/chip contact area is reduced contributing to the observed reduction in the cutting force;

- With workpiece hardness exceeding 40 HRC: chip segmentation appears (Figure 1.3), and an increase in the cutting force is showed (Figure 1.4). With increasing the hardness the yield stress due to the workpiece hardness increases and when the hardness of a steel reaches a specific value the steel machined at high chip cross sections is brittle and the deformation energy expended in cutting is small. For this effect the generated heat is reduced and the material softening does not take place, therefore the rake face results in a higher shear force when the segmented chip appears. The high friction force consequently causes a high cutting force and high strain in the chip.

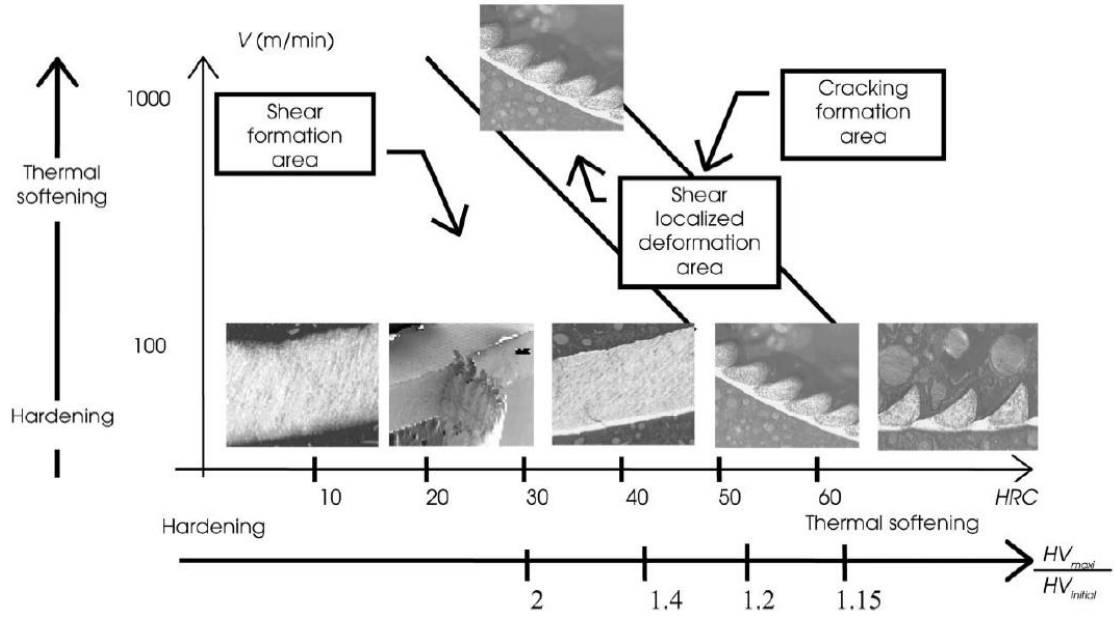

Figure 1.3 Chip morphology at varying workpiece hardness [26]

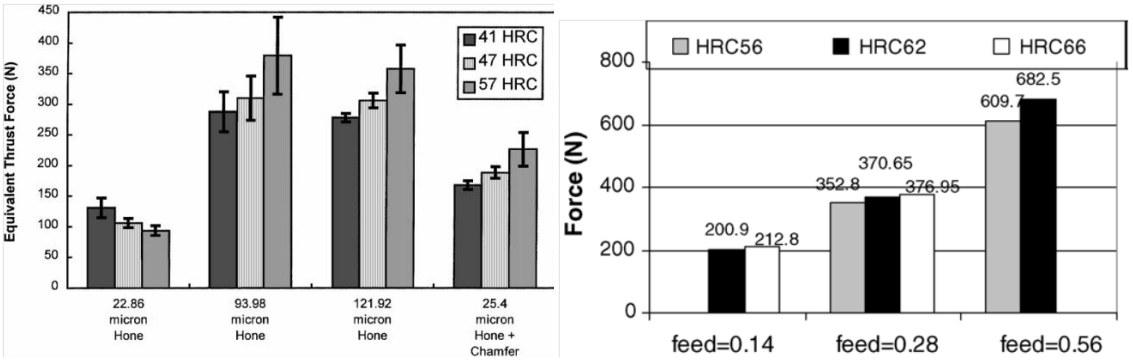

Figure 1.4 Cutting force at varying workpiece hardness [35, 36]

1.5 – CUTTING TEMPERATURES

During machining processes most of the mechanical energy used to form the chip is almost completely converted into heat and the mechanisms of material deformation, friction and material removal lead to the initiation of heat sources in the cutting region.

High cutting temperatures, which adversely affect tool life, dimensional and form accuracy, surface integrity of the product, inherently characterizes high-speed

machining. In industry, such high cutting temperatures and their detrimental effects are generally reduced by proper selection of process parameters, proper selection application of cutting fluid, and using heat and wear resistance cutting tool materials like carbides, coated carbides and high-performance ceramics.

Temperatures in the cutting zone considerably affect the stress–strain relationship, fracture and the flow of the workpiece material. Generally, increasing temperature decreases the strength of the workpiece material and thus increases its ductility.

The main regions where heat is generated during the cutting process are shown in Figure 1.5. Firstly, heat is generated in the primary deformation zone due to plastic work done at the shear plane. The local heating in this zone results in very high temperatures, thus softening the material and allowing greater deformation. Secondly, heat is generated in the secondary deformation zone due to work done in deforming the chip and in overcoming the sliding friction at the tool-chip interface zone. Finally, the heat generated in the tertiary deformation zone, at the tool workpiece interface, is due to the work done to overcome friction, which occurs at the rubbing contact between the tool flank face and the newly machined surface of the workpiece. Heat generation and temperatures in the primary and secondary zones are highly dependent on the cutting conditions while heat generation in the tertiary zone is strongly influenced by tool flank wear.

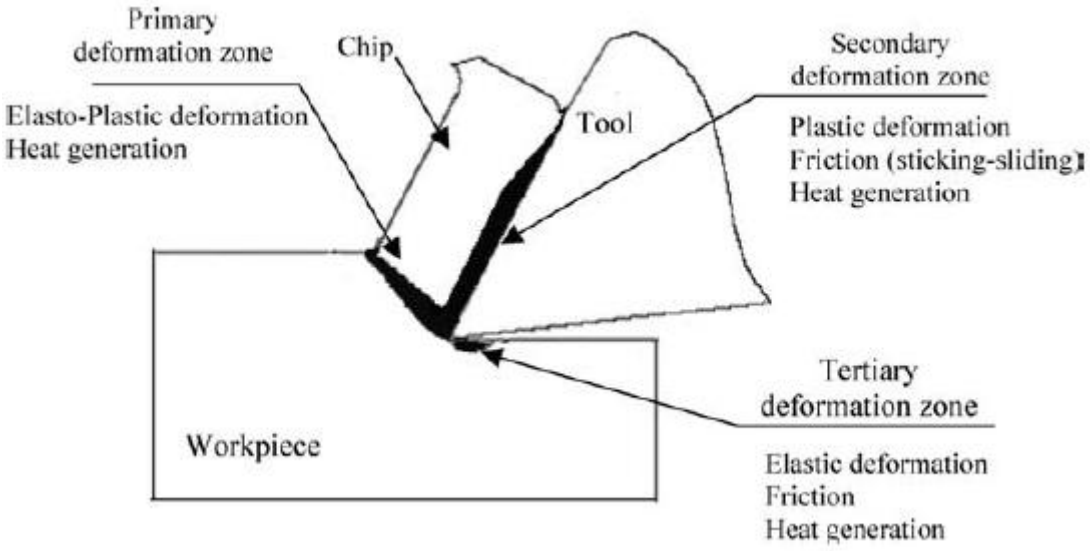

Figure 1.5 Sources of heat generation in cutting processes

Regarding the surface integrity of machined components, the friction between rake face and the new generated workpiece surface is the most important mechanism.

In 1999, Ueda et al [37] studied the influence of cutting parameters and workpiece material on the temperature of the cutting edge T_{te} (Figure 1.6). A two-color pyrometer is used to measure the temperature over the thermal radiation of the tool conducted through a hole of an internal tube. Different kinds of steels in different hardness level are investigated. It can be clearly stated that the temperature rises with cutting speed and with the hardness of the workpiece. The investigation of the influence of the workpiece material hardness on cutting temperatures confirms the results of the examination of the machining force. With the increase of the material hardness an increase in cutting force is registered, furthermore with increasing the cutting force cutting energy becomes higher and results in higher temperatures.

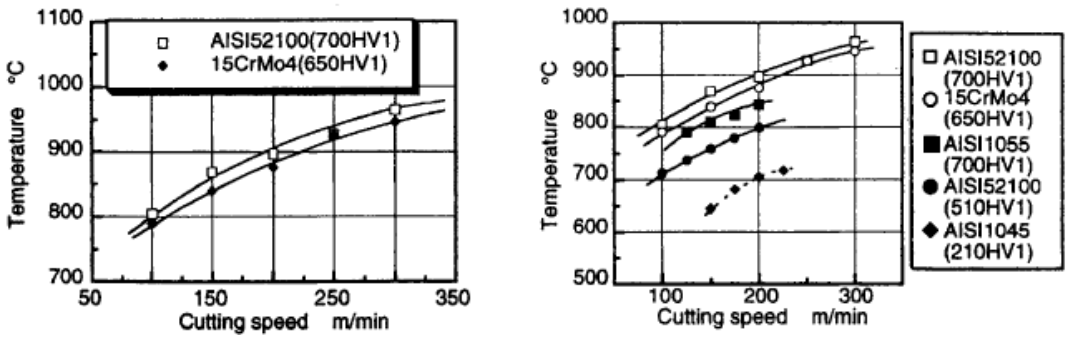

Figure 1.6 Influence of cutting speed and work materials on tool temperature: AISI 1045, HV1=210, a=0.8mm, f=0.15 mm/rev [22]

Studies conducted by Thoenshoff et al [38] on the thermal aspect demonstrates that during the machining operations two areas with different temperatures are formed below the cutting edge:

- The maximum temperature on the component surface develops at the beginning of the contact area near the material separation;
- A second maximum is produced if the minimum cutting depth is exceeded and only plastic and elastic deformation as well as friction take place.

In summary, the power consumption and the heat generation in metal cutting processes are dependent on a combination of the physical and chemical properties of the workpiece material and cutting tool material, cutting conditions and the cutting tool geometry.

1.6 – CUTTING MATERIALS

Another important aspect in hard turning processes is focused on cutting materials and tool shapes. In hard turning surface roughness and workpiece accuracy are usually comparable to those obtained by grinding processes, for this reason certain boundary characteristics on the applicable cutting tools can be defined with regard to the accuracy of the machined surface:

- High indentation hardness of the cutting tool is required in order to prevent deformations of the tool tip in the contact area of tool and workpiece. Usually, it has to be higher than three times the workpiece hardness;
- Due to the heat generated in the cutting process, materials with high thermal conductivity are needed to reduce the probability of deviations in the geometric accuracy of the workpiece;
- For the high cutting forces and temperatures, tool materials must have high resistance against mechanical stress combined with a high wear resistance;
- High thermal stability of the cutting tool material for the high process temperatures that are produced in the area of the contact zone.

Although hard turning is characterized by very high temperatures and specific forces, modern cutting tools are able to stand these thermal and mechanical loads.

Mechanical and Thermal Properties	Cemented Carbide K 10	Ceramic	PCBN	PCD
Density (g/cm^3)	14-15	3.8-5	3.4-4.3	3.5-4.2
Hardness HV 30	1500-1700	1800-2500	3000-4500	4000-5000
Young's Modulus (GPa)	590-630	300-400	580-680	680-810
Fracture Toughness (MPa)	10.8	2-3	3.7-6.3	6.8-8.8
Temperature Stability (°C)	800-1200	1300-1800	1500	600
Thermal Conductivity (W/(Km))	100	30-40	40-100	560
Thermal Expansion Coefficient ($10^{-6}K^{-1}$)	5.4	7.5-8.0	3.6-4.9	4.2-4.9

Table 1.1 Mechanical and thermal properties of different cutting tool materials [38]

Depending on the several aspects above reported on the hard turning processes Al_2O_3/TiC-ceramics and PCBN are of interest for hard turning operations for their high tensile strength, fracture toughness and thermal stability. In particular the higher thermal conductivity and lower thermal expansion coefficient lead PCBN tools as the more adapted tool material for hard cutting processes compared to ceramics [39-42].

In fact, Al_2O_3-ceramic possesses high chemical stability and hardness but the resistance to fracture is insufficient; the higher toughness and chemical reactivity of SisN4-ceramics cannot be utilized in hard turning and SiC-whisker reinforced ceramics show short tool life.

For this reasons PCBN are the main used cutting tools for turning hardened steels. Figure 1.7 shows tool life in turning of hardened steel, using a low PCBN content (60% of CBN) and an alumina-based ceramic (reinforced with silicon carbide) insert.

PCBN is the cutting tool material with the longest possible tool life. But the composition of the tool material exerts an influence on the wear mechanisms. The material properties of PCBN can be influenced by the PCBN content, the grain size and distribution as well as the composition of the binder phase which can be ceramic or metallic. For hard turning operations usually ceramic binders are preferred. The range of PCBN content in the different tool materials is varied in a percentage of 50% to 90%.

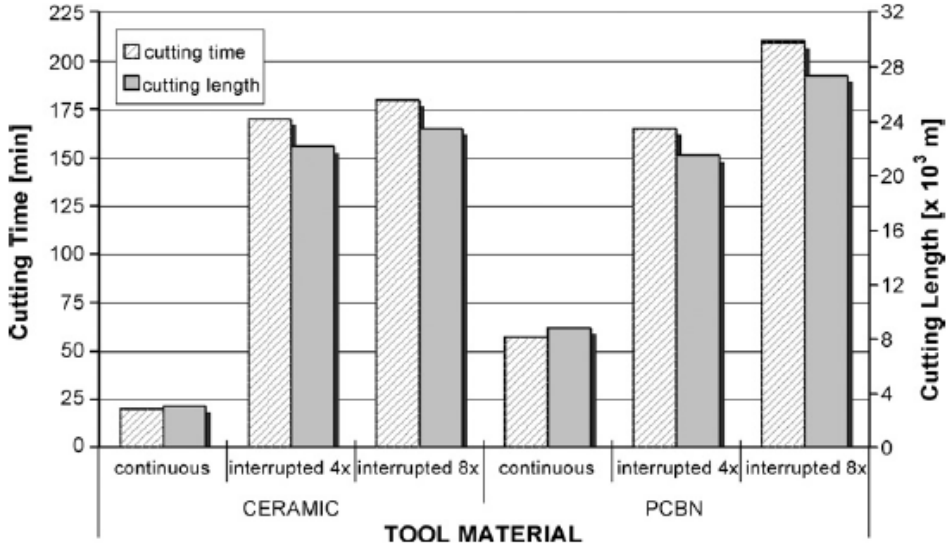

Figure 1.7 Efficiency of ceramic and PCBN cutting tool materials: workpiece AISI 4340, HRC=56.0, V=150 m/min, f=0.08 mm/rev, a=0.15 mm [43]

The mechanical and thermal loads in the cutting process require additional properties of the tool material, especially at low values of uncut chip thickness. The tool material with a lower content of PCBN shows advantages due to lower thermal conductivity and higher toughness. Furthermore, additional properties of the cutting tool material are of importance. This is based upon possible deviations of tool life in relation to different cutting tool manufacturers. Finally, the highest potential for turning hardened steel is shown by PCBN-tools with a low content of PCBN of small grain size.

1.7 – MACHINE TOOL

Technology has played an enormous role in advancing the metal working industry and creating opportunities to reduce costs and improve quality. Consider the role technology has played in transforming routine metal cutting operations. At one time machining was very much an operator dependent, skill critical process. Today, CNC machine tools, which operate with mature technology and provide both consistency and reliability, have now become the biggest contributor to part quality and cost.

Recent efforts in machine tool development lead to new machine concepts of high-precision lathes to improve the quality of hard turned workpieces significantly (Figure 1.8). The accuracy demands on these machine tools are comparable with grinding machine tools concerning static, dynamic and thermal stiffness as well as accuracy of the spindle system and slides [44, 45]. The application of such types of machine tools enables to reach workpiece qualities in the accuracy range of IT 6-7 in hard cutting under appropriate condition reliability [46].

Figure 1.8 High CNC precision lathe suited for hard turning processes: Mazak: Nexus 200-II, laboratory of university of calabria

Precision turning lathes with components designed for increased accuracy and high-precision, equipped with NC-controls with high resolution are capable to reach the accuracy of grinding processes. For high grade applications as e.g. for gear components or roller bearings finishing operations need to be made by grinding, for the inaccuracy reached by hard turning with particular attention to the geometrical accuracy as well as on the stiffness of the machine tool: each deviation of the relative position between cutting tool and workpiece reflects its effect on the machined surface.

With the recent conjunction between lathes machine and hydrostatic systems high quality machined parts it is possible to obtain by hard turning processes. By the introduction of hydrostatic guide ways and bearings, resolutions of 0.1 µm in the positioning of the tool tip are possible now. These innovations in lathe machines permit to obtain the final accuracy of grinding by hard turning.

Another important aspect of the finishing processes, especially when accuracy is taken into account, is the surface roughness. This aspect represents one of the main limits of the hard turning compared with grinding; in fact, by high precision lathes surface roughness of about R_z=1 µm can be reached, while by fine grinding it is possible to reach values of R_z lower than 1 µm.

Besides the surface roughness also the surface micro-profile is of high importance for the functional behavior of the machined components especially for the precision parts that are characterized by very fine and smooth profile. Using fine grinding machine tools it is possible to realize the production of these fine contours; in contrast, by hard turning processes this aspect is strictly related to both NC-control resolution and high precision lathe machines.

One of the main advantages of hard turning is the possibility to perform the process in dry conditions avoiding the use of cooling lubricants, on the other hand form errors gain more importance. The temperatures reached during hard turning are usually higher than 500 °C at the tool tip-workpiece contact zone for this reason the thermal effects lead to deviation of parallelism on the surface lines. New developed high-precision lathes offer the possibility to compensate form errors due to thermal effects and to receive a smooth profile without recognizable NC-control steps after dry turning. In order to prevent the form errors, due to the thermal effect, increasing the workpiece quality the application of cooling lubricants seems to be best alternative so that deviation of diameter does not occur during the cutting and the dimensional accuracy is not infected.

1.8 – SURFACE INTEGRITY

Among all the important aspects of a machined part, the functional characteristics (workpiece geometry, surface roughness and surface integrity) need an accurate analysis for the good performance of the component during its application. Mainly attention is usually directed to the surface integrity and attributes, that are particularly influenced by the cutting processes for the complex thermo-mechanical effects typical of the cutting

processes. In order to reduce the thermo-mechanical cutting effects and obtain high quality and applicability of machined components, the final cutting operation must be carried out with small cutting depth: low cutting forces, low temperatures and cutting loads reduce dimensional deviations, surface roughness and the influence in terms of surface integrity. Surface integrity includes the presence of micro-cracks, microstructural changes, surface roughness, phase transformations, residual stress, plastic deformation and changes in the microhardness, Figure 1.9 and Figure 1.10.

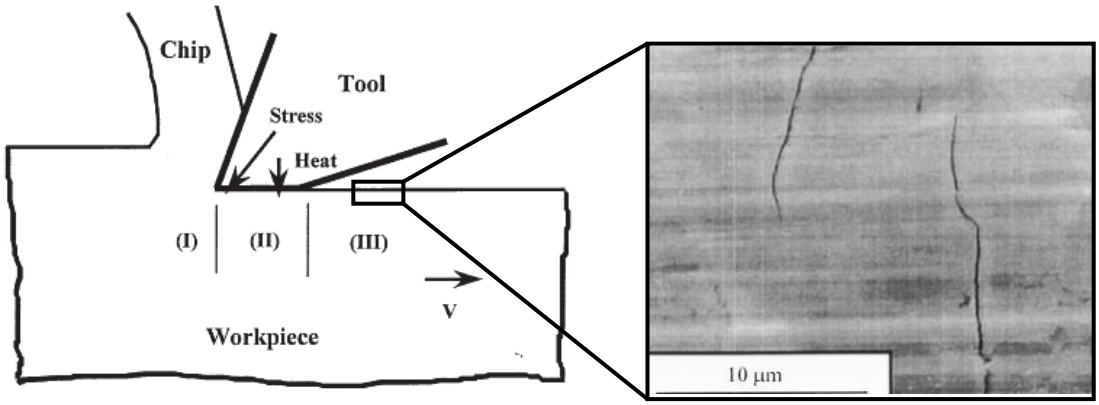

Figure 1.9 A sketch of the thermo-mechanical cutting loads in different zones and possible surface microcraks [47]

These factors determine the behavior and service failures of the produced components. For the cited reasons related to the machined surface integrity, a comprehensive understanding of the machining process is essential in order to better design the machining process, choosing the correct process conditions.

Due to the combination of extremely high temperatures and mechanical loads in the tool-tip-workpiece contact zone, the austenite-start temperature of the workpiece material is reached, then for the rapid cooling the workpiece material is self-quenched, so microstructural changes take place and residual stresses influence the surface integrity.

Furthermore the machined surface is characterized by the formation of a thin layer, often called as white layer because of its color when observed by optical microscope or featureless when observed by a scanning electron microscope, Figure 1.10. This

microstructural variation seems to be mainly due to the thermal effect caused by hard turning process.

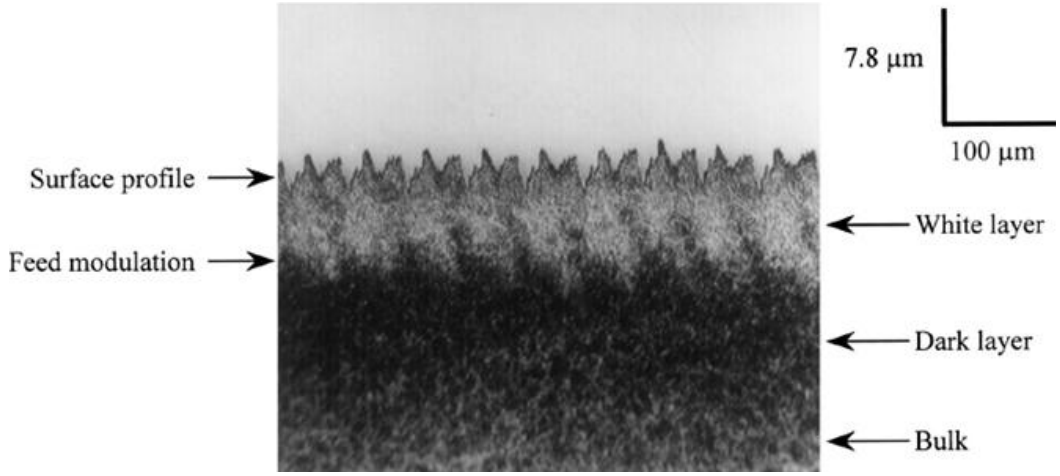

Figure 1.10 An example of surface integrity analysis on hard turned surface of AISI 52100 steel, optical micrograph: microstructural changes (white and dark layers) and surface roughness [48]

However, before starting to deeply analyze the phase transformations during hard turning it is essential to investigate the material composition and the structure of machined components.

From the literature [49-51] it is widely reported that with white layer formation a considerable increase of the amount of austenite can be observed in the subsurface. White layer consists of over 60% austenite which is a non-etching white component in contradiction to the dark martensite scorching. The martensite components also show a mostly tetragonal twisted lattice.

In order to generate white layers by the machining of hard materials, two conditions must be given:

- The contact temperature must exceed austenizing level of the workpiece material;
- The cooling of the surface area must take place in very short time.

Therefore, a description of the thermo-mechanical mechanisms about the formation of white layers should be able to explain the extremely fast heating phase which is related with austenization.

During hard turning processes, the contact time between tool and workpiece is often less than 0.1 ms, this condition leads to have different material structures if hard turning or grinding operation is performed.

In hard turning, the contact time is very short as well as the time for heat conduction, furthermore hard turning is a single point turning operation; the explanation of these conditions finds its only justification in the specific combination between friction and plastic deformation during hard turning processes. In fact, plastic deformations can produce a high amount of heat in a short time which also heats up the workpiece. The combination of high plastic deformations and extreme short heat up times cause the lattice shearing with the formation of a very fine austenitic grain structure for the rapid cooling that does not allow the grain growth after tool-workpiece contact: a quenching thermal treatment takes place on the machined surface; thus, the combination of martensite and fine grained austenite structure causes the increase of the hardness in the area of the white layer. Consequently, the surface integrity is affected due to the microstructural changes that take place during hard cutting. Also the residual stresses of the austenite material components are clearly shifted towards compressive strain. Under the surface and as a consequence of high mechanical stress, compressive residual stress occurs with a maximum compressive peak positioned near the white-dark layer transition [52].

Finally another important aspect of the hard turning processes is focused on the functional behavior of the machined components.

As it was above mentioned, hard turning deeply influences the surface integrity, and this is an important aspect that must be taken into account for the performance of the component during the applications. This influence on the surface integrity has a direct consequence on the fatigue life behavior; it becomes of real importance especially when rolling contact loads are analyzed [53-55]. Also the in depth residual stresses have an high importance when the fatigue life of hard turned components are taken into account. Figure 1.11 describes the influence of residual stresses and initial workpiece hardness during fatigue life tests.

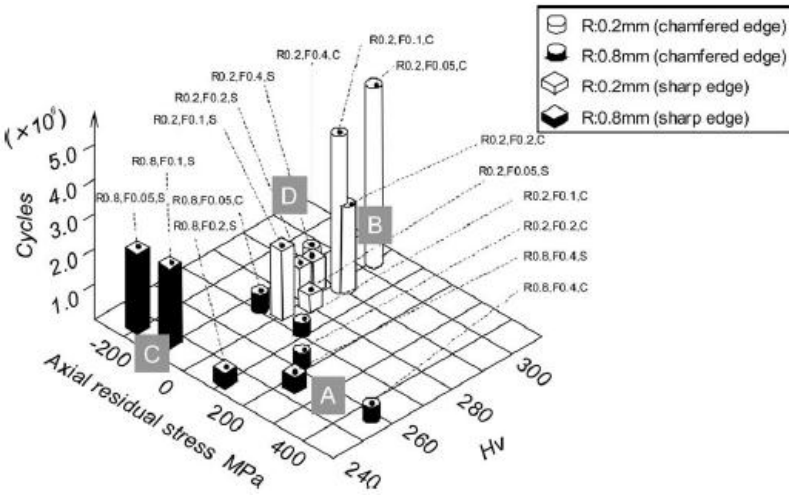

Figure 1.11 Interaction of axial residual stress and hardness on fatigue life [56]

In case of roller contact loads, residual stresses in hard turned surfaces change to values in direction of compressive stresses which is known for its positive influence in case of the fatigue live of components.

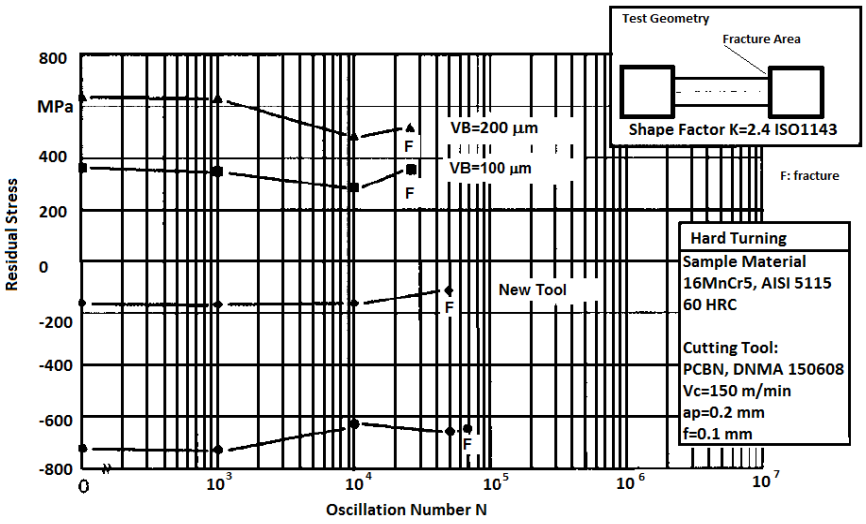

Figure 1.12 Residual stress in relation to the oscillation number [57]

Another important component characteristic is the fatigue strength against bending or oscillating loads. Here, sensitive influences from the area of the subsurface, surface topography, microstructure and residual stresses are known. As an example, case hardened components are common in automotive applications. Bending fatigue strength

is a main criterion for components because the maximum of the load directly occurs in the surface, the machined area. In this case, the subsurface residual stresses caused by hard machining are of special meaning. For investigations on the influence of hard turning to bending fatigue life, sample pieces with different residual stresses by the turning processes were selected. Stress cycle diagrams of a Wohler fatigue test reveal the influence of hard cutting conditions to the oscillating fatigue strength (Figure 1.12).

The results of the investigations show that the residual stresses are almost not influenced by the number of oscillating loads. A reduction of residual stresses as shown in rolling contact loads does not occur.

To evaluate the productivity of a cutting process the material removal rate is the most important economical parameter.

Compared to the material removal rate, the surface rate gains particular importance in the case of machining smaller workpiece diameters with lower over measures and smaller cutting depth. As a typical example, the efficiency of centerlines grinding of roller bearings can hardly be achieved in turning. However, the productivity effect of the turning process in appropriate cases is due to the high form flexibility. Different surfaces and shapes can be machined with one tool and one machine tool is needed for outer and inner diameter machining. Because of these advantages, in many applications the machining time can be shortened significantly by hard turning, Figure 1.13. However, the final determination of machining times and costs can only be made according to a specific production task.

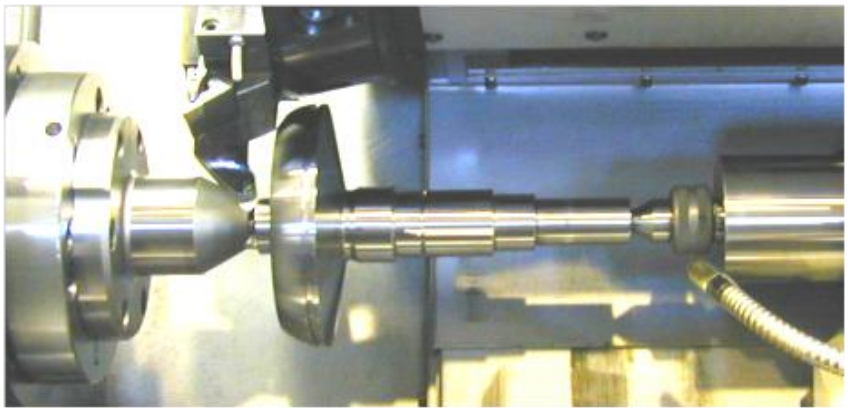

Figure 1.13 Typical hard turned component [11]

1.9 – ACCURACY OF THE PROCESS

The primary task of hard turning, as a finishing operation, is to ensure the quality and reliability of the parts. The quality criteria of hard turning as a cutting operation can be found in the technical drawings. The most important aspect for any process to be accepted by the industry it should be robust and accurate as far as the performance is concerned. For analysis of the geometrical accuracy in hard turning four characteristics are taken into account, Figure 1.14:

- Higher cutting forces;
- Dry condition;
- Single point form generation;
- Minimum value of the depth of cut.

The passive force occurring in hard turning – the component perpendicular to the cutting speed – is a multiple of the main cutting force, while in traditional turning it is only a fraction of this value. The extraordinarily high passive force significantly loads the elements of the machining system, causing elastic deformation and deteriorating the machining accuracy. This issue related to the passive force can be solved increasing the machine tool rigidity. Hard turning is usually performed in dry conditions at relatively high speed resulting in high temperatures, these cause thermal expansion of the workpiece, which also deteriorates the machining accuracy. The surface generating element of hard turning is the single-point tool tip, which shapes the surface of the workpiece and is accompanied by significant force and heat effects. Under such conditions the single-point tool tip reacts sensitively to any irregularities. It abreacts the allowance distinctions, the hardness differences and the other heterogeneities of the material with the creation of machining errors. The fourth aspect influencing the accuracy is the depth of cut. In hard turning this cannot be reduced arbitrarily, although this is possible in grinding. Because of the necessity of a minimum depth of cut, hard turning is followed by higher forces than in grinding, even in the finest smoothing

operations. Most unfavorable effects can be eliminated by an increase in the robustness of the machining system: high static and dynamic stiffness of the machine tool and rigid clamping devices for workpiece and tool.

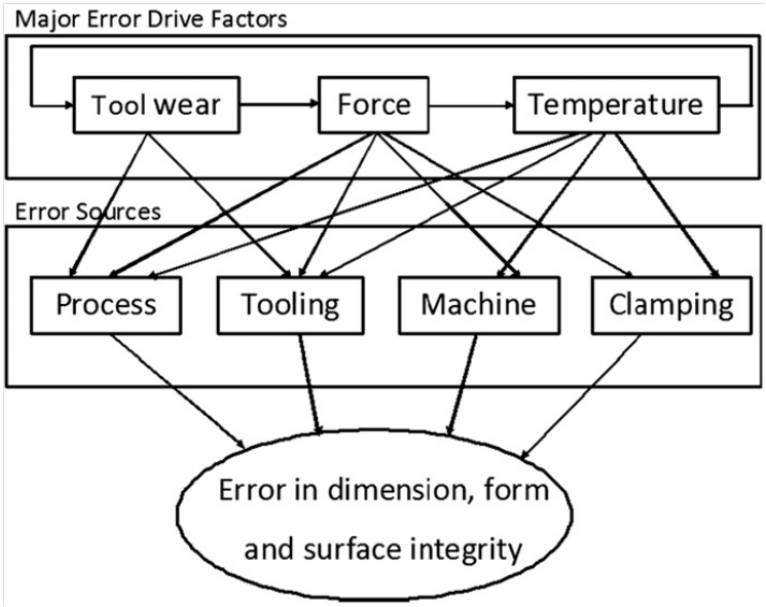

Figure 1.14 Major error driver factors and error sources in precision hard turning [58].

1.10 – COST

Hard machining applications show high potential to replace grinding operations. The finishing of a hydraulic component is one example for the economical advantages possible by substitution of grinding by turning. Because of many short and different shapes, inner and outer diameter machining, this component is a typical example suited for hard turning.

Compared to the former production by grinding operations, the production sequence is reduced noticeably. Only one machine tool and one single set up is necessary. Reducing the manufacturing process will reduce the number of setting and that will reduce the machining time then the total cost. Workpiece quality achieved in hard turning is at least at the level of the grinding operation. Significant improvements can be

seen concerning production times and costs. For instance machining time for batch size is about 60% shorter compared to grinding. In comparison to hard turning, grinding is a more complex process. The repeated conditioning of the grinding wheel occupies the machine itself while tool preparation in hard turning can be done off-line. An additional bonus of hard turning is avoiding cutting fluids. The possibility of dry machining means saving considerable costs otherwise caused by buying, monitoring, treatment and disposal of cutting fluids.

Furthermore cutting leads to more favorable conditions. Due to the possibility of dry machining, there are only chips consisting of not contaminated workpiece material that can easily be recycled [59]. Tool can be disposed (ceramics) or reused after sharpening, but there is no mixture of different materials. Thus, cutting of hard materials can be considered as a very efficient possibility for protection of environment.

1.11 – RESIDUAL STRESSES INFLUENCE

It is widely reported that in a finishing process, surface integrity is often a relevant key factor because of its impact on the product performance. In fact, in many cases where unexpected failure occurred, it can be due to the presence of residual stresses which have combined with the service stresses to seriously shorten component life; on the other hand, beneficial residual stresses (usually compressive residual stresses) can be introduced to improve fatigue resistance.

Residual stresses are a tension or compression stresses, that remain after the external cause of the stresses is removed and in hard machining are the results of interactions of thermal and mechanical effects. Three distinct phenomena are thought to contribute to residual stress formation during machining of hardened steel:

1. Mechanical phenomenon: inhomogeneous plastic deformation of the workpiece material. This is inherent to the cutting operation and is usually associated with compressive residual stress;

2. Thermal phenomenon: material flow and loads caused by a thermal source. The machining process results in considerable heat generation due to plastic deformation in the shear zone and friction at the secondary and tertiary deformation zones;

3. Metallurgical phenomenon: phase transformations during machining lead to a volume expansion.

The first two phenomena are always present in hard machining, while the third one depends on the machining conditions. Considering the mechanical deformation taking place during cutting in the near-surface region of the workpiece, the workpiece material undergoes compressive plastic deformation ahead of the cutting edge and tensile plastic deformation behind it. If the tensile deformation is greater than the compressive one, the net result will be tensile plastic deformation, which would induce surface compressive residual stresses upon relaxation as the near-surface layer is restricted by the underlying bulk material. The opposite would take place if the net plastic deformation was compressive [60, 61]. During cutting, the surface layer is heated more than the underlying material, and since cooling occurs mainly from the inside by conduction, the surface layer stays hotter than the bulk material after cutting, and tends to expand experiencing compressive stresses. If these compressive stresses exceed the yield strength, the material will be plastically deformed under compression resulting in tensile residual stresses after cooling [62]. The occurrence of phase transformation mainly depends on the cutting temperatures as well as the cooling rate; these are both significant to the workpiece material [63, 64]. When phase transformation takes place, the mechanical and thermal properties of the material change, as well as its grain size. Consequently, residual stresses would be induced due to the non-uniform permanent changes that took place, where the type of residual stresses (whether being tensile or compressive) differs from a material to another.

Component service life is affected to a significant extent by these residual stresses, depending on their nature. Resistance to fatigue, creep and stress corrosion cracking are influenced by the nature and magnitude of residual stresses. In addition, component geometry is likely to be affected, resulting in parts that do not meet required tolerances. Therefore, it is of great importance to predict the residual stresses in the machined

component. These types of stresses can be present in any mechanical structure because of their many causes and they may be due to the technological process used to make the component. Manufacturing processes are common causes of residual stress, virtually all manufacturing and fabricating processes such as casting, welding, machining, molding, heat treatment, plastic deformation during bending, rolling or forging introduce residual stresses into the manufactured object. The residual stresses effects on the different properties of a material (fatigue, fracture, corrosion, friction, wear, etc.) can be considerable; in the modern design of mechanical components, residual stresses have therefore to be taken into account. Hence, it is important that the effect of the finishing process on the residual stress profile is accurately predicted, so that the machining parameters can be optimally selected to enhance fatigue life of machined components.

For this reasons related to the machined surface integrity this thesis wants to give a contribute in this direction correlating machining process parameters and workpiece properties to the workpiece surface and subsurface characteristics and residual stress distribution for hard turning processes.

1.12 – FINITE ELEMENT MODELING

The main indicators of machined surface integrity are surface roughness, presence of microcracks and residual stresses but also microstructural changes, phase transformation and microhardness changes on the machined surface of hardened steels must be taken into account for the good process feasibility. Furthermore, to make the hard turning process economically competitive, accurate models for surface integrity analysis are needed, that are capable to predict the several aspects related to the surface integrity as a function of the machining conditions, in order to allow the identification of the cutting conditions that will result in the best state (residual stress state, microstructural changes, roughness, etc.) of the component in function of its utilization.

Following this direction, since the early cutting model by Merchant et al [65], based on a simple material flow definition under orthogonal cutting assumption, many

researchers in metal cutting are attempting to develop and improve hard turning finite element based models.

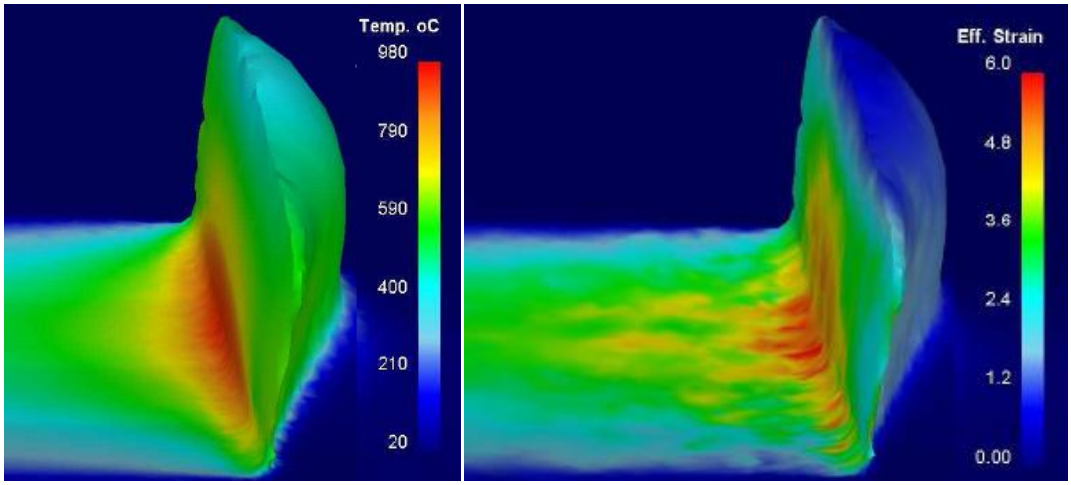

Figure 1.15 Temperature (a) and strain (b) analysis by a Deform 3-D post processor [66]

FE software packages consist normally of three parts. These are pre-processing, processing, and post-processing components. The function of the pre-processing is to specify the environment for the actual modeling situation. Both process and material are defined, as well as tool parameters. The solver (or the processing component) is the heart of the program. It is here where the data are treated and all the computations are performed. The third component is the post-processing which is a visualization and analysis tool that provides the user with the capability to analyze, extract, and communicate the results achieved, Figure 1.15.

Since the first finite element studies of the 1970s to the last years several models of the machining processes have been shown by the researchers who work in this direction. Several enhancements have been obtained in the last decade thanks to the use of Finite Element simulations. Numerous researchers used FEM to predict some typical machining variables, such as cutting forces, chip morphology, surface integrity, etc. [67].

In computational mechanisms it is usual to define simulation models which depend on nature of the results. Obviously all the phenomena analyzed during machining processes need appropriate reference scales to be studied: separation of physical effects

having large lengths of variation from those with smaller characteristic lengths must be done. Two different scales are introduced to study the turning operations:

- Macroscopic scale: to analyze the whole workpiece-tool-machine system particularly the geometry of machined surface;
- Mesoscopic scale: to analyze at the tool-tip workpiece scale the chip formation, chip geometry, stresses and temperatures, friction, cutting forces and thermo-mechanical characteristics along the tool-tip.

At the macroscpic scale accurate models have been built to predict the behavior of the workpiece-tool machine system, the cutting forces and the correlated thermal aspects and the roughness and form of the final machined surface.

High evolutive interaction between tool and workpiece is the main characteristic of the machining processes at the macroscopic scale. This interaction is “history” dependent due to the evolution during machining of the workpiece domain.

The cutting law is a central point in machining simulation, for this reason a lot of works are focused in this direction. The first model, based under orthogonal cutting assumptions, was introduced by Merchant [65]. Many efforts and improvements were then proposed. The most relevant enhancements are found in [68] and [69] taking into account wear and thermal aspects and in [70] where thermal diffusion is incorporated. To accurately simulate cutting forces it is necessary to know the instantaneous cutting conditions: cutting speed, feed rate, cutting section, etc. To define the latter geometrical models are needed while the relative motion between workpiece and tool is described by static or dynamic models. To study the dynamic behavior of the process, time domain methods [71] are usually used.

To simulate machining processes it is necessary to have good representative mechanical models; at the macroscopic scale these models are the cutting law with discontinuous cutting condition and dynamic models of the machine.

Concerning the mesoscopic analysis of the machining processes, very relevant enhancements have been registered in the last ten years mainly focused on the reliability of the effectiveness of the obtained results.

Some improvements have been registered as concern the flow stress modeling: Johnson-Cook and high shear tests are utilized to identify the material parameters appearing in such law [72]. Most recently some innovative models including the effect of material hardness at high temperatures have been proposed [73].

Friction modeling is generally based on Coulomb models, constant shear models or finally sticking-slide models. Finally chip generation is generally taken into account by means of numerical remeshing in machining modeling, while several advanced damage mechanics models have been implemented to simulate blanking [74].

Today the amount of results provided by machining models is really huge:

- Prediction of mechanical variables in machining;
- Prediction of chip geometry;
- Prediction of thermal variables in machining;
- Prediction of tool wear in machining;
- Prediction of the surface integrity in machining.

Concerning mechanical variables in machining (strain, stress, cutting forces, etc.) these are dependent on the workpiece parameters (temperature, material type, etc.), cutting tool parameters (material, geometry, etc.) and cutting parameters (cutting speed, feed rate, etc.). Mainly attention was focused on the prediction of cutting forces and pressure distribution on the rake face of the tool [75]. Furthermore the latter studies are pursued to a greater comprehension of the complex physical phenomena underlying the specific machining process: in this sense the development of effective friction models has been pursued by several researchers [76]. Several materials are considered, the most common are steels and aluminum alloys although several efforts are oriented also to titanium alloys, two-phase alloys and other materials.

Since metal cutting is a chip-formation process, the prediction of chip geometry is another important aspect to take into account when modeling is considered. The problem of chip formation and its control has been studied trying to define the mechanism of chip formation, chip flow and chip breaking [73]. Chip flow along the contact length with the tool is a very important factor, because it influences in a relevant

way energy dissipation by friction and heat transfer conditions: most of the heat generated in machining is removed from the cutting zone by the chip. Chip control is necessary especially in turning and drilling.

High temperatures in machining are the main cause of unsatisfactory tool life and limitations on cutting speed. Several numerical techniques were proposed to study the thermal problems in machining and to calculate the temperature distributions within both the workpiece and the tool [77]. However the prediction of the thermal aspects is probably the most critical task up to now due to implemented numerical formulation. In fact, most of the numerical analyses of machining are based on the updated-Lagrangian formulation and carry out a coupled thermo-mechanical analysis. In this case only few milliseconds of cutting time can be simulated. This aspect is an heavy limitation for the effectiveness of the numerical modeling, since in this short time thermal steady state cannot be achieved. Furthermore temperature prediction influences other important process variables, such as tool wear and residual stresses.

The above drawback was highlighted by several authors [77], which have proposed different numerical strategies to overcome this problem [78].

Wear prediction in machining has been recently studied by using FEM technique although it still represents a "border" application. A couple of relevant research issues have to be strongly enhanced to achieve an effective prediction: the former is related to the reliability of the calculated temperature field, the latter is connected to the absence of predictive models for coated tool.

Whereas these problems, several authors tried to model tool wear by FEM [55, 60] taking into account advanced tool wear models, mainly based on diffusive wear models.

More in detail, Nouari and Molinari [70] proposed a tool wear model considering the diffusion mechanism to predict uncoated tungsten carbide wear when cutting steels are machined. They also investigated the influence of the process variables as well as of the tool geometry on the tool wear. However, in the last few years the research on tool wear mechanism appears to be reduced, although tool wear prediction is one of the most critical issues. Probably the reason is strictly related to the unreliability of temperature prediction in machining. Only once this problem is solved, tool wear prediction can be heavily carried out and extended to coated tools.

Finally the reliability of mechanical components depends to a large extent on the physical state of their surface layers. This state includes the distribution of residual stresses induced during the machining process.

Residual stresses can enhance or impair the ability of a component to withstand loading conditions in service (fatigue, creep, cracking, etc.), depending on their nature: compressive or tensile, respectively. Therefore, prediction and control of the residual stresses in machining is absolutely necessary. For these reasons several researchers were oriented on this field [70, 79] even if more efforts must be done to improve the prediction of the surface integrity in terms of advanced flow stress models, temperature prediction and modeling of tool wear when advanced tool materials are used.

It is evident that the finite element method (FEM) simulations are today a very important and helpful instrument in hard turning processes analysis, and several are the researchers who work in this field with the aim to give a valid contribute to the science. So the results that will be showed direct to a more consistent utilize of the FEM in the tools design and in the simulation of the hard turning process.

1.13 – MOTIVATION OF THE PRESENT WORK

The following observations explain the motivation for the present thesis:

1. Recent researches have shown that machining of components directly in the hardened state can lead to substantial productivity improvement by eliminating extra processing steps such us grinding. For this reason the hard turning process is going to be applied in industry with the aim to replace the costly and slow grinding process in finishing mechanical components. Furthermore in the latter, the relatively more aggressive grinding process parameters employed under typical production conditions could result in the deterioration of the surface integrity of hardened components and hence on their life under service conditions;

2. In machining of hardened materials, maintaining surface integrity is one of the most critical requirements. Often, the major indicators of surface integrity of machined parts are surface roughness and residual stresses. However, the material microstructure also changes on the surface of machined hardened steels and this must be taken into account for process modeling. Therefore, in order for manufacturers to maximize their gains from utilizing hard finish turning, accurate predictive models for surface integrity are needed, that are capable of predicting also both white and dark layers formation as a function of the machining conditions;

3. The good agreements, between numerical and experimental results, showed by the several researchers in the literature of the hard turning processes induce to an increasing use of the FEM for the optimization of cutting tool design (tool material and geometry, coatings) and cutting conditions (cutting speed, feed rate, depth of cut) such that product quality, productivity, and tool life are maximized.

The above observations indicate that it is necessary to:

1. Have a series of experimental cutting tests conducted under several cutting conditions;

2. Study the effect of cutting tool edge geometry and cutting conditions (cutting speed, feed rate and initial workpiece hardness) in terms of surface integrity: residual stresses profile, microstructural changes, phase transformations, etc.;

3. Develop a valid methodology and Finite Element Model to predict the several aspects related to the surface integrity during hard turning process.

1.14 – OBJECTIVES AND CONTRIBUTIONS

The main objective of the proposed research is to develop an innovative finite element model for predicting the effects of the cutting tool edge design and cutting parameters (feed rate, cutting speed and initial workpiece hardness) on the machined surface integrity and microstructural changes during hard turning.

Thus, the single specific objectives are to:

1. Study and determine the influence of cutting tool geometry (honed and chamfered edge) and process parameters (feed rate, cutting speed and workpiece initial hardness) on the machined surface in terms of residual stresses, hardness modification, white and dark layers formation, etc.;

2. Investigate and understand the nature of the microstructural alteration from a metallurgical point of view;

3. Establish a procedure for predicting the surface integrity and the microstructural alterations on the machined surface using 2D FE software;

4. Demonstrate the importance and the utility of the FEM in hard turning processes.

1.15 – ORGANIZATION

In the following flow chart (Figure 1.16) the organization of the present work is reported:

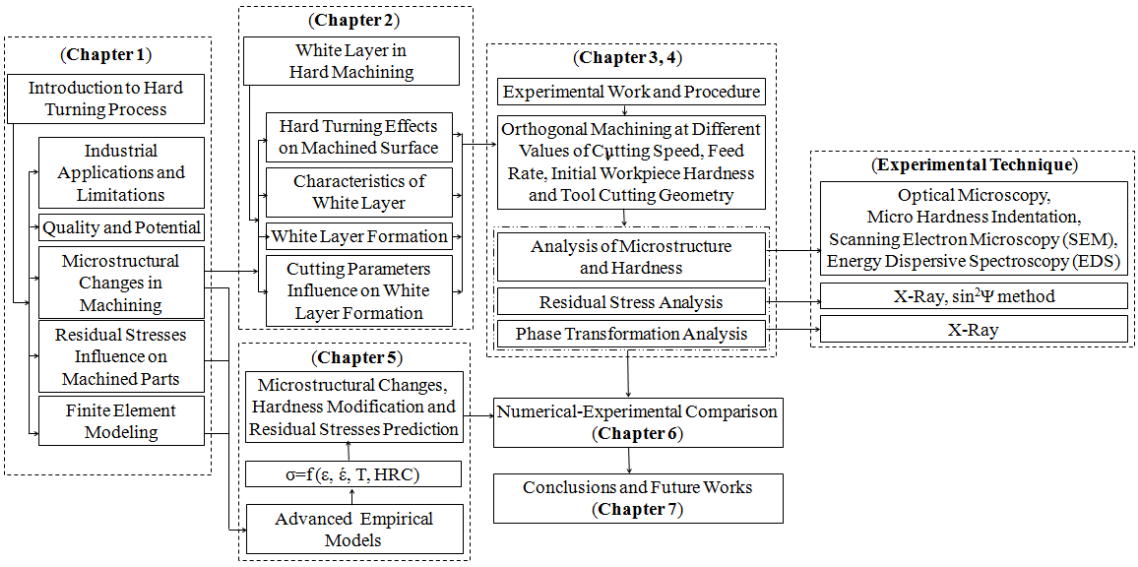

Figure 1.16 Flow chart summarizing the present research

CHAPTER II

WHITE LAYER IN HARD MACHINING

The aim of this chapter is to provide a review on the influence and interaction of different process parameters (cutting speed, feed rate, initial workpiece hardness, tool geometry, etc.) on white layer formation. In addition, influence of cooling conditions: WET, Minimum Quantity of Lubrication (MQL) and cryogenic are analyzed. Finally a review on the effect of the white layer formation on the components fatigue life is presented.

2.1 – WHITE LAYER FORMATION

White layer refers to hard surface layers appearing white under the microscope, which is formed in a variety of ferrous materials during manufacturing processes [80] which induce white layers that often contain fine-grained martensitic structures (Figure 2.1). These affected layers are highly brittle and often subjected to cracking. In some cases, austenitic layers were also detected.

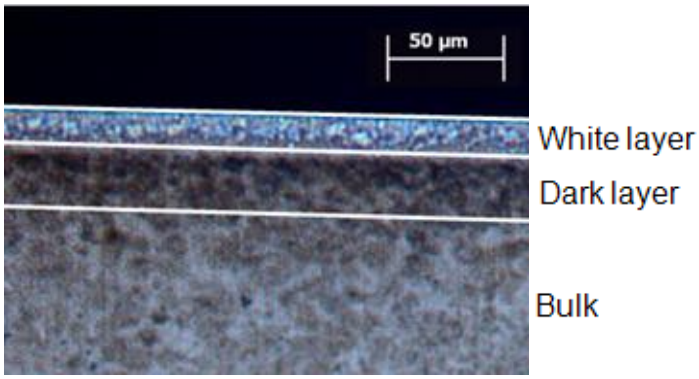

Figure 2.1 Optical observation of white and dark layers

The first approach to the study of the possible causes of the white layer was carried out in 1912 [81] when, analyzing the surfaces of used steel wire ropes, the formation of white layers was observed. After that, many research have found the occurrence of this phenomenon in different areas: on the surface of many used engineering components (such as pistons, rail heads, roller bearings, etc.), and on the surface of manufactured components such as ground, drilled or turned pieces. It is found that different types and forms of white layers can be created depending on the operating conditions and the materials used.

In sum, three main mechanisms have been identified for white layer formation [82]:

(I) Surface reaction with the environment;

(II) Severe plastic deformation (high strain, strain rate and temperature);

(III) Rapid heating and quenching which result in phase transformation.

It has been reported that each of these phenomena alone or in combination reduces the subsurface microstructure of the materials, specifically the grain size, to a point where its structure cannot be observed optically [83]. The hypothesis of surface reaction with the environment was elaborated upon after finding white layer on worn surface. Although, how atmospheric reaction can contribute to the sub-surface white layer formation is still unknown, several mechanisms of surface reaction have been suggested to prove it [11]. More often, the formation of this layer with ultrafine grains or nanocrystalline structure is attributed to manufacturing processing induced large strain (shear strain > 2) [84], strain rates and temperature [26]). Therefore, the mechanical effect has been explored as the possible dominant factor for the white layer formation.

Mybokwere et al [85], Cho et al [86] and Zhang et al [87] showed that dynamic recrystallization and dynamic recovery are the dominant processes in the formation of surface white layers and internal white adiabatic shear bands, which are internal non-etching white bands in steels, deformed at high strain rates (from 10^3 to 10^6 s^{-1}). Mao et al [88] investigated the affected layers formed in grinding of AISI 52100 steel. They found that the retained austenite and white layer can be formed at the grinding temperature which is below the nominal phase transformation temperature of the workpiece material. More specifically, the percentage of retained austenite in the white layer of the ground workpiece of hardened steel is lower than that of the unmachined workpiece. This confirms that the mechanical effect can influence the white layer formation, and the dominant factor in annealed steel grinding is the plastic deformation.

Regarding to the third white layer formation mechanism, it is well known that temperatures in machining can reach very high values, it is likely that at the tool-workpiece interface, temperatures are high enough to cause phase transformation of ferrous alloys. In particular, for steels, Ramesh et al [89] found that the influence of stress and strain on the austenite-start temperature produces an approximate austenite-start temperature of 550°C–650°C (Figure 2.2).

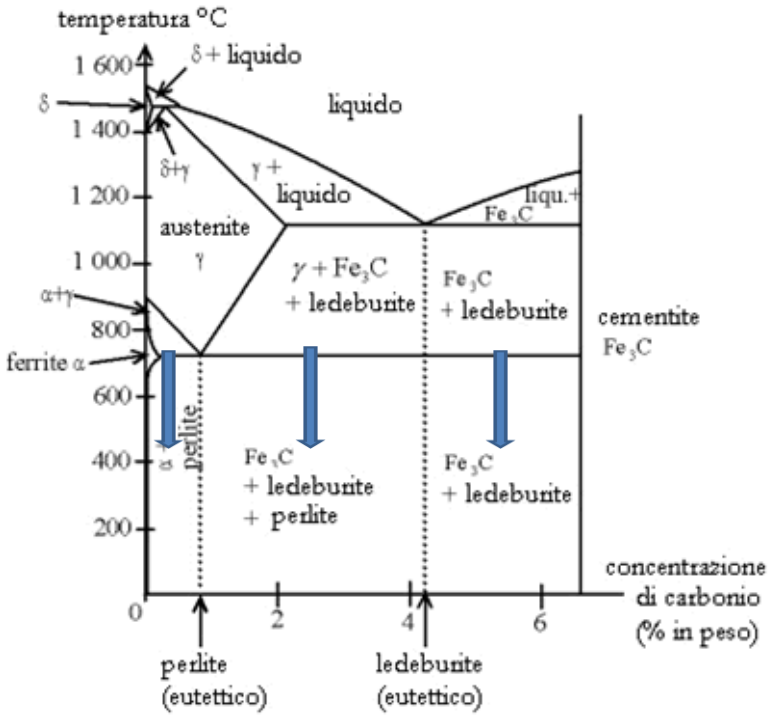

Figure 2.2 Influence of stress and strain on the austenite-start temperature

Barry and Byrne [90] and Chou and Evans [48] affirmed that the high austenite content of the surface white layer clearly confirms the occurrence of the reverse martensite transformation during machining. Such metallurgical change is due to the rapid increase in temperature, combined with high pressure generated by the action of the tool, transforming the machined surface to the austenitic state. When the tool and the workpiece separate, the surface cools down and the critical speed of martensite formation is reached by thermal convection into air and by conduction with the workpiece. Also, due to the high thermal cooling in machining (10^4 °C/s [48]), austenite has insufficient time to fully transform and some retained austenite traces can be found in the surface layer.

Brinksmier and Brockhoff [91] showed that, due to a critical rate of heating and "quenching" (as in machining), fine-grains structures can be formed, especially in martensitic steels. In addition, they noticed that the white layer thickness increases when the temperature was above the austenitising temperature of the considered steel. Barbacki et al [92] studied the formation mechanism of white and dark layers during the turning process with particular focusing on the coupled mechanical and thermal effects during processing. Österle et al [93] analyzed the white layer generated in pearlitic steels. Their research also demonstrated that the formation of white layer was due to the coupled effects: the mechanical due to the presence of severe plastic deformations and the thermal, tied to the rapid heating followed by quenching.

The same conclusion was drawn by Qi et al [94]. They investigated the white layers produced on the machined surfaces and on the inner side part of the chips in dry hard turning of GCr15 with PCBN tools. Their results also showed that white layer formation in hard turned surfaces was the concurrent effects of rapid heating and cooling processes, as well as plastic deformation. Plastic deformation will assist in the grain refinement and phase transformation processes. As the cutting speed increases, the thermal softening effect becomes greater than the influence of plastic deformation.

Wang et al [83] have reported that during wear of steels AISI 52100 and AISI 1080, when frictional heating is insufficient to induce phase transformation, white layer is generated due to plastic deformation purely by the action of frictional shear stress. While at higher speed and/or higher loading conditions, the temperature at the asperity contacts may be sufficiently high for re-austenitization to take place followed by rapid

quenching, where the base material acts as heat sink; this process results in the formation of very fine secondary martensite. Even in the latter mechanism of white layer formation, the plastic deformation's important role is also pointed out by Li et al [95] and Torrance and Cameron [96].

Ramesh et al [97] performed tests on hard turning AISI 4340 and 52100 (57 HRC) steel alloys and observed the clear formation of white layer and absence of dark layer in alloy 4340, this absence was attributed to the fact that the tempering temperature would have never been reached in the subsurface layers.

2.1.1 – EFFECT OF MATERIAL CHARACTERISTICS ON WHITE LAYER FORMATION

It is assessed that material characteristics of steels such as carbon content, alloying and heat treatment play a role in the formation of white layer in machining. Shaw and Vyas [98] highlighted that carbon diffused into the γ phase during rapid heating leading to formation of untempered martensite during quenching in the grinding process. They deduced from the Fe-C phase diagram that 0.025 wt. % carbon content is the minimum amount needed to achieve the observed phase change to cause the microstructural change because austenite (γ) transformed to ferrite (α) without martensite phase (α′) with less than 0.025 wt. % carbon. Okusa et al [99] performed experimental tests on several types of steels, with different levels of alloying, to study their effect on the white layer formation. The authors showed that white layer is observed in the built-up edge formed on the tool in machining carbon steel and a low alloy steel such as Cr-Mo steel, while no white layer is observed in the built-up edge formed during machining high alloy steels such as alloy tool steel and stainless steel. Kim and Kwon [100] performed experimental tests on AISI 1045, 1070 and 4340 annealed steels, with different levels of carbon or alloying. The authors showed that white layer occurs in 1070 steel at a machining speed as low as 225 m/min, in 1045 steel only at the higher machining speed of 275 m/min, while thicker white layer is observed in machining of 4340 steel

compared to that in 1045 steel for the lower A_3 temperature of the 4340 steel. Shaw and Vyas [98] ground 1045 annealed steel comparing the microstructure changes in the surface with that produced in grinding of 4340 hardened steel (51 HRC). A very thick (130μm) heat affected zone and a more complex structure was observed in the ground 1045 annealed steel surface. Large pearlite patches in the 1045 annealed steel are thought to hinder carbon diffusion into the γ phase and are responsible for the complex structure in the heat affected zone. Coolant application during grinding of 1045 annealed steel is considered to be a factor responsible for the fine pearlite structure formed on the surface because coolant application provides another quenching source on the surface in addition to quenching by the bulk. However, since several different conditions are used in the study for the two materials, it results difficult to compare the structure of the ground 1045 with the ground 4340 in order to identify the effect of each material on white layer formation.

2.2 – INFLUENCE OF THE CUTTING PARAMETERS

Since it is widely reported that white layer formation and its thickness are function of the cutting conditions (i.e., cutting speed, feed rate, depth of cut) as well as initial workpiece hardness, tool geometry and cooling condition a review of the literature about their influence on the white layer formation will be showed in the next paragraphs, with the aim to better understand the influence of each single parameters on the phase transformations during hard turning.

2.2.1 – INFLUENCE OF THE CUTTING SPEED

Concerning the influence of the cutting speed on the microstructural changes during hard turning processes a wide series of experimental analysis and investigations are

reported in the literature, resulting in an increase of the white layer thickness with the increase of the cutting speed. Chou and Song [101] found that when samples in AISI 52100 are machined, the white layer thickness shows a rapid increase with the increase of the cutting speed until 3-4 m/s (180-240 m/min), after that a steady condition is reached in which the thickness remains constant with the increase of the cutting speed; for higher cutting speed the white layer slightly decreases showing a negative slope (Figure 2.3).

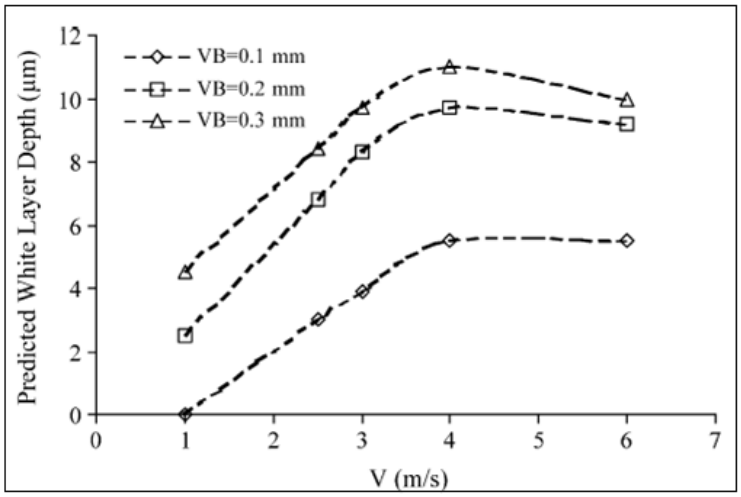

Figure 2.3 Influence of cutting speed on White Layer thickness [101]

Warren et al [102] studied the influence of machining induced residual stress and phase transformation on the measurement of subsurface mechanical behavior using nanoindentation. In order to investigate the fundamental relationships between subsurface mechanical behavior, residual stress, and microstructures, several group samples were prepared using the machining conditions (Table 2.1).

The chosen machine tools provide enough stiffness to conduct hard turning since the surface finish Ra 0.15 µm is within the production range. The testing specimens were prepared by slicing the samples with an abrasive cutter and then filing by hand to remove all burrs. Each specimen was then set in an epoxy mold in order to expose the cross-sections and reduce edge rounding during polishing. A series of polishing was manually performed with decreasing grit size and finished with a 0.03 µm aluminum polishing compound until mirror like surface was obtained

Work material (HRC)	Operation	Surface characteristic	Speed (m/s)	Feed (mm/rev)	Depth of cut (mm)
AISI 52100 (62 ±1)	Dry turning	No white layer (WL)	1.78	0.0254	0.254
AISI 52100 (62±1)	Dry turning	Thin WL (5 μm)	2.82	0.0254	0.254
AISI 52100 (62±1)	Dry turning	Thick WL (12 μm)	2.82	0.05	0.2
AISI 1070 (61.7±0.4)	Grinding (fluid: CSN)	No WL	15	0.02	0.1
AISI 1070 (61.7±0.4)	Honing (fluid: E)	No WL	1	NA	0.05

Table 2.1 Machining Conditions [102]

At the end of each test subsurface structure characterization and nanoindentation tests were performed. Subsurface structures at different magnifications were characterized using optical microscopy to differentiate microstructure changes in the machined layer. Taking into account the two first machining conditions reported in Table 2.1, in which AISI 52100 is hard dry turned increasing the cutting speed, the authors were able to find a machined surface without white layer and one with the white layer formation. These evidences were reported in Table 2.1 after the analysis of the microstructures obtained by optical microscope (Figure 2.4).

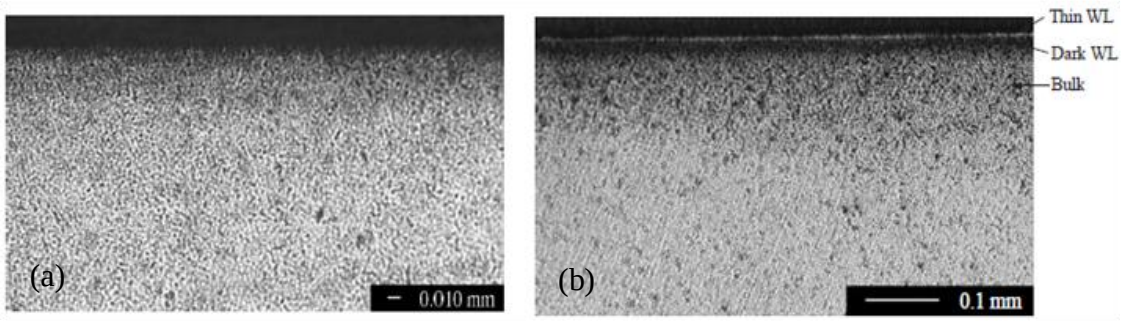

Figure 2.4 Cross section of turned surface (a) with no visible white layer and (b) with a thin white layer [102]

As above mentioned, observing Figure 2.4 (a) there is no visible phase transformed region in the subsurface and the grain size is relatively constant throughout the depth, while in Figure 2.4 (b) the subsurface is characterized by a thin phase transformed region. The phase transformed region consists of the white layer (WL) of approximately

5–10 µm thick and the 30 µm dark layer (DL) directly beneath the WL. Beneath the dark layer is the bulk material which has little variation in microstructure and grain size. So the increase of the cutting speed results in an increase of the white layer thickness.

Ramesh et al [50] conducted an analysis of white layer formed in hard turning of AISI 52100 steel. Bars of 35 mm diameter were heat treated by holding at 829 °C for 1.5 h, quenching in oil, then tempering at 163 °C for 2 h, which yielded a tempered martensitic bulk structure with a hardness of approximately 62 HRC. White layers were generated by turning the hardened steel at three different cutting speeds of 300 SFPM (91.4 m/min), 600 SFPM (182.9 m/min), and 900 SFPM (274.3 m/min). The feed and depth of cut were kept constant at 0.127 mm/rev and 0.254 mm/rev, respectively, and all cutting were performed dry. Since machining with cutting tools is a thermo-mechanical process, it is impossible to completely isolate the mechanical and thermal effects. Consequently, the choice of cutting speeds from low-to-high was designed to emphasize the expected dominant role of thermal phenomena at the highest cutting speed. In contrast, the lowest cutting speed was selected to emphasize the expected dominant role of mechanical (plastic) deformation. Each of the three conditions employed a low CBN-content insert (Kennametal KD050 grade, ANSI TNG-432 geometry) mounted in a standard tool holder (Kennametal DTGNL- 164D). Hard turning was carried out on a rigid super precision CNC lathe (Hardinge T-42SP).

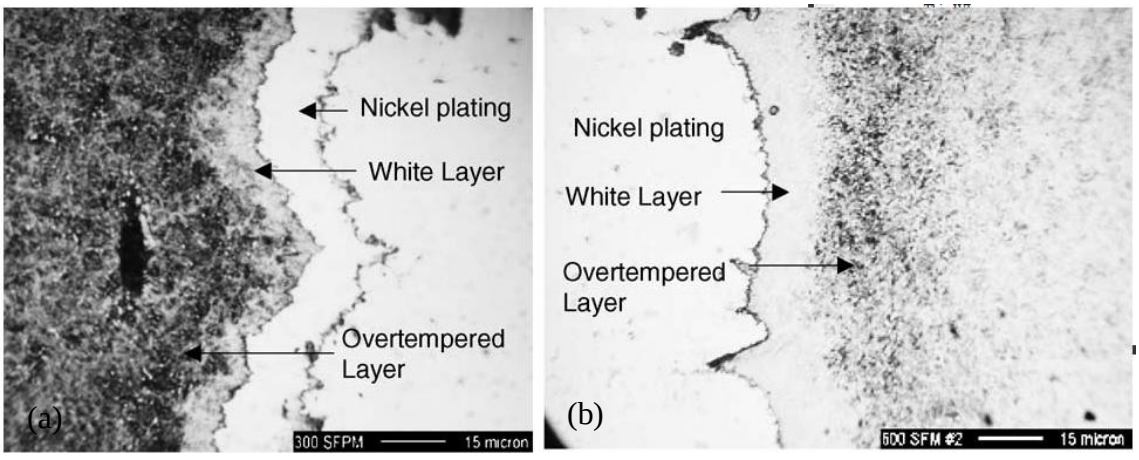

Figure 2.5 Taper section of the white layer generated (a) at 300 SFPM (91.4 m/min) and (b) at 600 SFPM (182.9 m/min) [50]

In Figure 2.5 are reported the optical micrographs results. In accordance with the other research the authors show as white layer thickness increases when cutting speed rises; furthermore it is showed an opposite trend for the dark layer (overtempered layer) that decreases with the increase of the cutting speed.

Sangil Han of the Georgia Institute of Technology [103] in his PhD thesis on mechanism and modeling of white layer formation in orthogonal machining of steels studied the influence of several cutting parameters on microstructrual changes. He showed that with the increase of the cutting speed from 100 to 300 m/min an evident increase in white layer thickness was registered when AISI 52100 (53 HRC) was machined (Figure 2.5).

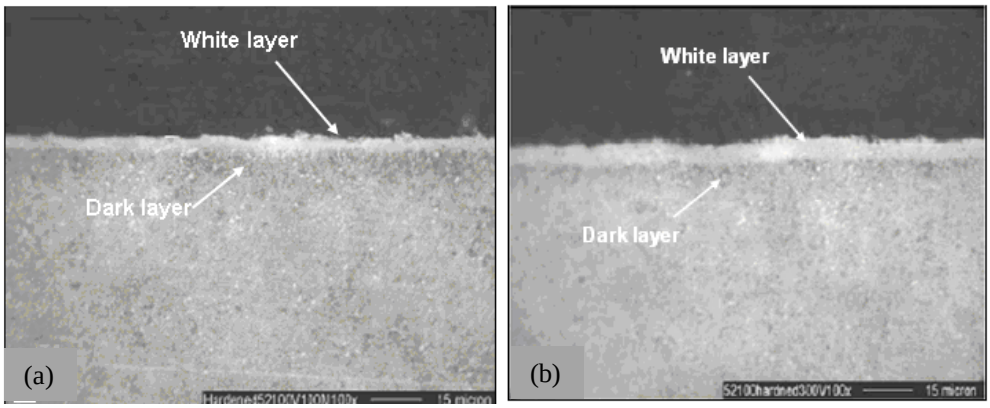

Figure 2.5 Micrographs of the machined surface at: (a) V = 100 m/min and (b) V = 300 m/min [103]

Other experimental work of Shi et al [104] was conducted on turning of AISI 52100 steel (62 HRC) to study the white layer thickness based on the cutting parameters of hard machining. The authors performed more than 60 experiments with the following cutting conditions (Table 2.2).

Tool flank wear, μm	102, 203, 305, 406, 508
Cutting speed, m/min	91.4, 144.8, 198.1, 251.5
Tool rake angle, °	–5, 25
Tool nose radius, mm	0.8, 6.35
Feed rate, μm/rev	38, 76
Tool thermal conductivity, W/m/°C	38, 100
Cooling condition	Dry, wet (liquid nitrogen)

Table 2.2 Cutting parameters in machining of hardened AISI 52100 Steel [104]

In this way it was possible to have a wider idea on the on the influence of several parameters on surface structural changes including the comparison between dry and cooling condition too. Taking into account the influence of the cutting speed also in this case the increase of the cutting speed is followed by an increase in the white layer thickness (Table 2.3).

Index	Cooling	V_b µm	U m/min	γ °	R mm	f µm/rev	K W/m/°C	WL thick-ness, µm
1	No	508	91.4	−5	0.8	38	100	1.4
2	No	508	144.8	−5	0.8	38	100	2.7
3	No	508	198.1	−5	0.8	38	100	3.4
4	No	508	251.1	−5	0.8	38	100	4.5
5	No	406	91.4	−5	0.8	38	100	0.0
6	No	406	144.8	−5	0.8	38	100	0.3
7	No	406	198.1	−5	0.8	38	100	1.1
8	No	406	251.1	−5	0.8	38	100	2.8
9	No	305	91.4	−5	0.8	38	100	0.0
10	No	305	144.8	−5	0.8	38	100	0.0
11	No	305	198.1	−5	0.8	38	100	0.3
12	No	305	251.1	−5	0.8	38	100	1.6
13	No	203	91.4	−5	0.8	38	100	0.0
14	No	203	144.8	−5	0.8	38	100	0.0
15	No	203	198.1	−5	0.8	38	100	0.0
16	No	203	251.1	−5	0.8	38	100	0.0
17	No	102	91.4	−5	0.8	38	100	0.0
18	No	102	144.8	−5	0.8	38	100	0.0
19	No	102	198.1	−5	0.8	38	100	0.0
20	No	102	251.1	−5	0.8	38	100	0.0

Table 2.3 Cutting conditions and white layer thickness [104]

Finally Chou and Evans [48] studied the effect of the thermal modeling of hard turned surfaces on white layer formation. Moreover, the effects of two process parameters (i.e., cutting speed and flank wear) on white layer depth were investigated. They were selected because cutting forces are insensitive to cutting speed, and thus most mechanical effects are similar, and because most literature suggested flank wear as a critical variable. Bars of 25 mm, made of VIMVAR 52100 steel with a hardness of 61–63 HRC were turned on outside diameter. Cutting tools were 55° diamond-shaped Al2O3–TiC inserts (Kennametal K090,1 DNGA432T) with - 30° rake, 5° clearance and 0.8 mm nose radius. Cutting conditions were 50 µm/rev feed rate and 200 µm depth of cut. Cutting speed ranged from 0.5 m/s to 4.5 m/s. The results in terms of white layer thickness are reported in Figure 2.6.

This results gives the best idea about the influence of the cutting speed on white layer formation during hard turning processes. Similarly to Chou and Song [101] also Chou and Evans found an evident increase of the white layer for increasing values of the cutting speed until 3-4 m/s; after this value a constant or decreasing thickness, depending on the tool wear value, was detected.

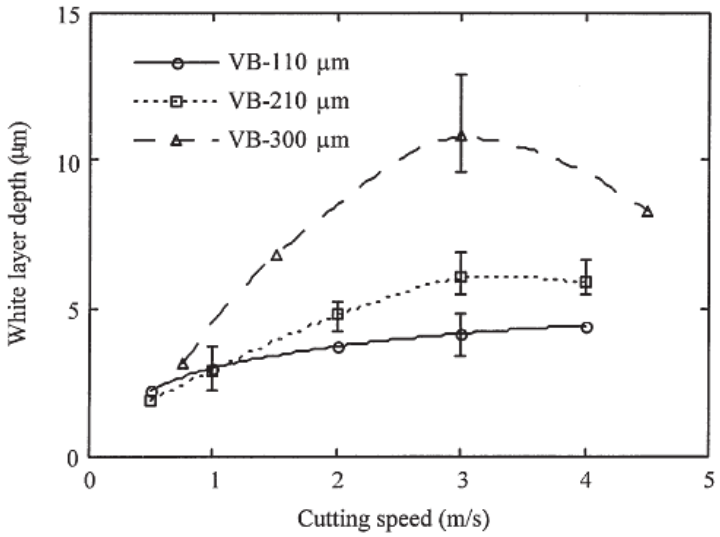

Figure 2.6 Measured white layer depth as a function of flank wear and cutting speed [48]

2.2.2 – INFLUENCE OF THE FEED RATE

The influence of the feed rate on the white layer formation shows a general behavior similar to that found for the cutting speed: with the increase of the feed rate an increase in white layer thickness is also observed.

Chou and Song [101] conducted experimental tests on AISI 52100 (60-62 HRC), using a feed rate ranging from 0.3 mm/rev to 0.6 mm/rev, while maintaining depth of cut and cutting speed constant and using a ceramic tool used (chamfer 20°x0.1 mm). Their experimental results are illustrated in Figure 2.7.

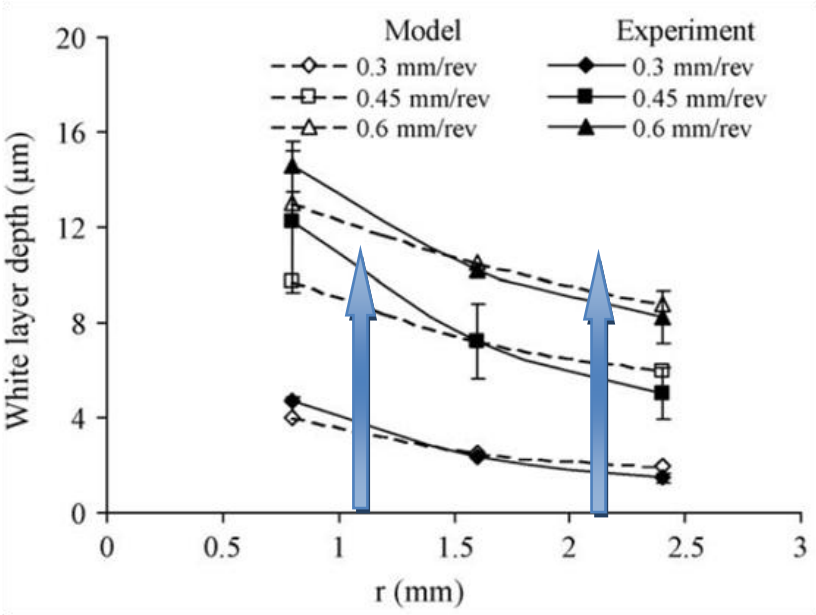

Figure 2.7 Feed rate influence on white layer thickness on AISI 52100 [101]

It may be noted as with the increase of the feed rate the white layer thickness also increases.

The experiments conducted by Ramesh et al [97] leads to the same conclusions. He made two tests on AISI 52100 (60-62 HRC), with different feed rates (0.127 mm/rev and 0.178 mm/rev) and fixed depth of cut and cutting speed, using a CBN tool.

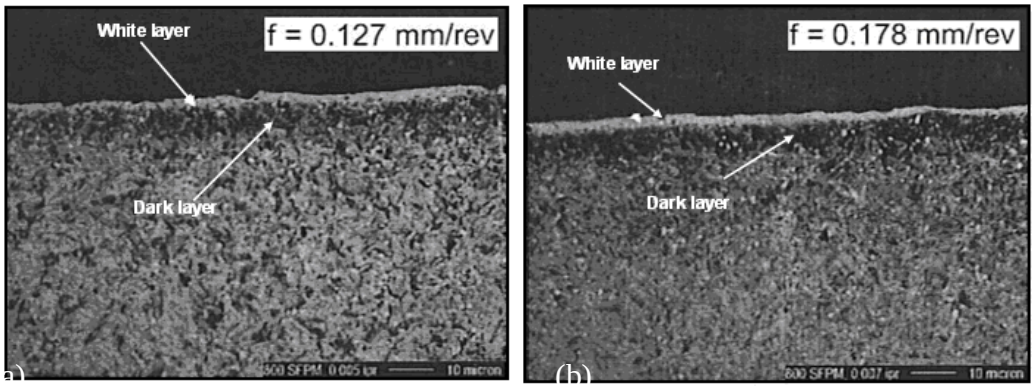

Figure 2.8 White and dark layers thicknesses at (a) *f*=0.127 mm/revand (b) *f*=0.178 mm/rev [97]

Observing the optical images, Figure 2.8, the white layer thickness rises when feed rate ranges from 0.127 mm/rev to 0.178 mm/rev. Also, analyzing the images in Figure 2.8 it can be observed the dark layer formation (overtempered martensite) and the

opposite influence of the feed rate on it: with the increase of the feed rate the dark layer decreases.

Also, A.W. Warren et al [102] studied the influence of feed rate on microstructural changes. Taking into account the second and the third Tests reported in Table 2.1, in which AISI 52100 is hard dry turned increasing the feed rate, the authors show an evident increase of the white layer thickness from 5 µm to 12 µm.

2.2.3 – INFLUENCE OF THE INITIAL WORKPIECE HARDNESS

The initial workpiece hardness represents another important cutting parameter to take into account when surface integrity is considered during hard turning, because of its influence on microstructural changes.

Studying the results observed by Sangil Han [103] and Ramesh et al [97] a consideration on hardness influence on white layer formation can be drawn.

Sangil Han [103] performed experimental analysis on hard turning of AISI 52100 (53 HRC), showing his results in terms of white layer formation varying the cutting speed from 100 to 300 m/min; he reported that with the increase of the cutting speed from 100 to 300 m/min an increase of the white layer thickness from 2.4 to 5.6 µm was registered (Figure 2.9).

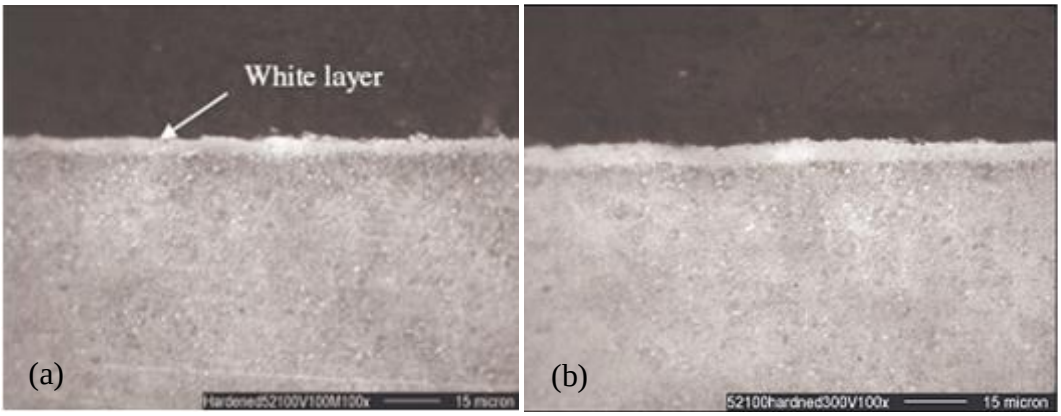

Figure 2.9 White and dark layers thicknesses at (a) 100 m/min and (b) 300 m/min [103]

Similar result was reported by Ramesh et al [97] during his study conducted on samples in AISI 52100 with an initial workpiece hardness of 62 HRC increasing the cutting speed from 100 to 300 m/min. He produced an evident increasing on white layer thickness from 8.6 µm to 12.6 µm (Figure 2.10).

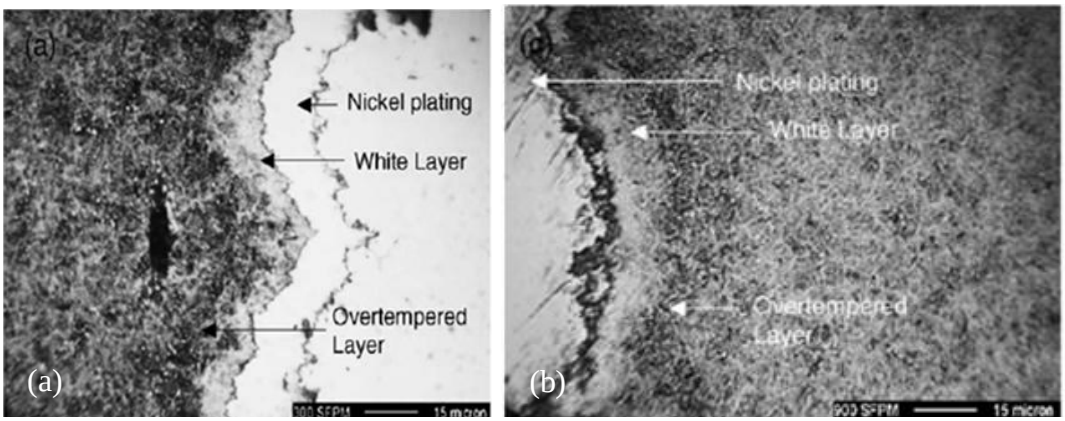

Figure 2.10 Taper section of the white layer generated (a) at 300 SFPM (91.4 m/min) and (b) at 900 SFPM (274.3 m/min) [97]

Thus, comparing their results [103, 97], at fixed cutting speed but varying the initial workpiece hardness an increase of the white layer thickness is registered when hardness increases. More in detail, for a fixed cutting speed of 100 m/min increasing the initial workpiece hardness from 53 to 62 HRC a white layer thickness of 2.4 µm and 8.6 µm is respectively reported. In addition, for a cutting speed of 300 m/min the increase of the hardness from 53 to 62 HRC produces a white layer thickness of 5.6 µm and 12.6 µm, respectively.

Moreover, other two important results can be seen from the comparison of their results [103, 97]:

- Confirmation of what was previously showed: as concerned the cutting speed when cutting speed rises an increase of the white layer thickness is observed;
- Higher initial workpiece hardness generates higher depth of overtempered martensite layer.

2.2.4 – INFLUENCE OF THE TOOL GEOMETRY

Another important parameter that is reported to have a significant influence on white and dark layers thickness during hard machining is the tool geometry. With the term tool geometry several aspects are analyzed in the literature: chamfered vs honed tools, tool wear, tool nose radius, etc.

Attanasio et al [105] performed a series of orthogonal hard turning tests are conducted to investigate the effects of tool wear and cutting parameters (cutting speed and feed rate), on white and dark layers formation of hardened AISI 52100 bearing steel, using PCBN inserts. Thickness of samples was equal to 1.2 mm, while its initial diameter was equal to 150 mm. The process parameters varied during their experimental campaign are shown in Figure 2.11.

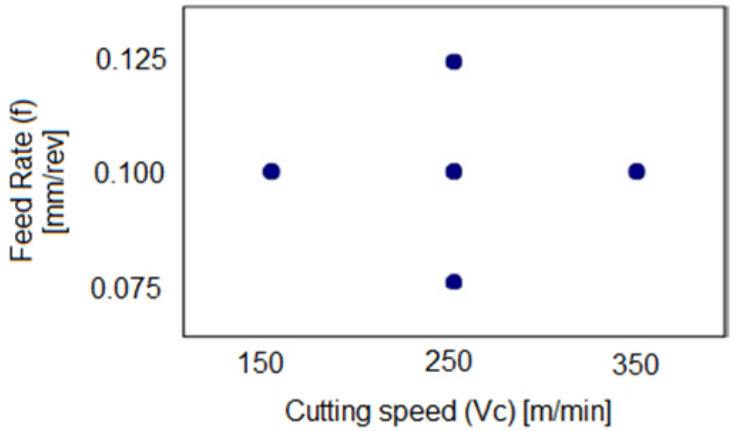

Figure 2.11 Experimental cutting data [105]

It should be pointed that the process parameters employed by Attanasio et al [105] were chosen in order to promote rapid tool wear and to facilitate the formation of white and dark layers in the machined surface. Metallographic inspection of polished and etched machined specimens was carried out using a Scanning Electron Microscope (SEM), (Figure 2.12).

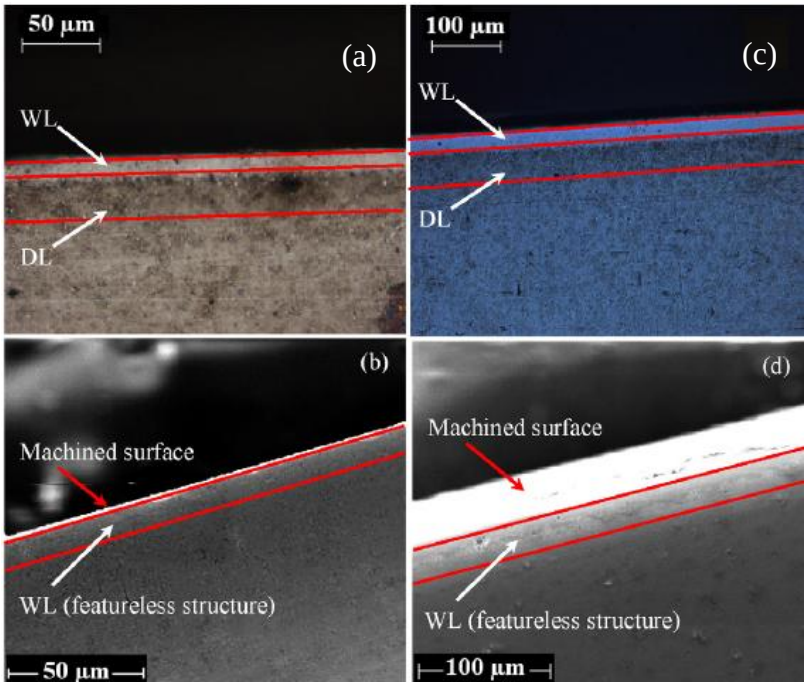

Figure 2.12 Optical observation (a) and SEM image (b) for test at 250 m/min, 0.1 mm/rev when critical flank wear VB* was relieved, optical (c) and SEM (d) images for test at 350 m/min, 0.1 mm/rev and critical flank wear (VB*) [105]

As general remark they found as for increasing tool wear and cutting velocity the white layers thickness increases; while the same behavior can be found only for feed rate higher than 0.1 mm (i.e., the chamfer length). Also the dark layers thickness increases with the tool wear.

Schwach and Guo [106] conducted a similar study in order to verify the effect of the tool wear. Then experiments were done on flat disc work samples of AISI 52100 (61–62 HRC). Four different machining conditions were used to produce distinct surface integrity conditions (Table 2.4).

Cutting conditions	Fresh surface #1 (FS-1)	Fresh surface #2 (FS-2)	White layer #1 (WL-1)	White layer #2 (WL-2)
V (m/min)	106.8	106.8	169.2	169.2
f (mm/rev)	0.1016	0.0254	0.0254	0.0254
DoC (mm)	0.254	0.254	0.254	0.254
VB (mm)	0	0	0.7	0.4

Table 2.4 Machining Parameters for Rolling Contact Life test Samples of AISI 52100 Steel (62 HRC) [106]

Comparing optical results of the last two experiments (Figure 2.13), the authors studied the influence of the tool wear, increased from 0.4 to 0.7 mm, on the surface and sub-surface microstructure.

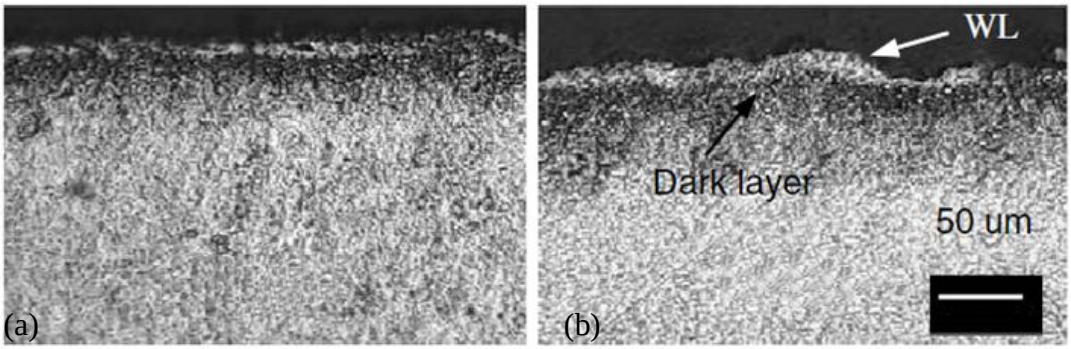

Figure 2.13 Subsurface microstructure at (a) VB=0.4 mm and (b) VB=0.7 mm [106]

With the increase of the tool wear it was reported an increase of the white layer from 4.5 to 7.5 µm; furthermore an increase of the dark layer was also observed.

Poulachon et al [80] conducted some orthogonal hard machining tests on four different work materials: X160CrMoV12 (AISI D2) with a ferritic and cementite matrix and coarse M_7C_3 primary carbides (20 µm); (ii) X38CrMoV5 (AISI H11) with a martensitic matrix (grain size 25 µm) and few MC carbides; (iii) 35NiCrMo16 with a martensitic matrix (grain size 10 µm) and rare carbides (no tempering); and (iv) 100Cr6 (AISI 52100) with a martensitic matrix (grain size 10 µm) and plenty of small M_7C_3 primary carbides (1 µm). Heat treatment conditions helped to reach hardness for all four work materials at HRC 54. The work material samples were prepared in a tube shape, 100 mm outside diameter with 12 mm thickness. In Figure 2.14 are reported the obtained experimental results.

Their results are of extreme importance because allow to have a general overview on the influence of the tool wear on white layer formation for hard machining since four different types of hard steels were kept into account. The results confirmed an evident increase of the white layer thickness with the increase of the flank tool wear.

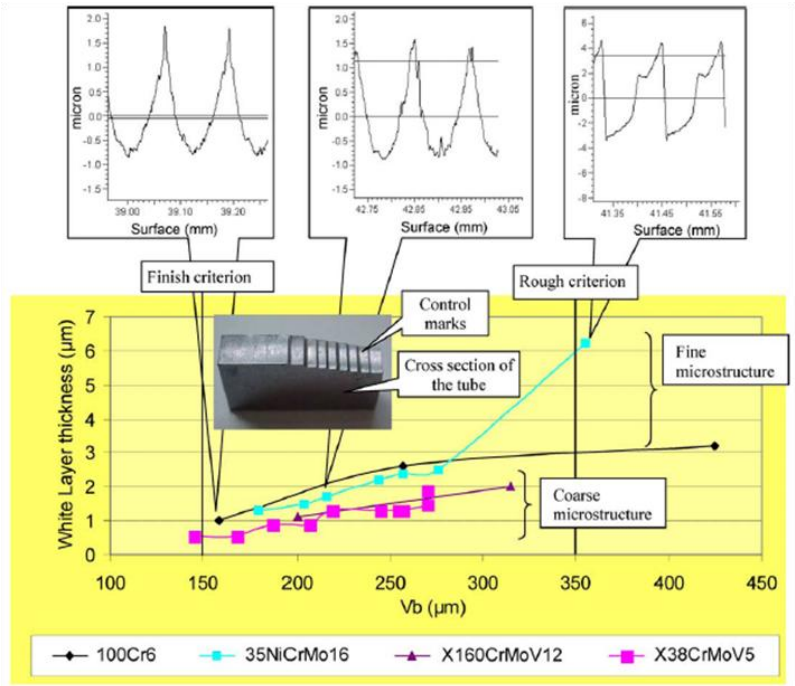

Figure 2.14 White layer thickness as a function of flank wear VB combined 35NiCrMo16 roughness profiles [80]

Also Akcan et al [84] studied the influence of the tool wear during hard machining of AISI 52100 and AISI 4340 (62 HRC). In Figure 2.15 are reported their results, also in this case an increase of the white layer is observed when the tool flank wear is increased.

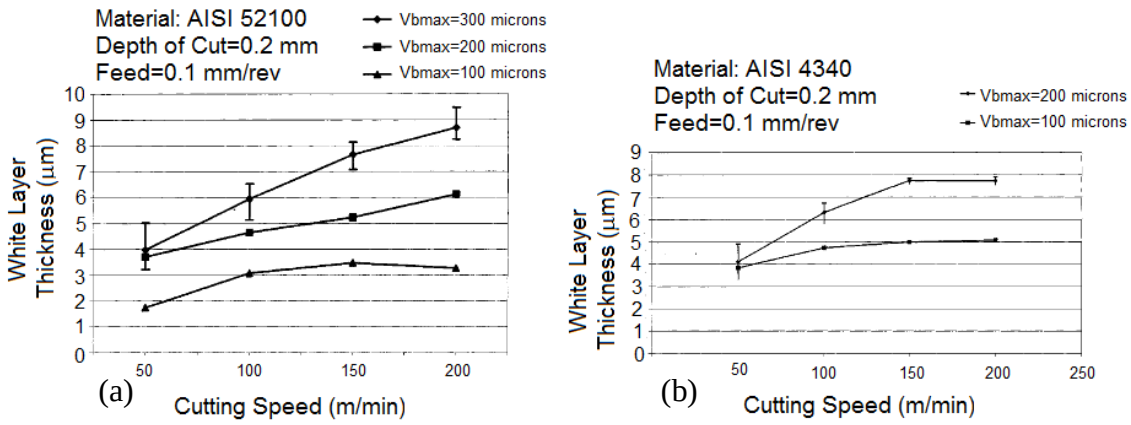

Figure 2.15 The variation of white layer thickness with cutting speed and flank wear (VBmax) in (a) 52100 steel and (b) 4340 steel, depth of cut=0.2 mm, and feed=0.1 mm/rev [84]

2.2.5 – INFLUENCE OF THE TOOL MATERIAL

In addition to the influence of cutting speed and tool flank wear on white layer depth, K. Chou and J. Evans [48] tested material effects of tool using a low CBN content, ceramic tool (Sumitomo BN250 DNMA432T), and an Al_2O_3–TiC inserts (Kenametal K090,1 DNGA432T).

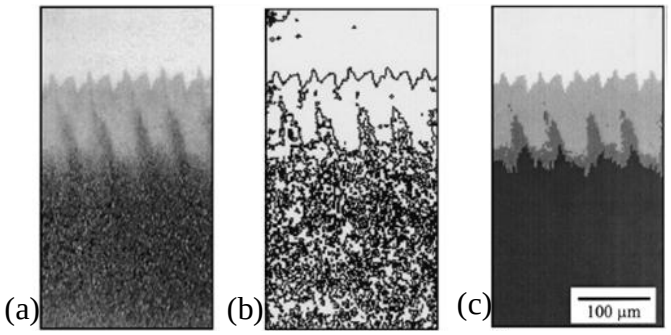

Figure 2.16 White layer images and depth measurement: (a) digitized photograph, (b) indexed contour image and (c) manipulated image with thresholds (marker in vertical direction is 6.7 μm) [48]

In Figure 2.16 is reported an example of the analysis conducted to identify, characterize and measure the white layer thickness. The experiment investigating material effects indicates a strong material dependence; in fact, the CBN tool, though having a higher thermal conductivity which should reduce heat partition into the workpiece, does not result in a smaller white layer.

2.2.6 – INFLUENCE OF THE COOLING CONDITIONS

Because of the main importance of the thermal effect on the machined parts, especially when surface integrity is considered, recently researches were interested in evaluating the influence of the cooling conditions when hard turning processes are

performed. In the following paragraphs the effect of three of the main used cooling techniques on microstructural changes are showed:

- WET: use of continuous flow of cooling lubricant;
- Minimum Quantity Lubrication (MQL): use of very small quantity of cooling lubricant;
- Cryogenic: use of materials (usually gases) at very low temperatures, below -150 °C: liquid nitrogen is the most commonly used element in cryogenics.

2.2.6.A – WET CONDITION

A. Devillez et al [107] focused their attention on the effect of dry machining on surface integrity when machining Inconel 718 superalloy (54 HRC) tests are performed. Wet and dry turning tests were performed at various cutting speeds using a coated carbide tool. For each cutting test machined surface was observed and additional observations and measurements were performed with the samples corresponding to the cutting speed of 60 m/min: wet and dry subsurface microstructures in the direction of cutting were studied and compared (Figure 2.17).

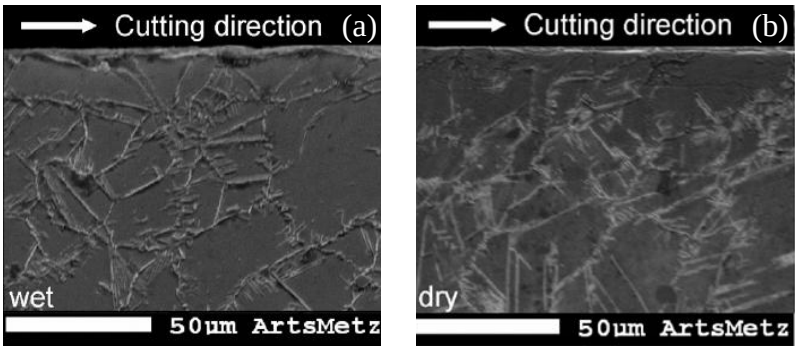

Figure 2.17 Subsurface microstructure after (a) wet and (b) dry cutting at 60 m/min [107]

Although a low value of cutting speed was analyzed Figure 2.17 reveals that dry condition shows an incidence on the microstructure deformation and damage. In fact, additional data about microstructure and microhardness led the authors to state that in dry conditions the surface quality is altered by the higher temperatures generated.

2.2.6.B – MINIMUM QUANTITY LUBRICATION (MQL) CONDITION

R. Da Silva et al [108] conducted an experimental analysis in order to investigate the effect of minimum quantity lubricant technique on surface integrity when ABNT 4340 steel (60 HRC) is ground. In particular, the samples where machined by an Al_2O_3 grinding wheel with conventional cooling, dry condition and with the use of the MQL technique. Figures 2.18 are micrographs of sample cross-sections illustrating the comparison of subsurface alterations that took place in the workpieces under dry condition and with the use of the MQL technique.

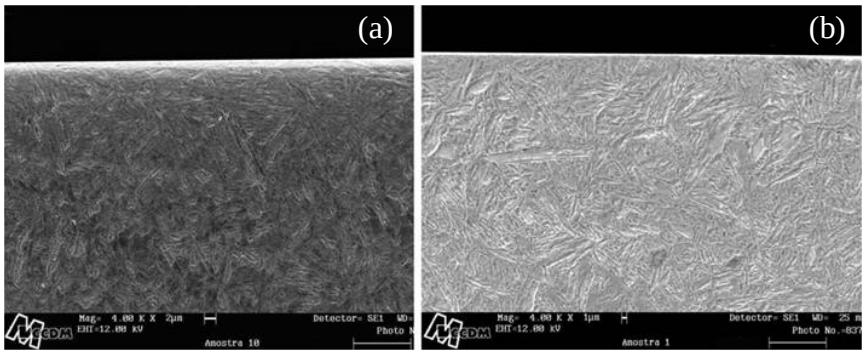

Figure 2.18 Subsurface microstructure: (a) dry condition and (b) MQL [108]

Observing Figure 2.18 the authors noted that the microstructure under dry condition shows thinner martensitic structure in the subsurface, which is probably due to the more effective tempering because of higher temperature and slow cooling. All the energy spent in grinding is converted into heat in the grinding zone, which leads to higher

temperatures and possible thermal damages in the workpiece. Several thermal damages may occur in grinding of annealed steel, including tempering and re-hardening due to formation of fragile martensite if the grinding temperature is high enough to cause the reaustenitization. These damages can be avoided if the grinding process is carried out in such a way that the maximum temperature in the grinding zone is kept below the minimum value for reaustenitization, normally near the eutectoid temperature of the carbon steel and many alloy steels.

In fact, it can be noticed when analyzing the microstructures the lack of meaningful circumstantial evidence of subsurface alterations in the microstructure when the MQL technique was employed. The metallurgical alterations clearly seen for all conditions tested (MQL, conventional, dry grinding and heat treatment) were essentially restricted to the changes in the microstructure. Again, the MQL technique efficiency was also confirmed in the microstructure analysis, reinforcing the thesis of significant effects on cooling and lubrication, providing a positive aspect of the surface integrity of the workpiece.

2.2.6.C – CRYOGENIC COOLING

Z. Zurecki et al [109] examined the impact of cryogenic liquid nitrogen spray cooling on white layer formation during orthogonal hard machining on AISI 52100 (62 HRC) at different cutting conditions.

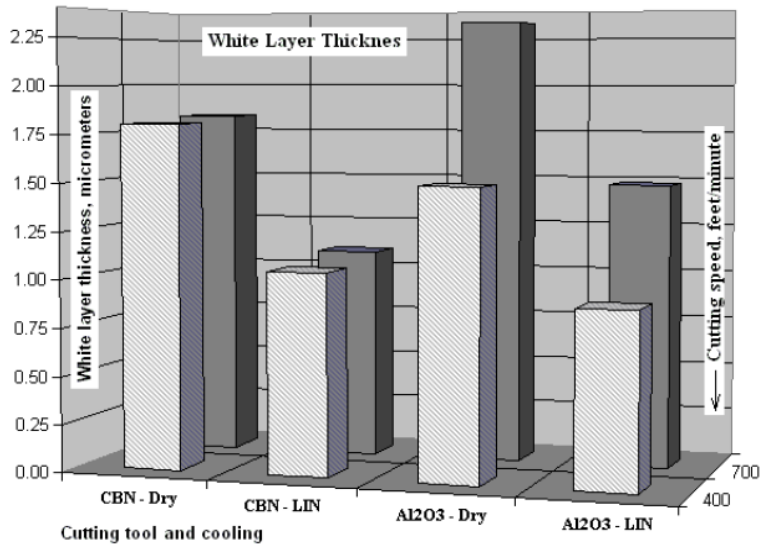

Figure 2.19 Results of SEM image-based white layer measurements on samples hard turned at the speed of 400 and 700 ft/min (122 and 213 m/min, respectively) [109]

Analyzing the results reported in Figure 2.19 the authors concluded that white layer is a purely thermo-mechanical phenomenon involving dissolution of low-alloy carbides into austenitic matrix, and catastrophic flow of that 1-phase material resulting in its nano-scale refinement. Furthermore, it was showed that the depth and extent of the refinement are controlled by cooling, in fact, with the cryogenic nitrogen reduction in white layer thickness, loss of hardness, and improving residual stress distribution were observed. Also a drastic reduction of dark layer was registered during their experiments, in fact, although it is not shown in Figure 2.19, the average thickness of dark layer was about 50 μm for LIN-cooled tools and 100 μm for dry-machining.

Other experimental work by Shi et al [104] was conducted on turning of AISI 52100 steel (62 HRC) to observe the white layer thickness during hard machining performed

under dry and wet conditions. The authors performed more than 60 experiments with the following cutting conditions (Table 2.5).

Tool flank wear, μm	102, 203, 305, 406, 508
Cutting speed, m/min	91.4, 144.8, 198.1, 251.5
Tool rake angle, °	−5, 25
Tool nose radius, mm	0.8, 6.35
Feed rate, μm/rev	38, 76
Tool thermal conductivity, W/m/°C	38, 100
Cooling condition	Dry, wet (liquid nitrogen)

Table 2.5 Cutting Parameters in Machining of Hardened AISI 52100 Steel [104]

Then it was possible to have a wider idea on the influence of several parameters on surface structural changes including the comparison between dry and cryogenic cooling condition. Their results highlight as in the case of cryogenic cooling a drastic reduction of the white layer thickness sometime (even of 6 times) is observed. Table 2.6 reports the overall results in which the direct comparison of the corresponding dry and cryogenic conditions are highlighted.

Cooling	V_b μm	U m/min	γ °	R mm	f μm/rev	K W/m/°C	WL thick-ness, μm
No	508	91.4	−5	0.8	38	100	1.4
Yes	508	91.4	−5	0.8	38	100	0.2
No	508	144.8	−5	0.8	38	100	2.7
Yes	508	144.8	−5	0.8	38	100	1.0
No	508	198.1	−5	0.8	38	100	3.4
Yes	508	198.1	−5	0.8	38	100	2.0
No	508	251.1	−5	0.8	38	100	4.5
Yes	508	251.1	−5	0.8	38	100	2.9
No	406	198.1	−5	0.8	38	100	1.1
Yes	406	198.1	−5	0.8	38	100	0.7

Table 2.6 Cutting condition and white layer thickness [104]

Finally, another investigation on cryogenic effects on the machined surface was made by D. Xavier et al [110]. The authors studied the influence of cryogenic influence in terms of surface integrity (roughness, white layer) during hard machining of AISI 52100 (62-64 HRC) by liquid nitrogen cooling with the use of special PCBN cutting

tool. By comparing the SEM analysis, Figure 2.20, the authors reported that only in dry cutting condition a thin white layer is formed, while no white layer is observed in cryogenic condition.

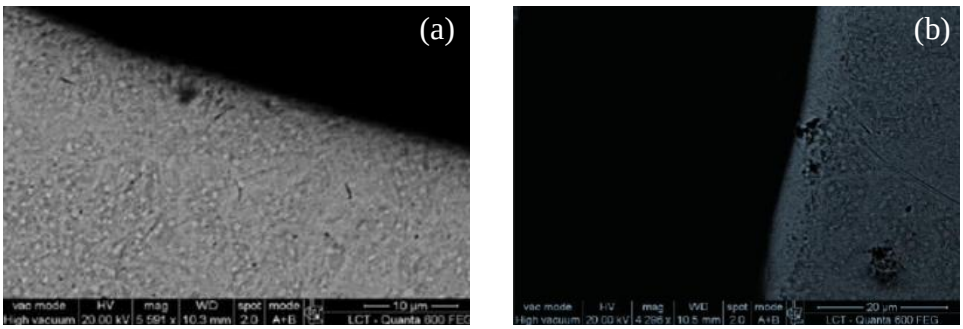

Figure 2.20 Metallographic aspect of transversal sections: (a) hard turning with liquid nitrogen cryogenic cooling Vc=160/min, ap 0.15 mm, fn = 0.2 mm/rev., (b) thin white layer formation for hard turning under dry condition Vc=160m/min, ap = 0.15 mm and fn = 0.2 mm/rev [110]

As overall, depending on these results what appears as important is the influence of the thermal effect on the white layer formation during hard turning processes. In fact, are of a great importance because since are directly related to the third theory proposed by Griffiths [82]: white layer formation can be attributed to the rapid heating and quenching, on the machined surface, which result in phase transformation.

2.3 – INFLUENCE OF THE WHITE LAYER ON FATIGUE LIFE

In order for hard turning to gain acceptance as an alternative to grinding in finishing processes, it is imperative that it provides comparable surface integrity, service life, and dimensional accuracy. Machining induced surface integrity can be characterized by surface roughness, micro-hardness, microstructure, residual stresses, etc. Although there is a substantial amount of research on the surface integrity resulting from hard turning [111–113, 12] and on the relationship between surface integrity and process parameters [92, 97, 115-118], the relationship between the surface integrity and the fatigue life of

hard turned surfaces is still not clearly understood, so it is important to understand how the surface integrity can affect the fatigue, or service life of machined components. Hard turning has the potential to produce favorable surface integrity such as a relatively deep ‘‘surface’’ compressive residual stress when compared with grinding, which may significantly increase a component’s fatigue life [15, 119, 114, 115]. As previously reported, hard turning may also induce white layer formation and, although its thickness is usually only several micrometers, its presence causes great concerns in the machining industry because of the effects on a component’s performance, such as fatigue life. Furthermore the white layer affects the nature and the profile of the residual stresses. Guo and Schwach [120] conducted a preliminary study that compared the fatigue performance of a component with the presence of white layer and a component free of white layer showed. They shown as the presence of the affected layer decreases fatigue life of hard turned surfaces in rolling contact. Following this direction other studies reported that white layer might reduce the fatigue strength [15, 114, 115, 119, 120-122]. In contrast, hard turned steels may have greater fatigue strength than ground steels, despite white layer occurrence, as shown by Konig et al [114]. Due to this discordance, deeply investigations are needed to fully understand as the white layer and residual stress patterns affect fatigue life. Schwach and Guo [120] revealed that a white layer with an approximate thickness of 5 μm would decrease the rolling fatigue life when compared to a surface free of a white layer. Utilizing acoustic emission monitoring, they also found that the white layer might initiate more crack growth/propagation throughout the rolling contact life, significantly increasing the potential for a catastrophic failure. Konig et al [114] cite various studies indicating that the surface integrity of hard turned parts even with pronounced white layer demonstrate substantial fatigue strength in rolling contact life. Tonshoff et al [12] performed rotating bending tests on hard turned specimens, which demonstrated that as tool wear increased, bending fatigue life decreased with all fractures initiating on the workpiece surface. This degradation in fatigue strength was mainly attributed to the formation of white layers on the surface and increase in surface roughness with increased tool wear. In their experiments carried out with various hard turned specimens, Agha and Liu [123] showed that cutting conditions have a significant effect on fatigue life. They also showed that the fatigue life of hard turned specimens is more repeatable than ground specimens. Matsumoto et al.

[15] presented statistically significant evidence that hard turning (prior to superfinshing) improved the fatigue life when compared to ground and superfinished components.

Finally S. Smith et al [124] studied the relationship between surface integrity and fatigue life of hard turned AISI 52100 steel (60–62 HRC), with grinding as a benchmark. Specifically, the surface integrity and fatigue life of the following five distinct surface conditions were examined: hard turned with continuous white layer (HTWL), hard turned with no white layer (HTnoWL), ground (G), and superfinished hard turned (HTSF) and ground specimens (GSF). High cycle tension–tension fatigue tests show that the presence of white layer does not adversely affect fatigue life and that, on average, the hard turned surface performs as well or better than the ground surface (Figure 2.21).

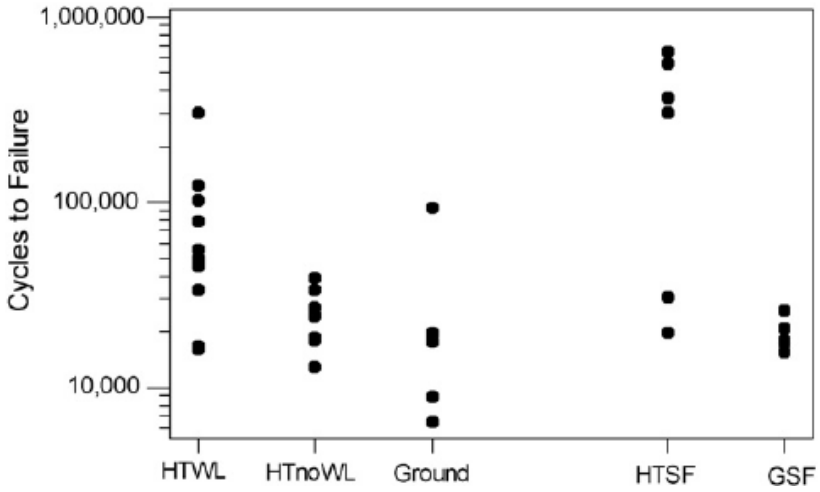

Figure 2.21 Axial high cycle fatigue life results [121]

Figure 2.22 suggests that the effect of residual stress on fatigue life is more significant than the effect of white layer and that for the hard turned surfaces, the fatigue life is found to be directly proportional to both the surface compressive residual stress and the maximum compressive residual stress.

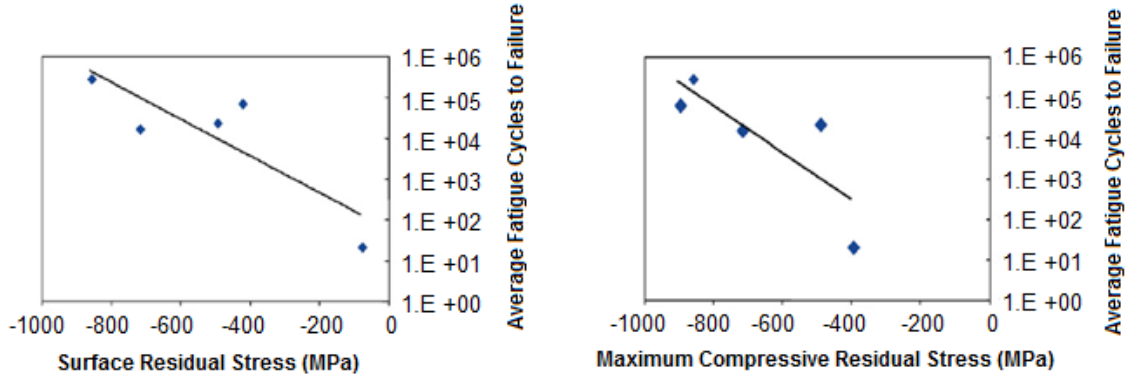

Figure 2.22 Fatigue life vs. (a) surface residual stress and (b) maximum compressive residual stress in the axial direction [121]

2.4 – SUMMARY

Several studies based on experimental tests were reviewed, allowing to perform an accurate investigation on the sensitivity exhibited by white layer (and sometimes by dark layer) to the various process parameters.

To conclude this chapter, a detailed overview of the discussed phenomena is reported and, a global summary of the results is shown.

As concern the cutting speed it was shown that its increase results in an thicker white layer (at least to a certain speed value), while the opposite is registered for the dark layer thickness that showed a decreasing trend.

When feed rate was analyzed, the same influence reported for the cutting speed was noted: an increase of the feed rate results in an increase of the white layer thickness and a decrease of the dark layer.

Higher initial workpiece hardness generates higher white and dark layers thickness.

The effect of the tool wear was equal for both the affected layers, its increase corresponds to an increase in both the white and dark layers thickness.

Tool geometry analysis showed that the use of a chamfered tool generates a thicker white layer than an honed tool.

Finally, concerning to the conventional cooling condition on the innovative one, the cryogenic effect, a drastic reduction is reported for the white layer thickness in presence of cooling system.

Table 2.23 reports the overall and the trends of affected layer varying the cutting process parameters.

INPUT		OUTPUT	
Cutting Parameter	Trend	White Layer	Dark Layer
Cutting Speed	↑	↑ ★	↓
Feed Rate	↑	↑	↓
Tool Wear	↑	↑	↑
Tool Geometry	-	The use of chamfered tool shows thicker white layer than honed tool	The use of chamfered tool shows thicker dark layer than honed tool
Initial Workpiece Hardness	↑	↑	↑
Cryogenic Condition	↑	↓	↓
★ The white layer trend rises until a certain value after that it gradually decreases up to settle around a constant value			

Table 2.23 Influence of cutting process parameters on white and dark layers formation

CHAPTER III

EXPERIMENTAL PROCEDURE FOR INVESTIGATING THE SURFACE INTEGRITY

This chapter contains the description of the materials (tool and workpiece), techniques and methods used to realize the experimental campaign and relative investigations.

The experimentation is carried out by machining disks of AISI 52100 hardened steel via orthogonal cutting tests using PCBN cutting tools. The disks were machined varying the cutting speed, the feed rate, the initial workpiece hardness and the tool geometry. For each of the investigated cases the depth of white and dark layers, the hardness, the cutting forces and the cutting temperatures were measured. Furthermore scanning electron microscopy modification (SEM), energy dispersive spectroscopy (EDS) and X-Ray diffraction (XRD) analysis were performed with the aim to better understand the reasons that lead to microstructural changes during hard turning of AISI 52100 and the effect of these on the machined components. The results of the study show the influence of each single cutting parameter on microstructural changes, and the impact of these on the residual stress profile in the machined components.

3.1 – EXPERIMENTAL PROCEDURE

The machining tests consist of orthogonal dry turning of disks made of AISI 52100 (100Cr6) hardened steel. Tests were performed on a CNC lathe provided of a piezoelectric dynamometer for the forces acquisitions and thermo-couples and infrared thermo-camera for thermal acquisitions. After machining, subsurface microstructure alteration in the form of white and dark layers were observed using an optical microscope (1000x) (Figure 3.1).

Figure 3.1 Optical microscope Leica: DM4000M, laboratory of university of Calabria

Scanning electron microscopy (SEM) was also used to examine the white layer thickness and to conduct energy dispersive spectroscopy (EDS) analysis for investigating its chemical composition. Microhardness was measured on the machined surface using a micro-indentation Vickers hardness tester with a certificated diamond indenter. Furthermore X-Ray diffraction (XRD) technique and electropolishing procedure were used in order to study the influence of the thermally-induced phase transformations on the surface and in-depth residual stress state. Finally, some machined samples were also analyzed with X-ray diffractometer to obtain the metallurgical structure of the crystalline material under consideration.

3.2 – CUTTING TOOL MATERIAL PROPERTIES

In general, cutting tools used for hard turning require extreme hardness, high compressive strength, high resistance to abrasive wear, thermal resistance and chemical stability at elevated temperatures. For interrupted cuts, tool materials with high toughness are more frequently required to prevent chipping and edge failure; however, these materials tend to have lower wear resistance instead despite to avoiding the use of coolant, as it causes higher variation in temperature, leading to premature tool failure. Ceramic and Cubic Boron Nitride (CBN) tools are currently the only choices available that can meet the demands of turning hardened steels.

Low CBN content cubic boron nitride tools (Seco grade: CBN 100) with two different edge geometries: chamfered (ISO TNGN 110308S with a chamfer of 20°x0.1 mm) and honed (ISO TNGN 110308E with an edge radius of 0.025 mm), were used to perform the experiments reported in this thesis (Figure 3.2).

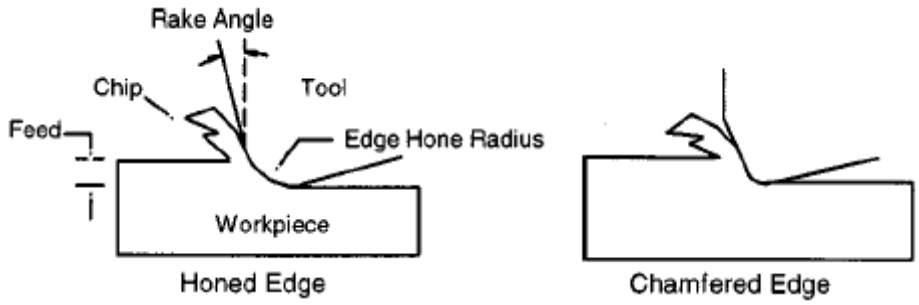

Figure 3.2 Typical PCBN cutting-edge preparation (orthogonal cutting geometry shown)

Polycrystalline Cubic Boron Nitride (PCBN) is a composite material comprising Cubic Boron Nitride (CBN) grains in a binder matrix; it is the dominant tool material for hard turning of alloy steel (45 – 65 HRC) due to its high hot hardness, high wear resistance, low solubility in iron, good fracture toughness [25, 125] and high thermal stability; furthermore PCBN cutting tools offer the possibility of greater process flexibility, reduced machining time, lower energy consumption, recycling possibilities, and the optional use of a coolant.

Since the market trends today are toward higher cutting speeds and increasing material removal rates, the number of commercially available PCBN tool grades is increasing with many being tailored for very specific applications. PCBN cutting tool materials are categorized as high CBN content material or low CBN content. High CBN content grades are approximately 80–95% CBN with a metallic-type binder. Low CBN content grades can contain from 40–70% CBN and the majority have ceramic based binder systems such as TiC and TiN. Tools with high PCBN content display greater toughness than those with an added ceramic phase. On the other hand, low PCBN is more resistant to diffusion wear, which is very important, especially in continuous turning.

Studies using these two classes of PCBN tools in continuous turning [126, 127, 48] have shown that, when the part and tool fixturing system were rigid to prevent either micro-chipping or breakage on the cutting edge, the life of the low PCBN tool was longer than that of the tool with high PCBN content. This fact is attributed to the added ceramic phase in PCBN material, which increases the tool's chemical stability, reducing the tendency for diffusion of tool particles into metallic elements of the chip, despite the decrease in the thermal conductivity of the tool material.

Narutaki and Yamane [128] showed the case of machining soft steels, where the wear resistance of the tool is controlled by the bonding strength of the tool grains. The authors concluded showing that PCBN with low content of CBN grain (~60%) produces an excellent performance in machining hard materials not containing many of ultra-hard grains (low alloy steels, case-hardening steels, tool steels, etc.). On the other hand, PCBN with high content of CBN grains (~90%) offers a better performance for abrasive wear and is suitable for machining hardened high speed steel products. Furthermore, they pointed out that the possibility of diffusion wear of CBN tool seems to be relatively low since the cutting temperature is not high enough and CBN grains are chemically stable for iron.

Ohtani and Yokogawa [129] stated that the main wear mechanism of CBN and ceramic tools in the machining of cold work tool SKD11 (hardness range 18–60 HRC) is abrasion by hard alloy carbide particles contained in the workpiece structure. The lifespan of carbide tools decreases as workpiece hardness increases, while the ceramic and CBN tool-life shows the opposite results.

Chryssolouris [130] carried out experimental cutting tests with four different work materials with the same hardness (55 HRC), but with different structures, in order to determine the influence of the work material structure on the wear behavior of CBN cutting edges. He showed that the cutting times for the same wear criterion for these various materials were different. A large difference in wear behavior was highlighted: ratio 1/2 for flank wear criterion (300 µm) and 1/4 for crater depth criterion (50 µm). Davies et al [131] performed similar experiments to compare the tool-wear rates for three steels of the same chemistry but different microstructures. They showed that the tool-wear rate decreases with decreasing CBN grain size and noted however, that bulk hardness and transverse rupture strength also increase with decreasing grain size.

In industrial applications, many components that are quenched and tempered before the finish turning operation have surfaces interrupted by holes, lubrication channels and key slots [132]. Interrupted turning of hardened surfaces imposes extra difficulties on machining operations. In such cases, a PCBN rather than a ceramic tool is preferable, due to its high hardness allied to moderate toughness.

Table 3.1 contains elastic and thermal properties of various CBN grades that are found in the literature.

CBN Grade	Young's Modulus (Gpa)	Poisson's Ratio	Thermal Conductivity at 20°C (W/m °K)	Heat Capacity (W/mm^2/°C)	Specific Heat (J/Kg/°C)	Emissivity	Thermal Expansion Coefficient (x10-6/°C)	Reference
Low-CBN	-	-	40	2.76		0.45		[Umbrello, 2004]
High-CBN	680	0.22	100	-	960	-	4.9	[Guo, 2002]
Low-CBN	800	0.15	40	-	793	-	5.6	[Mamalis, 2002]
Low-CBN	587	0.15	44	-	-	-	4.7	[Heat, 1986]
High-CBN	680	0.22	100	-	-	-	4.9	[Heat, 1986]
High-CBN	630	0.14	-	-	-	-	-	[Sandvik, 2005]
High-CBN	680	0.22	300-600	-	-	-	-	[Pierson, 1996]
Low-CBN	588	0.171	44	-	750	-	-	[Ng, 1999]
High-CBN	652	0.128	100	-	960	-	-	[Ng, 1999]
Low-CBN	-	-	44	-	-	-	-	[Ezugwu, 2005]
High-CBN	-	-	138	-	-	-	-	[Ezugwu, 2005]
High-CBN	680	0.22	100	-	750	-	-	[Ramesh, 2002]

Table 3.1 Elastic and thermal properties of CBN [133]

3.3 – WORKPIECE MATERIAL PROPERTIES

AISI 52100 hardened steel was chosen as the workpiece material used during the experimental tests performed in this work.

This material finds is main applications in making bearings, for its suitable properties.

The bearing is defined ‘‘as a part of a machine that allows one part to rotate or move in contact with another part with as little friction as possible’’. Additional functions include the transmission of loads and enabling the accurate location of components. A bearing may have to sustain severe static as well as cyclic loads while serving reliably in difficult environments so AISI 52100 and other steels are well-suited in this context, and in their many forms represent the material of choice in the manufacture of bearings.

AISI 52100 (commonly, UNI 100Cr6 in Europe) is a high carbon-chrome-manganese through hardening steel which finds applications in several rotating parts like anti-friction bearings, cams, crank shaft and other mechanical power transmission components.

Description	Value
C	0.9-1.05
Mn	0.25-0.45
Si	0.15-0.35
Cr	1.35-1.65
Ni	< 0.3
Mo	-
Other	S < 0.025
Young's Modulus (GPa)	210
Poisson Ratio	0.3
Mass Density (Kg m-3)	7853
Heat Capacity (N mm-2 /°C)	Fig. 1a
Thermal Conductivity (N s /°C)	Fig. 1b
Emissivity	0.7

Table 3.2 Chemical, mechanical and physical properties of the 52100 steel [134]

The Fe-C phase diagram illustrating the nominal Ac_1 and Ac_3 temperatures for is shown in Figure 3.3.

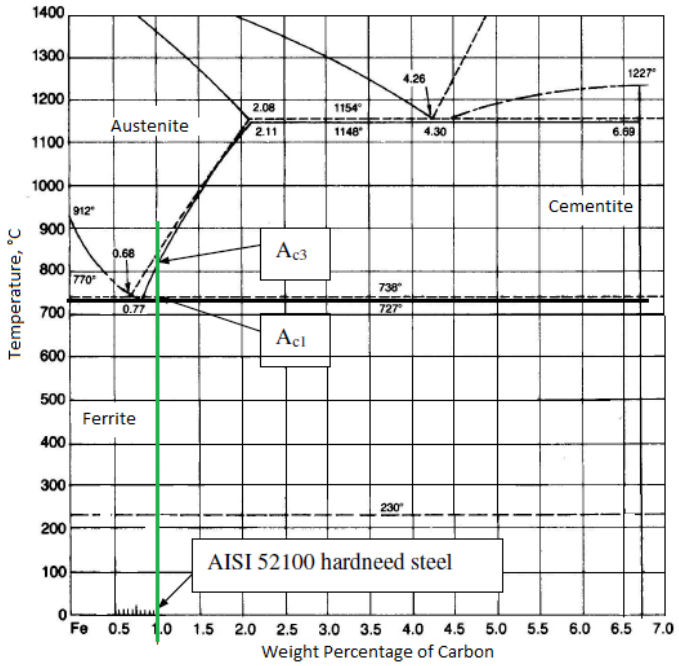

Figure 3.3 Fe-C phase diagram

Another important aspect related to the AISI 52100 are the heat treatment processes, usually made in order to change some superficial and in depth properties of the component as the hardness; quenching and tempering are the two main heat treatment processes usually made in order to reach an high specified hardness in a component. Related to the thermal aspect, with particular attention to the heat treatment processes made to obtain a specific hardness, the TTT and CCT curves specific of the AISI 52100 are below reported (Figure 3.4).

These curves are of main importance especially when the effect of the temperature, during hard machining, on the surface integrity is analyzed. In particular taking into account the behavior reported in the above figures it is possible to well understand and justify the formation of a martensitic structure on the machined surface when hard machining processes are performed. The temperatures reached on the machined surface are higher than the nominal A_{c1} temperature (Figure 3.3) and the cooling rate, after the tool cutting operation, is very high; depending on these two aspects and analyzing

Figure 3.4 it is evident that a quenching thermal treatment is made on the machined surface with the consequent martensitic structure formation that results in an higher material hardness compared to the initial workpiece hardness. This is the explanation that also Griffiths shows to explain the main influence of the thermal aspect on the formation of the white layer and its higher hardness value when compared to the bulk material. Same procedure can be followed to explain the formation of the dark layer in the sub-surface, in this case a tempering thermal treatment is considered. So high hardness is achieved in this steel by the induction hardening process.

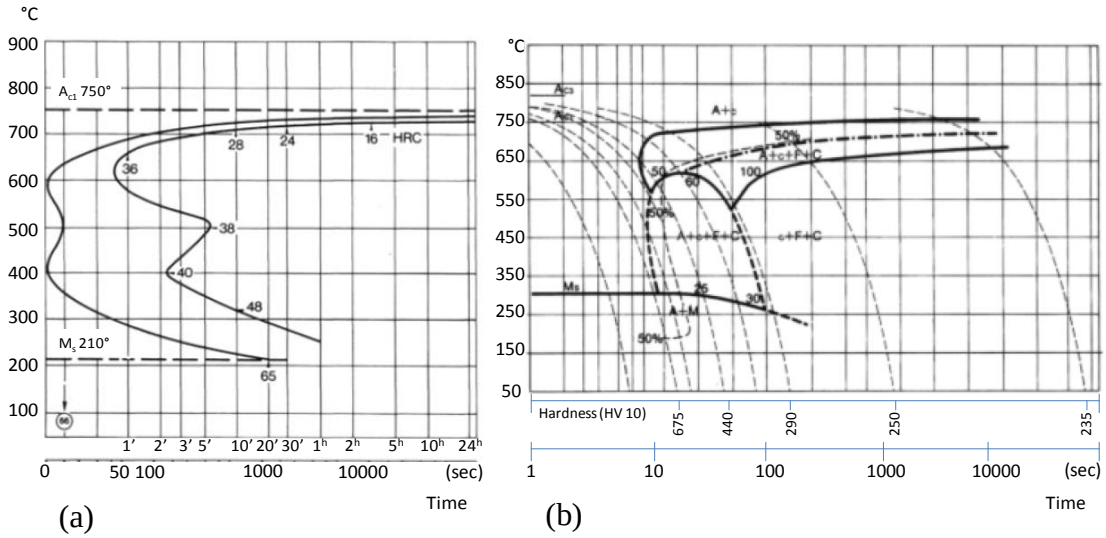

Figure 3.4 (a) TTT diagram and (b) CCT curve for 100Cr6 (AISI 52100)

This material is generally solution-treated to a temperature of 850 °C followed by oil quenching, and then tempered in the range 180–250 °C. This results in a microstructure of lightly tempered martensite, primary carbides and up to about 5% retained austenite. The hardness of AISI 52100 can reach 58–62 HRC. Higher hardness possess lower fracture toughness and ductility. Due to its high hardenability this steel achieves a uniform "through" hardness.

As shown in Table 3.3, several works presented in the literature consider the mechanical properties of the AISI 52100 steel workpiece with constant values taking into account the results of the tests conducted at room temperature.

Young's Modulus (Gpa)	Poisson's Ratio	Thermal Conductivity (W/m °C)	Heat Capacity (N/mm^2/°C)	Specific Heat (J/Kg/°C)	Emissivity	Thermal Expansion Coefficient (x10-6/°C)	Reference
-	-	60.5	-	433	-	-	[Hamdi, 2004]
167	-	32	-	745	-	-	[Poulachon, 2001]
210	0.3	16.8	-	460	-	16.5	[Mamalis, 2002]
206	-	-	-	-	-	-	[Caccialupi, 2003]
210	0.3	46.6	-	475	-	-	[ASM, 1999]

Table 3.3 Elastic and thermal properties of AISI 52100 steel [133]

Other works also show that such assumptions are incorrect since the temperature plays a fundamental role in the material behavior; so some researchers achieved mechanical properties of AISI 52100 steel as a function of the temperature f(T). Table 3.4 contains mechanical properties along the temperature range that is encountered during hard machining operations.

Temperature (°C)	Young's Modulus (Gpa)	Thermal Expansion Coefficient (x10-6/ °C)	Poisson ratio
20	201	11.5	0.277
200	179	12.6	0.269
400	163	13.7	0.255
600	103	13.7	0.342
800	87	15.3	0.396
1000	67	15.3	0.490

Table 3.4 Mechanical properties of AISI 52100 in function of the temperature [135]

Furthermore Umbrello et al [134] reported that also for thermal conductivity and heat capacity the influence of the temperature is significant.

As shown in Figure 3.5 the heat capacity drastically arises when the phase changes from martensite to austenite at AS temperature ($\approx$ 730 °C). This is also the temperature where the linear decrease in thermal conductivity changes to a constant value for temperatures higher than 730 °C.

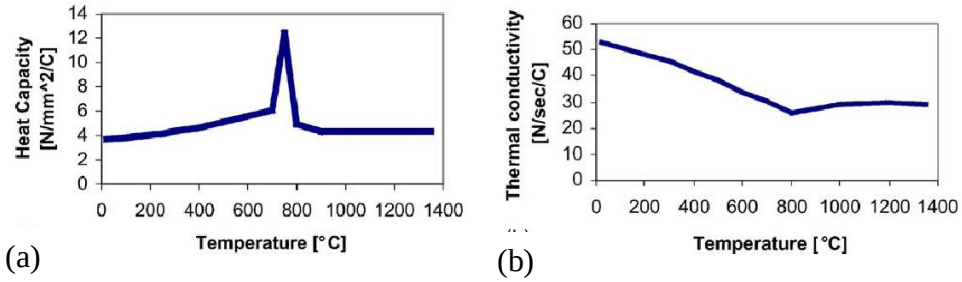

Figure 3.5 Physical properties of the AISI 52100 steel: (a) heat capacity and (b) thermal conductivity [134]

As concerned the sample geometry, in the present work disks of hardened AISI 52100 steel (outer diameter=150 mm; thickness=1.4 mm) were prepared by sawing from a round bar stock, followed by machining, heat treatment, and gentle grinding to restore flatness and parallelism resulting from the distortion during quenching.

In Figure 3.6 is reported the shape of the sample used in the experiments, the presence of the holes near the centre of the disk is necessary to correctly fix the disk in the lathe machine, so that the orthogonal cutting condition is respected.

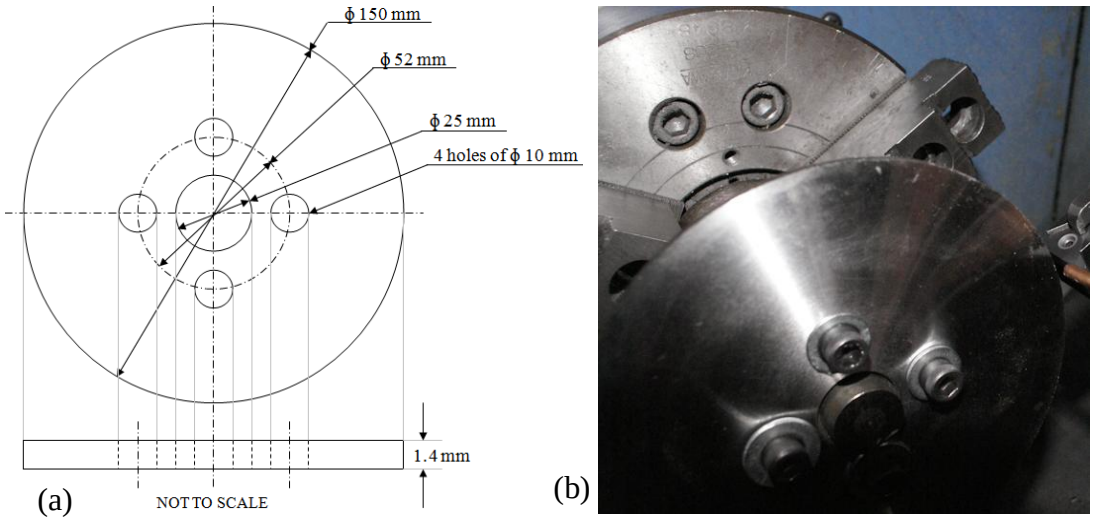

Figure 3.6 Experimental set-up: (a) disk shape and (b) orthogonal cutting test

The disks were divided into three lots and different quenching and tempering treatments were used in order to achieve three levels of initial hardness: 54.0±1 HRC, 56.5±1 HRC and 61.0±1 HRC before beginning the tests.

In Table 3.5 the heat treatments to achieve the three different initial workpiece hardness are reported.

	54.0 ± 1 HRC		56.5 ± 1 HRC		61.0 ± 1 HRC	
Heat Treatments	Temperature	Time	Temperature	Time	Temperature	Time
Heating	850 °C	30 min	850 °C	30 min	850 °C	30 min
Quenching	70 °C/oil	30 min	60 °C/oil	20 min	30 °C/oil	10 min
Tempering	175 °C	80 min	175 °C	60 min	175 °C	30 min

Table 3.5 Heat treatments on AISI 52100 steel

3.4 – EXPERIMENTAL SET-UP FOR HARD MACHINING OPERATION

Dry cutting tests were conducted on a stiff high speed CNC lathe by means of orthogonal operation using cubic boron nitride (CBN) tool inserts mounted on a CTFNR3225P11 tool holder (providing a rake angle of -8°) which was held in a Kistler 9121 three-component piezoelectric dynamometer for measuring forces as illustrated in Figure 3.7.

In order to avoid effects on the produces machined surface related to transient condition (in either feed or speed) due to the orthogonal configuration, the experiments were executed in the following sequence:

1. The disk was mounted in the mandrel held in the chuck of the CNC turning center (Figure 1) and the cutting insert was mounted in the tool holder;

2. The tool was aligned and brought close to the rotating workpiece by single-stepping through the CNC program (i.e., only one block/line of program code is executed with each press of the button by the operator);

3. All the instruments are set to “record” mode and the CNC program is taken out of single-step mode;

4. With the next press of the button the rest of the program is executed uninterrupted – i.e., the tool enters the workpiece and continues cutting at the prescribed feed rate up till the prescribed end-of-cut diameter, and then instantaneously retracts at maximum feed. This insures that the rubbing of the tool against the final machined workpiece surface is minimal (though it may not be zero) and, equally importantly, invariant/constant for all the experimental conditions. Further, since the feed rate employed is in the low range (0.05-0.175 mm/rev) according to the tool makers, and due to the relatively large workpiece diameter (150 mm at start and 80 at the end) the rpms corresponding to the cutting speeds employed are also relatively low (159-743 rpm), it is possible for the CNC machine's hardware to change from radially inward feed to outward extraction almost instantaneously for all practical purposes. Hence, the transient effects were minimal, and this was confirmed from the force signals recorded during the cutting.

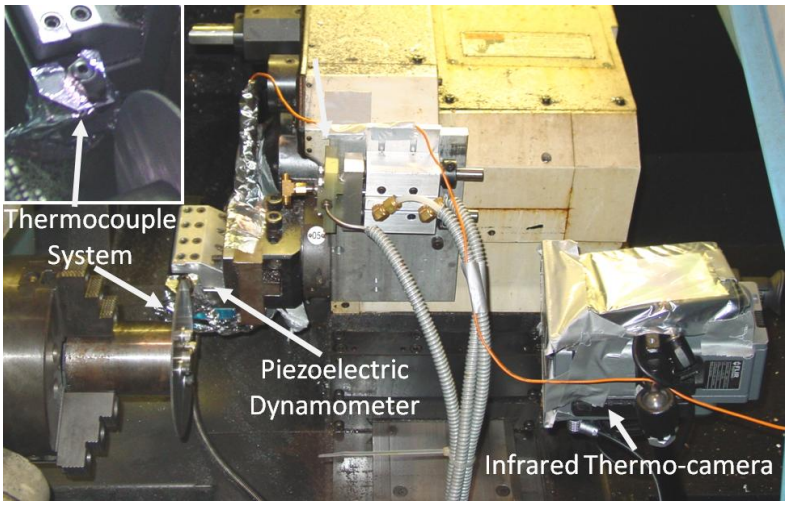

Figure 3.7 Experimental equipments

The disks were machined under dry conditions varying the cutting speed, the feed rate, and the initial workpiece hardness, and using low CBN content cubic boron nitride tools (Seco grade: CBN 100) with two different edge geometries: chamfered (ISO TNGN 110308S with a chamfer of 20°x0.1 mm) and honed (ISO TNGN 110308E with an edge radius of 0.025 mm); the flank angle was -8°. The cutting time of each test was 15-20 sec in order to reach the mechanical and thermal steady state conditions. In such

conditions a flank wear of 0.03 – 0.05 mm was revealed on the utilized CBN tools. Due to this latter evidence, in this research the influence of tool-wear was not investigated. Table 1 shows the details of the experimental plan.

A thermocouple system and an infrared thermo-camera were used during the experiments in order to detect the whole thermal field. The local workpiece emissivity was evaluated to be 0.21 and the transmission due to the external optic screen was estimated to be 0.5.

3.5 – CUTTING CONDITIONS

To study the relationship between the thickness of white and dark layers and cutting parameters, and the influence of the two affected layers on the residual stress profile several cutting parameters were considered during the machining experiments of this study.

The disks were dry machined varying cutting speed, V, initial workpiece hardness, tool shape, and feed rate, f; in particular four levels of cutting speed, three levels of feed rate, three levels of hardness and two types of cutting tool geometry were considered in the experimental design as indicated in Tables 3.6 and 3.7.

Each test was performed 3 times for the repeatability that interests each experimental analysis.

Chamfered Tool									
Test	1/2/3/4	5/6/7	8	9	10/11/12/13	14	15/16/17	18	19
Cutting Speed [m/min]	75/150/250/350	75/150/250	75	250	75/150/250/350	250	75/150/250	75	75
Feed Rate [mm/rev]	0.075	0.125	0.175	0.075	0.125	0.175	0.075	0.1	0.125
Hardness [HRC]	61			56.5			54		

Table 3.6 Experimental plan tests for chamfered tool

Honed Tool								
Test	20	21/22/23	24	25	26/27/28	29/30	31	32
Cutting Speed [m/min]	250	75/150/350	250	250	75/150/250	75/150/250	75	75
Feed Rate [mm/rev]	0.075	0.125	0.175	0.075	0.125	0.075	0.1	0.125
Hardness [HRC]		61			56.5		54	

Table 3.7 Experimental plan tests for honed tool

3.6 – EXPERIMENTAL SET-UP FOR MICROSTRUCTURAL CHANGES ANALYSIS

After machining, samples of 5x5 mm^2 were sectioned by wire-EDM for microstructure analysis and microhardness measurements. Then, the samples were polished and etched for about 5 s using 5% Nital solution to observe white layer using a light optical microscope (1000X) and scanning electron microscope (SEM). Microhardness was measured on the machined surface using a micro-indentation Vickers hardness tester with a certificated diamond indenter. Five measurements were made for each machined surface, with measurement locations well-spaced to avoid interference between indentations. The applied load was 25 g for 10 s. Then the Vickers micro-hardness values were converted in Rockwell macro-hardness C scale (HRC) by technical conversion charts.

An energy-dispersive X-ray spectroscopy (EDS) was also performed (Figure 3.8). Energy dispersive X-ray analysis, also known as EDS, EDX or EDAX, is a technique used to identify the elemental composition of a sample or small area of interest on the sample. It is one of the variants of X-ray fluorescence spectroscopy which relies on the investigation of a sample through interactions between electromagnetic radiation and matter, analyzing X-rays emitted by the matter in response to being hit with charged particles. Its characterization capabilities are due in large part to the fundamental principle that each element has a unique atomic structure allowing X-rays that are characteristic of an element's atomic structure to be identified uniquely from one another.

To stimulate the emission of characteristic X-rays from a specimen, a high-energy beam of charged particles such as electrons or protons, or a beam of X-rays, is focused into the sample being studied. At rest, an atom within the sample contains ground state (or unexcited) electrons in discrete energy levels or electron shells bound to the nucleus. The incident beam may excite an electron in an inner shell, ejecting it from the shell while creating an electron hole where the electron was. An electron from an outer, higher-energy shell then fills the hole, and the difference in energy between the higher-energy shell and the lower energy shell may be released in the form of an X-ray. The number and energy of the X-rays emitted from a specimen can be measured by an energy-dispersive spectrometer. As the energy of the X-rays are characteristic of the difference in energy between the two shells, and of the atomic structure of the element from which they were emitted, this allows the elemental composition of the specimen to be measured.

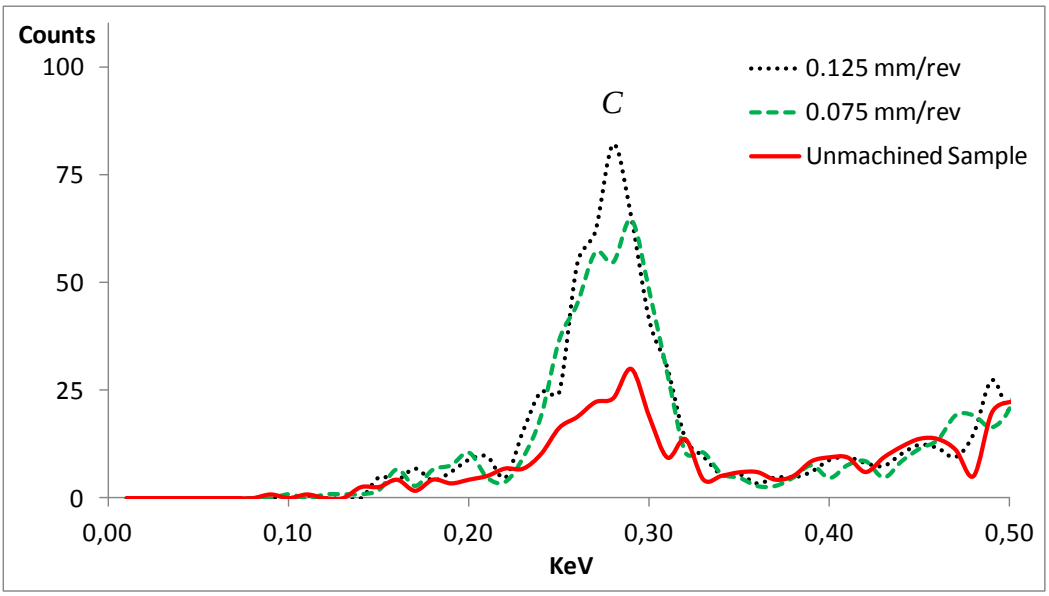

Figure 3.8 Typical EDS spectrum

Several issues can perturb an EDS spectrum, i.e. peak broadening and peak distortion. In addition, several hardware-related problems, such as pulse pileup rejection by the main amplifier, acoustic coupling on the co-axial connector between the detector and the amplifier, and ground loops, can occur.

Peak broadening results from statistical variations in the number of charge carriers and thermal noise in the amplification process. While the natural width of an x-ray peak might be on the order of 0.04% of the peak energy, the statistical and thermal artifacts increase this width to around 0.1% of the peak energy. The only method for reducing this problem is to increase the number of counts in the spectrum.

Peak distortion is caused by non-uniform regions of the detector near the faces and sides. Traps and recombination sites result in recombination of electron-hole pairs, thus distorting the output. In addition, a phenomenon known as the background shelf will increase the background at the energies below a peak. This can be quite noticeable with a strong peak. This is caused by continuum x-ray being inelastically scattered from the detector, which reduces the number of charge carriers collected. This results in even lower energy counts and fewer higher energy counts.

In order to achieve maximum energy resolution, the amplifier must have sufficient time to recover after processing each signal. The use of a long time constant can result in a second pulse arriving at the amplifier before the first pulse is completely processed. This problem results in the need for pulse pileup rejection. When two pulses arrive close together, a peak at double the energy or at a sum of the energies can result. The pulse pileup rejection circuitry cannot eliminate this problem, but it can reduce it substantially.

Acoustic interference can cause an extremely high background count for low energies (from 2 keV down to 0 keV). This is the result of noise coupling into the amplifier from the wire between the detector and the amplifier. Because this length of wire can act as a very sensitive microphone, it must be shielded adequately from mechanical vibrations.

Finally, *ground loops* can cause distorted spectra by introducing 60 Hz noise and other signals into the detection electronics. Because the EDS signals are very low level signals, the metal components of the system must be adequately grounded so that no potential difference can exist. Voltage differences on the order of microvolts can cause problems that introduce noise into the EDS spectra.

Finally, an X-ray diffraction (XRD) test gave the information about microstructural phase composition of the machined material.

In fact X-ray diffraction technique is a non-destructive analytical method which reveals information about the crystallographic structure, chemical composition, and physical properties of materials and thin films. This technique is based on observing the scattered intensity of an X-ray beam hitting a sample as a function of incident and scattered angle, polarization, and wavelength or energy. By this technique it is possible to characterize the crystallographic structure, grain size and preferred orientation in polycrystalline or powdered solid samples. It is commonly used to identify unknown substances, by comparing diffraction data against a database maintained by the International Centre for Diffraction Data. It may also be used to characterize heterogeneous solid mixtures to determine relative abundance of crystalline compounds and, when coupled with lattice refinement techniques can provide structural information on unknown materials. Finally it is also a common method for determining strains in crystalline materials: an effect of the finite crystallite sizes is seen as a broadening of the peaks in an X-ray diffraction, from the broadening it will be possible to calculate the residual strain and then the corresponding residual stress.

In the present work the X-ray diffraction tests for phase composition analysis was conducted by using a X-ray equipment Bruker AXS D8 Discover with a quarter Ellurian cradle sample holder. The X-ray diffraction patterns were measured using CuK_α radiation (λ=1.54184Å, $K_{\alpha1}/K_{\alpha2}$=0.5) from a source operated at 40 kV, and 40 mA. Samples were accordingly positioned at the center of plate into the X-ray goniometer in order to ensure a correct beam irradiation. The 2θ scans were carried out between 40 and 92 deg 2θ. The scan increment was 0.02 degree; the corresponding acquisition time was varied.

Finally, estimation of the volume fractions of the retained austenite was carried out according to the ASTM E975 method [136, 137].

3.7 – EXPERIMENTAL PROCEDURE AND SET-UP FOR RESIDUAL STRESS ANALYSIS: X-RAY DIFFRACTION TECHNIQUE

In X-ray diffraction residual stress measurement, the strain in the crystal lattice is measured, and the residual stress producing the strain is calculated, assuming a linear elastic distortion of the crystal lattice. Although the term stress measurement has come into common usage, stress is an extrinsic property that is not directly measurable. All methods of stress determination require measurement of some intrinsic property, such as strain or force and area, and the calculation of the associated stress. Mechanical methods (dissection techniques) and nonlinear elastic methods (ultrasonic and magnetic techniques) are limited in their applicability to residual stress determination. Mechanical methods are limited by assumptions concerning the nature of the residual stress field and sample geometry. Mechanical methods, being necessarily destructive, cannot be directly checked by repeat measurement. Spatial and depth resolution are orders of magnitude less than those of X-ray diffraction. All non linear elastic methods are subject to major error from preferred orientation, cold work, temperature, and grain size. All require stress-free reference samples, which are otherwise identical to the sample under investigation. Nonlinear elastic methods are generally not suitable for routine residual stress determination at their current state of development. In addition, their spatial and depth resolutions are orders of magnitude less than those of X-ray diffraction. To determine the stress, the strain in the crystal lattice must be measured for at least two precisely known orientations relative to the sample surface. Therefore, X-ray diffraction residual stress measurement is applicable to materials that are crystalline, relatively fine grained, and produce diffraction for any orientation of the sample surface. Samples may be metallic or ceramic, provided a diffraction peak of suitable intensity and free of interference from neighboring peaks can be produced in the high back-reflection region with the radiations available. X-ray diffraction residual stress measurement is unique in that macroscopic and microscopic residual stresses can be determined nondestructively.

Macroscopic stresses, or macrostresses, which extend over distances that are large relative to the grain size of the material, are of general interest in design and failure

analysis. Macrostresses are tensor quantities, with magnitudes varying with direction at a single point in a body. The macrostress for a given location and direction is determined by measuring the strain in that direction at a single point. When macrostresses are determined in at least three known directions, and a condition of plane stress is assumed, the three stresses can be combined using Mohr's circle for stress to determine the maximum and minimum residual stresses, the maximum shear stress, and their orientation relative to a reference direction. Macrostresses strain many crystals uniformly in the surface. This uniform distortion of the crystal lattice shifts the angular position of the diffraction peak selected for residual stress measurement.

Microscopic stresses, or microstresses, are scalar properties of the sample, such as percent of cold work or hardness, that are without direction and result from imperfections in the crystal lattice. Microstresses are associated with strains within the crystal lattice that traverse distances on the order of or less than the dimensions of the crystals. Microstresses vary from point to point within the crystal lattice, altering the lattice spacing and broadening the diffraction peak. Macrostresses and microstresses can be determined separately from the diffraction peak position and breadth.

In order to better understand the fundamental principles of X-ray diffraction instruments, it is important to be aware of the theory behind these systems.

About 95% of all solids can be described as crystalline (the atoms are arranged in a regular pattern) and the orientation and interplanar spacings of the planes are defined by the three integers h, k, l called *Miller's indices* that become the order of diffraction along the unit cell axes. X-ray analysis can be done only on these types of materials.

The basic principle of X-ray diffraction is based on *Bragg's law*, which states that when a monochromatic x-ray beam with wavelength λ is projected onto a crystalline material at an angle θ, diffraction occurs only when the distance traveled by the rays reflected from successive planes differs by an integral number n of wavelengths. This is schematically illustrated in Figure 3.9.

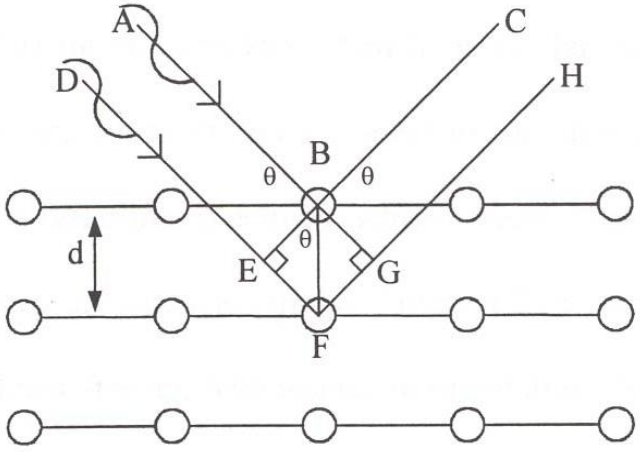

Figure 3.9 Diffraction of X-rays by a crystalline material

X-ray lines ABC and DEFGH have a wavelength representative of x-ray radiation. Initially, lines AB and DE have the same wavelength. These lines will remain in phase if EFG is an integral multiple of this wavelength. This causes reinforcement of the incident x-ray beam, which is known as constructive interference or diffraction. If EFG is not an integral multiple of the incident beam wavelength, then the lines will be out of phase resulting in destructive interference and diffraction will not occur. This can be expressed using $n\lambda = 2dsin\theta$, where n is an integer, λ is the wavelength of a beam of x-rays incident on a crystal with lattice planes separated by distance d, and θ is the Bragg angle.

X-ray diffraction relies on the elastic deformation of a material to measure internal stresses in a material. The deformation cause changes in the spacing of the lattice planes from their stress-free value to a new value that corresponds to the magnitude of the applied stress. Because the wavelength is constant, the unknown parameters in Bragg's equation are the interplanar spacing d and Bragg angle θ. Thus, if θ becomes known, the d value can be obtained using Bragg's law.

As a result, X-ray method measures strains by measuring the interplanar spacing in different directions, then the measured strains are converted into stresses using linear elasticity theory

This process can be explained by considering a polycrystalline specimen subjected to an unknown residual stress. The angles φ and ψ are interpreted as specimen rotation

and specimen tilt, respectively. The interplanar spacing at a particular combination of ϕ and ψ can be obtained using Bragg's law, as described previously.

If $d_{\varphi\psi}$ is the spacing between the lattice planes measured in the direction defined by the two angles φ and ψ, the strain can be expressed in terms of changes in the linear dimensions of the crystal lattice [138]:

$$\varepsilon_{\phi\psi} = \frac{\Delta d}{d_0} = \frac{d_{\phi\psi} - d_0}{d_0} = \frac{\sin\theta_0}{\sin\theta} - 1$$

Or by derivation from Bragg's law

$$\varepsilon = -\cot g\,\theta_0 \cdot \Delta\theta$$

For this expression notice that the precision of result is not proportional to $cotg\theta$, this can be done with a diffraction angle over 140°.

After calculating strain, stress can be obtained with mechanical law, but some hypothesis must be done:

- Elastic linear domain;
- The material can be considered isotropic;
- Stress and strain must be constant on the considered volume.

For a stress-free material, the interplanar distance corresponding to the selected diffraction peak is relatively independent of the orientation of the planes to the surface of the sample. This orientation is defined through the angle ψ that the normal to the plans considered form with the normal to the surface of the piece. When the material is subjected to a stress, the interplanar distance and, consequently, the deformation become functions of the angle ψ (Figure 3.10 for uniaxial tension).

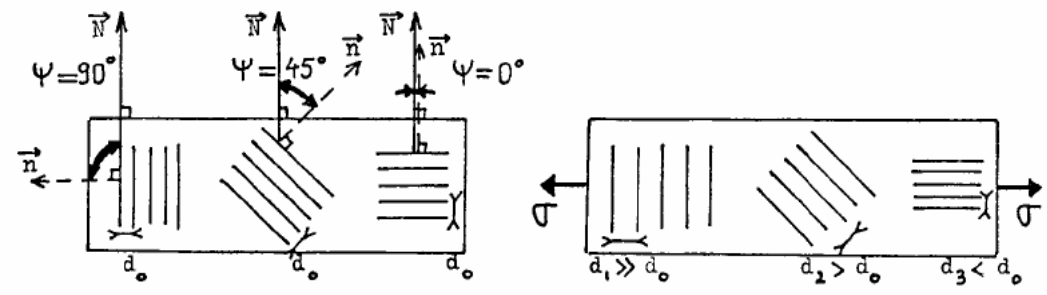

Figure 3.10 Physical interpretation of stress in a polycrystalline specimen [138]

Depending on these considerations and by applying the laws of the mechanics continuous media it is possible to write the following relation called the $\sin^2\psi$ method:

$$2\theta_{\phi\psi} = 2\theta_0 + \left(\frac{1}{K_1}\right)_{hkl}\left[\left\langle\sigma_{11}^{\phi}\right\rangle\sin^2\psi + \left\langle\sigma_{13}^{\phi}\right\rangle\sin 2\psi\right] + \left(\frac{1}{K_2}\right)_{hkl}\left[\left\langle\sigma_{11}^{\phi}\right\rangle + \left\langle\sigma_{22}^{\phi}\right\rangle\right]$$

Were K_1 and K_2 are the X-ray elasticity parameters.

By plotting the $2\theta_{\phi\psi}$ values versus $\sin^2\psi$ a straight line is obtained in the case of a biaxial stress state Figure 3.11: the stress is then calculated from the slope of the best fit line.

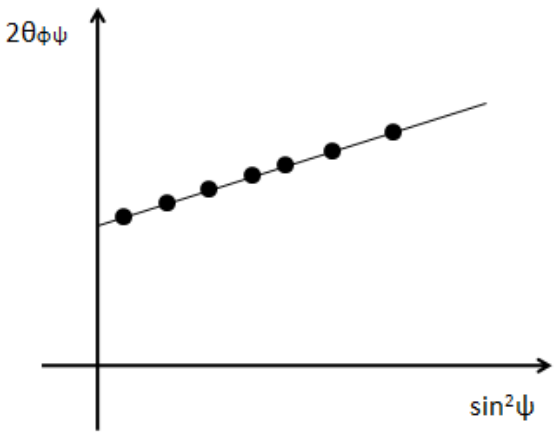

Figure 3.11 Plot of crystallographic strain vs. $\sin^2\psi$

By measuring the $2\theta_{\phi\psi}$ in at least three ϕ directions it is possible to obtain the compete stress tensor.

The residual stress determined by using X-ray diffraction is the arithmetic average stress in a volume of material defined by the irradiated area, which may vary from square centimeters to square millimeters, and the depth of penetration of the x-ray beam. The linear absorption coefficient of the material for the radiation used governs the depth of penetration, which can vary considerably. Furthermore the X-ray diffraction stress measurement is confined to the surface of the sample. Electropolishing is used to expose new surfaces for subsurface measurement. In the exposed surface layer, a condition of plane stress is assumed to exist: a stress distribution described by principal stresses σ_1 and σ_2 existing in the plane of the surface, and no perpendicular stress to the surface, $\sigma_3 = 0$. However, a strain component perpendicular to the surface ε_3 exists as a result of the Poisson's ratio contractions caused by the two principal stresses.

After the above description on the fundamentals of X-Ray diffraction method on residual stress evaluation, it is necessary to take into account also the errors and the limitations related to this procedure [138]:

Instrumental and Positioning Errors. The principal sources of error in X-Ray diffraction residual stress measurement are related to the high precision with which the diffraction-peak position must be located. Errors of approximately 0.025 mm in alignment of the diffraction apparatus or positioning of the sample result in errors in stress measurement of approximately 14 MPa for high diffraction angle techniques and increase rapidly as the diffraction angle is reduced. Instrument alignment requires coincidence of the θ and ψ axes of rotation and positioning of the sample such that the diffracting volume is centred on these coincident axes. So, the fundamental problem can be summarized as finding small changes in interplanar distances and then subtracting to get strain.

Effect of Sample Geometry. Excessive sample surface roughness, curvature of the surface within the irradiated area, or interference of the sample geometry with the diffracted x-ray beam can result in systematic error similar to sample displacement.

X-ray Elastic Constants. A major source of potential systematic proportional error arises in the determination of the X-ray elastic constants. The residual stress measured is proportional to the value of the X-ray elastic constants, which may differ by more than 40% from the bulk value due to elastic anisotropy. The X-ray elastic constant must be determined empirically by loading a sample of the material to known stress levels and measuring the change in the lattice spacing as a function of applied stress, by which the X-ray elastic constant can be calculated.

Finally general aspects on the X-ray diffraction method related to this work are:

- General Applications:
  - Nondestructive surface residual stress measurement;
  - Determination of subsurface residual stress distributions combined with material removing technique as electropoloshing;
  - Measurement of residual stresses associated with failures caused by fatigue or stress corrosion.

- Cases of Applications:
  - Measurement of surface and subsurface residual stresses;
  - Determination of the depth and magnitude of the maximum compressive residual stress.

- Estimated Analysis Time
  - 1 min to 1 h per measurement, depending on the diffracted X-ray intensity and technique used. Typically, 1 hr. per measurement for subsurface work, including electropolishing material removal and sample repositioning.

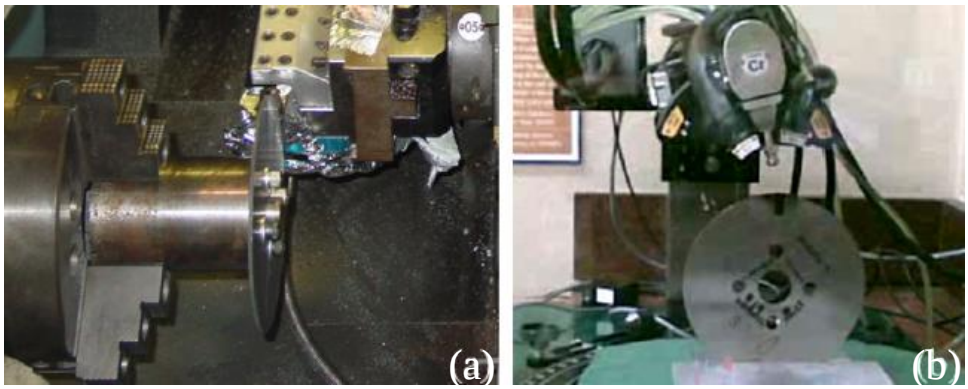

Figure 3.12 Experimental set-up: (a) orthogonal cutting test, (b) residual stresses measurement by X-ray diffraction technique

Depending on the above description the residual stress state in machined disk surfaces of the present thesis was analyzed by X-ray diffraction technique Figure 3.12 using the $\sin^2\psi$ method. The parameters used in the X-ray analysis are shown in Table 3.8.

X-ray radiation	Young's modulus	Poisson ratio	Bragg angle 2θ	Lattice plane	Number of ψ angles ($\pm 40^\circ$)
Cr-Kα	210 GPa	0.3	156.3°	{211}	15

Table 3.8 X-ray diffraction parameters for residual stress measurement

To determine the in-depth residual stress profile, successive layers of material were removed by electropolishing to avoid the modification of machining-induced residual stress. Further corrections to the residual stress data were made due to the volume of material removed. Due to the specific shape of the workpiece a rectangular mask was applied on the surface to limit the region of the X-ray analysis. Both axial and circumferential (hoop) residual stresses were measured.

3.8 – EXPERIMENTAL PROCEDURE AND SET-UP FOR THERMAL ANALYSIS

Since the main requirement of any hard machining operation is to realize component taking into account its good performance in service, the importance of monitoring temperatures during these operations and assessing their effects on both the workpiece and the cutting edge of the tool becomes of main interest [139-141]. The importance of the several works present in the literature on the temperature measurements is strictly related to three main objectives: to improve the quality of the finished workpiece, especially when surface integrity is considered, to predict tool wear and to have the availability of experimental thermal data for improving of predictive software modeling. Furthermore it was widely showed in the previous paragraphs that the temperature history is directly related to part quality, resulting in surface and sub-surface phase transformation (white and dark layers formation) and introducing residual stresses.

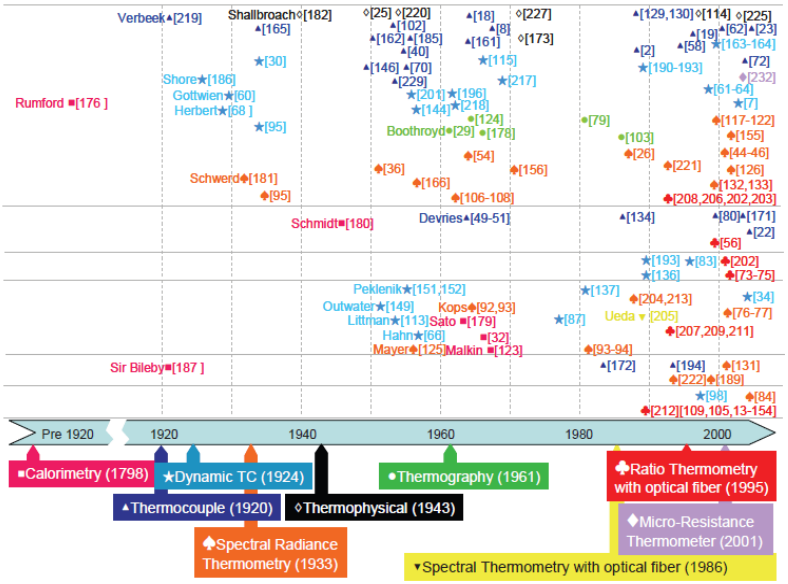

Figure 3.13 Historical outline of thermal measurements in material removal processes Reference [142]

However, in current manufacturing processes temperature is still not easily measured or controlled, in fact when coolants are used especially during cryogenic analysis, many current measurement methods do not apply. Since diffusion, chemical

reactions and thermal softening depend exponentially on temperature, the productivity and efficiency of material removal operations is adversely affected by increased temperature; furthermore the high temperatures at the tool-workpiece interface deeply affect the tool geometry resulting in an exponentially mechanism of the tool wear, that leads to have, for example, the presence of the brittle white layer on the machined surface [105].

The primary difficulty in understanding the thermal behavior in material removal is the inability to measure temperatures accurately and with high resolution. While technology has improved, the list of phenomena exploited to measure temperature has changed little. Even so, agreement between different methods is difficult to assess.

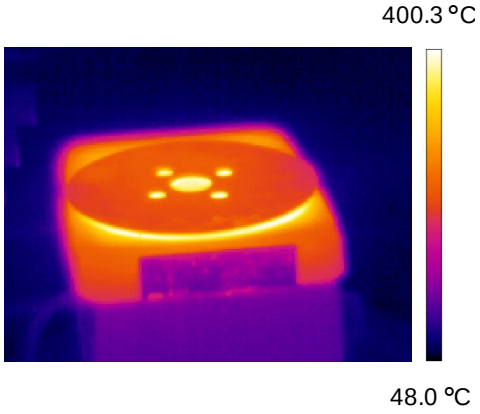

Figure 3.14 Experimental procedure for thermo-camera calibration

How it is well reported in Figure 3.13 starting from the use of calorimeter and thermocouples, today the use of the thermo camera has replaced any method providing fast and extensive temperature analysis including: isotherms, spot measurements, line and area measurements, histogram charts for more in-depth analysis of area and line tools; furthermore the thermo camera gives the possibility to have the time vs. temperature trend in real time or with recorded images and sequences and the plot files can be saved and imported into Excel for more detailed analysis.

Before to start with the thermal analysis a specific thermal calibration, for our specific thermo-camera, was conducted to find the right thermal emissivity and transmission related to our workpiece material in order to improve the accuracy and the quality of the results (Figure 3.14).

A value of 0.21 and 0.5 was respectively found for the thermal emissivity and transmission.

3.9 – SUMMARY

In this Chapter the tool and workpiece material properties, from mechanical and thermal point of view, was reported; a wide experimental plan was made in order to have a deep and clear knowledge about the several aspects related to this analysis. Furthermore all the several experimental techniques and methods used for measuring the various surface integrity parameters were presented, well showing the capabilities of all the machines utilized for this research.

CHAPTER IV

EXPERIMENTAL RESULTS AND ANALYSIS

In this chapter the experimental procedure, the used equipments and the experimental results (i.e., cutting forces, surface and subsurface microhardness and microstructural alterations, phase transformations, residual stresses, etc.) will be reported and discussed, with the aim to establish the effects of the cutting process parameters on the investigated outputs. Table 4.1 reports all the experimental analysis performed for each conducted test, highlighting the wide range of machining conditions carried out in order to pursue a deep knowledge of the studied phenomena. Also, the choice of a large range of cutting process parameters allow to have enough data for an accurate development of the advanced numerical cutting model, which will be discussed in the follow Chapter V.

Input Parameters				Output data							
Tool	*Initial Workpiece Hardness (HRC)*	*V (m/min)*	*f (mm/rev)*	*Hardness Profile (HRC)*	*Optical Microscopy*	*SEM*	*EDS*	*XRD PHASE*	*XRD RS*	*T (°C)*	*F (N)*
CHAMFER	56.5	75	0,125	x	x	x		x	x		x
		150	0,125	x	x			x	x		x
		250	0,075	x	x				x		x
		250	0,125	x	x				x		x
		250	0,175	x	x						x
		350	0,125	x	x				x		x
	61	75	0,075	x	x			x	x	x	x
		75	0,125	x	x				x	x	x
		75	0,175	x	x						
		150	0,075	x	x			x	x	x	x
		150	0,125	x	x				x	x	x
		250	0,075	x	x	x	x	x	x	x	x
		250	0,125	x	x	x			x	x	x
		350	0,075	x	x				x	x	x
	54	75	0,075	x	x	x	x			x	x
		75	0,1	x	x	x	x			x	x
		75	0,125	x	x	x	x	x	x	x	x
		150	0,075	x	x	x	x			x	x
		250	0,075	x	x	x	x	x	x	x	x
HONE	56.5	75	0,125	x	x			x		x	x
		150	0,125	x	x			x	x		
		250	0,075	x	x				x	x	x
		250	0,125	x	x				x	x	x
	61	75	0,125	x	x	x	x	x		x	x
		150	0,125	x	x	x	x		x	x	x
		250	0,075	x	x	x	x		x	x	x
		250	0,175	x					x	x	x
		350	0,125	x	x	x	x		x	x	x
	54	75	0,075	x	x	x	x			x	x
		75	0,1	x	x	x	x			x	x
		75	0,125	x	x		x	x		x	x
		150	0,075	x	x	x	x			x	x
		250	0,075	x	x		x		x	x	x

Table 4.1 Experimental cutting conditions and analyzed results

4.1 – CUTTING FORCES

Figures 4.1, 4.2, 4.3, 4.4, 4.5, 4.6 show the trend of the average cutting forces when mechanical and thermal steady-state conditions were reached, while the error bars represents the standard deviations of the signal.

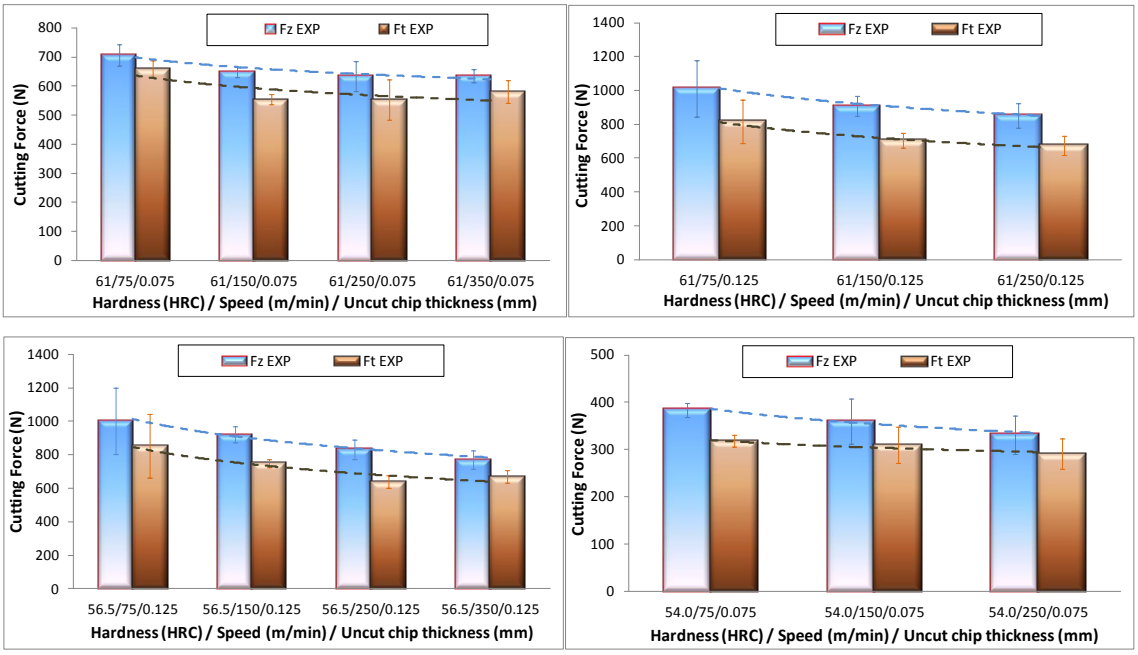

Figure 4.1 Variation of cutting (Fz) and thrust (Ft) forces during dry hard turning by chamfered tool varying the cutting speeds

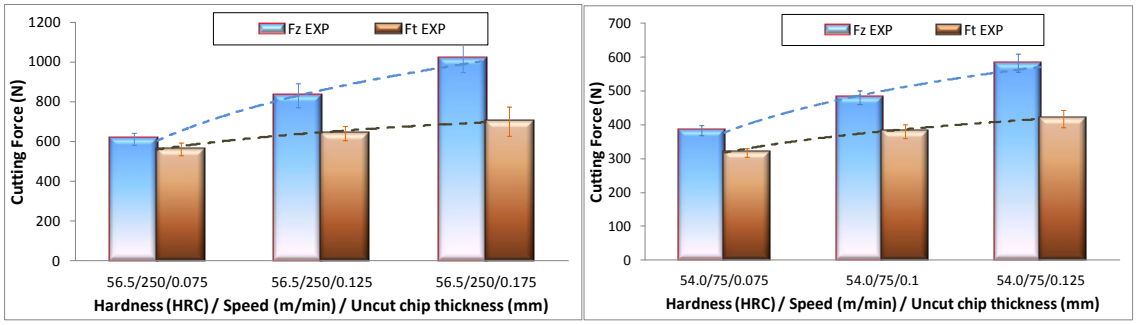

Figure 4.2 Variation of cutting (Fz) and thrust (Ft) forces during dry hard turning by chamfered tool varying the feed rates

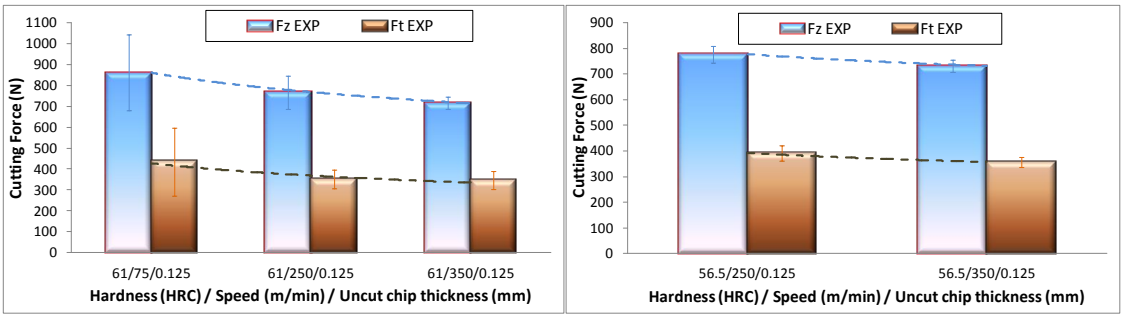

Figure 4.3 Variation of cutting (Fz) and thrust (Ft) forces during dry hard turning by honed tool varying the cutting speeds

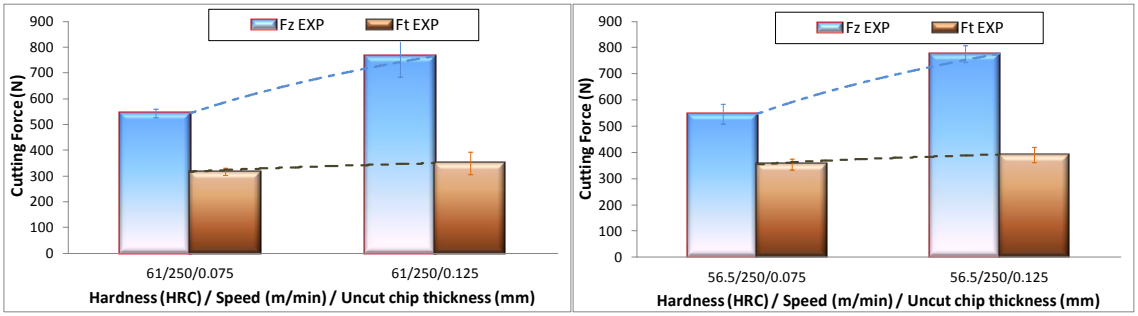

Figure 4.4 Variation of cutting (Fz) and thrust (Ft) forces during dry hard turning by honed tool varying the feed rates

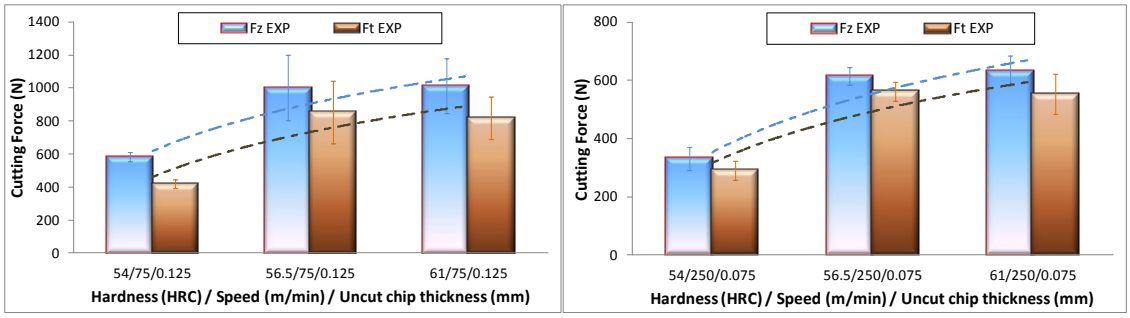

Figure 4.5 Variation of cutting (Fz) and thrust (Ft) forces during dry hard turning by chamfered tool varying the initial workpiece hardness

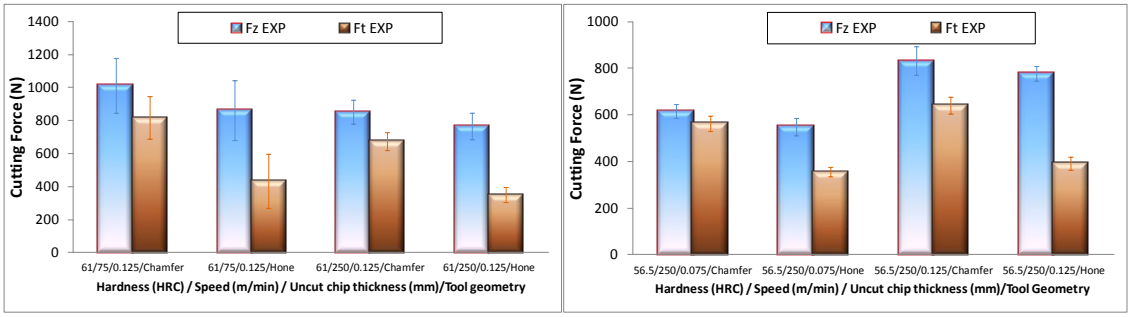

Figure 4.6 Variation of cutting (Fz) and thrust (Ft) forces during dry hard turning varying the tool geometries

Depending on which cutting parameter is considered (Table 4.1) several discussions can be done on the reported results. By analyzing the influence of the cutting speed on both cutting (F_z) and thrust (F_t) forces it is reported that the increase of cutting speed shows an evident decrease in both the cutting forces; this is due to the increased thermal softening at the higher temperatures reached when cutting speed rises. Such evidence is not influenced by the tool shape (chamfer or hone) as illustrated in Figures 4.1-4.3. On the contrary, the increase of uncut chip thickness shows a considerable increase in cutting forces due to the increase in contact area between the workpiece and cutting tool (Figures 4.2-4.4). Considering the influence of the initial workpiece hardness (Figure 4.5) its increase results in an increase of the cutting forces due to the evolution of the machined material resistance. Finally, by comparing the two tool geometries considered in the present study (Figure 4.6) a slight increase of the cutting forces is reported when cahmfered tool is used, due to higher effective rake angle.

4.2 – CUTTING TEMPERATURES

Also in this case, for a detailed analysis, the influence of the several cutting parameters is considered as reported in Table 4.1.

Usually, comparison of the temperatures is often based upon the maximum temperatures measured on the tool rake face.

In contrast, in this study, in order to have a more complete map of thermal profiles, different measurements were taken within the three main zones involved in machining as shown in Figures 4.7-4.8.

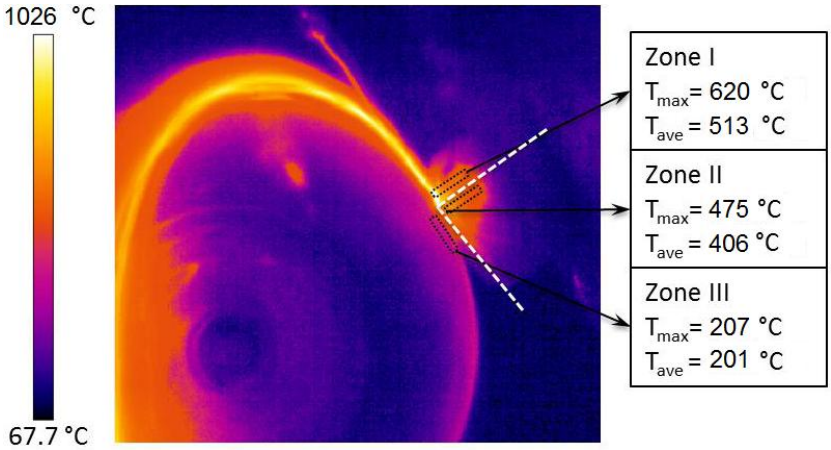

Figure 4.7 Temperature fields in the three analyzed zones for Test at V= 75 m/min, f=0.075, 54 HRC, chamfered tool

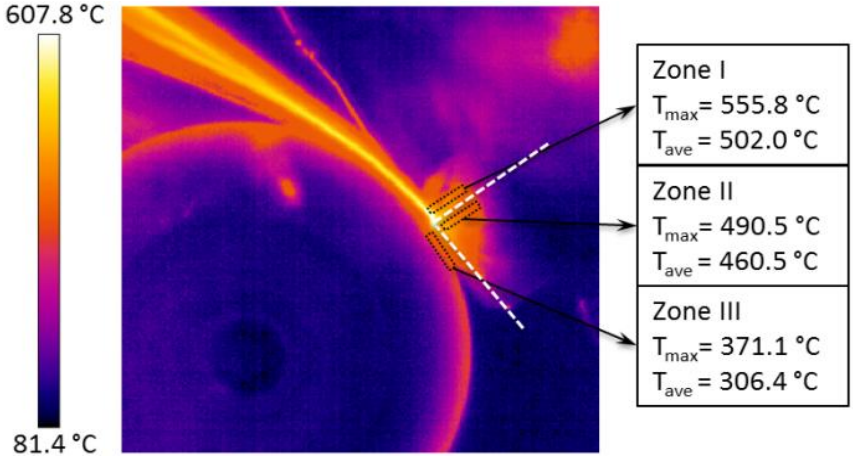

Figure 4.8 Temperature fields in the three analyzed zones for Test at V= 75 m/min, f=0.125, 61 HRC, honed tool

More precisely, zone 1 is located on the tool-chip interface, zone 2 is localized below the tool rake in correspondence of the primary shear plane (effect on the tool) while zone 3 is located on the machined surface downstream of the tool contact.

Also to study the influence of each cutting parameters on the temperatures some of the collected data are plotted in Figures 4.9, 4.10, 4.11 and 4.12.

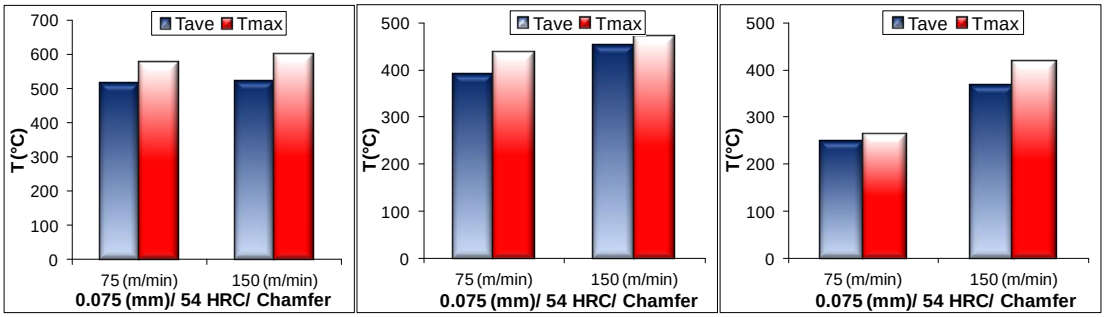

(a) (b) (c)

Figure 4.9 Variation of the cutting temperatures varying cutting speed:
(a) zone 1, (b) zone 2 and (c) zone 3

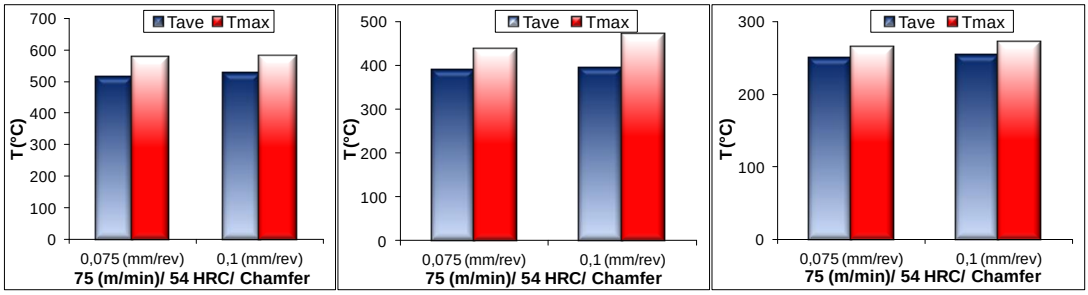

(a) (b) (c)

Figure 4.10 Variation of the cutting temperatures varying feed rate:
(a) zone 1, (b) zone 2 and (c) zone 3

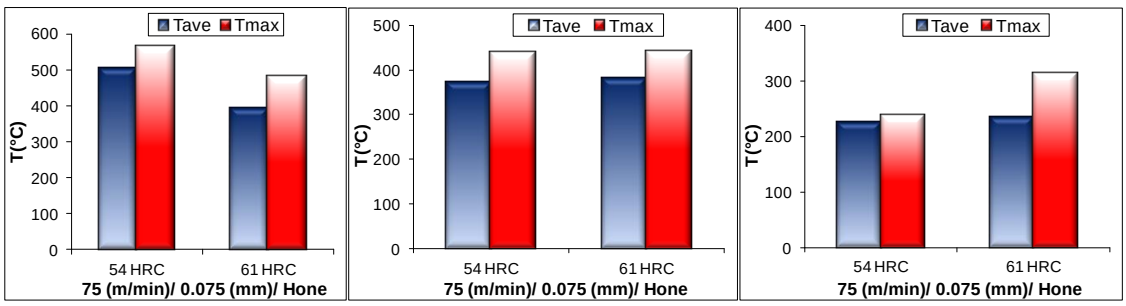

(a) (b) (c)

Figure 4.11 Variation of the cutting temperatures varying initial workpiece hardness:
(a) zone 1, (b) zone 2 and (c) zone 3

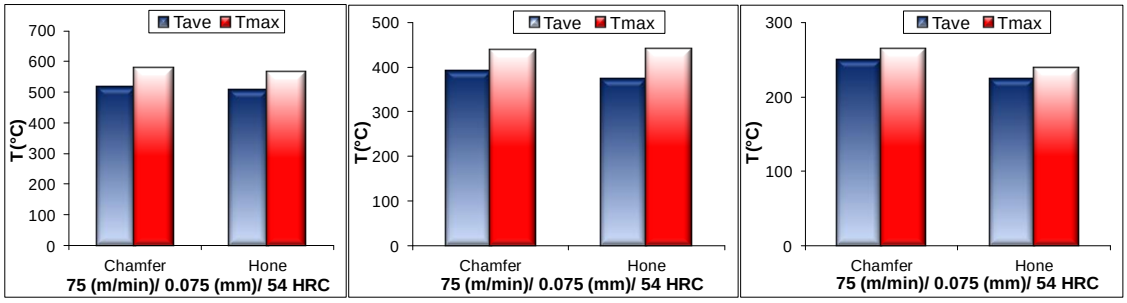

Figure 4.12 Variation of the cutting temperatures varying tool geometry:
(a) zone 1, (b) zone 2 and (c) zone 3

The results show as generally temperature increases with all the considered parameters; in particular higher cutting speed, feed rate and initial workpiece hardness lead to an increase of the temperatures in the three analyzed zones.

Furthermore, also the use of chamfered tool shape leads to an increase of both maximum and average temperatures in the three zones. The reason is due to the higher rake angle near the primary and secondary shear zones (-28° instead of only -8° in the case of honed tool) which produces higher chip curvature, localized severe plastic deformation and, consequently, more mechanical work. In table 4.2 are reported the complete data collection, for tests at 54 HRC machined by chamfered tool, as far as the temperature is regarded.

54 HRC		Zone I	Zone II	Zone III
75 m/min - 0.075 mm	T_{ave}	515	389	249
	T_{max}	575	437	264
75 m/min - 0.1 mm	T_{ave}	524	392	253
	T_{max}	582	470	272
75 m/min - 0.125 mm	T_{ave}	553	487	304
	T_{max}	597	501	287
150 m/min - 0.075 mm	T_{ave}	521	451	368
	T_{max}	599	472	418
250 m/min - 0.075 mm	T_{ave}	532	589	455
	T_{max}	632	531	543

Table 4.2 Cutting temperatures results with chamfered geometry

Furthermore it is possible to highlight an important aspect from the above reported thermal analysis: the maximum reached temperatures on the machined surface are very lower than theoretical value of the austenite start temperature for steels. This aspect will be helpful, with the other experimental results obtained by EDS and XRD phase analysis, in order to investigate what is the main dominant aspect for microstructural changes during machining of hardened steels.

4.3 – WHITE AND DARK LAYERS THICKNESS

Figure 4.13 shows typical micrographies of the machined workpiece surfaces where are evident the presence of both white and dark layers, while Figure 4.14 shows some of the scanning electron microscopy (SEM) images with evidence of a featureless structure since white layer is etch resistant.

The observations obtained by optical microscope show that, under varying process conditions, there is white layers formation with thicknesses between 3 and 15 microns. Once more, it is feasible to see that the thickness of white layer was larger in the case of higher cutting speed, higher initial workpiece hardness and when chamfered tool is used (Figure 4.13).

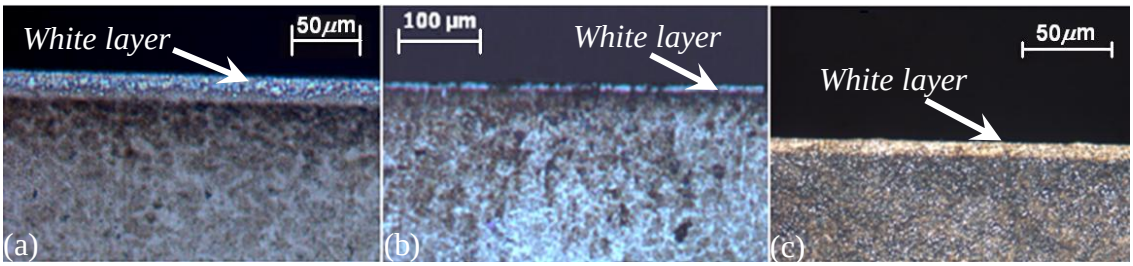

Figure 4.13 Optical microscope observations: (a) 250 m/min, 0.125 mm/rev, 61 HRC, Chamfered tool, (b) 75 m/min, 0.125 mm/rev, 56.5 HRC, Chamfered tool (c) 250 m/min, 0.125 mm/rev, 61 HRC, Honed tool

SEM micrographs, for the same cases reported in Figures 4.13, also show the effects due to machining, in particular, the variation on the surface layer caused by the

microstructure changes of steel (Figure 4.14). These transformations, determined either by the temperature change and/or the plastic deformation of the sample during processing, result in a refinement of the grains, creating a very compact and homogeneous microstructure corresponding to the white layer (*featureless* structure).

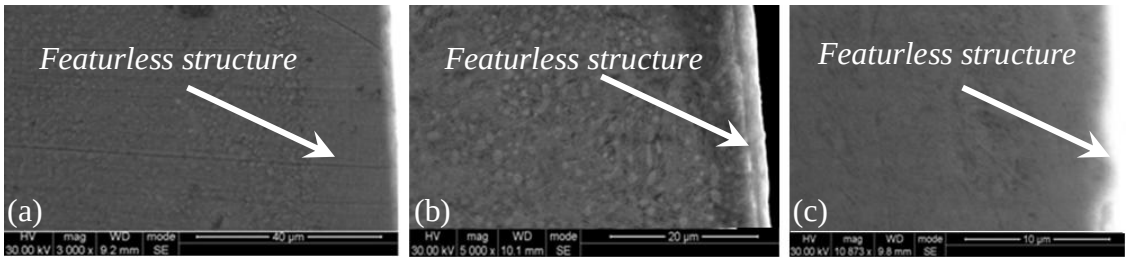

Figure 4.13 SEM micrographs: (a) 250 m/min, 0.125 mm/rev, 61 HRC, Chamfered tool, (b) 75 m/min, 0.125 mm/rev, 56.5 HRC, Chamfered tool (c) 250 m/min, 0.125 mm/rev, 61 HRC, Honed tool

In Figures 4.14, 4.15, 4.16, 4.17 the results obtained by optical and SEM analysis, on the white and layers thickness, are reported varying the studied cutting parameters.

In Figure 4.14 the influence of the cutting speed on the white and dark layers formation is shown.

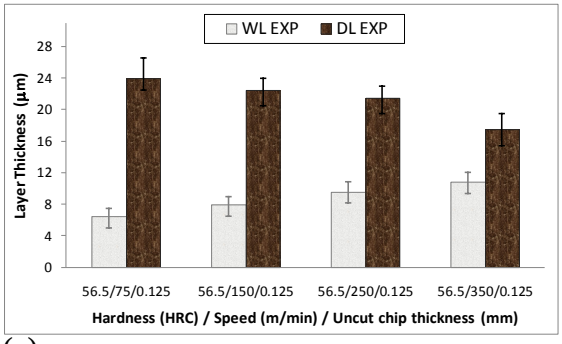

(a)

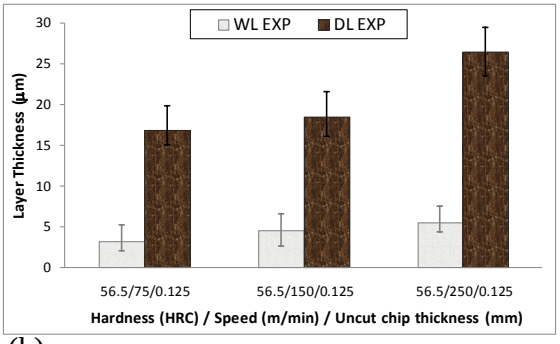

(b)

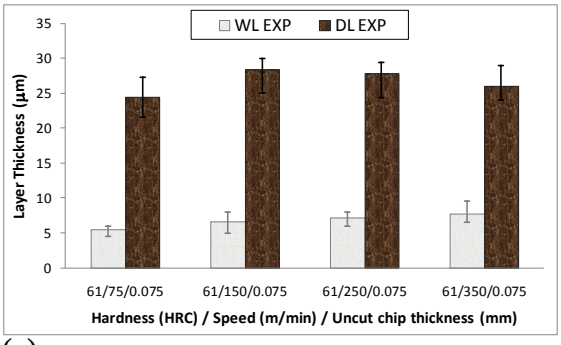

(c)

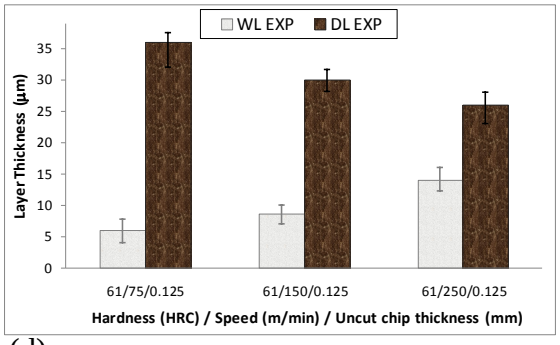

(d)

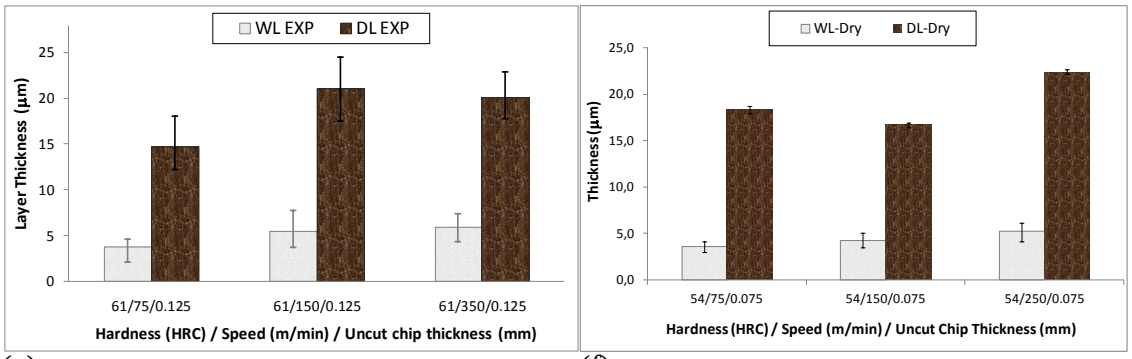

(e) (f)

Fig. 4.14 Experimental microstructural changes varying cutting speed:
with chamfered tool (a), (c), (d), (f) and honed tool (b), (e)

It is evident that with the increase of the cutting speed white layer thickness increases too (until to reach a steady value that is not overcome for increasing value of the cutting speed), in contrast dark layer thickness decreases. These results are in agreement with those present in the literature [101, 102, 103-106, 108].

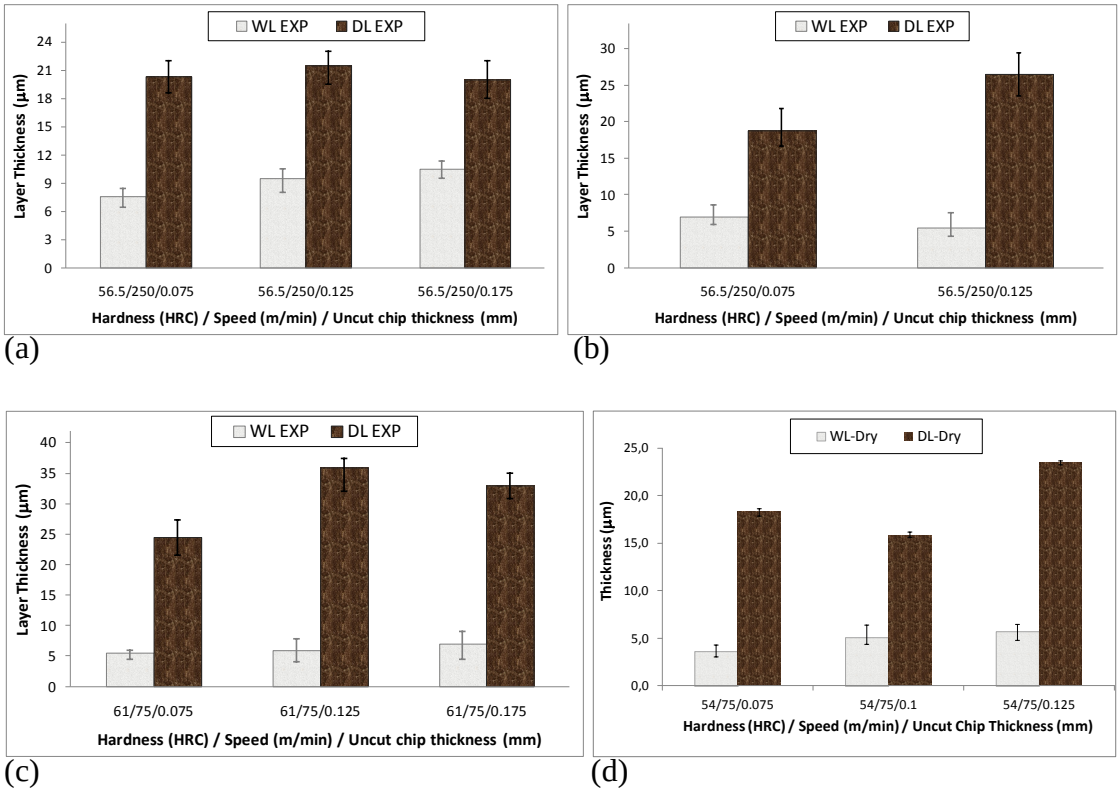

(a) (b)

(c) (d)

Fig. 4.15 Experimental microstructural changes varying feed rate:
with chamfered tool (a), (c), (d) and honed tool (b)

The influence of the feed rate on white and dark layers formation is reported in Figure 4.15.

White layer registers an evident increase with the feed rate increasing; in contrast, a slightly decrease trend is registered for the dark layer thickness, in accordance with the literature [101, 102, 103-106, 108]. The increase in white layer thickness, with increasing cutting speed and feed was expected since the higher temperatures generated in the machining zone should lead to localized thermal softening of the workpiece material, as well as a greater depth below the machined surface where the temperature exceeds the austenitizing temperature for subsequent quenching through self-cooling, and consequent martensitic transformation. However, it was interesting to note that this trend did not apply to the dark layer thickness. This is probably due to the lowering of austenitizing temperature at high stress, as the machining conditions are made more aggressive, a greater fraction of the subsurface is sufficiently above the local austenitizing temperature would seem to undergo quenching, with the bulk material acting as a heat sink, rather than tempering (i.e., a greater fraction of the subsurface will transform into untempered martensite (white layer) instead of overtempered martensite (dark layer)).

The influence of the initial workpiece hardness on white and dark layers formation is analyzed in Figure 4.16.

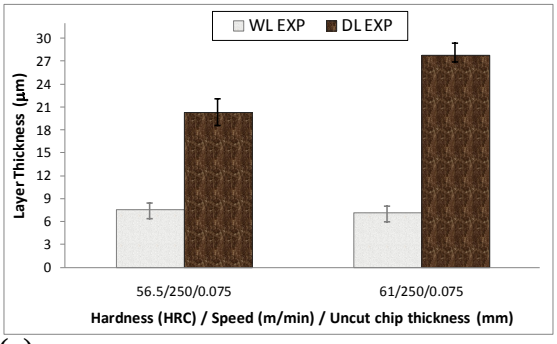

(a)

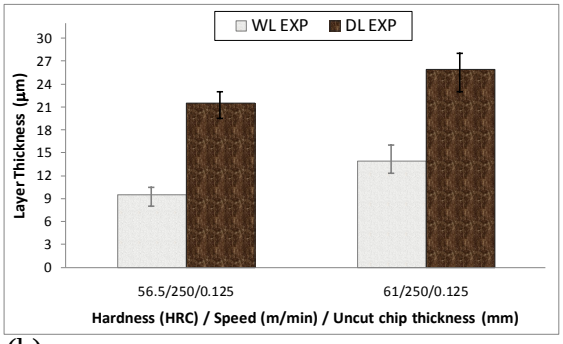

(b)

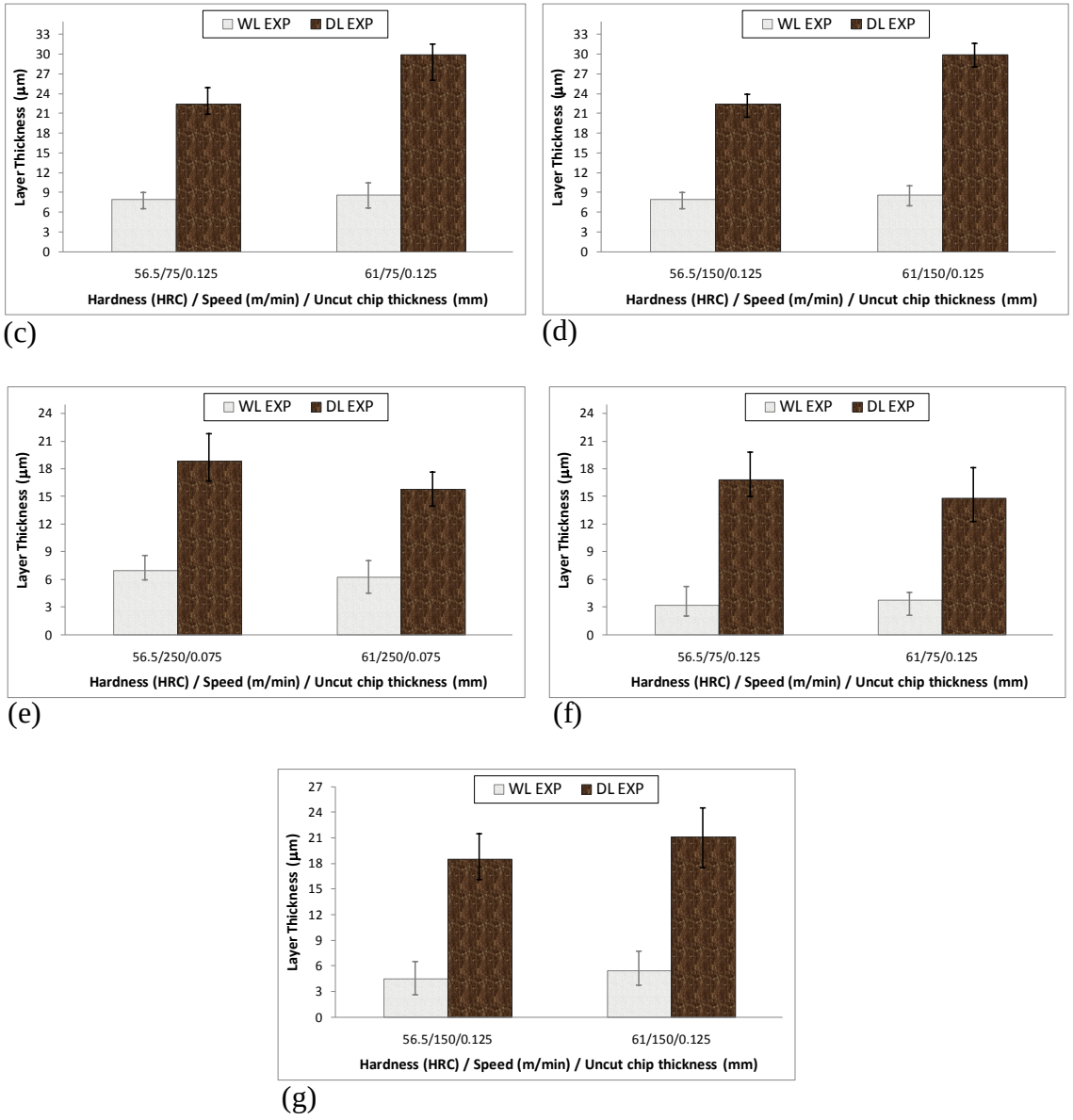

Fig. 4.16 Experimental microstructural changes varying initial workpiece hardness: with chamfered tool (a), (b), (c), (d) and honed tool (e), (f), (g)

In this case both white and dark layers thickness increase is registered when the initial workpiece hardness increases. This is mainly because the higher material hardness leads to higher stresses and temperatures during the severe plastic deformation, causing a greater region of the subsurface to undergo martensitic transformation and/or tempering.

Finally the effect of the tool geometry on white and dark layers thickness reported in Figure 4.17.

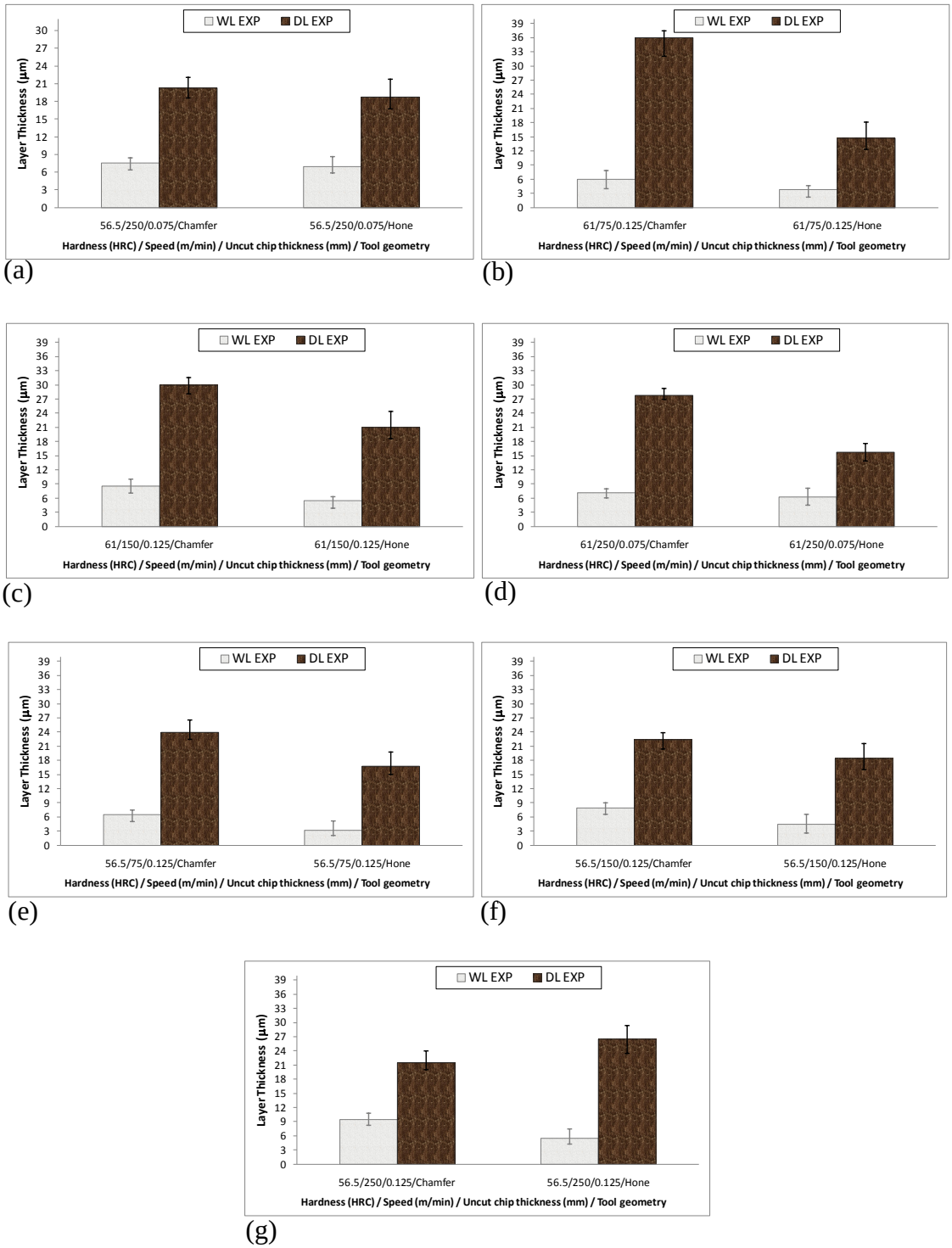

Fig. 4.17 Experimental microstructural changes varying the tool geometry

The two specific analyzed tool geometries show that the honed tool studied in the present work leads to have reduced white and dark layers thicknesses if compared with the chamfered one.

4.4 – WHITE AND DARK LAYERS HARDNESS

Figure 4.18 show the variation of microhardness values for the different experimental conditions employed.

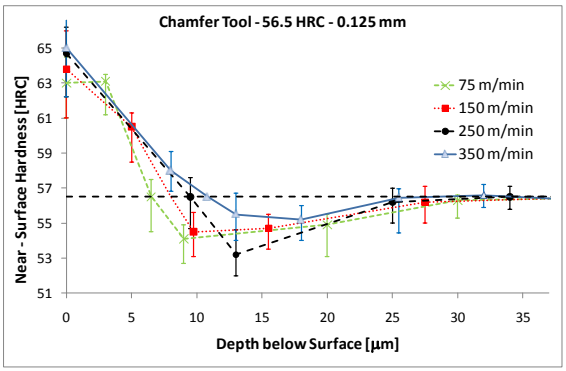

(a)

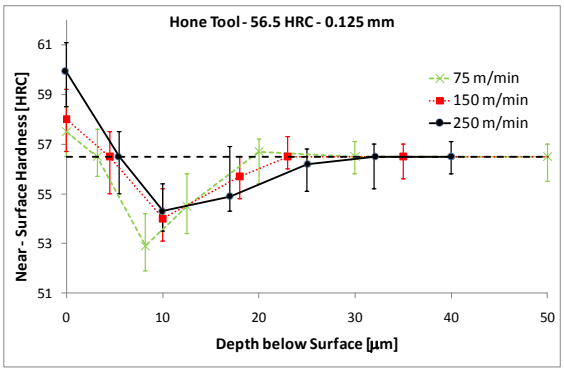

(b)

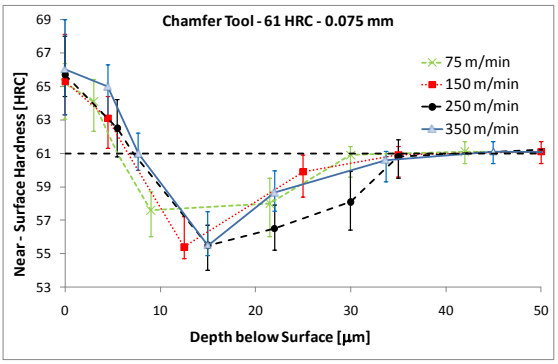

(c)

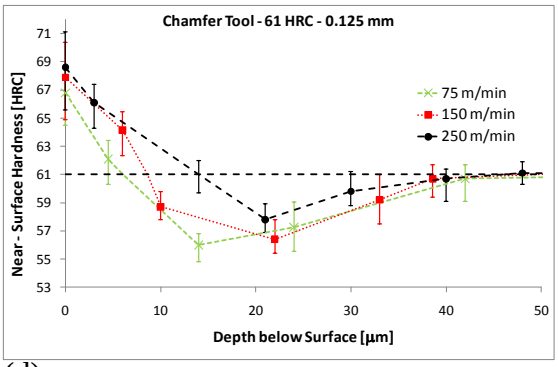

(d)

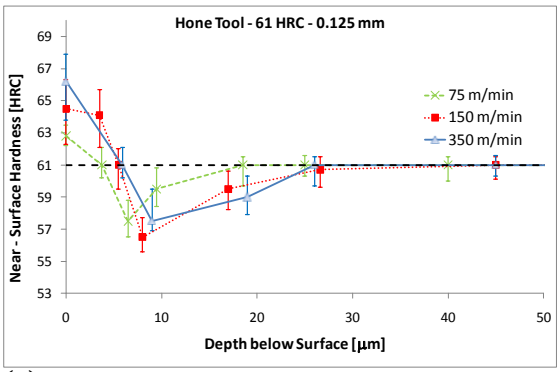

(e)

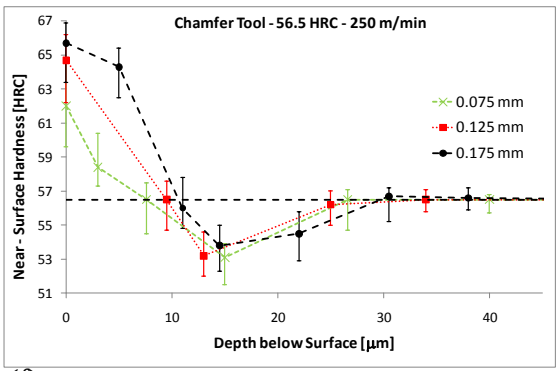

(f)

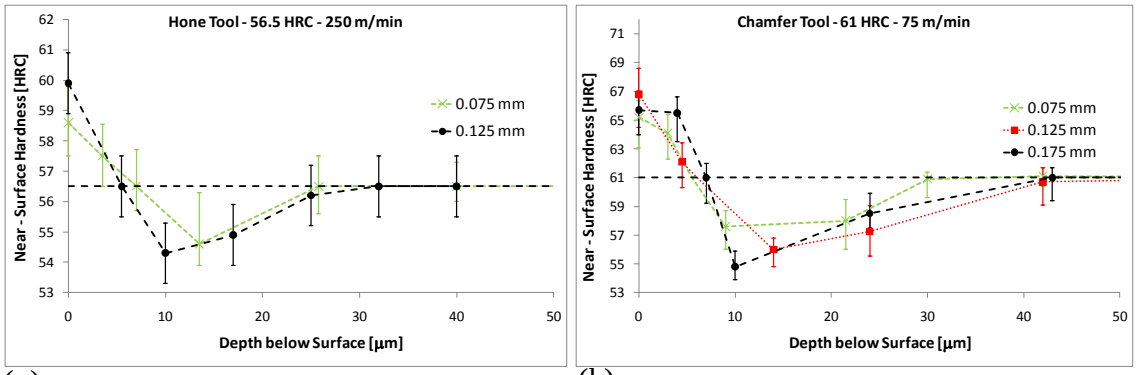

(g) (h)

Fig. 4.18 Experimental hardness profile of the hard turned disks varying cutting speed (a), (b), (c), (d), (e) and feed rate (f), (g) and (h)

In particular, the results highlight that, in all of the investigated cases, the surface hardness is higher than that of the bulk material.

Figure 4.18 shows the measured macrohardness (HRC) profiles for fixed cutting speed and feed rate, respectively. In general, hardness variation is expected since, as also mentioned in Chapter II, the white layer is much harder than the dark layer and bulk material. Moreover, the dark layer is softer than the bulk material. The reason of an higher hardness for the white layer is due to the martesitic transformation (as well described in Chapter II), that takes place during the turning process, for the rapid heating and quenching on the machined surface. Since among the various microstructures that can be obtained in a steel, martensite is the hardest, this leads to have in the white layer the hardest microstructure. The same consideration can be done for the dark layer: since dark layer is due to tempering process a softer microstructure than bulk material takes place; this explanation well justify what is reported in Figure 4.18 in which the hardest part is represented by white layer (untempered martensite), the softer part is represented by dark layer (overtempered martensite) and finally there is the bulk material in which there is not influence of the machining process.

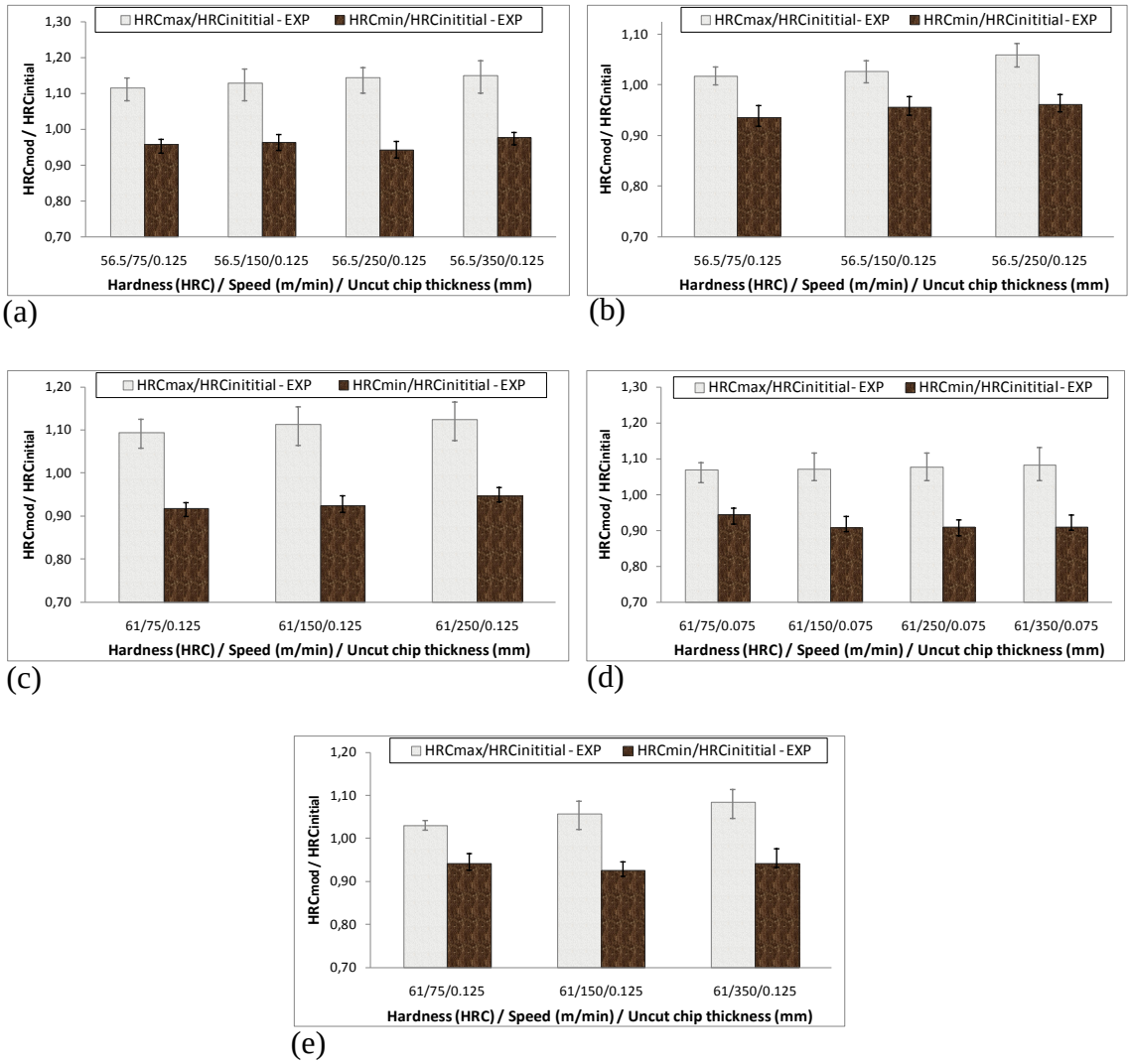

Fig. 4.19 Experimental hardness modification varying cutting speed with chamfered tool (a), (c), (d) and honed tool (b), (e)

Another interesting aspect, analyzed and reported in Figures 4.19, 4.20, 4.21 is the value of hardness modification, relative to the initial hardness condition prior to machining.

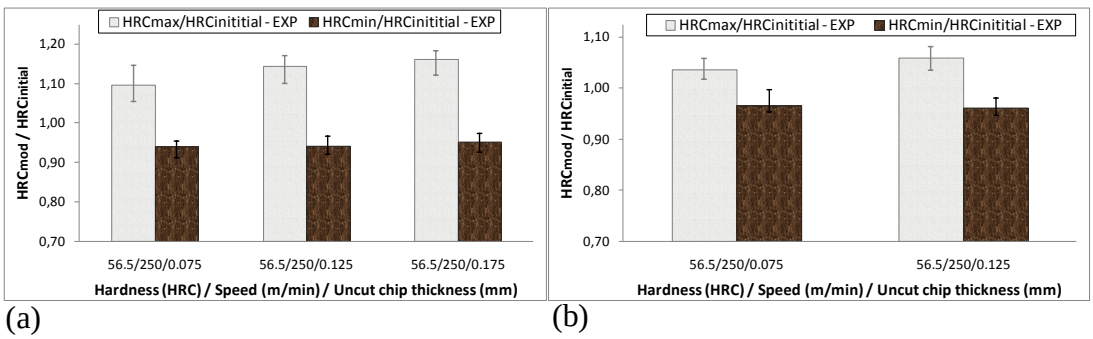

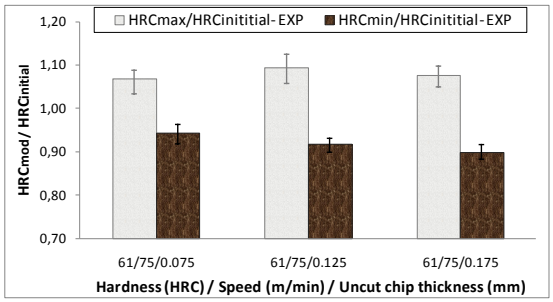

(c)

Fig. 4.20 Experimental hardness modification varying feed rate with chamfered tool (a), (c) and honed tool (b)

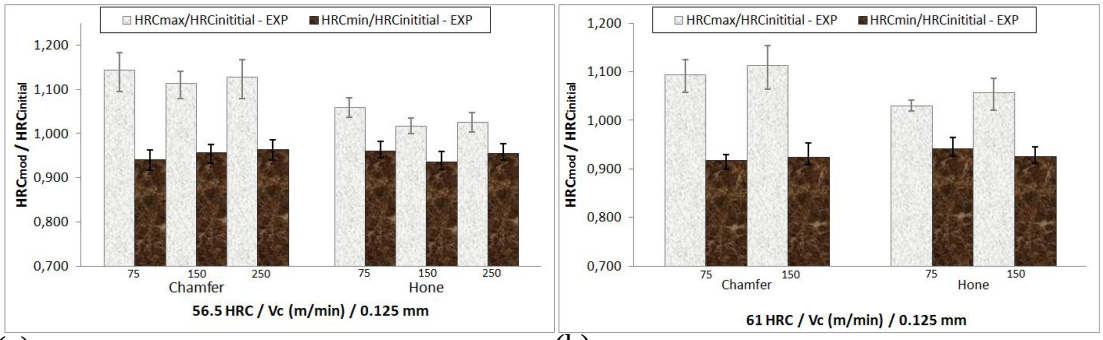

(a) (b)

Fig. 4.21 Experimental hardness modification varying tool geometry (a) 56.5 HRC and 61 HRC (b)

The results for maximum hardness modification correspond to the white layer, which is harder than the bulk material, while the results for minimum hardness modification correspond to the dark layer, which is softer than the bulk material. It is important to underline that the parameter $HRC_{max}/HRC_{Initial}$ decreases with the increasing of the initial workpiece hardness and increases with the increasing of the cutting speed and feed rate (Figures 4.19, 4.20). Similar trends were experimentally observed by [26]. The possible reasons for these trends are that at higher initial hardness there is relatively less scope for the material to further harden through martensitic transformation, while increasing cutting speed and feed rate increases the extent of quenching due to the higher temperatures attained. Same thermal considerations can be done if the tool geometry influence is considered; in fact surface hardness modifications can be attributed either to rapid heating and quenching, which results in microstructural transformation, as well as to severe plastic deformation and consequently grain size

refinement; since by using chamfered tool higher temperatures were reached (Figure 4.21) this results in higher quenching effect in which the final structure is harder.

4.5 – WHITE AND DARK LAYERS EDS ANALYSIS

SEM-EDS microanalysis of both the surface layer and the bulk material of the test was performed, giving the opportunity to check the variation of the chemical elements. In particular, it is noticed a difference in carbon content between the machined surface and the sub surface material of the workpiece (bulk or unmachined material), confirming the microstructural changes.

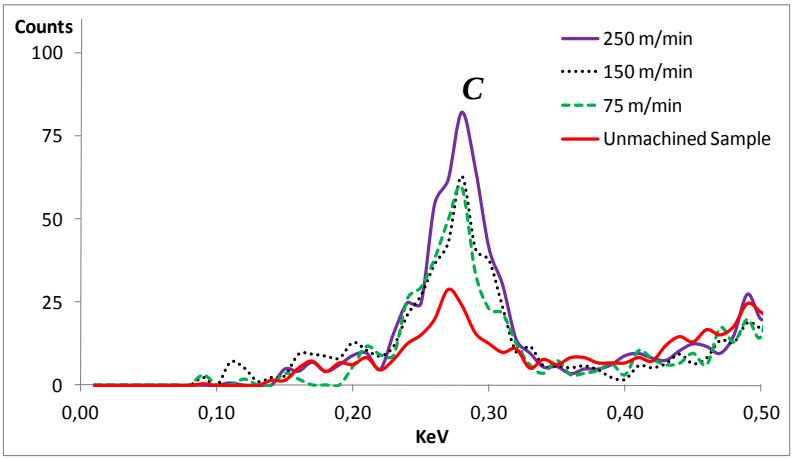

Fig. 4.22 Energy Dispersive Spectroscopy (EDS) on machined specimens vs. unmachined sample: f=0.075 mm/rev, 54 HRC, honed tool

Figure 4.22 depicts the data acquired by energy-dispersive spectroscopy (EDS) analysis when experiments varying cutting speed were considered. As seen, higher carbon content (*C*) on both machined surfaces was detected, this is mainly due to the presence of retained austenite within the white layer. What is important to emphasize is that a slight increase of carbon content was estimated on the machined surface with the increase of the cutting speed from 75 to 150 m/min, while an evident increase of carbon content is reported when cutting speed is increased to 250 m/min; that evidence is mostly due to the temperature increase for the increase of the cutting speed and

consequently more microstructural transformations due to heating and quenching are created.

This effect is more evident in Figure 4.23 in which the influence of the feed rate is considered.

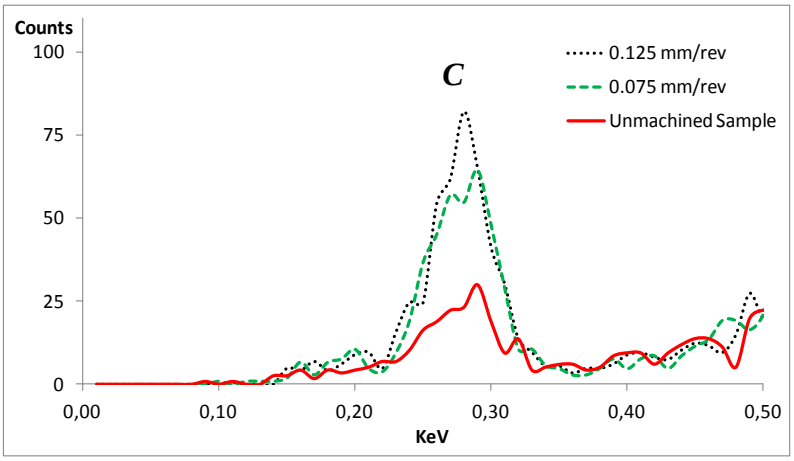

Fig. 4.22 Energy Dispersive Spectroscopy (EDS) on machined specimens vs. unmachined sample: V=75 m/min, 54 HRC, chamfered tool

Also in this case an increase of the carbon content is registered when machining operations are performed, showing the presence of microstructural changes on machined surface; furthermore, an evident increase of the carbon content is showed when feed rate increases from 0.075 to 0.125 mm/rev. Again thermal analysis can explain this behavior, in fact it was reported that the increase of the feed rate results in higher cutting temperatures that lead to microstructural transformations for the heating and quenching on the machined surface (white layer formation); thus the presence of higher content of retained austenite within the white layer shows in Figure 4.22 an increase of the carbon content. The same considerations can be done if the variation of the initial workpiece hardness is considered, Figure 4.23.

.

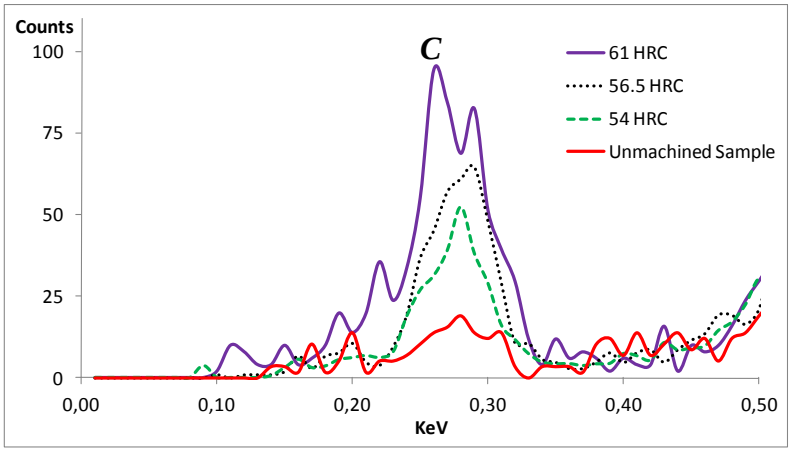

Fig. 4.23 Energy Dispersive Spectroscopy (EDS) on machined specimens vs. unmachined sample: V=75 m/min, f=0.125, honed tool

Higher cutting temperatures reached with the increase of the initial workpiece hardness result in higher carbon content on the machined surface for the presence of more microstructural changes.

Finally, in Figure 4.24 the influence of the cutting tool geometry is reported. As expected, since the higher rake angle produces more mechanical work and higher temperatures compared to the honed tool, higher carbon content are showed when chamfered tools are used.

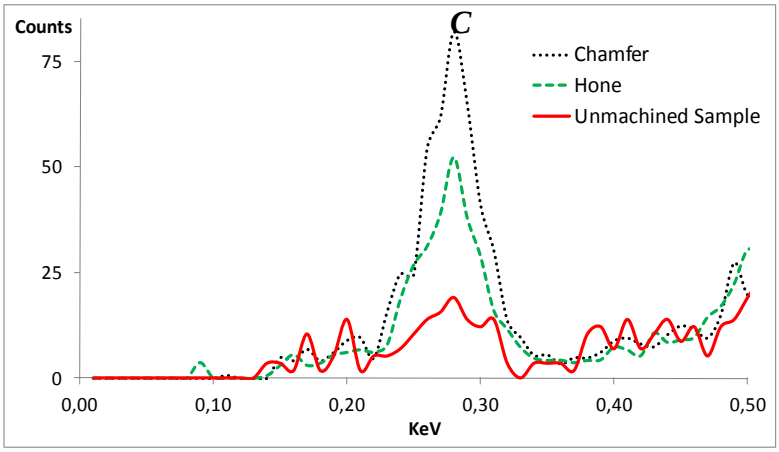

Fig. 4.24 Energy Dispersive Spectroscopy (EDS) on machined specimens with chamfered and honed tool vs. unmachined sample: V=75 m/min, f=0.1 mm/rev, 54 HRC

4.6 – X-RAY DIFFRACTION FOR PHASE ANALYSIS

Figure 4.25 shows the phase analysis obtained by means of X-ray diffraction technique on samples prior to the machining operation and, therefore, without the presence of the white layer on the investigated surface.

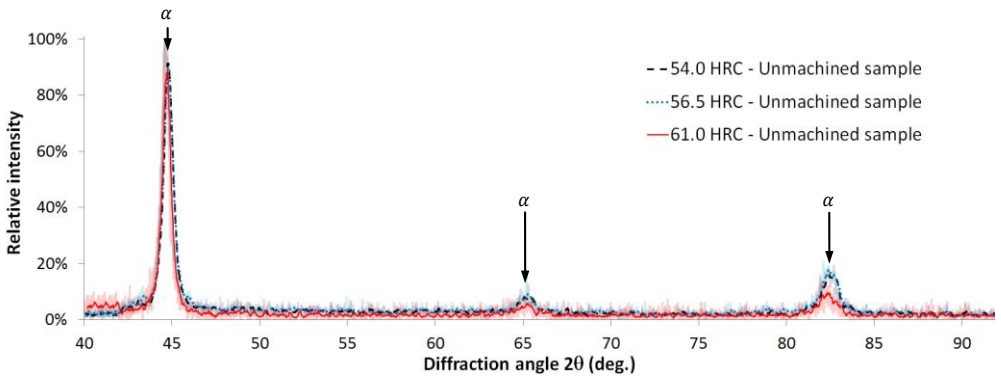

Fig. 4.25 X-ray phase analysis on specimens before machining operation (α=ferrite- α)

In particular, the X-ray phase analysis on the unmachined surface shows three peaks at 44.67°, 65.02° and 82.33° which, according to Bragg's law and data reported in materials handbook [143], correspond to ferrite-α respectively at (110), (200) and (211) Miller's indices.

On the other hand, when machined samples are investigated, the X-ray phase analysis shows several peaks.

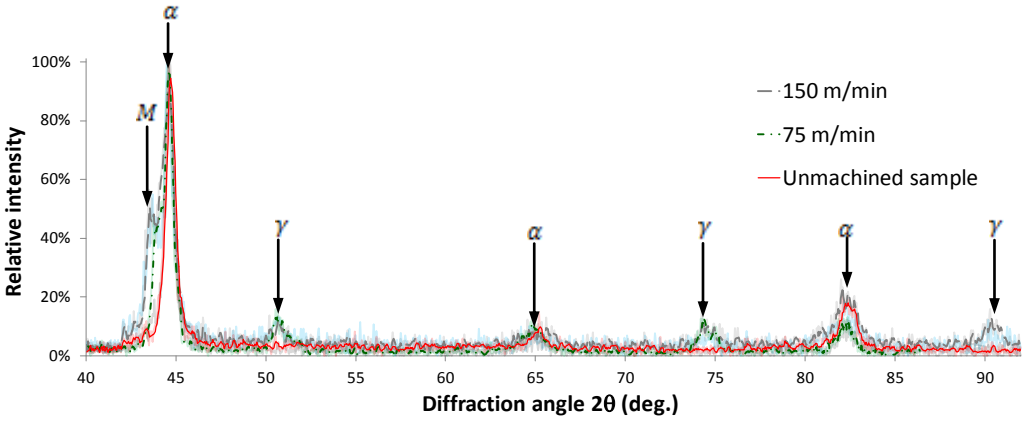

Figure 4.26 X-ray phase analysis on machined specimens vs. unmachined sample: 56.5 HRC and f = 0.125 mm/rev, chamfered tool (α=ferrite-α; γ=austenite; M=Fe_3C-martensite)

Figures 4.26 shows the phase analysis obtained by means of X-ray diffraction technique on samples machined varying cutting speeds when chamfered tool is used. As can be observed high cutting speeds create the higher temperature changes and, therefore, the microstructural phase transformation occur. Once again, three peaks are located at 44.67°, 65.02°, and 82.33° which correspond respectively to ferrite-α. Furthermore, four additional peaks are found at 43.74°, 50.67°, 74.68° and 90.67°. Specifically, the peak at 43.74° corresponds to Fe_3C-martensite (102) while peaks at 50.67°, 74.68° and 90.67°correspond to retained austenite respectively at (200), (220) and (311) Miller's indices as reported in the materials handbook [144, 145] and found by Bragg's law. It is important to note that these results are consistent with other experimental XRD observations [11, 51, 109] for this material. These results combined with EDS analysis (increasing of carbon content on machined samples) lead to state that the thermal effect is the main cause for white and dark layers formation during machining of hardened steels. This fact confirms the first theory proposed by Griffiths in which the white layer formation is principally due to the rapid heating and quenching on machined surface that results in microstructural transformations.

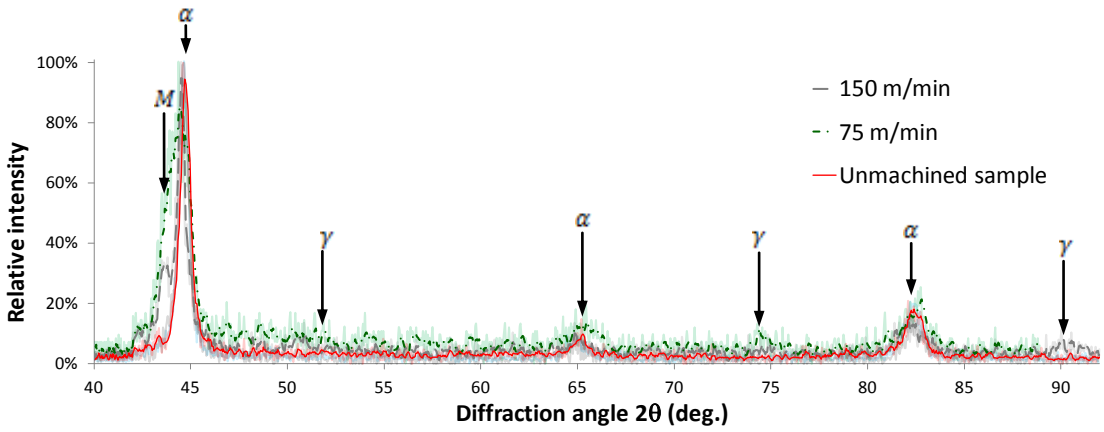

Figure 4.27 X-ray phase analysis on machined specimens vs. unmachined sample: 56.5 HRC and f=0.125 mm/rev, honed tool (α=ferrite-α; γ=austenite; M=Fe_3C-martensite)

Such evidence is also confirmed when samples were machined with honed tools (Figure 4.27). Therefore, for certain conditions the tool geometry has an effect on white layer formation. In fact, the higher negative effective rake angle of the chamfered tool produces a shift in maximum cutting temperature from the tool rake face to near the tool cutting edge (i.e., high maximum temperature on the machined surface).

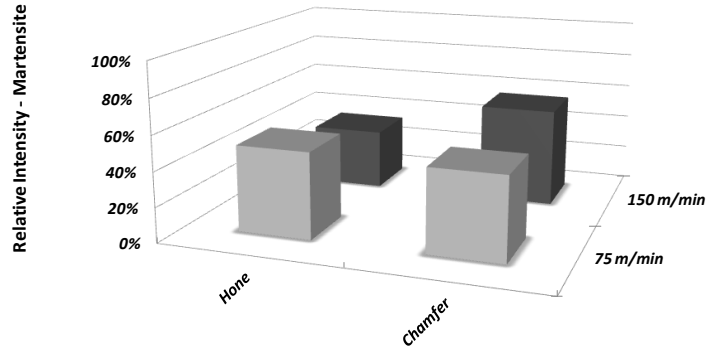

	Hone	Chamfer
75 m/min	49,60%	47,90%
150 m/min	34,80%	56,50%

Figure 4.27 Martensite transformation at varying cutting speed and tool shape for samples at 56.5 HRC and machined with feed rate=0.125 mm/rev

Figure 4.28 depicts as the relative intensity of the martensite peak from chamfered tool is often higher than those from honed tool especially when high cutting speed are considered.

Figure 4.28 (a) reports the phase analysis on samples machined with chamfered tool at varying feed rate. As can be observed, the highest martensite peak is registered for the highest feed rate value, in fact the feed rate increase creates higher temperature changes and, therefore, the microstructural phase transformation occur. Such evidence is also confirmed when samples were machined with honed tools (Figure 4.28 (b)).

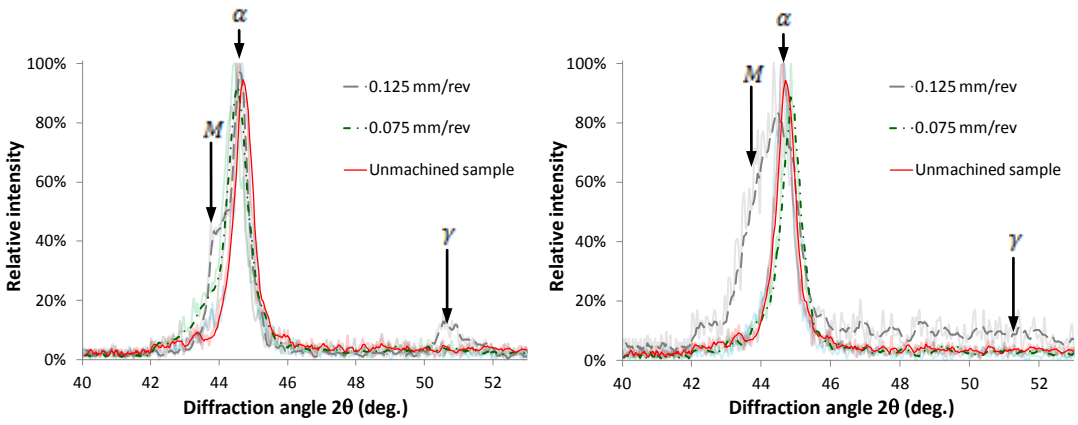

Figure 4.28 X-ray phase analysis on samples at 56.5 HRC machined at 75 m/min: (a) chamfered tool vs. unmachined sample; (b) honed tool vs. unmachined sample (α=ferrite-α; γ=austenite; M=Fe_3C-martensite)

Once again, the chamfered tool preparation is more drastic than the honed edge one as far as white layer formation is regarded.

The relative intensities of the martensite peak at varying feed rate and tool shape are shown in Figure 4.29; in this case the difference between chamfered and honed tool is more evident when low feed rates are considered.

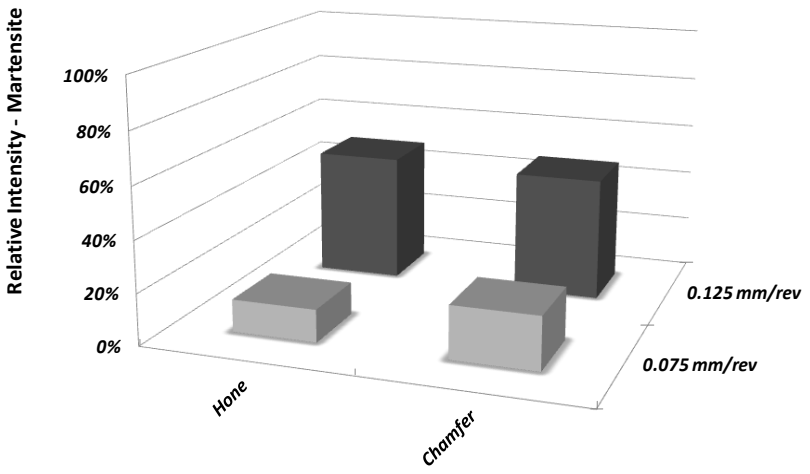

	Hone	Chamfer
0.075 mm/rev	12,70%	20,60%
0.125 mm/rev	49,60%	47,90%

Figure 4.29 Martensite transformation at varying feed rate and tool shape for samples at 56.5 HRC and machined with cutting speed=75 m/min

Finally Figures 4.30 and 4.31 report the phase analysis obtained by means of X-ray diffraction technique on samples machined at varying initial workpiece hardness and tool shape. Also in this case it can be observed, the highest martensite peak is registered for the highest initial workpiece hardness, in fact with the increase of the initial workpiece hardness higher temperature changes are reached and, therefore, the microstructural phase transformation occur. Such evidence is also confirmed when samples were machined with honed tools (Figure 4.31).

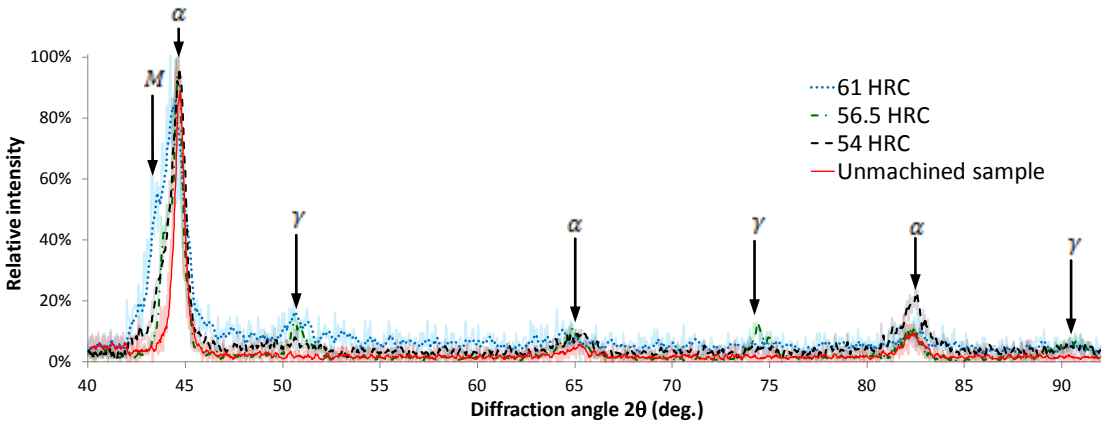

Figure 4.30 X-ray phase analysis on machined specimens vs. unmachined sample: V=75 m/min and f=0.125 mm/rev, chamfered tool (α=ferrite-α; γ=austenite; M=Fe_3C-martensite)

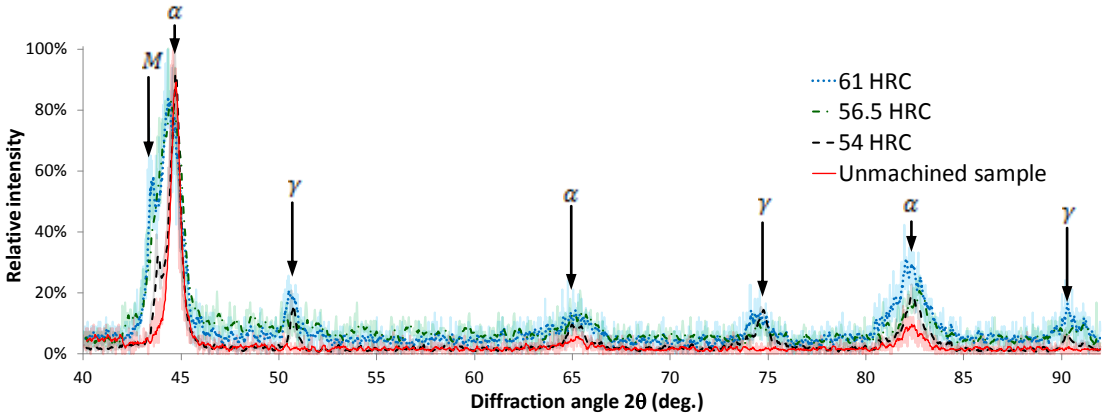

Figure 4.31 X-ray phase analysis on machined specimens vs. unmachined sample: V=75 m/min and f=0.125 mm/rev, honed tool (α=ferrite-α; γ=austenite; M=Fe_3C-martensite)

The relative intensities of the martensite peak at varying initial workpiece hardness and tool shape are shown in Figure 4.32.

In this case not evident differences are reported in the relative intensity of martensite if the tool geometry influence is considered; while more evident is the increase of the retained martensite if the initial workpiece hardness is considered: an increase more than two times is reported passing from 54 HRC to 61 HRC.

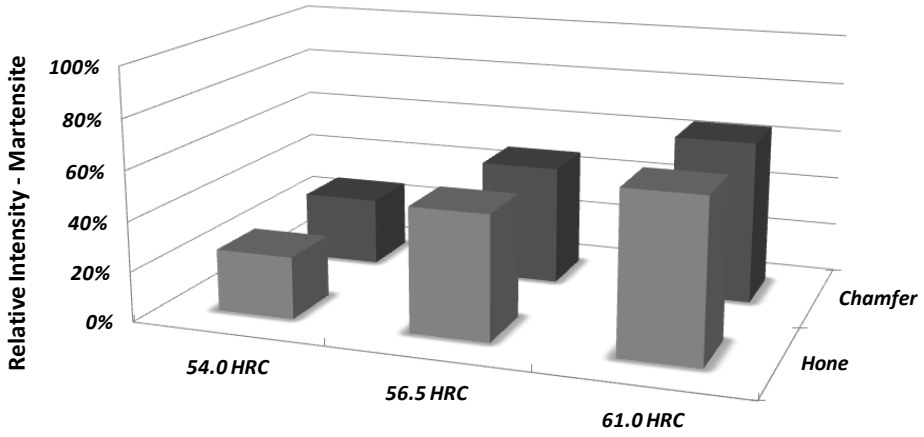

	54.0 HRC	56.5 HRC	61.0 HRC
Hone	24,80%	49,60%	64,00%
Chamfer	27,30%	47,90%	65,00%

Figure 4.32 Martensite transformation at varying initial workpiece hardness and tool shape machined with cutting speed=75 m/min and feed rate=0.125 mm/rev

These experimental evidences of the X-ray phase analysis confirm what EDS analysis have qualitatively showed, i.e., a reduction of white layer formation when cutting speed, feed rate and initial workpiece hardness were reduced and when honed tool is used, because lower cutting temperatures are reached and consequently less microstructural transformation due to rapid heating and quenching (formation on untempered martensite structure). In fact, as it can be seen the relative intensity of the martensite peak increases with the increase of cutting speed, feed rate and initial workpiece hardenss and when chamfered tool is used to perform the experiments.

Finally some considerations concerning retained austenite are below reported.

Retained austenite is an important phase in AISI 52100 bearing steel when martensitic microstructure is formed. Whereas it is definitively established that the dimensional changes that occur when it appears can compromise the mechanical performance of machined components, there are contradictory studies on its role in determining the fatigue properties. In fact, retained austenite enhances the development of a mean compressive stress [146] which is beneficial for improving surface integrity of machined parts. On the other hand, when dimensional stability due to the decomposition of retained austenite during service is an issue, an appropriate choice of austenitisation and tempering conditions can completely remove it without

compromising the hardness [147]. There are also two aspects to the mechanical behaviour of retained austenite that can be considered: (i) its susceptibility to ordinary plastic deformation; (ii) the stress or strain-induced martensitic transformation. Concerning the former, in [148] it is demonstrated as the austenite in AISI 52100 type steel is relatively soft and hence in the composite microstructure, undergoes microscopic plastic deformation during the early stages of straining, resulting in an overall reduction of the elastic limit. The second aspect of the stability of the retained austenite is related to diffusionless martensitic transformation since it can be stimulated by applying an external stress [149]. Therefore, when machined components containing retained austenite are put into service, the imposed stresses may stimulate martensite to form.

Also, when bearings in AISI 52100 are subjected to heavy loads, plasticity occurs at the contact surfaces causing the formation of shallow grooves which can develop into significant damage [150]. The presence of austenite can exasperate this effect if it leads to a reduction in the yield strength.

Then, taking into account the important role plays by the retained austenite, the advantage and the drawbacks, it is of cardinal interest to quantitatively evaluate its volume fraction on the affected layer. That can be done based on the relative peak areas depicted in the XRD plots and the procedures given in [136, 137], permitting to estimate the volume fraction of retained austenite by the following equation:

$$\%\ of\ RA = (V_\gamma) \cdot 100 = \left(\frac{\frac{I_\gamma}{R_\gamma}}{\frac{I_\gamma}{R_\gamma} + \frac{I_\alpha}{R_\alpha}} \right) \cdot 100 \qquad (1)$$

where R is a scale factor associated with phases and materials used, I is the calculated integrated intensity total for a phase, and V is the volume fraction of the phase. The austenite phase is represented by γ and the ferrite/martensite phase is represented by α. Thus, the calculated volume fraction of retained austenite (200) for the investigated tests are reported in Figures 4.33, 4.34, 4.35.

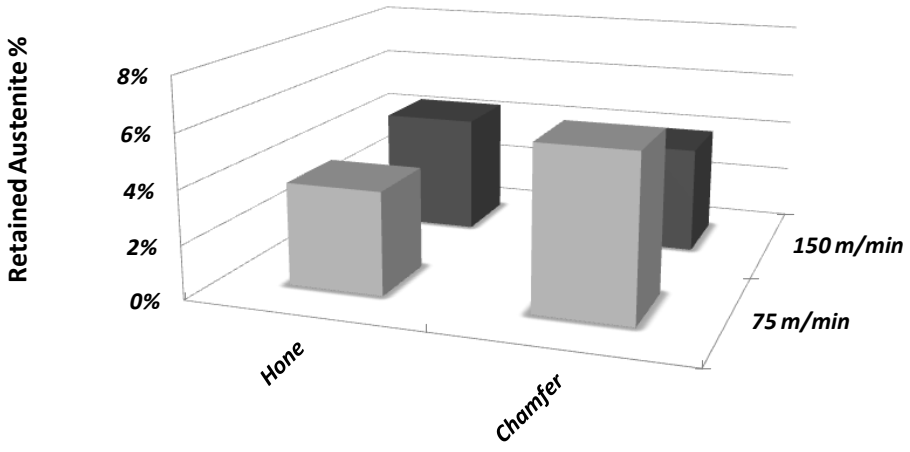

	Hone	Chamfer
75 m/min	3,83%	6,05%
150 m/min	4,44%	3,98%

Figure 4.33 Volume fraction of retained austenite at varying cutting speed and tool shape for samples at 56.5 HRC and machined with feed rate=0.125 mm/rev

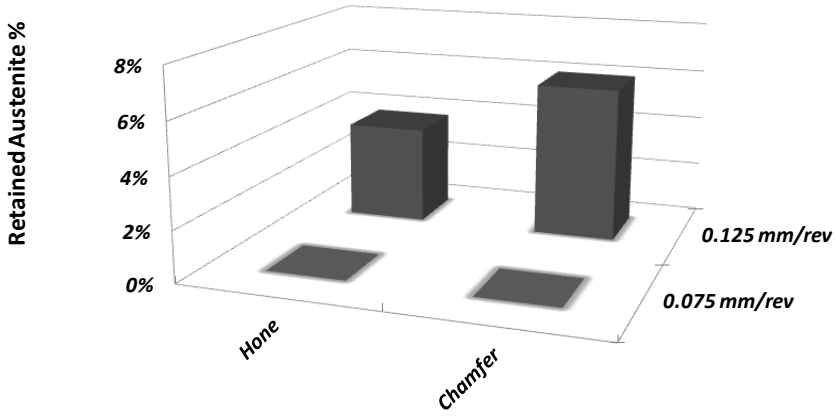

	Hone	Chamfer
0.075 mm/rev	0,00%	0,00%
0.125 mm/rev	3,83%	6,05%

Figure 4.34 Volume fraction of retained austenite at varying cutting speed and tool shape for samples at with 56.5 HRC and machined with cutting speed=75 m/min

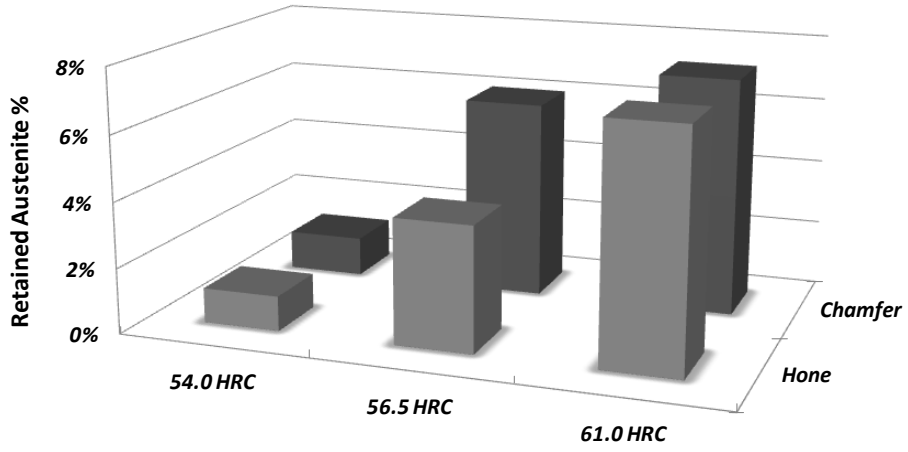

	54.0 HRC	56.5 HRC	61.0 HRC
Hone	1,07%	3,83%	7,19%
Chamfer	1,20%	6,05%	7,25%

Figure. 4.35 Volume fraction of retained austenite at varying initial material hardness and tool shape for samples at cutting speed=75 m/min and feed rate=0.125 mm/rev

In particular, Figure 4.35 shows as there is an high content of retained austenite when samples at 56.5 HRC and 61 HRC are machined. In contrast, the volume of retained austenite is only contained on samples at 54 HRC.

Finally Figure 4.34 highlights as for the employed cutting conditions low feed rates can significantly reduce or totally avoid the amount of the retained austenite.

4.7 – RESIDUAL STRESS ANALYSIS

In this paragraph a detailed description of the influence of cutting speed, feed rate, initial workpiece hardness, tool shape and microstructural changes on the surface and sub-surface residual stresses profile will be shown. To better describe the influence of each single cutting parameter on the residual stress shape four different factors were considered (figure 1 b): a: Surface residual stress; b: Maximum compressive residual stress below surface; c: Penetration depth; d: Thickness affected by machining residual stress.

Both axial and circumferential (hoop) residual stress were measured to provide a more accurate and complete study on the material. Before analyzing the obtained results it is important to point out the principal parameters to refer in order to understand a typical residual stress profile, Figure 4.36

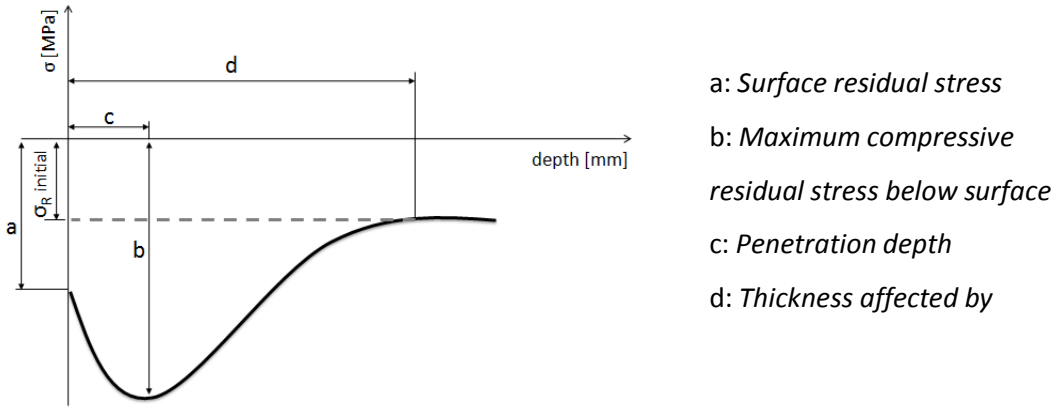

Figure 4.36 Residual stress parameters

Besides these parameters it needs to clarify about the residual stress pre-existing in the base material due to both heat treatments and grinding processes necessary for sample preparation and not related to the machining process.

It is important to exactly know the right value of the pre-existing residual stress because the experimental residual stress value obtained from the X-ray machine is the sum of the residual stress due to the machining process and the pre-existing residual stress; so to know the only amount of the residual stress due to the turning process it is necessary to subtract the pre-existing residual stress to the X-ray machine analysis.

In order to evaluate the residual stress in the base material X-Ray analysis were performed making measurements at three different points on the disk along the radial direction, as shown in figure 4.37.

For each point residual stress profile was defined for depths over than 300 microns until to reach a stable value that represents the residual stress due to the sample preparation.

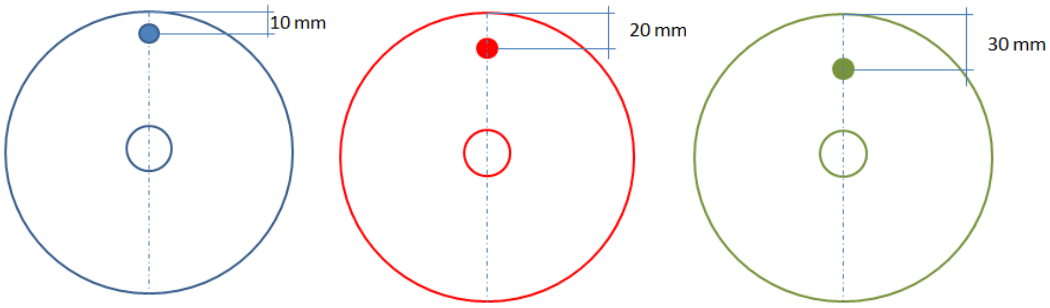

Figure 4.37 X-ray analysis in the base material

It was found that the pre-existing residual stress was about -150 MPa for the sample at 54 HRC, -180 MPa for the sample at 56.5 HRC (Figure 4.38), and -190 MPa for the disk at 61 HRC.

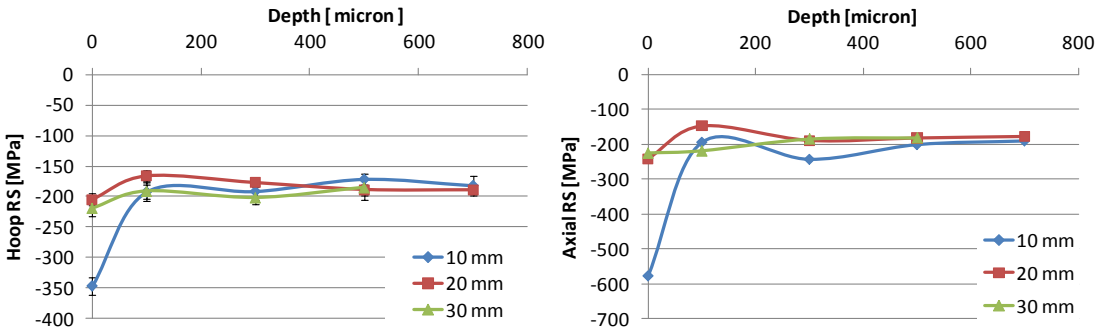

Figure 4.38 Residual stress profile in the base material 56.5 HRC

4.7.1 – INFLUENCE OF THE CUTTING SPEED

Figure 4.39 shows the influence of the cutting speed on the residual stress profile; taking into account the four parameters above reported (and also depicted in Figure 4.36), it is possible to describe how the residual stress profiles are affected (both for the axial and circumferential directions). In particular, the results highlight that with the increase of the cutting speed a deeper compressive surface residual stress is registered by the X-Ray analysis either in the axial direction as well as in the circumferential one.

In addition, the maximum compressive residual stress below surface becomes larger (i.e. deeper) when cutting speed increases and its location is shifted further than surface. These variation are more evident on the axial direction.

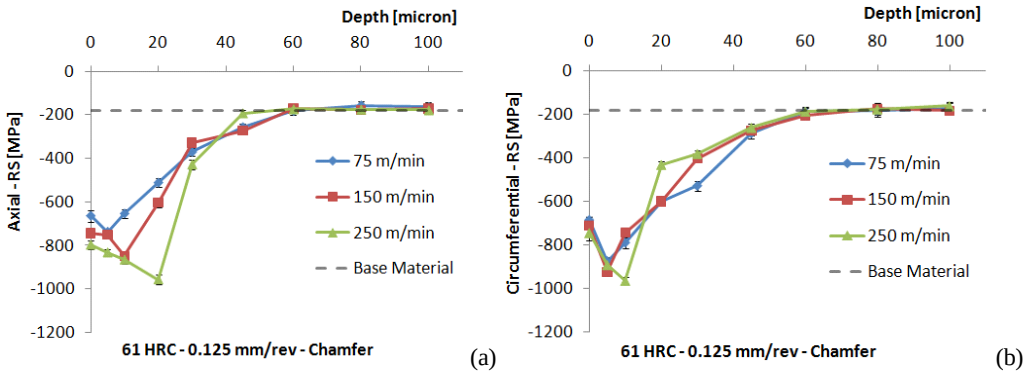

Figure 4.39 Effect of cutting speed on the residual stress for 61 HRC along the axial (a) and circumferential (b) directions: chamfered tool

On the contrary, when cutting speed rises the thickness affected by machining residual stresses decreases. The reason of these trends, as it will be better described in paragraph 4.7.5, is strictly related to the presence of the white layer, which becomes thicker and harder with increasing cutting speed [151].

4.7.2 – INFLUENCE OF THE FEED RATE

In Figure 4.40 is reported the influence of the feed rate on the residual stress profile at different cutting speeds.

It can be noted that the feed rate has not evident influence on the residual stress profile; for both 75 m/min and 250 m/min the position of the four factors (Figure 4.36), used to describe the changes of the residual stress at varying of the cutting conditions, is not changed. This shows that with the cutting conditions chosen in the present work the feed rate has not influence when the residual stress profile is taken into account.

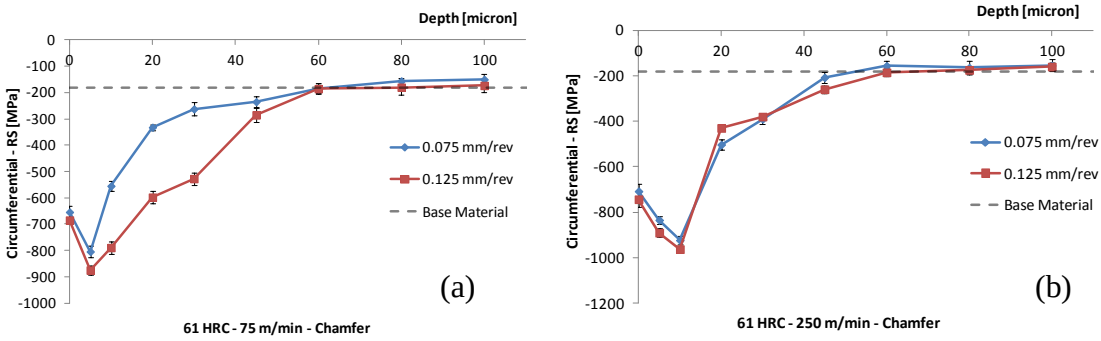

Figure 4.40 Effect of feed rate on the residual stress for 61 HRC along the axial (a) and circumferential (b) directions: chamfered tool

4.7.3 – INFLUENCE OF THE INITIAL WORKPIECE HARDNESS

In figure 4.41 (a) is reported the influence of the initial workpiece hardness on the residual stress profile. It is evident as the increment of hardness produces more compressive axial and circumferential residual stress profiles although the position of maximum compressive stress below surface remains almost constant. Also the surface residual stress in both the directions increase with higher initial hardness. The reason is related to the hard structure on the machined surface which produces more compressive residual stresses [118]. Finally, the thickness affected by machining residual stress depth slightly increases with the increasing of the initial workpiece hardness.

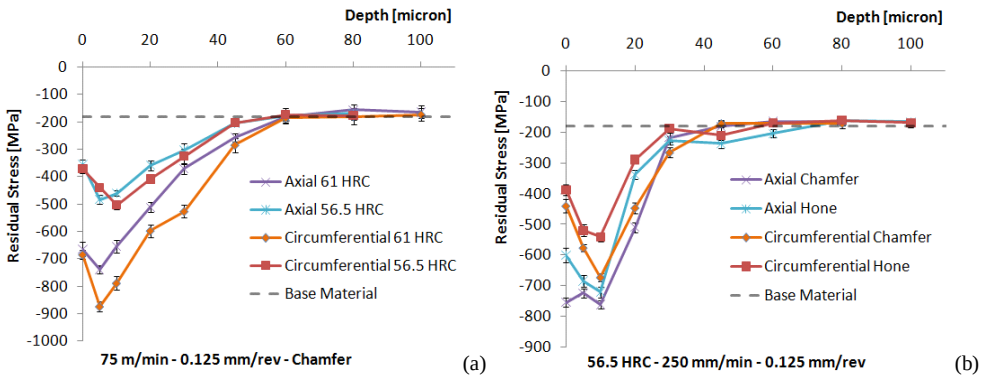

Figure 4.41 Effect of initial workpiece hardness (a) and tool geometry (b)

4.7.4 – INFLUENCE OF THE TOOL GEOMETRY

Figures 4.41 (b) reports the influence of the tool geometries on the residual stress profiles. It is showed that the use of a chamfered tool generates higher axial and circumferential compressive residual stress than for the equivalent test case with a honed tool in terms of both surface residual stress and maximum compressive stress below surface. In contrast both the tool shapes report similar location of the penetration depth either for the axial direction as well as for the circumferential one.

4.7.5 – INFLUENCE OF THE MICROSTRUCTURAL CHANGES (WHITE AND DARK LAYERS)

Figure 4.42 shows the influence of the white and dark layers on residual stress state. As can be observed, for a lower cutting speed (Figure 4.42 (a)) the max compressive residual stress for both the axial and the circumferential directions is positioned in the while layer region. Such evidence was also observed for the specimens at 56.5 HRC machined at the same cutting speed. In contrast, at higher cutting speed (Figure 4.42 (b)) the maximum compressive stress is positioned near the white-dark layer transition (circumferential direction) or in the dark layer (axial direction). Similar observations were done for specimens at 56.5 HRC (Figure 4.43). The reason of these evidences are related to the fact that both white layer thickness and position of the penetration depth increase with the increasing of the cutting speed, although the latter rises more than the white layer thickness.

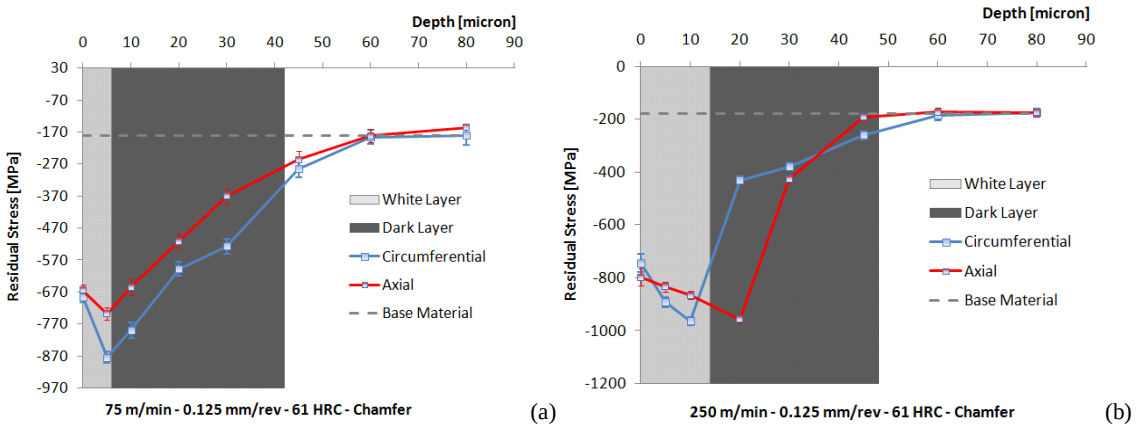

Figure 4.42 Effect of the microstructural changes on the residual stress profiles at 75 m/min (a) and 250 m/min (b) for specimens at 61 HRC: chamfered tool

Moreover, it is widely assessed that in orthogonal cutting of AISI 52100 with the increase of the cutting speed an increase in while layer and a decrease in dark layer thicknesses are registered; furthermore, when the initial workpiece hardness increases both while and dark layers thickness increase [118, 151]; furthermore, Thiele et al [118] showed that with the increase of the hardness the residual stress state becomes more compressive. Therefore, taking into account all the investigated cases and the above mentioned knowledge, the overall reported in Table 4.2 can be drawn.

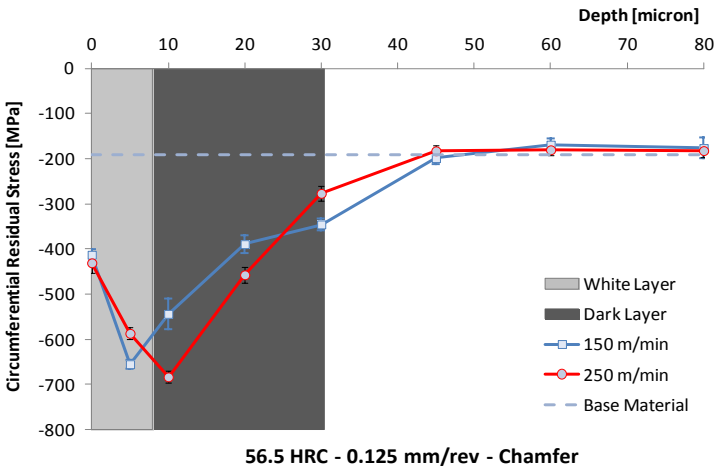

Figure 4.43 Effect of the microstructural changes on the residual stress profiles at varying cutting speed

Finally in the [151] was showed that the ratio HRCmax/HRCinitial increases with the increase of the cutting speed and this (according also to Thiele et al [118]) leads to an increase in the compressive surface residual stress and in the maximum value of the compressive peak. In contrast, the thickness affected by machining residual stress is related to the dark layer thickness; in fact when the dark layer thickness increases the parameter d increases. Therefore, when cutting speed increases: (i) the hardness of the white layer increases [151] and consequently the residual stress state becomes more compressive [118]; considering Figure 4.36, parameters a and b increase; (ii) dark layer thickness decreases [151] and consequently the thickness affected by machining residual stress decreases; considering Figure 4.36, parameter d decreases.

Similar considerations can be done as concerned the residual stress profiles affected by the different initial workpiece hardness.

$HRC_{WHITE-LAYER} > HRC_{BULK-MATERIAL} > HRC_{DARK-LAYER}$				
Cutting Speed	↑	White Layer	↑	Dark Layer ↓
Hardness	↑	White Layer	↑	Dark Layer ↑
Hardness	↑	Compressive RS	↑	-

Table 4.2 Effect of cutting speed and hardness on the microstructural changes and residual stress

4.8 – SUMMARY

In this Chapter an experimental and detailed analysis of the several aspects related to the microstructural changes during orthogonal hard turning of disks of AISI 52100 (54, 56.5 and 61 HRC) steel was carried out. It was shown the importance of each single cutting parameter on the white and dark layers formation in terms of white and dark layers thickness, hardness modification, microstructural phase transformations, residual stress state, etc. Furthermore the tool geometry was also taken into account.

The present analysis gives an helpful knowledge in order to understand what happens in terms of microstructural changes, phase transformations and residual stress state when the value of one of the studied parameters is increased or decreased. Moreover, the performed EDS and XRD analyses show that the thermal effect was the

main cause for the white layer formation in dry machining. In fact, the rapid heating and quenching on the surface creates an alteration with a consequent martensitic formation. Furthermore the presence of phase transformations for cutting temperatures below 723 ^{0}C (thermal analysis, Figures 4.9 - 4.12) shows that the influence of stress and strain during hard turning reduces the value of the austenite-start temperature.

Finally the effects of cutting speed, feed rate, initial workpiece hardness and tool cutting-edge geometry on the residual stress profile was investigated, correlating them with the microstructural phase transformations. Particularly, it was found that both the axial and circumferential surface and subsurface residual stress become larger (i.e., deeper) increasing the cutting speed, for harder material and using chamfered tools. Also the location of the maximum compressive residual stress rises in similar manner. Finally, microstructural changes deeply affect the residual stresses distribution and, for this reason, they have to be accurately taken into account during process design.

CHAPTER V

FINITE ELEMENT MODELING FOR WHITE AND DARK LAYERS FORMATION AND RESIDUAL STRESSES ANALYSIS

This chapter contains the description of the proposed FE model for predicting the microstructural alterations and, consequently, for investigating their effects on the surface integrity. An overview concerning the different FEM methodologies for studying the cutting processes and the previous numerical models based on the microstructural alterations in the literature will be carried out. Then, a new advanced empirical model for white and dark layers prediction will shown. In particular, a hardness-based flow stress model was implemented in the FE code and an empirical model was developed for describing the phase transformations, and therefore, the white and dark layers generation in AISI 52100 steel. An iterative procedure was utilized for calibrating the proposed empirical model for the micro structural changes above mentioned. Finally, the numerical technique for extracting residual stress profile from the numerical simulations will be illustrated.

5.1 – APPLICATION OF ANALYTICAL AND NUMERICAL APPROACHES FOR PREDICTING THE WHITE LAYER

A number of workers have made attempts to model microstructural changes in hard machining, but to date there has been no significant improvements to correctly model white layer formation in hard machining. The FE approach is attractive, as stress, strain and temperature distributions may be obtained for the tool and the workpiece. However, in order to model white layer formation, a working thermo-mechanical model needs to be developed.

Akcan et al [152], and Chou and Evans [48], used an analytical approach to predict white layer formation by assuming that it is due to thermally driven phase transformation effects. Recently, two interesting contributions have been made by Ramesh and Melkote [153], and Fischer and Bandar [154]. In particular, Ramesh and Melkote [153] presented a Finite Element model of continuous white layer formation. They modeled the problem as quenching by incorporating in the FE model the effects of stresses and strains on the transformation temperature, volume expansion and transformation plasticity. These characteristics were taken into account by developing extensive VUMAT FORTRAN subroutines in ABAQUS FE code. Furthermore, subroutines were also necessary for describing the basic elastic-plastic constitutive behavior. The study was conducted under thermally dominant cutting conditions that promote phase transformations. Unfortunately, although this work represents an initial attempt to simulate the white layer formation, some drawbacks are noted by the same authors such as: the software does not include automated remeshing, so a predefined separation plane is required; chip segmentation effects, which are known to occur in hardened materials, were neglected for numerical convenience since it was assumed that this does not influence surface behavior; the orientations of elements in the chip prior to the start of machining are altered and the basic shape of the chip is not changed. Starting from the above-mentioned research, Fischer and Bandar [154] proposed a finite element model of continuous white layer formation based on the austenitization of the surface layer and subsequent martensite formation due to rapid cooling. Material properties were determined by a mixture rule on the element and the hardness-based flow stress

model for AISI 52100 proposed by Umbrello et al [134] was used for defining the single mixture phases. The results found by Fischer and Bandar [154] showed good agreement in both white layer thickness and hardness with those experimentally found by Han [103]. However, the proposed physically-based approach requires large experimental databases, with complex metallographic analyses and time-consuming procedures for the identification of microstructure law coefficients. Furthermore, although the physically-based models reflect the knowledge of the physical phenomena underlying the deformation process, their use (with few exceptions) requires specialized scientific and computational knowledge, well beyond the ability of potential industrial users. Moreover, most of these models have not yet been validated for a sufficient number of realistic cases; thus, their accuracy and applicability remain practically unknown [155]. In addition, when physically-based models are incorporated for studying the micro structural changes in machining by FE codes, only the white layer formation can realistically be predicted by thermal analysis of the quenching process since the martensitic transformation is a diffusionless type transformation (time independent). In contrast, when Lagrangian formulation is used, the tempering effect (diffusion type transformation) cannot be practically simulated because the simulated time is 2-3 orders of magnitude lower that the physical one; therefore the overtempered martensite (microstructure present in the dark layer) is difficult to predict using physically-based models.

5.2 – NUMERICAL MODELING

In this paragraph the two advanced numerical empirical equations developed to simulate the white (quenching effect) and dark (tempering effect) layers formation will be shown. Furthermore, the customize FE numerical model in order to include the above mentioned equations will be reported.

5.2.1 – ADVANCED EMPIRICAL MODELS FOR PREDICTING WHITE AND DARK LAYERS FORMATIONS

Habak et al. [156] conducted an experimental work, reproducing the primary shear zone (shear band and the white layer) with special geometry "Hat-shaped shear specimens" (Figure 5.1, 5.2), to understand the effects of initial micro structure and temperature on adiabatic shear band generation.

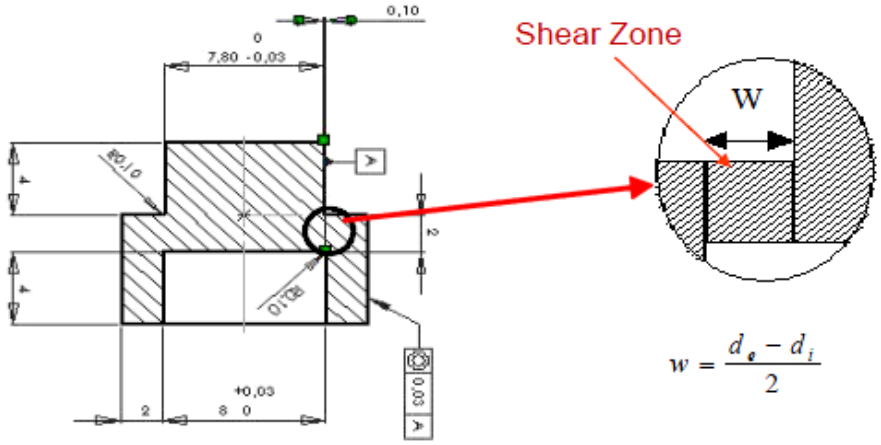

Figure 5.1 Geometry of the hat-shaped shear specimens [156]

They demonstrated that the origin of the white layer in hard machining processes is, in general, thermo-mechanical and, more precisely, it is initially generated by a mechanical effect involving a localized shear deformation. Consequently, the high strain-rate results in a localized temperature rise generating a thermal effect that leads to the white layer formation.

In addition to the experimental results reported in this thesis (Chapter IV), to study the nature of white layer formation when several metallurgical states and speeds are taken into account, a finite element model that numerically reproduces the experimental work done by Habak et al [156] was developed. The commercial FE code Deform 2D, based on the implicit updated Lagrangian formulation, was utilized for the analysis since this software includes coupled mechanical, thermal, and microstructure analysis.

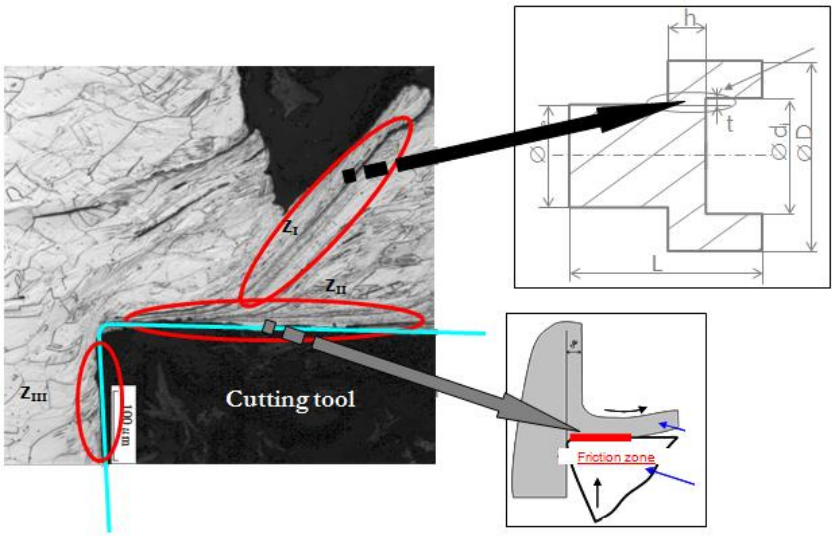

Figure 5.2 Reproduction of the primary shear zone by hat-shaped shear specimens [156]

As far as the microstructure analysis is concerned, the system is designed for both ferrous and nonferrous metals. Using carbon steel as an example, the austenite-ferrite and austenite-pearlite structure changes, and vice versa, are governed by the diffusion type transformation. The transformation is driven by a diffusion process depending on the temperature, stress history, and carbon content. The diffusionless transformation from the austenite to martensite involves a shear process which depends on the temperature, stress, and carbon content [157]. During Lagrangian analysis, at each time step, the phase volume fractions are calculated based on temperature and deformation results from that step. The updated properties are then used for the deformation and temperature calculations at the next step [158].

Phase	Phase hardness	Volume fraction			
		46 HRC	**51 HRC**	**55 HRC**	**62 HRC**
Martensite	64 HRC	5%	5%	5%	4%
Bainite	35 HRC	16%	4%	0%	0%
Pearlite	29 HRC	35%	31%	23%	0%
Austenite	17 HRC	44%	60%	72%	96%

Table 5.1 Volume fraction ratio and phase hardness for 46 HRC, 51 HRC, 55 HRC and 62 HRC metallurgical states in AISI 52100 steel

The different metallurgical states of AISI 52100 were determined by a mixture rule on the element and the hardness-based flow stress model for AISI 52100 [134] was used for defining the single mixture phases. In addition, using a hardness vs. time and tempering temperature chart presented in the ASM Handbook - *Heat Treating*, [159], and phase hardness estimates from the SFTC-DEFORM V9.1 material library [158], a mixture rule approach was used to estimate a volume fraction ratio of the different phases as reported in Table 5.1.

According to Habak et al [156], for the quasi-static tests at very low deformation rates (~1 mm/s) no white layer was observed (Figure 5.3 (a)).

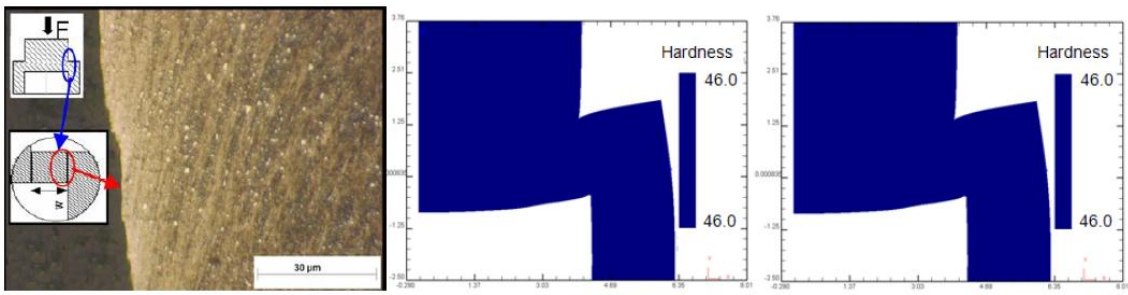

Figure 5.3 (a) Experimental observation for a metallurgical state of 46HRC, speed of 0.1 mm/sec and punch stroke of 1mm (Habak et al., 2007); (b) numerical observation at the end of the deformation path (time 10 sec); (c) final state after cooling down (time 100 sec)

The numerical simulations show the same results. In fact, no white layer was observed either at the end of the deformation path (Figure 5.3 (b)) or when the cooling down was completed (Figure 5.3 (c)).

In contrast, when the speed was experimentally set equal to 10 mm/s, Habak et al [156] noted that some trace of white layer appeared on the surface (Figure 5.4 (a)).

However, from the experiment it was not possible to distinguish the predominant effect. This can be deduced by observing the numerical results (Figures 5.4 (b) and 5.4 (c)). In fact, the structure presented traces of white layer only at the end of the cooling down (Figure 5.4 (c)), while no microstructural changes were observed during the deformation path.

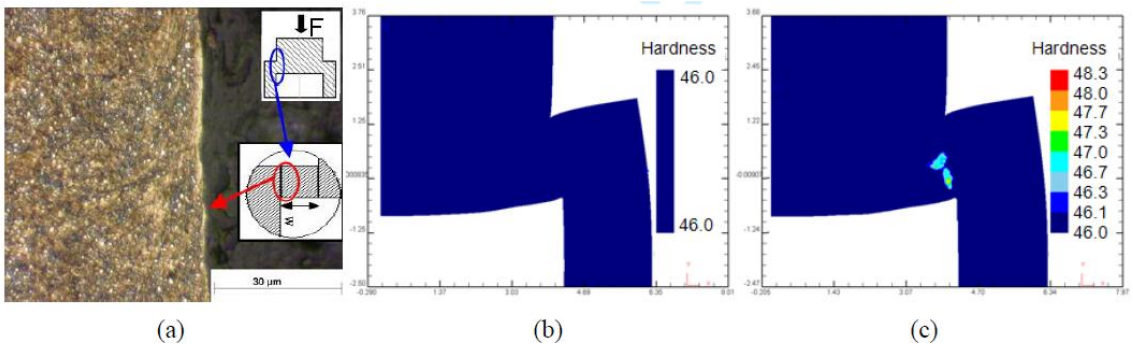

Figure 5.4 (a) Experimental observation for a metallurgical state of 46HRC, speed of 10 mm/sec and punch stroke of 1mm (Habak et al., 2007); (b) numerical observation at the end of the deformation path (time 0.1 sec); (c) final state after cooling down (time 100 sec)

Increasing both the speed as well as initial material hardness, Habak et al [156] found that the white layer thickness increased (Figure 5.5 (a)).

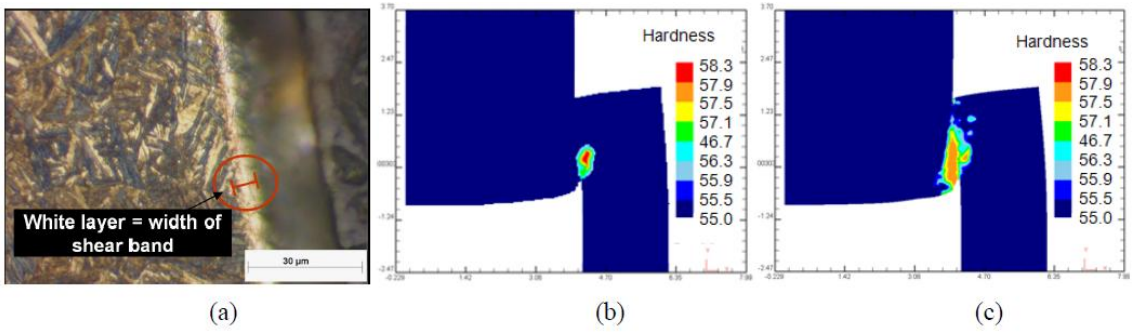

Figure 5.5 (a) Experimental observation for a metallurgical state of 55HRC, speed of 12500 mm/sec and punch stroke of 1mm (Habak et al., 2007); (b) numerical observation at the end of the deformation path (time $8*10^{-5}$ sec); (c) final state after cooling down (time 100 sec)

On simulating the experiment by finite element modeling it was possible to discern the fraction of white layer obtained after the mechanical process and the fraction related to the thermal effect. In particular, by analyzing the numerical results reported in Figures 5.5 (b) and 5.5 (c) using image processing software, it was possible to estimate that only 12% of the total white layer formation was directly due to severe plastic deformation.

Then, extending the numerical simulations to other combinations of metallurgical states (51 HRC and 62 HRC) and speeds, it was possible to develop a processing map

(Figure 5.6) characterized by several regions where the presence or not of white layer is reported.

Moreover, Figure 5.6 highlights the combinations of material hardness and deformation speed at which the thermal effect is dominant in white layer formation. Finally, it is important to note that for the common speeds and metallurgical states used in hard turning, the white layer formation is mainly due to thermal effect, as observed in Figure 5.6.

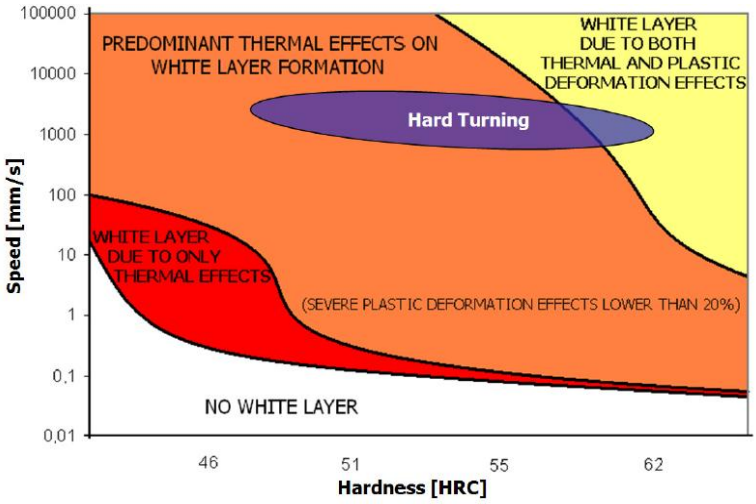

Figure 5.6 Nature of white layer formed at various speeds and metallurgical states

Following from these and from experimental results empirical models to predict white and dark layer formation (to be incorporated into the FE model in order to study the cutting process on hardened AISI 52100 steel) were developed based on the thermal effect – i.e., heat treatments of quenching and. Two simple thermal models based on the hardness modification (ΔHRC) were considered for describing the heat treatments of quenching and tempering, which are associated with white and dark layer formation, respectively. In particular, the hardness modification (ΔHRC) was related with white and dark layer formation since the material behavior in the FE model is described by a hardness-based flow stress. As far as the quenching process (related to white layer formation) is concerned, the empirical model implemented in the FE code by an user subroutine is:

$$\Delta HRC_{quenching} = F\left[\frac{67 - HRC_{initial}}{1030 - T_{AUS}}\right](T - T_{AUS}) \quad (1)$$

where $\Delta HRC_{quenching}$ is the hardness modification due to quenching heat treatment, $HRC_{initial}$ is the initial material hardness, T_{AUS} is the austenite-start temperature, T is the current temperature in the element, 67 represents the highest metallurgical state (in HRC hardness) that can be reached by AISI 52100 when it is quenched in oil starting from 1030°C [159].

In contrast, for the tempering process (associated with the dark layer formation), the empirical model employed is:

$$\Delta HRC_{tempering} = G\left[\frac{HRC_{initial} - HRC_{FT}}{T_{AUS} - T_{DLSTART}}\right](T_{DLSTART} - T) \quad (2)$$

where $\Delta HRC_{tempering}$ is the hardness modification due to tempering heat treatment, HRC_{FT} is the fully tempered material hardness when temperature corresponds to T_{AUS}, $T_{DLSTART}$ is the tempering-start temperature and T is the current temperature in the element.

F and G (which depend on both the investigated material and the initial hardness) will be empirically determined during FE model calibration and their correlation with the material hardness and process parameters will be found by a statistical approach.

Austenite start temperature (T_{AUS}) ranges between 300°C and 650°C (depending on the initial material hardness) according to the experimental results showed in Chapter IV in which the presence of white layer was registered also for surface temperatures below Ac_1 (Figure 5.7).

These experimental observations confirm that there is a reduction of the austenite start temperature.

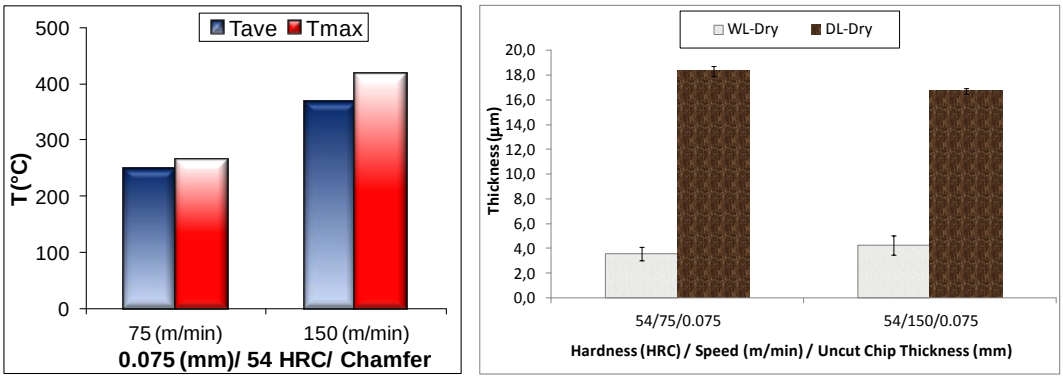

(a) (b)

Figure 5.7 (a) Experimental cutting temperatures on machined surface and (b) corresponding microstructural changes: V = 75 and 150 m/min, f = 0.075 mm/rev, 54 HRC, chamfered tool

In fact the influence of stress and strain reduces the value of the theoretical austenite-start temperature, due to high dislocation density associated with large strain, as observed by Ramesh [160]. Finally, parameter HRC_{FT} was derived from ASM Handbook - Heat Treating [159], in which the variation of hardness with tempering temperature in AISI 52100 is reported. As far as $T_{DLSTART}$ is concerned, it was initially set as illustrated in ASM Handbook [159], then the value was ranged during the FE calibration and the results were analyzed by the statistical approach.

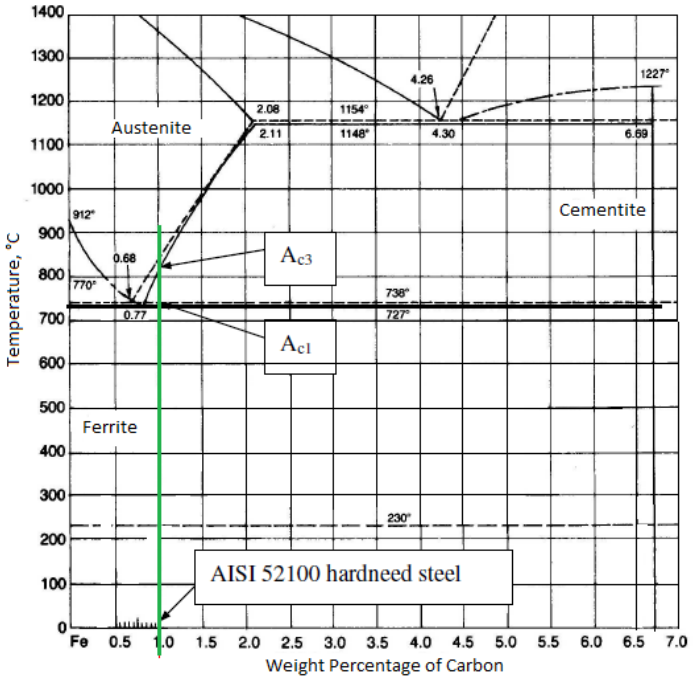

Figure 5.8 Fe-C phase diagram

5.2.2 – PROPOSED NUMERICAL PROCEDURE

The proposed numerical procedure developed employs a FE based thermo-mechanical model formulation of the orthogonal hard turning process. In particular, 2D plane strain simulation was carried out using SFTC Deform 2D®, and it was based on the following assumptions (Figure 5.9):

1. Rigid cutting tool (divided into 3500 elements);

2. Isotropic hardening for workpiece material, modelled as elastic-plastic and divided into 8500 elements;

3. High mesh density was defined on the workpiece. In particular, the elements located around the cutting edge and along the machined surface were 50 times as dense as the other ones (average element edge length on the surface ≈ 5-6 μm);

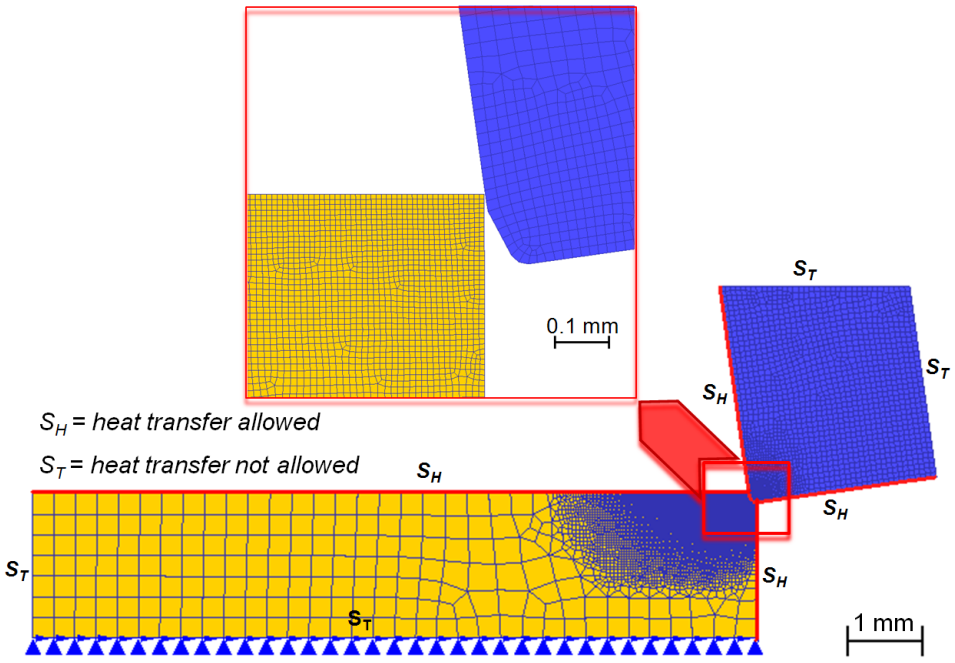

Figure 5.9 Model constrains and assumption

4. Non–isothermal elastic–viscoplastic material governed by incremental theory of plasticity and Von Mises yield condition. A hardness-based flow stress rule [134] was implemented in the FE code as the material constitutive law:

$$\sigma(\varepsilon,\dot{\varepsilon},T,HRC)=B(T)\left(C\varepsilon^{n}+J+K\varepsilon\right)\left[1+\left(\ln(\dot{\varepsilon})^{m}-A\right)\right] \quad (3)$$

where *B* is the temperature dependant factor, *C* represents the work hardening coefficient, *J* and *K* are two linear functions of hardness, and *A* is a factor related to a reference strain rate;

5. Brozzo's fracture criterion [161] was used to predict the effect of the stress on the chip segmentation during orthogonal cutting;

6. Constant shear stress on the tool chip interface model ($\tau=m\tau_0$) was implemented in the FE model, setting m=0.9 (estimated in [162]). In the mentioned equation, τ is the shear stress and τ_0 the flow shear stress obtained as $\tau_0=\sigma_0/\sqrt{3}$;

7. As regards the global heat transfer coefficient at the tool-chip-workpiece interfaces, a constant value of 28 kW/(m^{2}K) was set in the FE model [162].

8. Finally, as far the microstructure changes are concerned, the two previous proposed thermal models based on the hardness modification (*ΔHRC*) were considered to describe the heat treatments of quenching and tempering, which are associated with white and dark layer formation, respectively. In particular, the hardness modification (*ΔHRC*) was related to white and dark layer formation since the material behaviour in the FE model is described by a hardness-based flow stress.

Lastly, the proposed updating strategy implemented in the FE code in order to simulate the material microstructure changes is reported in Figure 5.10: each element undergoes quenching or tempering depending on its temperature calculated during FE simulation. If temperature is higher than T_{AUS}, Equation 1 is invoked. On the other hand, if temperature ranges between T_{AUS} and $T_{DLSTART}$, Equation 2 is invoked.

Actually, quenching phenomenon is physically non-diffusive, thus it is scientifically rigorous to simply apply Equation 1, if the hypothesis of fast cooling is consistent. In contrast, tempering phenomenon is here empirically modeled in order to obtain a consistent relationship based on the current temperature.

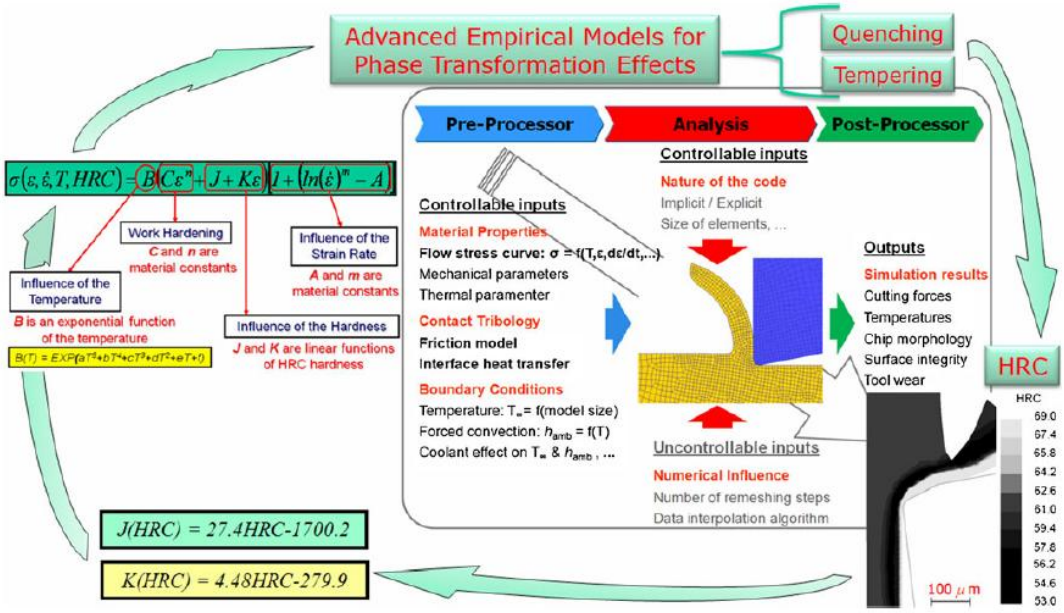

Figure 5.10 FE model to simulate white and dark layers formation in machining

It is important to emphasize that the temperature is checked at each time step in the simulation and for each element of the workpiece in order to update the current element hardness. The latter is stored before the next simulation step. Furthermore, it is also important to highlight that if the hardness variation happens, the material strength is locally different (harder or softer) than the bulk material, reflecting the reality of machining process.

5.3 – RESIDUAL STRESS ANALYSIS

The proposed FE strategy was, finally, used to predict the residual stresses evolution in the workpiece after machining. A manual routine is required at this stage since, using DEFORM-2D^{TM}, is not possible to obtain directly the numerical residual stresses. Therefore, the follow procedure was used:

1. an elastic-visco-plastic analysis was implemented for the investigated machining cases and it was executed for a total time long enough to reach the steady-state condition;

2. for several time steps, the tool was released from the machined surface (unloading phase) and the workpiece was cooled down to the room temperature; and

3. residual stress profiles at several locations of the machined surface were collected and the average values were calculated, as described in [163].

Concerning the third point, a deeper description is needed: in order to avoid the influence of chip formation on residual stresses, they should be extracted from the FE model far away from the chip formation zone. After tool relaxation, residual stress profile is plotted and the region is chosen correspondingly to its stabilized value (Figures 5.11).

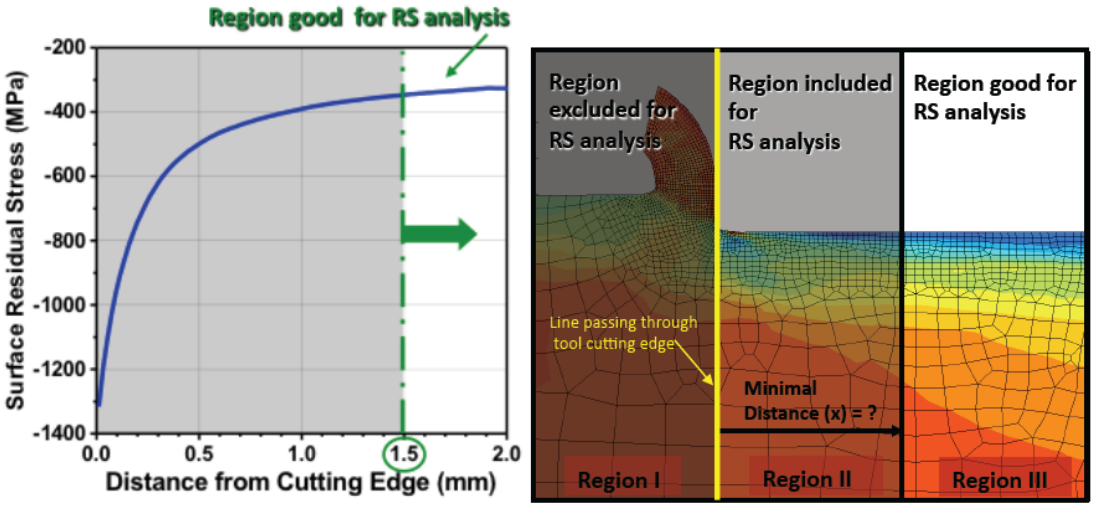

Figure 5.11 Chosen region for RS analysis

In addition, since by XRD the measured residual stresses are averaged over a finite volume of the work material, the predicted residual stresses should be also averaged over the same volume and the mean value should be taken (Figure 5.12).

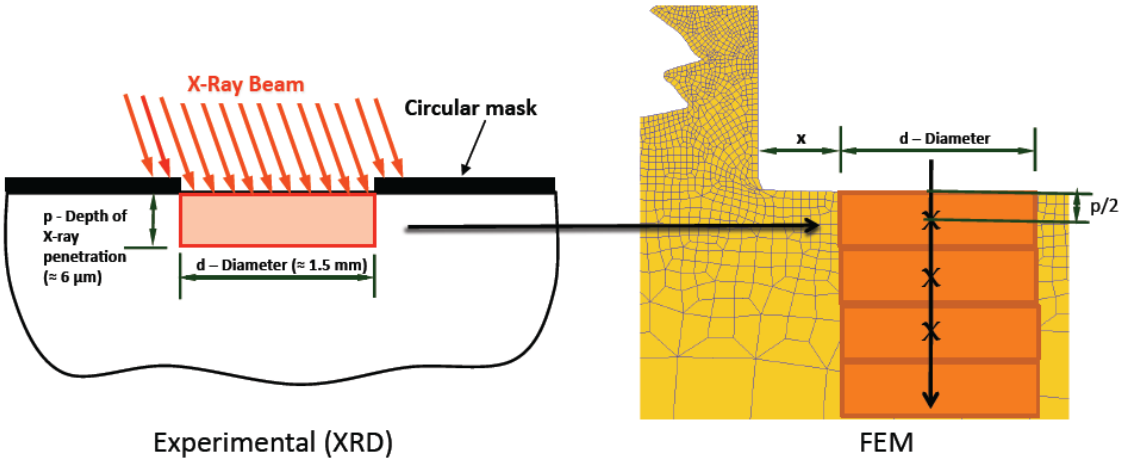

Figure 5.12 RS averaged over the chosen region

5.4 – SUMMARY

In this paragraph an FE model for studying the hard turning process in terms of white and dark layers formation and residual stress is developed and presented. For the microstructural changes, two empirically built equations were proposed. These equations, as well as the entire FE model, will be calibrated and validated, in the next Chapter VI using a wide range of experimental observations.

CHAPTER VI

NUMERICAL AND EXPERIMENTAL COMPARISON

In this chapter the detailed description of the proposed numerical models for white and dark layers prediction is carried out. Particularly the FE model will be calibrated and then validated using the wide range of experimental observations obtained in previous researches and also found in this study. An iterative procedure capable to predict the white and dark layers formation and their thickness in function of cutting conditions (i.e. cutting speed, feed rate, depth of cut) as well as of the initial workpiece hardness and tool geometry will be utilized. In addition a numerical approach will also be applied to evaluate the correlation between the process parameters and initial hardness with the coefficients of the two advanced empirical models. Finally, the proposed FE strategy will be used for investigating the microstructural changes formation and their control and evaluation as well as their influence on the residual stress profile.

6.1 – FE CALIBRATION

The calibration strategy was carried out by means of a Finite Element Analysis (FEA) of machining process for a range of cutting speeds, feed rates and workpiece hardness values, and by comparing the predicted results with those experimentally found in literature and other performed in the present work (Table 4.1).

The aim of this calibration phase was to empirically determine the coefficients F, G, T_{AUS} and TDL_{START} to be set in the thermal-based white and dark layer models implemented by user-subroutine in the commercial FE code Deform 2D utilized for the FE model calibration.

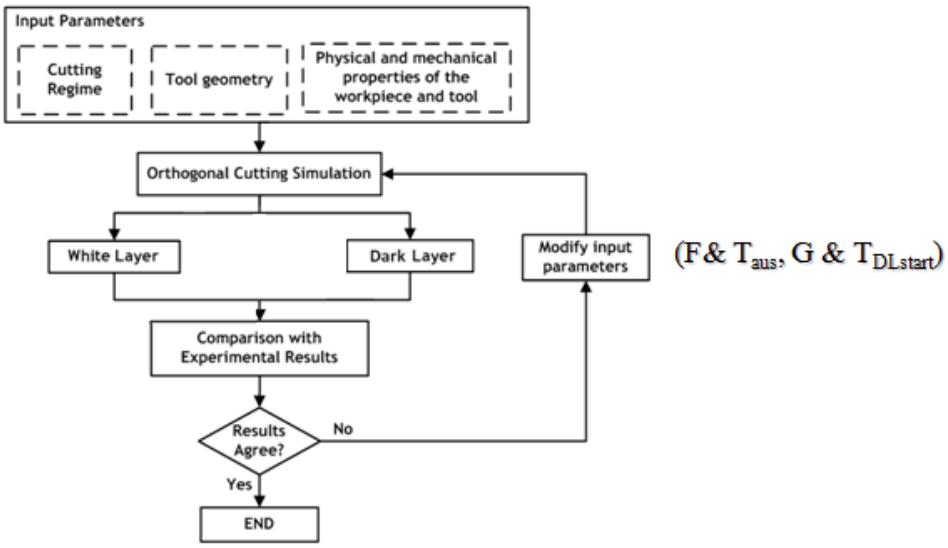

Figure 6.1 Iterative procedure for calibration phase

After created the numerical model in Deform 2-D: tool and workpiece geometries with respective physical and mechanical properties and boundary conditions, the calibration strategy reported in Figure 6.1 was implemented. A "*Trial and Error"* procedure, for each single experimental case, in which the right value of the four coefficients is found when a very low relative error is reached between the experimental results and the numerical one.

The calibration procedure was conducted for some of the experimental results observed in this study. In Figures 6.2 and 6.3 the calibration results between measured and predicted thicknesses of white and dark layers are reported.

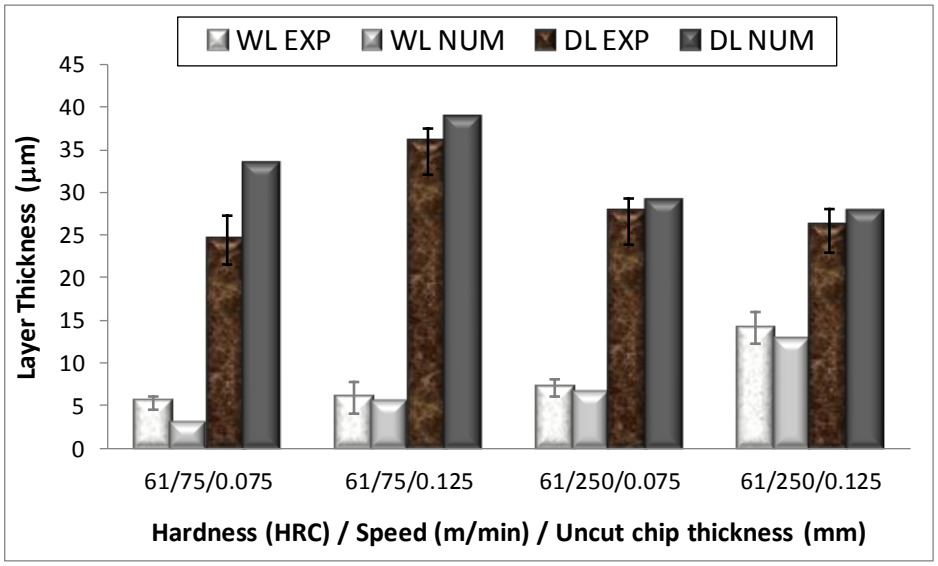

Figure 6.2 White and dark layers formation: comparison of the experimentally measured layers thickness with the numerically predicted (tests at 61 HRC)

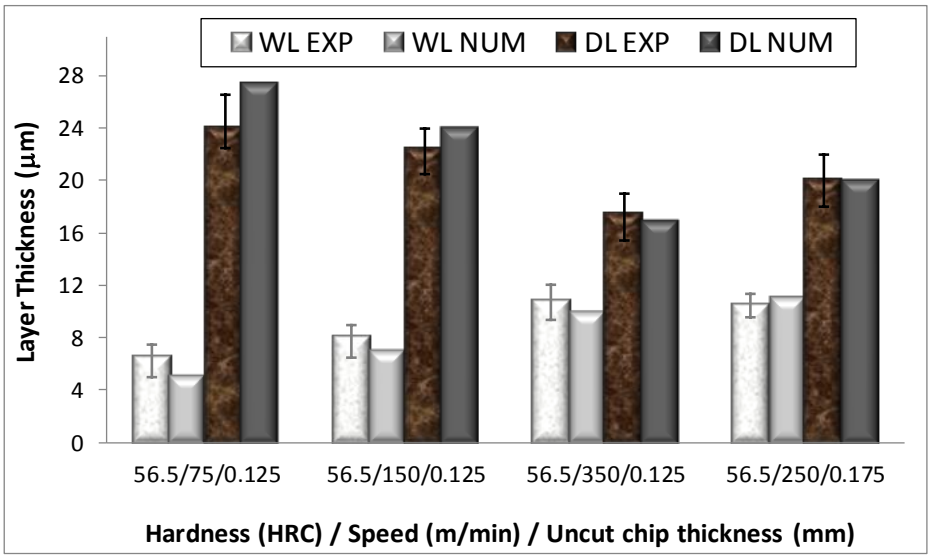

Figure 6.3 White and dark layers formation: comparison of the experimentally measured layers thickness with the numerically predicted (tests at 56.5 HRC)

Observing these results, it is evident the good agreement reached for both white and dark layers thickness.

Figures 6.4 and 6.5 show the calibration results concerning the cutting forces.

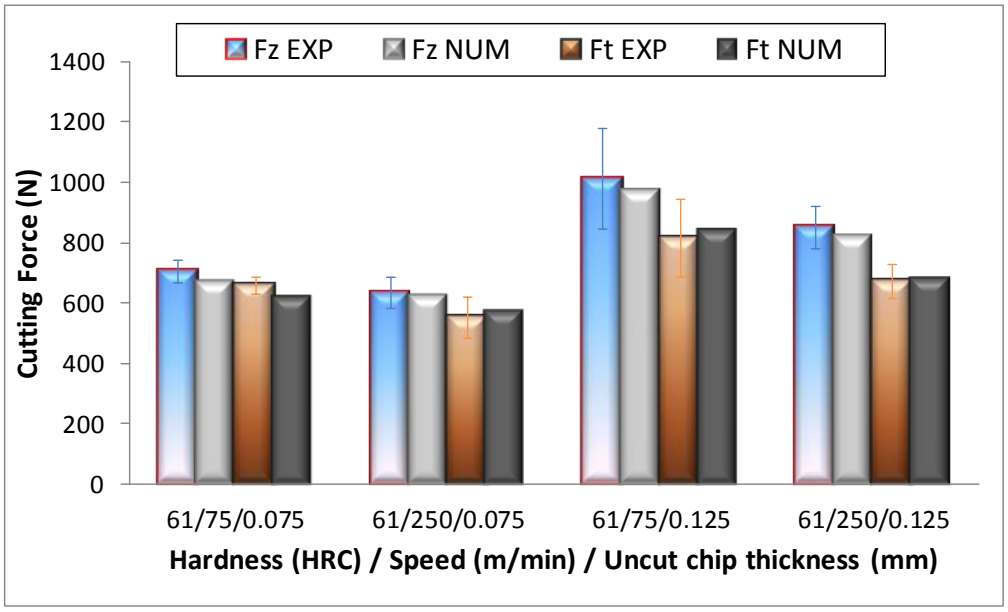

Figure 6.4 Comparison of the experimentally measured with the numerically predicted cutting forces (tests at 61 HRC)

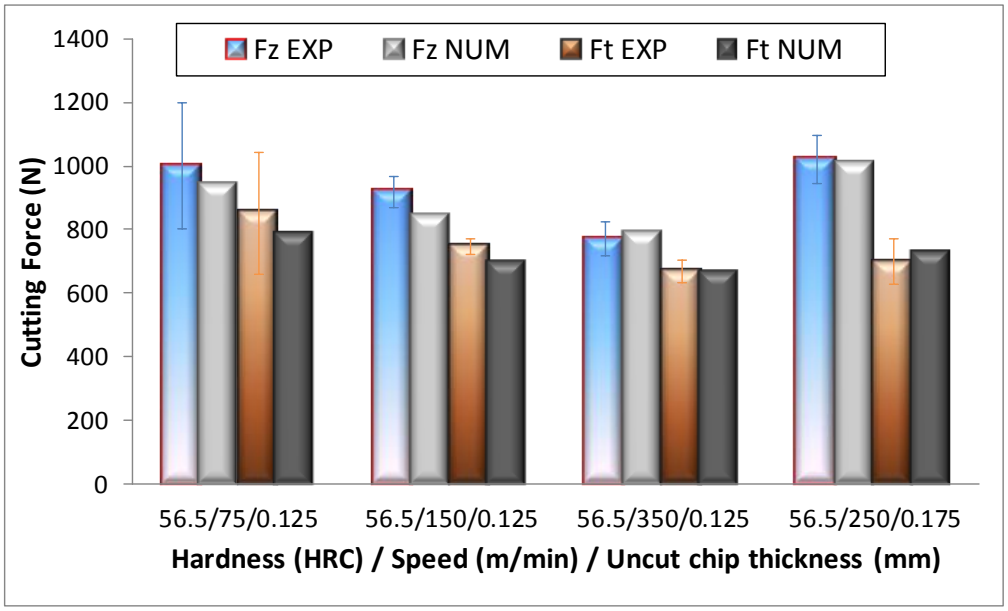

Figure 6.5 Comparison of the experimentally measured with the numerically predicted cutting forces (tests at 56.5 HRC)

Also in this case a good agreement was reached at the end of the calibration.

In Figures 6.6 and 6.7 the comparison between numerical and experimental results of the parameter $HRC_{mod}/HRC_{initial}$ is reported.

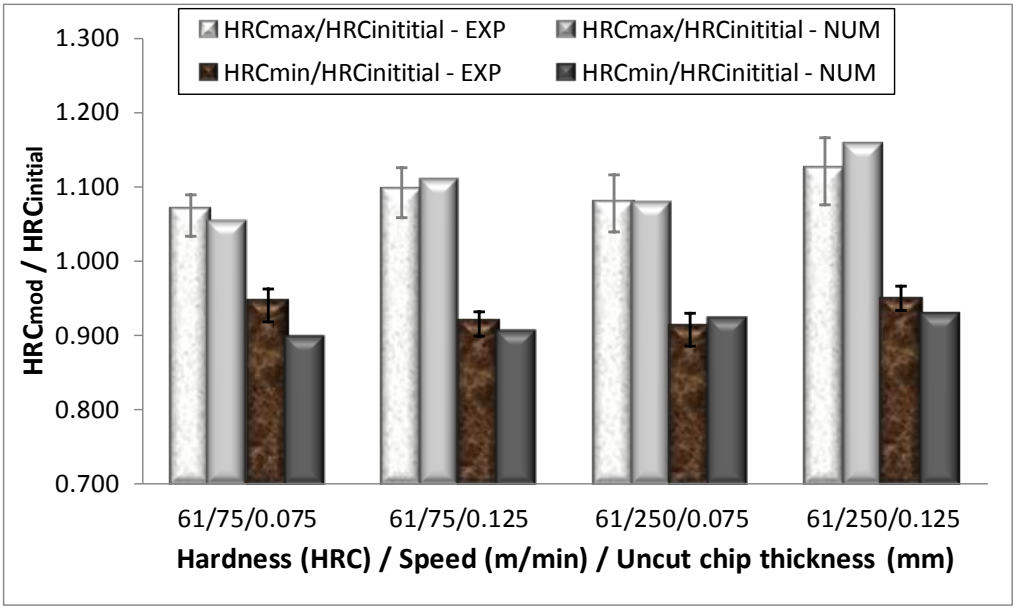

Figure 6.6 Comparison of the experimentally measured with the numerically predicted hardness modification (tests at 61 HRC)

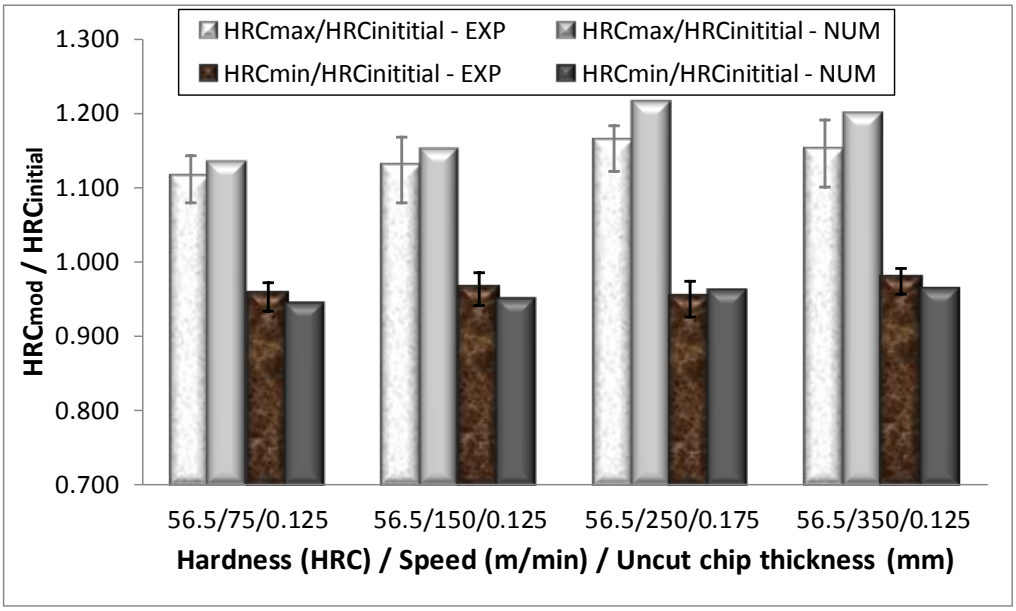

Figure 6.7 Comparison of the experimentally measured with the numerically predicted hardness modification (tests at 56.5 HRC)

Furthermore three different cases were taken into account from literature: Guo and Sahni [164], Poulachon et al [26], and Han, [103].

The conditions for the first numerical case were set equal to the experimental conditions employed by Guo and Sahni [164], in which the cutting conditions were: cutting speed = 169.2 m/min and uncut chip thickness = 0.2 mm. The cutting tool material was high-content CBN with a chamfered tool edge (20°x0.1mm). The tool holder reproduced a rake angle of -6° and a clearance angle of 6°. Finally, the initial hardness of the workpiece (AISI 52100 steel) specimen was 63 HRC. Figure 6.8 and 6.9 report the calibration results, including the relative errors between the measured and estimated thicknesses of both white and dark layers and the comparison of the near-surface hardness (Figure 6.9). These numerical results refer to the final iterative step in the calibration procedure, in which the values of coefficients F, G, T_{AUS} and $T_{DLSTART}$ were found equal to 15, 1, 650°C and 200°C, respectively.

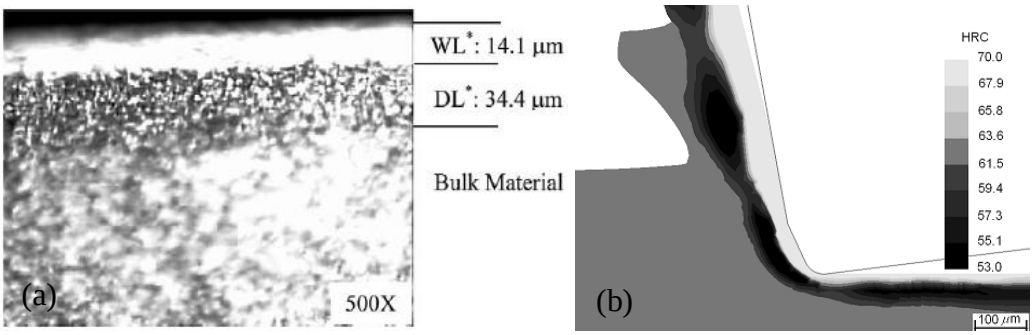

Figure 6.8 White and dark layers formation: (a) observed [164] and (b) predicted

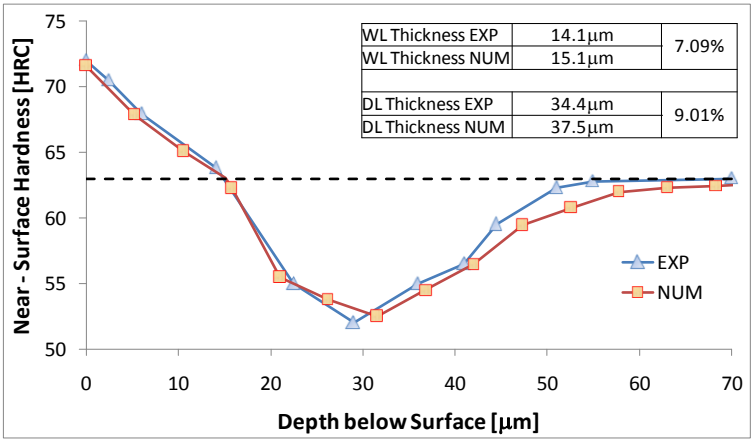

Figure 6.9 White and dark layers formation: comparison of the experimentally measured near-surface hardness profile with the numerically predicted and the absolute error between predicted and measured layers thickness

The second case for model calibration was based on the experimental observations made by Poulachon et al [26], where an AISI 52100 specimen (61HRC) was orthogonally machined using a high-content CBN tool with a chamfer of 20°x0.1mm. The cutting parameters were 100 m/min as cutting speed and 0.1 mm as uncut chip thickness. Figure 6.10 and 6.11 show the calibration results, including the relative errors between the measured and estimated thicknesses of both white and dark layers and the comparison of the near-surface hardness (Figure 6.11). The values of coefficients F, G, T_{AUS} and $T_{DLSTART}$ found at the end of the calibration were equal to 13, 0.6, 650°C and 200°C, respectively.

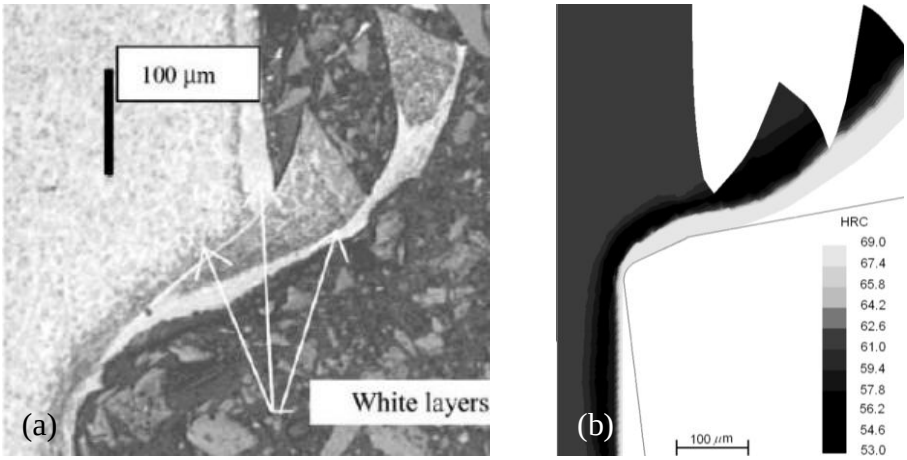

Figure 6.10 White and dark layers formation: (a) observed [26] and (b) predicted

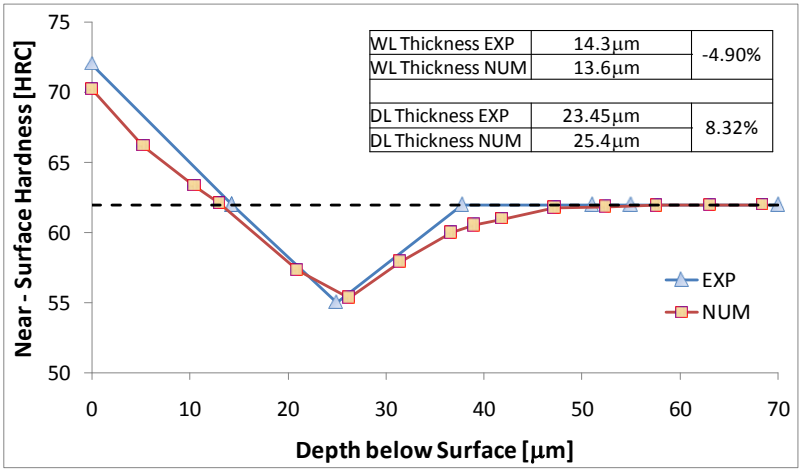

Figure 6.11 White and dark layers formation: comparison of the experimentally measured near-surface hardness profile with the numerically predicted and the absolute error between predicted and measured layers thickness

Finally, for the third case considered from literature, the experiment conducted by Han [103] was reproduced by FE simulation. In particular, the cutting speed and the uncut chip thickness were set equal to 100 m/min and 0.1 mm, respectively. The cutting tool material was a low-content CBN with an up-sharp edge (R = 0.03 mm) mounted on a tool holder characterized by a rake angle of 0° and a clearance angle of 6°. The initial hardness of the AISI 52100 specimen was 53 HRC. In Figure 6.12 and 6.13 the calibration results and the relative errors between measured and predicted thicknesses of white and dark layers are illustrated (Figure 6.13). The values of parameters F, G, T_{AUS} and $T_{DLSTART}$ were found to be 10, 0.4, 550°C and 385°C, respectively.

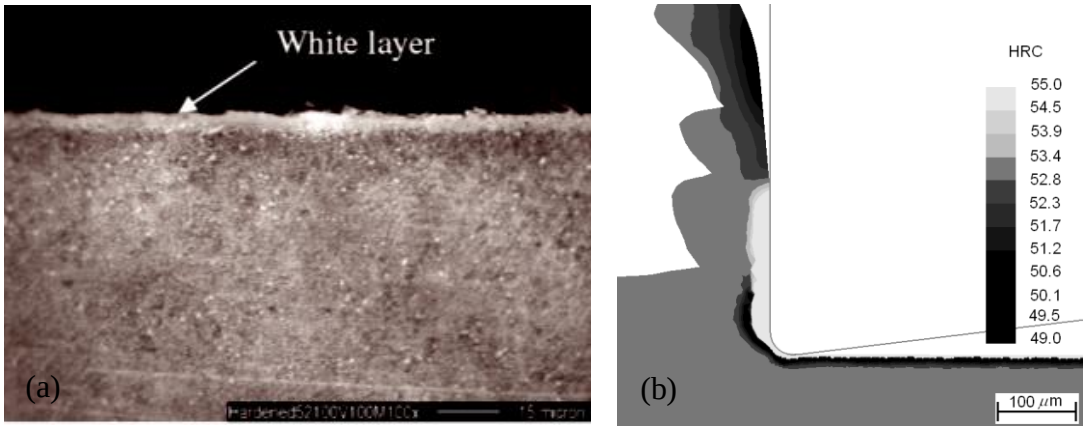

Figure 6.12 White and dark layers formation: (a) observed [103] and (b) predicted

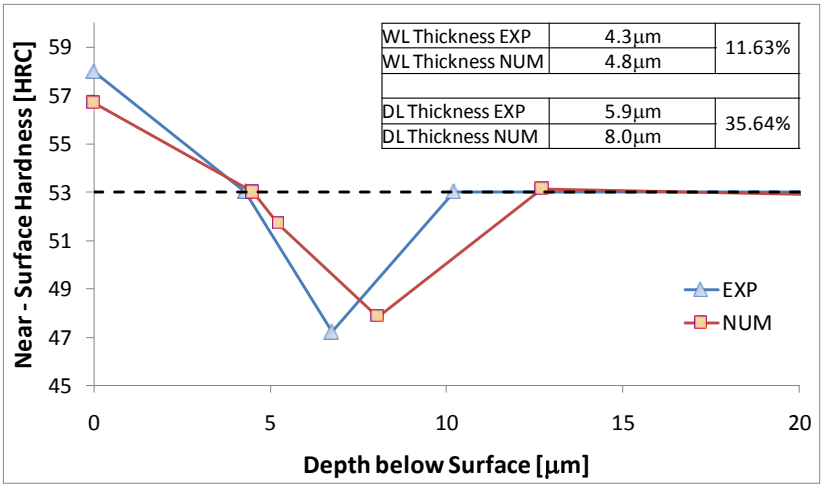

Figure 6.13 White and dark layers formation: comparison of the experimentally measured near-surface hardness profile with the numerically predicted and the absolute error between predicted and measured layers thickness

The good agreement between numerical and experimental results, found for all the investigated cases and parameters, suggests that the model development and calibration procedure is sufficiently robust for prediction of white layer thickness within the range of conditions employed here.

In Table 6.1 are reported all the experimental cases used in the calibration phase with the corresponding values of the four constants incorporated in the two empirical equations for hardening and tempering phenomena.

HRC	Speed (m/min)	Feed (mm/rev)	F	G	T_{AUS} (°C)	$T_{DLSTART}$ (°C)
53.0	100	0.1	10	0.4	550	385
56.5	75	0.125	10.8	0.58	580	350
61.0	75	0.125	11.5	0.6	600	230
62.0	100	0.1	13	0.6	650	200
63.0	169.2	0.2	15	1	650	200
61.0	250	0.125	12.5	0.75	620	230
56.5	150	0.125	9.7	0.55	600	340
56.5	350	0.125	9.2	0.62	620	345
61.0	75	0.075	12.95	0.45	550	235
61.0	250	0.075	12.87	0.6	565	230
56.5	250	0.175	8	0.6	650	360

Table 6.1 Experimental conditions used for FE model calibration

Taking into account these results (Table 6.1) the coefficients of the empirical models can be determined by using a regression analysis. Thus, robust equations for predicting the value of the empirical constants F, G, T_{AUS} and $T_{DLSTART}$ varying the process conditions can be found.

In detail the analysis of the historical data (cutting conditions and corresponding empirical coefficients values, Table 6.1) was applied to evaluate the influence of the single factors and theirs interactions on the empirical constants in the form of the following equation:

$$(F, G, T_{AUS}, T_{DLSTART}) = f\ (HRC, \text{cutting speed}, \text{feed rate}) \qquad (1)$$

Equations 2, 3, 4, 5 report the correlations obtained from the statistical approach:

$$F=a_o+a_1 HRC+a_2 V+a_3 f+a_4 (HRC*V)+a_5 (HRC*f)+a_6 (V*f) \quad (2)$$

$$G=b_o+b_1 HRC+b_2 V+b_3 f+b_4 (HRC*V)+b_5 (HRC*f)+b_6 (V*f) \quad (3)$$

$$T_{AUS}=c_o+c_1 HRC+c_2 V+c_3 f \quad (4)$$

$$T_{DLSTART}=d_o+d_1 HRC+d_2 V+d_3 f+d_4 (HRC*V)+d_5 (HRC*f)+$$
$$+d_6 (V*f)+d_7 HRC^2+d_8 V^2+d_9 f^2 \quad (5)$$

Coefficients associated with the constants contained in Equations 2, 3, 4 and 5 are reported in Table 6.2.

F		*G*	
a_0	5.304 E+01	b_0	1.142 E+00
a_1	-6.396 E-01	b_1	-1.772 E-02
a_2	-1.069 E-01	b_2	-3.179 E-03
a_3	-4.849 E+02	b_3	-1.248 E+01
a_4	1.639 E-03	b_4	7.839 E-05
a_5	7.683 E+00	b_5	2.735 E-01
a_6	8.065 E-02	b_6	-7.987 E-03

Taus		$T_{DLSTART}$	
c_0	2.816 E+02	d_0	-3.381 E+03
c_1	3.787 E+00	d_1	1.521 E+02
c_2	9.478 E-02	d_2	-7.542 E-01
c_3	6.724 E+02	d_3	-4.530 E-01
		d_4	8.920 E-03
		d_5	-7.930 E+00
		d_6	1.580 E+00
		d_7	-1.510 E+00
		d_8	4.930 E-04
		d_9	4.470 E+03

Table 6.2 Coefficients derived by historical data analysis and used to define the empirical constants in the quenching and tempering empirical models

6.2 – FE VALIDATION

The FE model, with empirical constants calibrated using the experimental data of Guo and Sahni [164], Poulachon et al [26] and Han [103] and others carried out in this study, will now validated by comparing numerical predictions from FE simulations with further experimental results found in references [118, 160, 103] and the remaining conditions reported in Table 4.1 not utilized during the calibration, for white layer and dark layer formation under different cutting speeds, uncut chip thicknesses and initial material hardness values.

The coefficients to be set in the empirical equations for hardening and tempering effects were obtained, for each single analyzed case, from Equations 2, 3, 4 and 5.

Concerning the other experiments, carried out in the present work, a comparison of experimentally determined forces and predicted values is shown in Figure 6.14, 6.15, 6.16. It can be observed that a good correlation is obtained since the maximum prediction error is less than 10% for both cutting and thrust forces and, as general trend, it can be noted as the machining forces decrease with cutting speed, while rapidly increase with the feed rate.

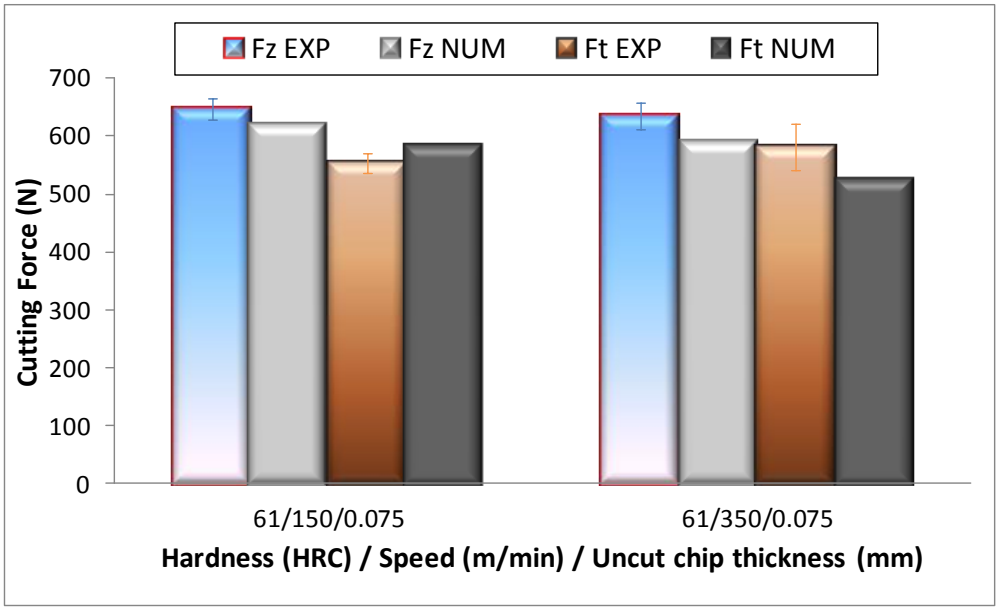

Figure 6.14 Comparison of experimental and predicted cutting forces (Fz principal cutting force, Ft thrust force) varying cutting speed (tests at 61 HRC)

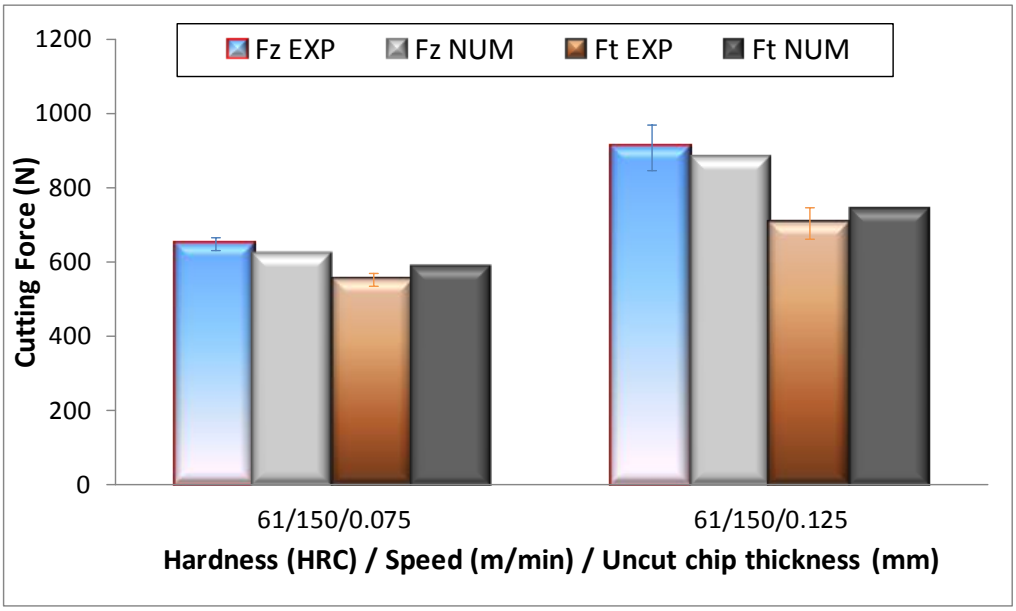

Figure 6.15 Comparison of experimental and predicted cutting forces (Fz principal cutting force, Ft thrust force) varying feed rate (tests at 61 HRC)

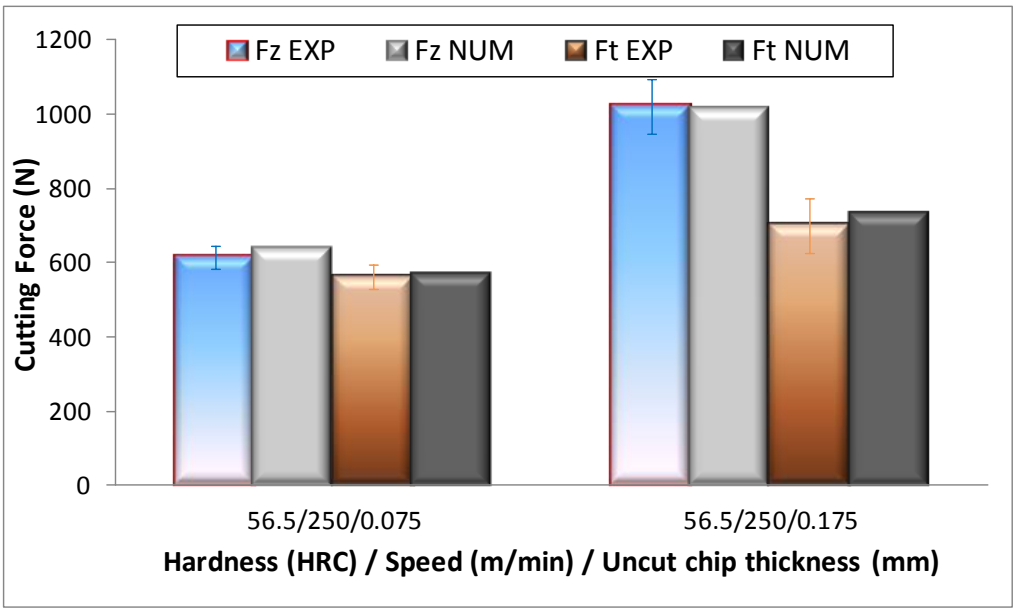

Figure 6.16 Comparison of experimental and predicted cutting forces (Fz principal cutting force, Ft thrust force) varying feed rate (tests at 56.5 HRC)

From Figure 6.17 to Figure 6.20 the comparison of the experimentally measured white and dark layers thickness with those numerically predicted is reported.

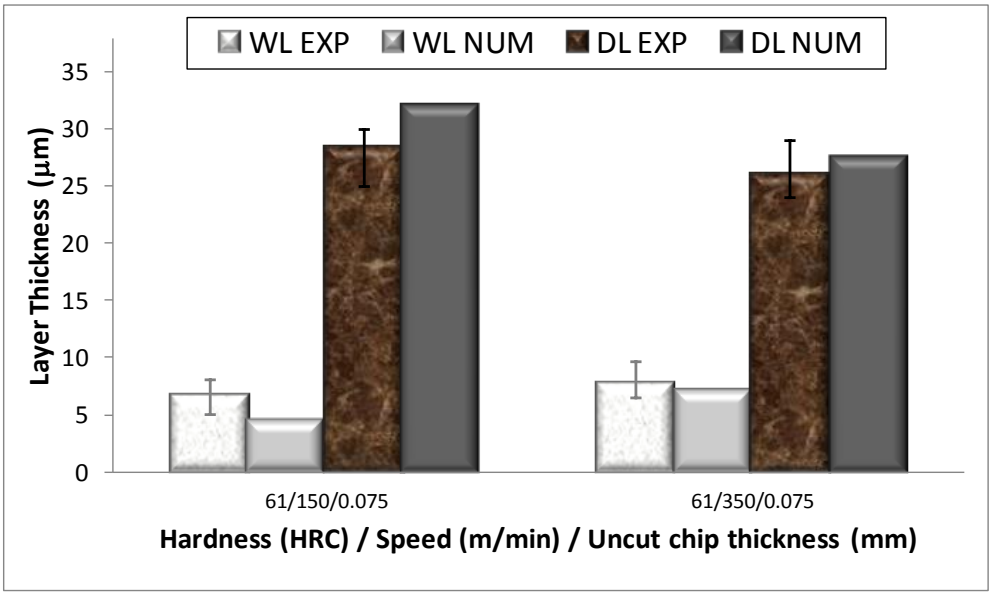

Figure 6.17 White and dark layers formation: comparison of the experimentally measured with the numerically predicted varying cutting speed (test with the chamfered tool)

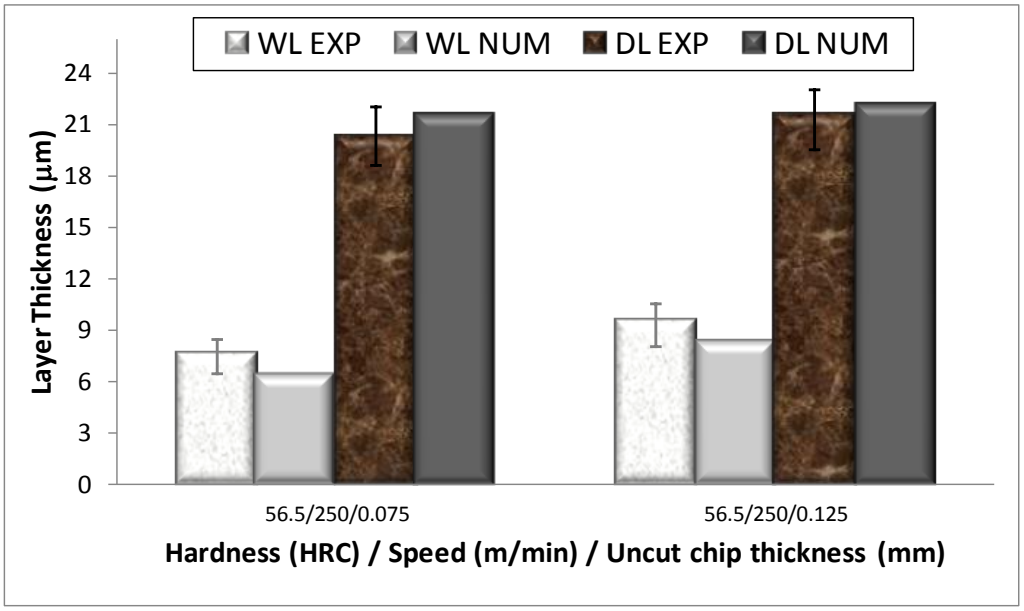

Figure 6.18 White and dark layers formation: comparison of the experimentally measured with the numerically predicted varying feed rate (tests with the chamfered tool)

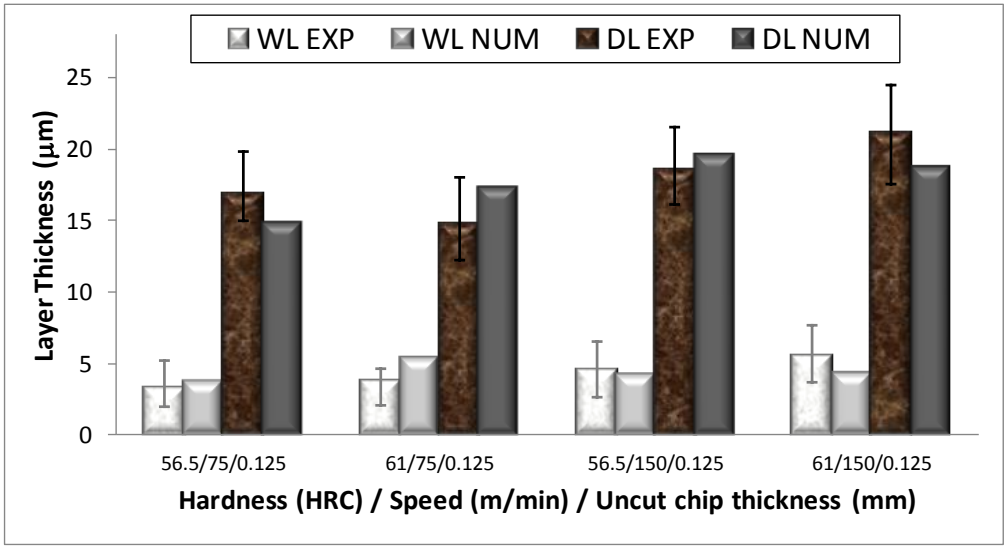

Figure 6.19 White and dark layers formation: comparison of the experimentally measured with the numerically predicted varying initial workpiece hardness (tests with the honed tool)

Observing these results, it is evident the good agreement for both white and dark layers prediction. Moreover, once more the results reported in Figure 6.17 show that white layer increases with increasing the cutting speed; in contrast dark layer decreases.

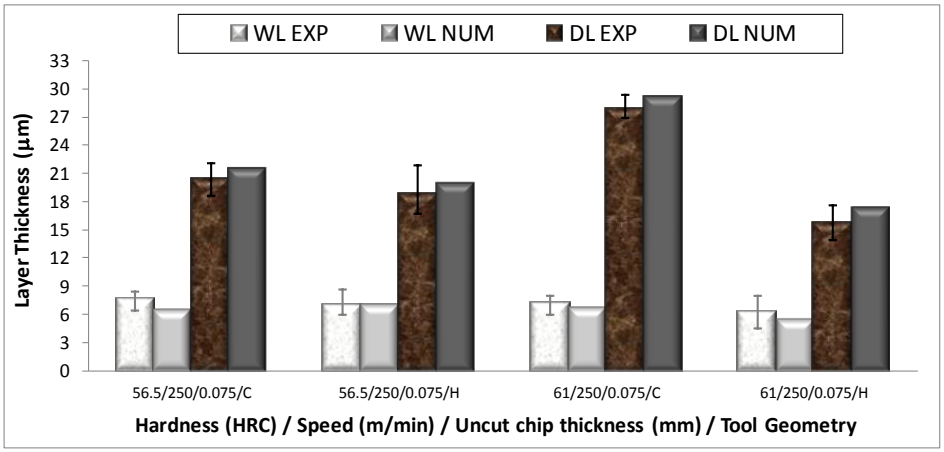

Figure 6.20 White and dark layers formation: comparison of the experimentally measured with the numerically predicted varying tool geometry

Figures 6.21, 6.22 and 6.23 show the comparison between the experimentally measured Rockwell C (HRC) hardness variation in both the machined surface and dark layer and those predicted. Also in this case, the good agreement is evident. Furthermore, the results confirm as a hardness variation is expected since the white layer is much

harder than the bulk material, while the dark layer is softer than the bulk material. Moreover, it is important to underline as parameter HRC_{max}/ $HRC_{initial}$ increases with increasing of the cutting speed. Similar results were obtained by Poulachon et al [14].

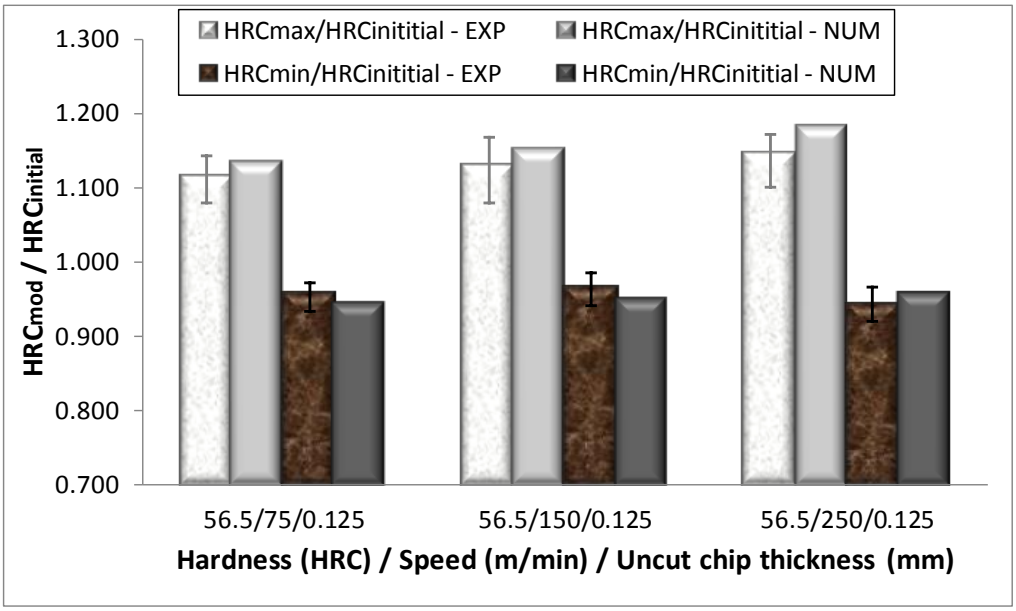

Figure 6.21 Simulative and experimental hardness modification varying cutting speed (tests with the chamfered tool)

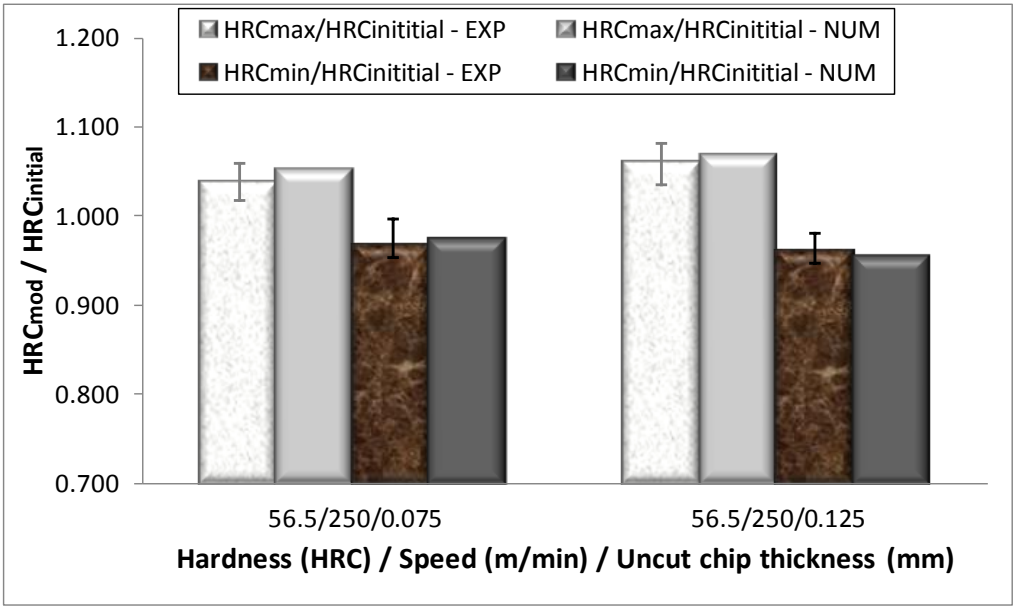

Figure 6.22 Simulative and experimental hardness modification varying feed rate (tests with the chamfered tool)

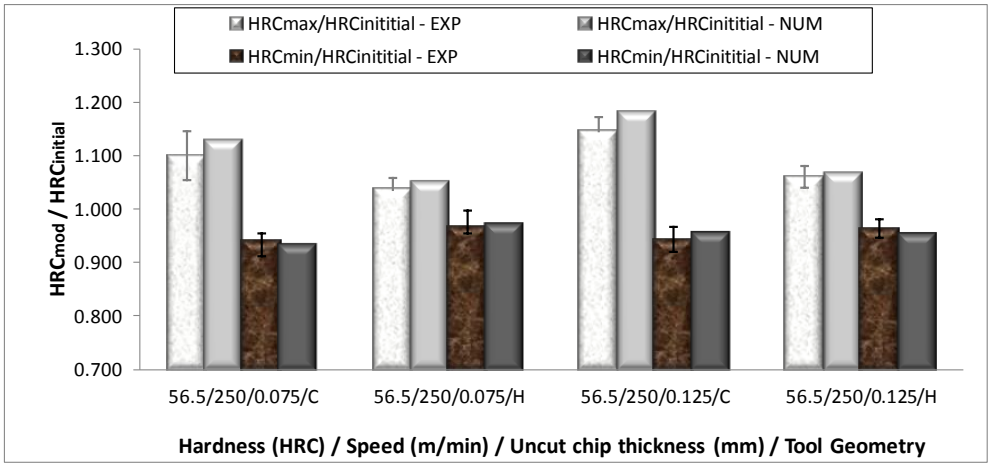

Figure 6.23 Simulative and experimental hardness modification at varying of tool geometry (tests with the honed tool)

Finally Figures from 6.24 to 6.31 show the validation results between the measured and predicted thicknesses of both white and dark layers and the comparison of the near-surface hardness for four of the cases chosen from literature.

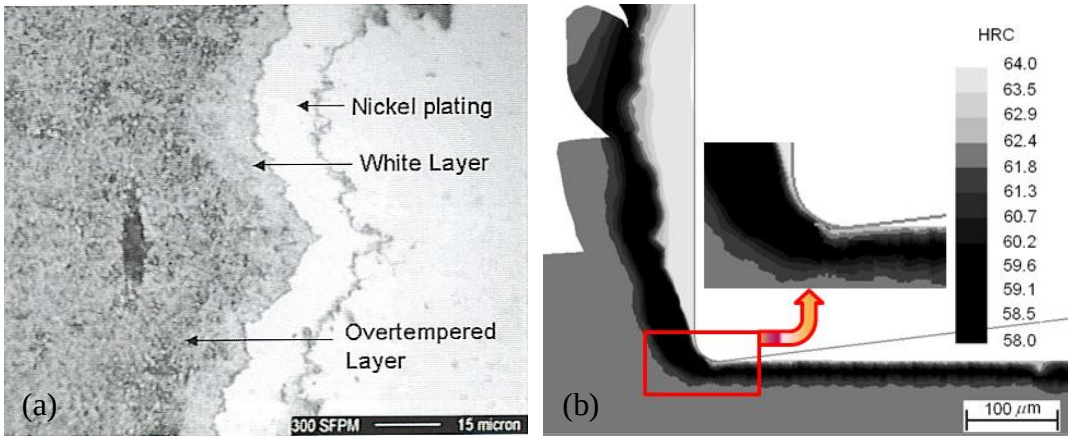

Figure 6.24 White and dark layers formation: (a) observed [160] and (b) predicted, V=91.44 m/min

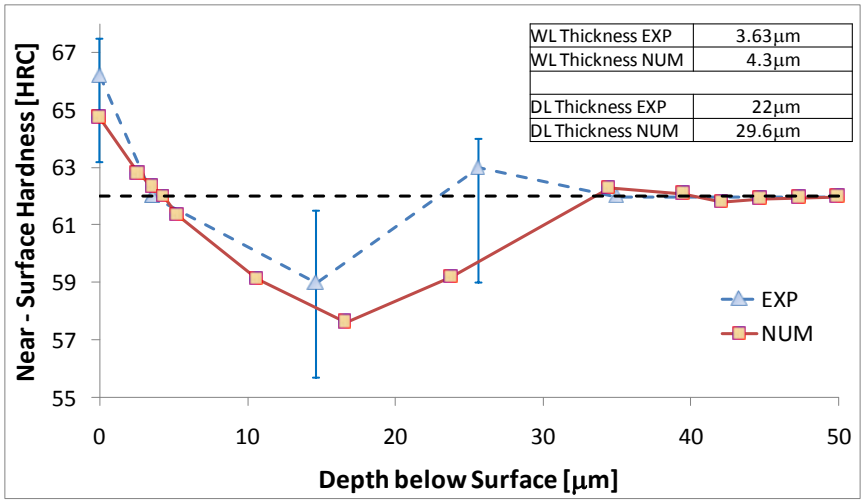

Figure 6.25 White and dark layers formation: comparison of the experimentally measured [160] with the numerically predicted near-surface hardness profile and layers thickness, V=91.44 m/min

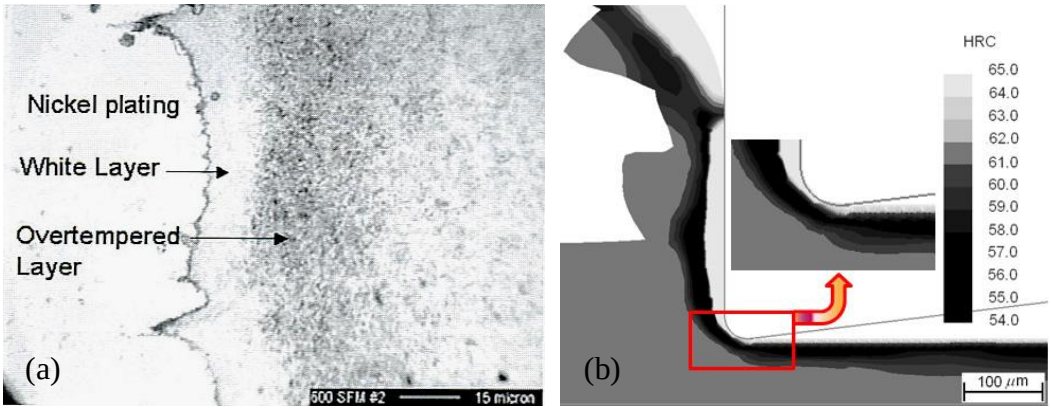

Figure 6.26 White and dark layers formation: (a) observed [160], and (b) predicted, V=182.88 m/min

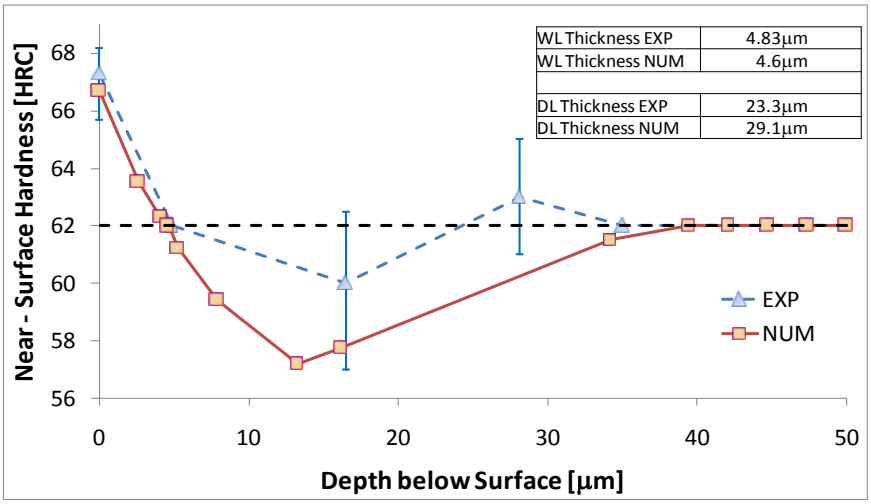

Figure 6.27 White and dark layers formation: comparison of the experimentally measured [160] with the numerically predicted near-surface hardness profile and layers thickness, V=182.88 m/min

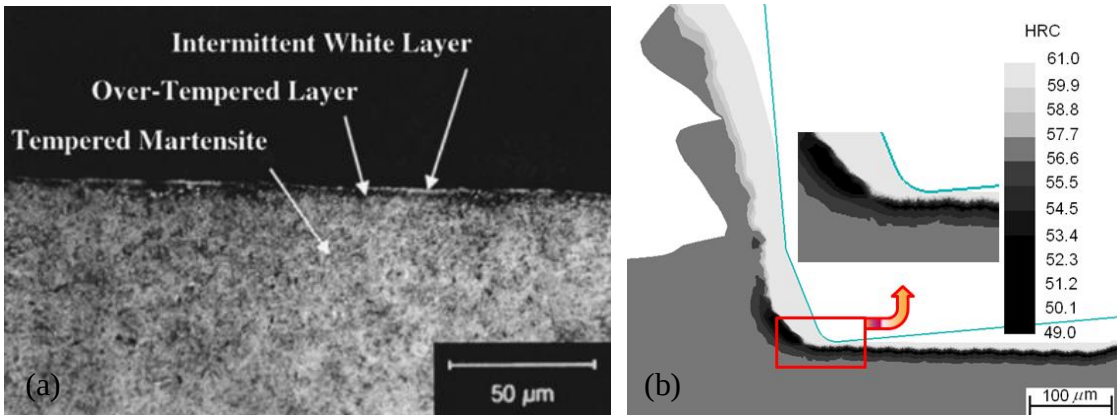

Figure 6.28 White and dark layers formation: (a) observed [118] and (b) predicted

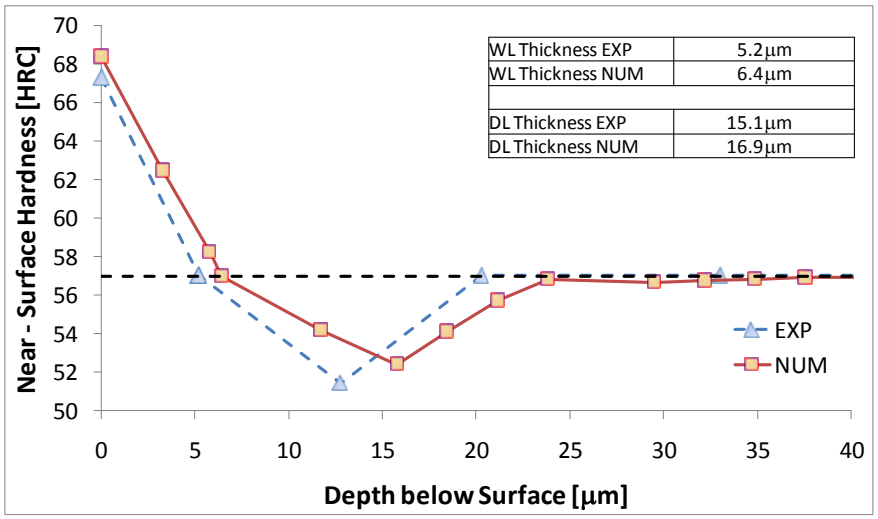

Figure 6.29 White and dark layers formation: comparison of the experimentally measured [118] with the numerically predicted near-surface hardness profile and layers thickness

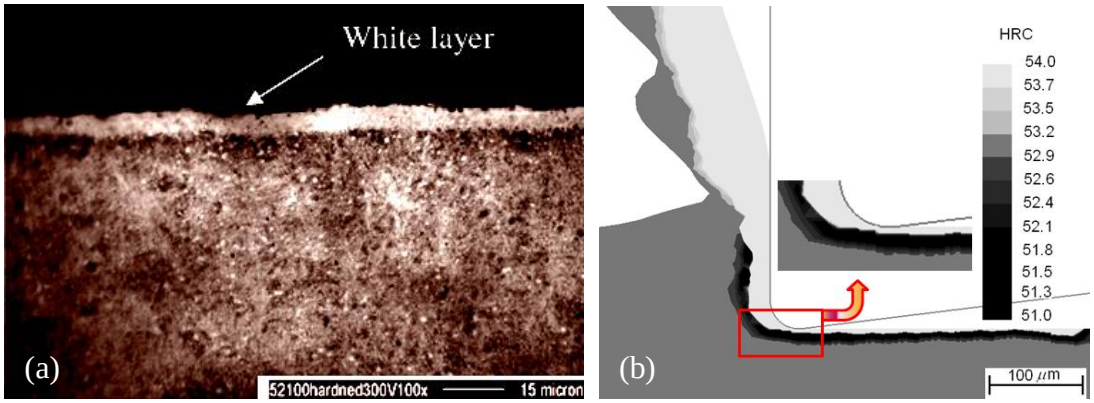

Figure 6.30 White and dark layers formation: (a) observed [103], and (b) predicted

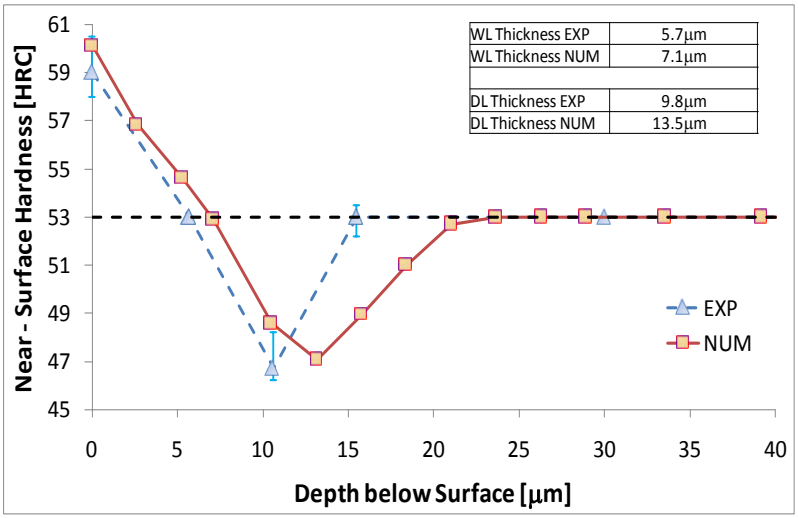

Figure 6.31 White and dark layers formation: comparison of the experimentally measured [103] with the numerically predicted near-surface hardness profile and layers thickness

As observed from Figures 6.24 - 6.31, the predicted results show a good agreement with the corresponding experimentally measured values and trends for the investigated cases found in literature.

6.3 – FE ANALYSIS

Depending on the good predictive quality of the developed numerical models, in both the calibration and validation phases, it is possible by an FE analysis to study the reasons that lead to have the above reported numerical and experimental trends of both white and dark layers in function of the cutting speed. The reasons of those trends are related to both the heat-affected zone (HAZ) and the relative maximum temperature.

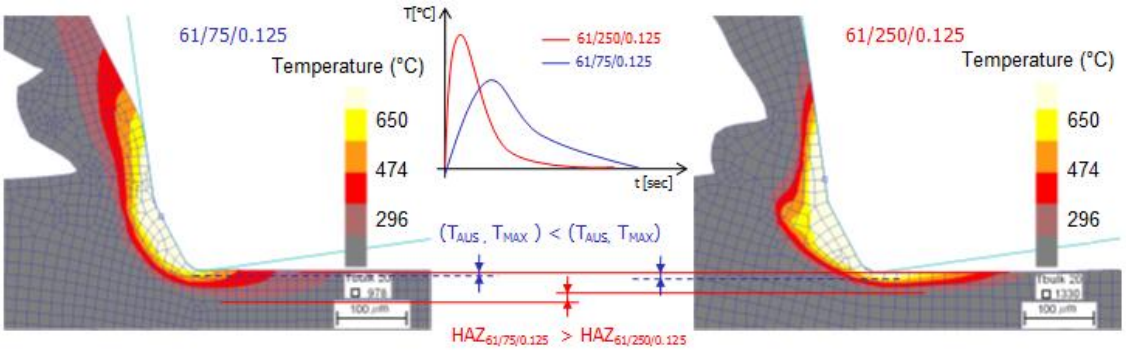

Figure 6.32 Influence of cutting speed on both temperature and heat-affected zone (HAZ)

As depicted in Figure 6.32, it is well known that temperature rises with the cutting speed while HAZ decreases. Therefore, when severe cutting velocities are utilized, deeper zones in which temperature is higher than T_{AUS} can be observed; thus higher white layers thickness is recognized. In contrast, due to smaller HAZ thickness, the region where temperature ranges within T_{AUS} and $T_{DLSTART}$ is reduced, consequently a reduced amount of overtempered martensite (dark layer) can be observed.

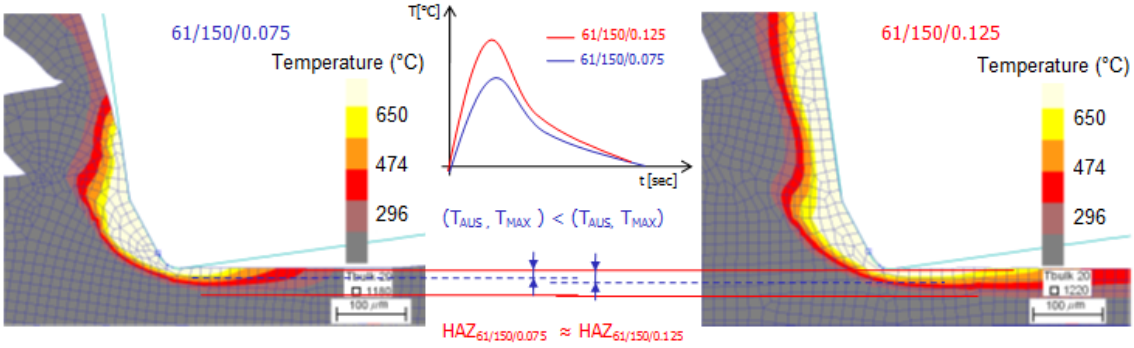

Figure 6.33 Influence of feed rate on both temperature and heat-affected zone (HAZ)

Same considerations can be done for the influence of the feed rate on white and dark layers formation: combination of similar heat-affected zone and higher temperatures (Figure 6.33) lead to have higher thickness of the white layer and lower thickness of the overtempered martensite (dark layer) at increasing of feed rate.

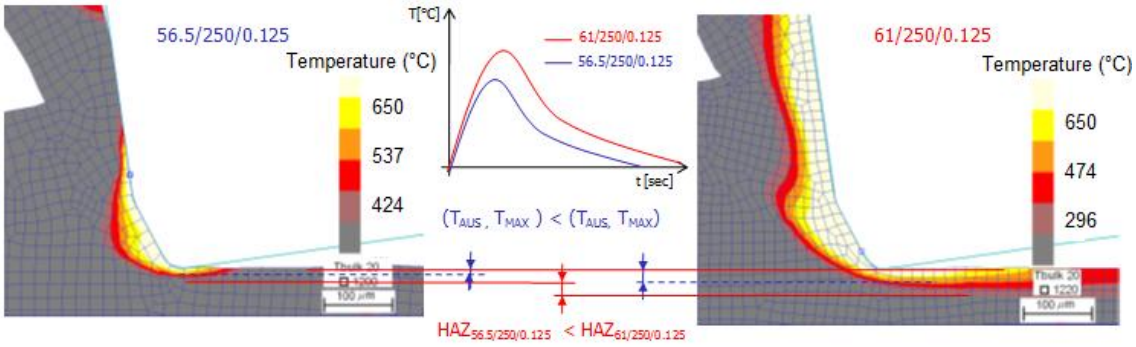

Figure 6.34 Influence of initial workpiece hardness on both temperature and heat-affected zone (HAZ)

On the contrary, both white and dark layers increase with increasing of initial material hardness (Figure 6.19) because, as illustrated in Figure 6.34, higher initial hardness generates higher temperatures on the machined surface and deeper HAZ due to the higher hardening effect.

6.4 – FE RESIDUAL STRESS PREDICTION

Finally to complete the present work a numerical study on the surface integrity in terms of microstructural changes effects on the residual stresses was conducted.

In order to verify the accuracy of the developed FE model, a first set of numerical simulations was performed and for sake of completeness, the obtained numerical results (both for the cases which incorporate or not the microstructural changes effects) were compared with those experimentally found. Although both axial and circumferential (hoop) residual stresses were experimentally measured, only the latter were predicted since they are more critical for part performance in service, and only this stress was predicted by the 2D Fe simulation, (Figures 6.35, 6.36).

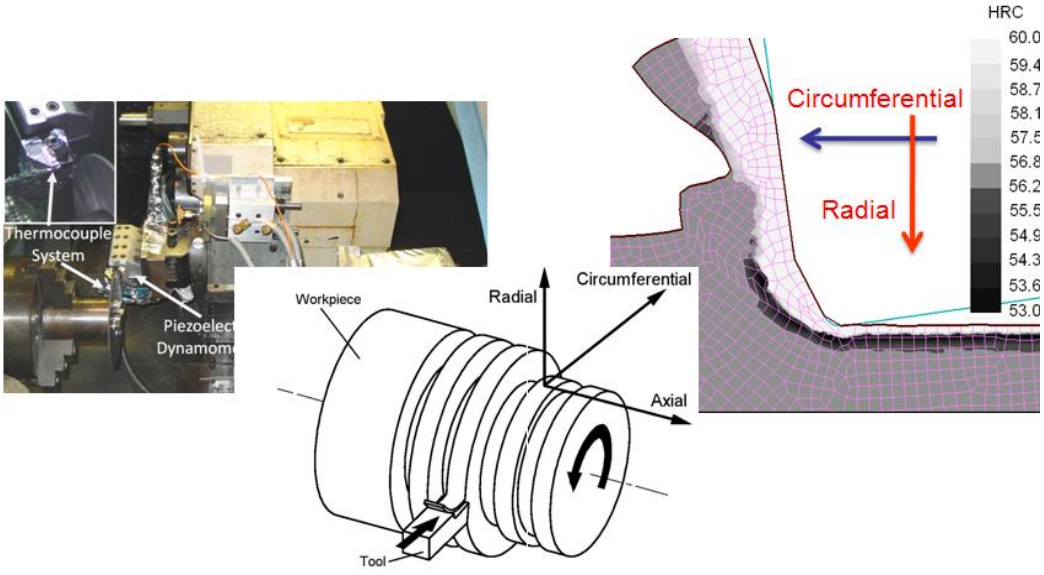

Figure 6.35 Experimental and numerical residual stress directions

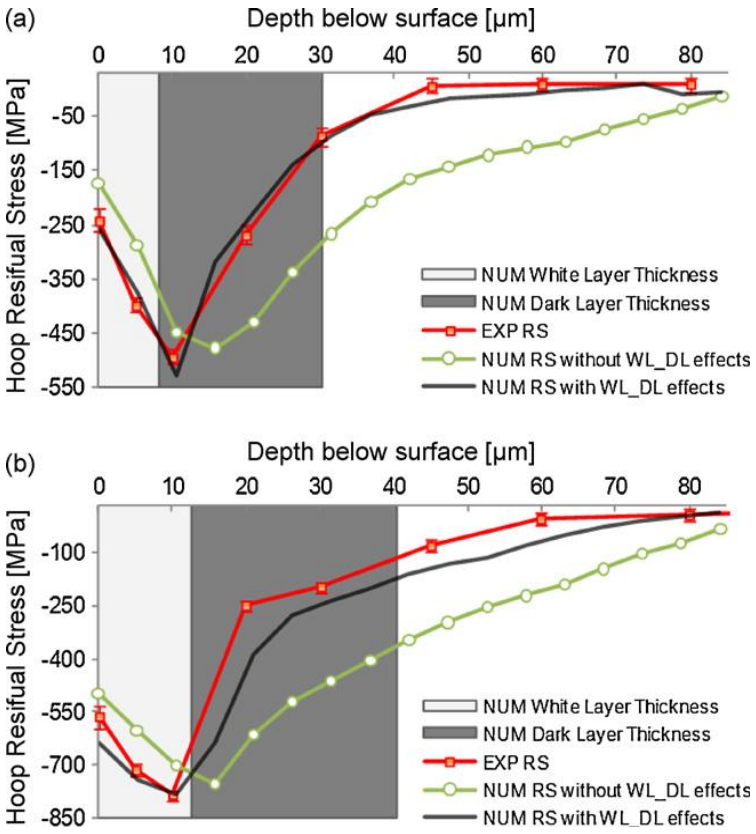

Figure 6.36 Effect of white and dark layers on the residual stress, and comparison of experimental (EXP) and numerical simulation (NUM) results with and without the effects of microstructural changes: (a) V=250 m/min, f=0.125 mm/rev, 56.5 HRC, chamfered tool, (b) V=250 m/min, f=0.125 mm/rev, 61 HRC, chamfered tool

The best agreement between numerical and experimental residual stress profiles is obtained when the microstructural transformations are considered in the model. Furthermore is evident that white layer has a significant impact on the magnitude and location of the maximum (peak) compressive residual stress below the surface, which is related to an increase in material hardness. In contrast, the presence of dark layer reduces the compressive residual stress. After it was demonstrated that the proposed model is adequate to investigate the influence of microstructural changes on residual stresses, the other tests were performed (Figure 6.37).

These results show that for both 56.5 HRC and 61 HRC workpieces hardness the maximum compressive stress below the surface becomes larger as cutting speed increases. This is related to the presence of the white layer, which becomes thicker and harder with increasing the cutting speed (Figure 6.17). It is also important to highlight that the increment of hardness produces more compressive residual stress profiles although the position of maximum compressive stress below surface remains almost constant. The use of honed tool generates lower compressive residual stress and white layer thickness than for the equivalent case with a chamfered tool in terms of both surface residual stress and maximum compressive stress below surface. Furthermore, the maximum compressive stress for the honed tool is positioned in the dark layer.

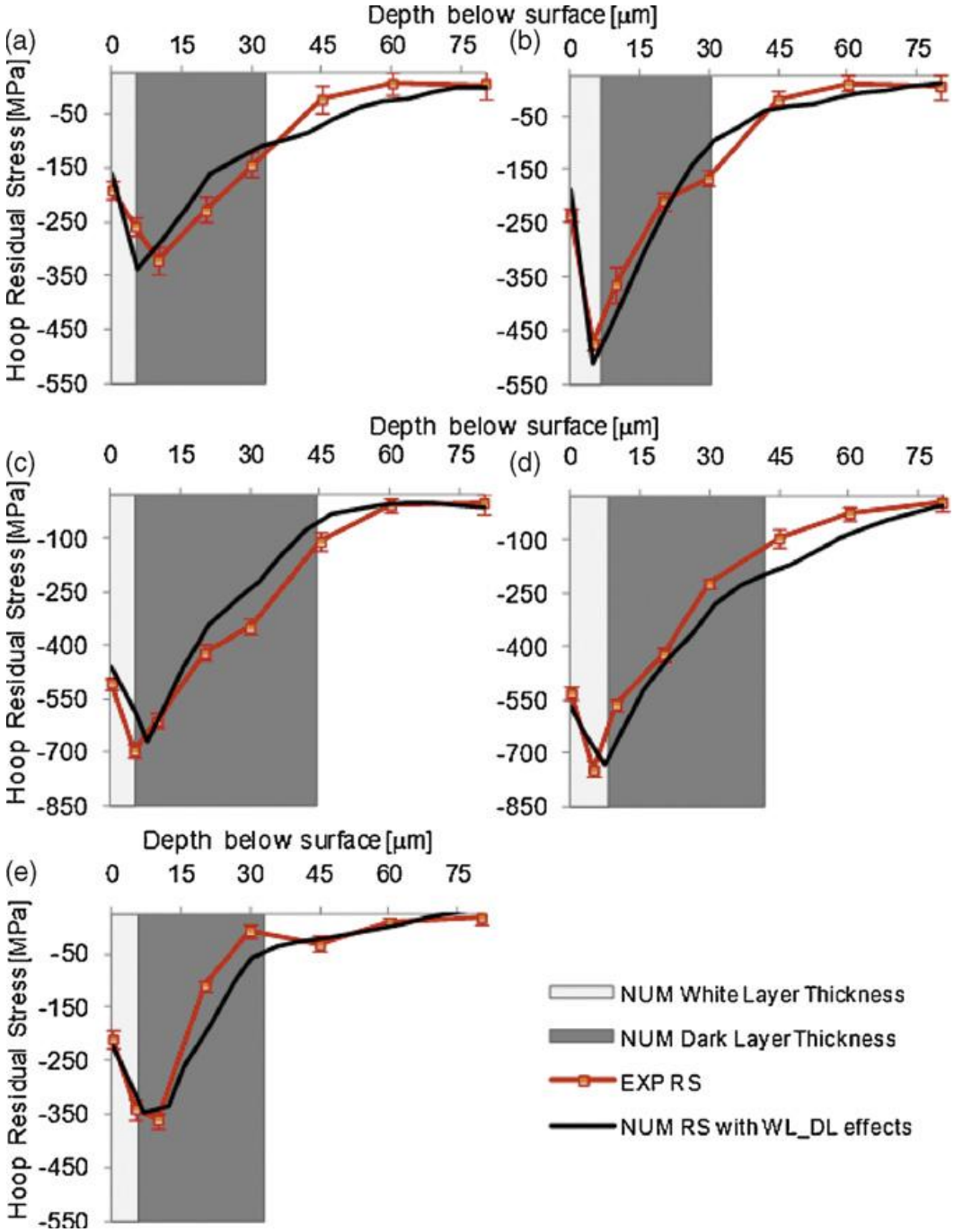

Figure 6.37 Effect of white and dark layers on residual stresses, and comparison of experimental (EXP) and numerical simulation (NUM) results: (a) V=75 m/min, f=0.125 mm/rev, 56.5 HRC, chamfered tool, (b) V=150 m/min, f=0.125 mm/rev, 56.5 HRC, chamfered tool, (c) V=75 m/min, f=0.125 mm/rev, 61 HRC, chamfered tool, (d) V=150 m/min, f=0.125 mm/rev, 61 HRC, chamfered tool, (e) V=250 m/min, f=0.125 mm/rev, 56.5 HRC, honed tool

6.5 – SUMMARY

In this chapter, the proposed FE procedure and the strategy for modeling the material microstructure changes were respectively calibrated and then validated by using experimental observations found in literature and other carried out during this study. In particular, numerical prediction of cutting forces, temperatures and white and dark layers thickness were found to be consistent with those experimentally measured by dynamometer, thermo couples and thermo-camera, and optical and SEM microscopes respectively. Finally, the good agreement obtained between the experimental and numerical results have indicated that the proposed FEM model was also suitable for studying the influence of white and dark layers formation on residual stresses during hard machining of AISI 52100 steel. Particularly, it was found that microstructural changes deeply affect the residual stresses distribution and, for this reason, they have to be accurately taken into account during the process design.

CONCLUSION

According to the results presented in the previous paragraphs of this thesis, the main results of the activity of the candidate may be summarized as follows:

- White layer depth in general increases with cutting speed, even if once the cutting speed reaches 250-300 m/min, the white layer slightly increases or remain almost constant. In contrast, inreasing the cutting speed a decrease for the dark layer is registered;
- Both white and dark layers thicknesses increase with the increasing of the initial workpiece material hardness;
- White layer depth increases choosing higher feed rate while a slight decrease for dark layer thickness is reported;
- Chamfered cutting tools induce thicker white and dark layers depth;
- EDS and X-Ray Diffraction characterization of the machined surface showed that the white layer is the result of the untempered martensite generation, since presence of retained austenite and phase transformation due to heating and rapid quenching are registered;
- Measurements of workpiece surface temperatures by thermo-camera suggested that phase transformation occurs below the nominal austenite-start temperature due to high dislocation density associated with large strain.

The scientific knowledge acquired from these results has also permitted to develop a new FE model based on two advanced empirical equations for white and dark layers prediction. The mentioned FE model was integrated with a hardness-based flow stress rule for material characterization and applied to simulate the orthogonal cutting operation of bearing steel AISI 52100. The FE model was then calibrated and validated by comparing white and dark layers formation, hardness modification, cutting forces and temperatures with the experimental results.

Based on the numerical results, it can be concluded that the present FE model can be successfully applied to simulate the orthogonal hard machining of AISI 52100 and to reproduce some characteristic features such as:

- White and dark layers formation;
- Hardness modification;
- Cutting forces and temperatures.

Finally, the proposed numerical strategy was used to predict the residual stresses profile of the machined component. Also, the influence of the microstructural changes on the residual stresses varying the cutting conditions, the workpiece hardness, and the tool edge geometry were studied and the following results were assessed:

- Better agreement between the experimental and predicted residual stress state in hard turned components can be achieved if the residual stress model incorporates the microstructural changes generated during machining operation;
- White layer influences the magnitude and the position of the maximum compressive residual stress peak;
- Dark layer reduces both the “penetration depth” and the thickness affected by machining residual stress.

In conclusion the research activities carried out during the Ph.D period have permitted to achieve some important objectives and to give a valid contribute in the direction of the FE analysis for microstructural changes prediction during hard turning.

Further improvements can be achieved using the developed numerical strategy for investigating other metallurgical aspects, such as the grain size and the correlated dynamic recrystallization, and for studying the effects of near-to-dry cooling methods (i.e., MQL, cryogenic, etc.) on the surface integrity, products life and their functional performance.

ACKNOWLEDGEMENTS

I wish to thank the research group TSL of the university of Calabria, composed by Prof. Luigino Filice, Ing. Domenico Umbrello, Ing. Giusy Ambrogio and Ing. Francesco Gagliardi, for the possibility to make my PhD study in the last three years with their contribution, help and friendship.

Obviously specials single notes are due to them:

-Thanks to Prof. Luigino Filice for his support and teaching not only in the professional life but also (end especially) in the everyday life with his humor and friendly way to do.

-Thanks to Giusy Ambrogio for her sisterly presence and for her suggestions and advices on my steps.

-Thanks to Francesco Gagliardi for his brotherly presence and for the funny times spent together.

-Finally special thanks to my HARD supervisor Domenico Umbrello for his HARD teaching, HARD review of my works and my final thesis and finally for his singular but inestimable HARD way to find in me the best allowing me to reach prestigious goals not only in the work but also in the life.

Particular thanks to Mr. Franco Pulice and his staff of the Department of Mechanical Engineering of the University of Calabria for their qualified involvement in the preparation and development of the experimental tests.

I wish to thank Professors I.S. Jawahir, O.W. Dilon Jr and A.D. Jayal of the University of Kentucky (KY, USA), Professor. J.C. Outeiro of the University Catolica Portuguesa (Lisbon, Portugal) and Eng. Rachid M'Saoubi of the SECO tool AB, (Fagersta, Sweden) for their support and teaching in my PhD.

Furthermore it was of main importance during these last three years the collaborative but also affective support of my colleagues Eng. Stefania Rizzuti, Eng. Giuseppe

Leonardo Manco, Eng. Giovanna Rotella, Eng. Serena Di Renzo and finally "*Thank you Mr. Chairman*" Eng. Francesco Greco.

Of course a special and particular thanks to my American relatives known during my study in US: Judge Raffaele J. Sposato and Nina Capalbo. It should be necessary several books to describe my real appreciation for them a for their affective presence although we are "*only several thousand miles of distance*".

Other important thanks to the unforgettable Eng. Roberto Caiaro and Angela Sposato and to their special children Silvio and Isabella.

One friendly thank also to Franca Sposato and her family, Zio Cenzino and his family, Rosanna, Loreta and Franco Sposato and their respective family.

Thanks to all the people I forgot without purpose.

Finally, I want to give many thanks to my parents and grandparents for their continuous presence on the way of my life . . .

Serafino

REFERENCES

[1] Raja Kountanya, Ibrahim Al-Zkeri, Taylan Altan, *Effect of tool edge geometry and cutting conditions on experimental and simulated chip morphology in orthogonal hard turning of 100Cr6 steel*, Journal of Materials Processing Technology, Volume 209, Issue 11, 21 June 2009, Pages 5068-5076.

[2] M.A. El Hakim, M.D. Abad, M.M. Abdelhameed, M.A. Shalaby, S.C. Veldhuis, *Wear behavior of some cutting tool materials in hard turning of HSS* ,Tribology International, Volume 44, Issue 10, September 2011, Pages 1174-1181.

[3] V.N. Gaitonde, S.R. Karnik, Luis Figueira, J. Paulo Davim, *Machinability investigations in hard turning of AISI D2 cold work tool steel with conventional and wiper ceramic inserts*, International Journal of Refractory Metals and Hard Materials, Volume 27, Issue 4, July 2009, Pages 754-763.

[4] Khaider Bouacha, Mohamed Athmane Yallese, Tarek Mabrouki, Jean-François Rigal, **S***tatistical analysis of surface roughness and cutting forces using response surface methodology in hard turning of AISI 52100 bearing steel with CBN tool*, International Journal of Refractory Metals and Hard Materials, Volume 28, Issue 3, May 2010, Pages 349-361.

[5] İlhan Asiltürk, Harun Akkuş, *Determining the effect of cutting parameters on surface roughness in hard turning using the Taguchi method*, Measurement, Volume 44, Issue 9, November 2011, Pages 1697-1704.

[6] H.A. Kishawy, Lei Pang, M. Balazinski, *Modeling of tool wear during hard turning with self-propelled rotary tools*, International Journal of Mechanical Sciences, Volume 53, Issue 11, November 2011, Pages 1015-1021.

[7] Y.B. Guo, S. Anurag, I.S. Jawahir, *A novel hybrid predictive model and validation of unique hook-shaped residual stress profiles in hard turning*, CIRP Annals - Manufacturing Technology, Volume 58, Issue 1, 2009, Pages 81-84.

[8] A.P. Paiva, P.H. Campos, J.R. Ferreira, L.G.D. Lopes, E.J. Paiva, P.P. Balestrassi, *A multivariate robust parameter design approach for optimization of AISI 52100 hardened steel turning with wiper mixed ceramic tool*, International Journal of Refractory Metals and Hard Materials, Volume 30, Issue 1, January 2012, Pages 152-163.

[9] Mohamed Athmane Yallese, Kamel Chaoui, Nassereddine Zeghib, Lakhdar Boulanouar, Jean-François Rigal, *Hard machining of hardened bearing steel using cubic boron nitride tool*, Journal of Materials Processing Technology, Volume 209, Issue 2, 19 January 2009, Pages 1092-1104.

[10] Kurt Adair, Shiv G. Kapoor, Richard E. DeVor, *Development of a unique topology for a hard-turning micro-scale machine tool*, Journal of Manufacturing Processes, Volume 13, Issue 2, August 2011, Pages 75-84.

[11] F. Klocke, E. Brinksmeier, K. Weinert, *Capability profile of hard cutting and grinding processes*, CIRP Annals - Manufacturing Technology, Volume 54, Issue 2, 2005, Pages 22-45.

[12] Töenshoff, H.K., Wobker, H.G., Brandt, D., *Hard turning influences on the workpiece properties*, NAMRI/SME, 1995, Volume 23, Pages 215-220.

[13] M.A. Elbestawi, A.K. Srivastava, T.I. El-Wardany, *A model for chip formation during dachining of hardened steel*, CIRP Annals - Manufacturing Technology, Volume 45, Issue 1, 1996, Pages 71-76.

[14] G. Poulachon, A. Moisan, *A contribution to the study of the cutting mechanisms during high speed machining of hardened steel*, CIRP Annals - Manufacturing Technology, Volume 47, Issue 1, 1998, Pages 73-76.

[15] Y. Matsumoto, F. Hashimoto, G. Lahoti, *Surface integrity generated by precision hard turning*, CIRP Annals - Manufacturing Technology, Volume 48, Issue 1, 1999, Pages 59-62.

[16] M.C. Shaw, A. Vyas, *The mechanism of chip formation with hard turning steel*, CIRP Annals - Manufacturing Technology, Volume 47, Issue 1, 1998, Pages 77-82.

[17] C. Guo, Y. Wu, V. Varghese, S. Malkin, *Temperatures and energy partition for grinding with vitrified CBN wheels,* CIRP Annals - Manufacturing Technology, Volume 48, Issue 1, 1999, Pages 247-250.

[18] F. Klocke, H. Kratz, *Advanced tool edge geometry for high precision hard turning,* CIRP Annals - Manufacturing Technology, Volume 54, Issue 1, 2005, Pages 47-50.

[19] M.Y. Noordin, V.C. Venkatesh, S. Sharif, *Dry turning of tempered martensitic stainless tool steel using coated cermet and coated carbide tools,* Journal of Materials Processing Technology, Volume 185, 2007, Pages 83–90.

[20] W. Grzesik, Z. Zalisz, *Wear phenomenon in hard steel machining using ceramic tools*, Tribology International, Volume 41, 2008, Pages 802–812.

[21] Ersan Aslan, Necip Camuscu, Burak Birgoren, *Design optimization of cutting parameters when turning hardened AISI4140 steel (63HRC) with Al_2O_3 + TiCN mixed ceramic tool*, Materials and Design, Volume 28, 2007, Pages 1618–1622.

[22] W. Grzesik, Z. Zalisz, *Wear phenomenon in hard steel machining using ceramic tools*, Tribology International, Volume 41, 2008, Pages 802–812.

[23] M.A. Yallese, K. Chaoui, N. Zeghib, L. Boulanouar, J. Rigal, *Hard machining of hardened bearing steel using cubic boron nitride tool*, Journal of Material Processing Technology, Volume 209, 2009, Pages 1092–1104.

[24] J.P. Costes, Y. Guillet, G. Poulachon, M. Dessoly, *Tool-life and wear mechanisms of CBN tools in machining of Inconel 718,* International Journal of Machine Tools and Manufacture, Volume 47, 2007, Pages 1081–1087.

[25] Abhijeet S. More, Wenping Jiang, W.D. Brown, Ajay P. Malshe, *Tool wear and machining performance of cBN–TiN coated carbide inserts and PCBN compact inserts in turning AISI 4340 hardened steel*, Journal of Materials Processing Technology, Volume 180, 2006, Pages 253–262.

[26] G. Poulachon, A. Moisan, I.S. Jawahir, *Tool-wear mechanisms in hard turning with polycrystalline cubic boron nitride tools*, Wear, Volume 250, 2001, Pages 576–586.

[27] T. Tamizharasan, T. Selvaraj, A. Noorul Haq, *Analysis of tool wear and surface finish in hard turning*, International Journal Advanced Manufacturing Technology, Volume 28, 2006, Pages 671–679.

[28] J.M. Zhou, M. Andersson, J.E. Stahl, *The monitoring of flank wear on the CBN tool in the hard turning process*, International Journal of Advanced Manu- facturing Technology, Volume 22, 2003, Pages 697–702.

[29] Y. Sahin, *Comparison of tool life between ceramic and cubic boron nitride (CBN) cutting tools when machining hardened steels*, Journal of Materials Processing Technology (2008) doi:10.1016/j.jmatprotec.2008.08.016.

[30] E.O. Ezugwu, R.B. Da Silva, J. Bonney, *A.R. Machado, Evaluation of the performance of CBN tools when turning Ti–6Al–4V alloy with high pressure coolant supplies*, International Journal of Machine Tools and Manufacture, Volume 45, 2005, Pages 1009–1014.

[31] Y. Huang, S.Y. Liang, *Modeling of cutting forces under hard turning conditions considering tool wear effect*, Transactions of the ASME, Journal of Manufacturing Science and Engineering, Volume 127, 2005, Pages 262–270.

[32] B. Fnides, H. Aouici, M.A. Yallese, *Cutting forces and surface roughness in hard turning of hot work steel X38CrMoV5-1 using mixed ceramic*, MECHANIKA, Volume Nr.2 (70), 2008, Pages 73–78 ISSN:1392–1207.

[33] T. Ozel, Y. Karpat, A. Srivastava, *Hard turning with variable microgeometry PCBN tool*, CIRP Annals Manufacturing Technology, Volume 57, 2008, Pages 73–76.

[34] A. Ebrahimi, M.M. Moshksar, *Evaluation of machinability in turning of micro-alloyed and quenched-tempered steels: tool wear, statistical analysis, chip morphology*, Journal of Material Processing Technology, Volume 209, 2009, Pages 910–921.

[35] Jeffrey D Thiele, Shreyes N. Melkote, *Effect of cutting edge geometry and workpiece hardness on surface generation in the finish hard turning of AISI 52100 steel*, Journal of Materials Processing Technology, Volume 94, Issues 2-3, 29 September 1999, Pages 216-226.

[36] Jiang Hua, Rajiv Shivpuri, Xiaomin Cheng, Vikram Bedekar, Yoichi Matsumoto, Fukuo Hashimoto, Thomas R. Watkins, *Effect of feed rate, workpiece hardness and*

cutting edge on subsurface residual stress in the hard turning of bearing steel using chamfer + hone cutting edge geometry, Materials Science and Engineering: A, Volume 394, Issues 1-2, 15 March 2005, Pages 238-248.

[37] Takashi Ueda, Mahfudz Al Huda, Keiji Yamada, Kazuo Nakayama, Hideaki Kudo, *Temperature measurement of CBN tool in turning of high hardness steel*, CIRP Annals - Manufacturing Technology, Volume 48, Issue 1, 1999, Pages 63-66.

[38] Toenshoff, H. K., Wobker, H.-G., Brandt, D.: *Hartbearbeitung aus der sicht der forschung*, VDI Berichte, Volume 988, 1993, Pages 189-209.

[39] Brandt, D., *Randzonenbeeinflussung beim hartdrehen*, Dr.-lng. Dissertation, Universitat-Hannover, 1995.

[40] Kaiser, M., *Hardfeinbearbeitung von einsatzgehartetem stahl mit PKB-werkzeugen,* IDR, Volume 1, 1992, Pages 24-33.

[41] Boemcke, A., *Ein beitrag zur ermittlung der verschleikmechanisrnen beim zerspanen mit hochharten polykristallinen schneidstoffen*, Dr.-lng. Diss. RWTH Aachen. 1989.

[42] Goldstein, M., *Optimierung der fertigungsfolge, kalffliekpressen - spanen' durch hartdrehen als feinbearbeitungsverfahren fur einsatzgehartete prekteile*, Dr.-lng. Diss. RWTH Aachen, 1991.

[43] Adilson José de Oliveira, Anselmo Eduardo Diniz, Davi Janini Ursolino, *Hard turning in continuous and interrupted cut with PCBN and whisker-reinforced cutting tools*, Journal of Materials Processing Technology, Volume 209, Issues 12-13, 1 July 2009, Pages 5262-5270.

[44] M.A. Elbestawi, A.K. Srivastava, T.I. El-Wardany, *A model for chip formation during machining of hardened steel,* CIRP Annals - Manufacturing Technology, Volume 45, Issue 1, 1996, Pages 71-76.

[45] Weck, M., Wieners, A., *Maschinen fur die hochund ultraprazision*, Technica Nr. 13/14/95, S. 14-19.

[46] Toenshoff, H.K., Karpuschewski, B., Borbe, C., *Prazisions-Hgrtdrehen von walzlagerringen,* 12.-14. Mai 1997, 14 International Plansee Seminar '97, Reutte, Tirol.

[47] T. I. El-Wardany, H. A. Kishawy, M.A. Elbestawi, *Surface integrity of die material in high speed hard machining, part 1: micrographical analysis*, Journal of Manufacturing Science and Engineering, Volume 122, 2000, Pages 620-631.

[48] Y.Kevin Chou, Chris J. Evans, *White layers and thermal modeling of hard turned surfaces*, International Journal of Machine Tools and Manufacture, Volume 39, Issue 12, December 1999, Pages 1863-1881.

[49] X Sauvage, J.M Le Breton, A Guillet, A Meyer, J Teillet, *Phase transformations in surface layers of machined steels investigated by X-ray diffraction and Mössbauer spectrometry*, Materials Science and Engineering: A, Volume 362, Issues 1-2, 5 December 2003, Pages 181-186.

[50] A. Ramesh, S.N. Melkote, L.F. Allard, L. Riester, T.R. Watkins, *Analysis of white layers formed in hard turning of AISI 52100 steel*, Materials Science and Engineering: A, Volume 390, Issues 1-2, 15 January 2005, Pages 88-97.

[51] Sangil Han, Shreyes N. Melkote, Michael S. Haluska, Thomas R. Watkins, *White layer formation due to phase transformation in orthogonal machining of AISI 1045 annealed steel*, Materials Science and Engineering: A, Volume 488, Issues 1-2, 15 August 2008, Pages 195-204.

[52] D. Umbrello, J.C. Outeiro, R. M'Saoubi, A.D. Jayal, I.S. Jawahir, *A numerical model incorporating the microstructure alteration for predicting residual stresses in hard machining of AISI 52100 steel*, CIRP Annals - Manufacturing Technology, Volume 59, Issue 1, 2010, Pages 113-116.

[53] Toenshoff, H. K., Karpuschewski, B., Borbe, C., *Hartbearbeitung: stand der forschung, hardmachining - state of research*, VDI Berichte Nr. 1399; 1998.

[54] Agha, S. R., Liu, R., *The effect of cutting conditions on rolling contact fatigue life of superfinish hard turned surfaces*, Proceedings of NSF and manufacturing Conference, Jan. 1999.

[55] Borbe, C., *Randzoneneigenschaften und bauteilverhalten beim hartdrehen*, DGM-Seminar, Werkstoffgefuge und Zerspanung, Hannover 1999.

[56] H. Sasahara, *The effect on fatigue life of residual stress and surface hardness resulting from different cutting conditions of 0.45%C steel*, International Journal of Machine Tools & Manufacture Volume 45, 2005, Pages 131–136.

[57] H. K.Toenshoff, C. Arendt, R. Ben Amor, *Cutting of hardened steel,* Keynote paper, Annals of the ClRP Volume 49/2, 2000, Pages 547-566.

[58] J. M. Zhou, M. Andersson, J. E. Stahl, *Identification of cutting errors in precision hard turning process, Journal of Materials Processing Technology*, 2004, Pages 746–750.

[59] K. Weinert, I. Inasaki, J.W. Sutherland, T. Wakabayashi, *Dry machining and minimum quantity lubrication*, CIRP Annals - Manufacturing Technology, Volume 53, Issue 2, 2004, Pages 511-537.

[60] C. Wiesner, *Residual stresses after orthogonal machining of AISI 304: numerical calculation of the thermal component and comparison with experiment results*, Metall. Trans. Volume A 23, 1992, Pages 989–996.

[61] C.R. Liu, A.C. Lin, M.M. Barash, *Thermal and mechanical stresses in the workpiece during machining*, ASME, Prod. Eng. Div., Volume 12, 1984, Pages 181–191.

[62] Y. Matsumoto, M.M. Barash, C.R. Liu, *Residual stress in the machined surface of hardened steel*, ASME, Prod. Eng. Div., Volume 12, 1984, Pages 193–204.

[63] S. Jeelani, J.A. Bailey, *Residual stress distribution in machining annealed 18% nickel maraging steel*, J. Eng. Mater. Technol. Trans. ASME, Volume 108/2, 1986, Pages 93–98.

[64] A.B. Sadat, *Effect of high cutting speed on surface integrity of AISI 4340 steel during turning*, Mater. Sci. Technol., Volume 6, 1990, Pages 371–375.

[65] Merchant, M. E., *Mechanics of the metal cutting process—II: plasticity conditions in orthogonal cutting*, J. Appl. Phys., Volume 16, 1945, Pages 318–324.

[66] Ozel, T; Llanos, I.; Soriano, J.; Arrazola, P. J., *3D Finite element modeling of chip formation process for machining Inconel 718: comparison of FE software predictions*, Machining Science and Technology, Volume 15, Number 1, January 2011, Pages 21-46.

[67] J. Mackerle, *Finite element analysis and simulation of machining: an addendum: A bibliography (1996–2002)*, International Journal of Machine Tools and Manufacture, Volume 43, Issue 1, January 2003, Pages 103-114.

[68] T. Matsumura, A. Ishii, T. Shirakashi and E. Usui, *Error compensation with simulating turning process,* Proc. of the 4th ESAFORM Conference, 2001, Pages 623-626.

[69] T. Matsumura, T. Shirakashi, T. Obikawa and E. Usui, *On the development of cutting process simulator for turning operation,* Proc. of the 6th ESAFORM Conference, 2003, Pages 519-522.

[70] M. Nouari and A. Molinari, *Modeling of the tool wear and optimization of the cutting process,* Proc. of the 4th ESAFORM Conference, 2001, Pages 643-646.

[71] A. Marty, S. Assouline, P. Lorong and G. Coffignal, *Prediction of the workpiece final surface taking into account the workpiece/tool/machine vibrations,* Proc. of the 6th ESAFORM Conference, 2003, Pages 535-538.

[72] B. Changeux, M. Touratier, J. L. Lebrun, T. Tomas, J. Clisson, *High speed shear stress for the identification of the Jhonson-Cook law,* Proc. of the 4th ESAFORM Conference, 2001.

[73] D. Umbrello, S. Shivpuri and J. Hua, *Modeling of the flow stress for AISI 52100 during hard machining processes,* Proc. of the 7th ESAFORM conference, 2004, Pages 725-728.

[74] V. Lemiale, P. Picart and J. Chambert, *Comparison of different fracture models for the metal blanking process,* Proc. of the 8 th ESAFORM Conference, 2005, Pages 757-768.

[75] O. W. Dillon, *FEM analysis of machining with a rounded tip cutting tool,* Proc. of the 6th ESAFORM Conference, 2003, Pages 563-566.

[76] P. J. Arrazola, F. Meslin and S. Marya, *Tool-chip contact analysis in numerical cutting modeling,* Proc. of the 6th ESAFOMR Conference, 2003, Pages 559-562.

[77] L. Filice, D. Umbrello, F. Micari, L. Settineri, *On the finite element simulation of thermal phenomena in machining processes,* Proc. of the 8th ESAFOMR Conference, 2005, Pages 729-732.

[78] W. Grzesik, P. Nieslony, and B. Bartoszuk, *A model for the cutting heat partitioning in multilayer coating-stell couples,* Proc. of the 7th ESAFORM Conference, 2004, Pages 749-752.

[79] T. Shirakashi, T. Obikawa and H. Sasahara, *Estimation of the residual stress distribution in machined surface and its control through fem simulation,* Proc. of the 4th ESAFORM Conference, 2001, Pages 639-642.

[80] G. Poulachon, A. Albert, M. Schluraff, I.S. Jawahir, *An experimental investigation of work material microstructure effects on white layer formation in PCBN hard turning*, International Journal of Machine Tools and Manufacture, Volume 45, Issue 2, February 2005, Pages 211-218.

[81] Stead JW, *Micro-Metallography and its practical application*, J West Scot Iron & Steel Inst, Volume 19, 1912, Pages 169-204.

[82] Griffiths BJ, *White layer formations at machined surfaces and their relationship to white layer formations at worn surfaces*, J Tribology, Volume 107, 1985, Pages 165-171.

[83] You Wang, Tingquan Lei, Jiajun Liu, *Tribo-metallographic behavior of high carbon steels in dry sliding: III. Dynamic microstructural changes and wear*, Wear, Volume 231, Issue 1, June 1999, Pages 20-37.

[84] Akcan S, Shah S, Moyal SP, Chhabra PN, Chandrasekar S, Yang HTY, *Formation of White Layers in Steels by Machining and Their Characteristics*, Metall & Mater Trans-A; Volume 33 (A), 2002, Pages 1245-1254.

[85] Mybokwere CO, Nutt SR, Duffy J, *Shear band formation in 4340 steel: a TEM study*. Mech Mater, Volume 17, 1994, Pages 97–110.

[86] Kyung-Mox Cho, Sunghak Lee, S.R. Nutt, J. Duffy, *Adiabatic shear band formation during dynamic torsional deformation of an HY-100 steel*, Acta Metallurgica et Materialia, Volume 41, Issue 3, March 1993, Pages 923-932.

[87] Baofa Zhang, Wanci Shen, Yingjie Liu, Xiangyun Tang, Yuanfei Wang, *Microstructures of surface white layer and internal white adiabatic shear band*, Wear, Volume 211, Issue 2, November 1997, Pages 164-168.

[88] Mao C, Zhou Z, Zhang J, Huang X, Gu D, *An experimental investigation of affected layers formed in grinding of AISI 52100 steel*, Int J Adv Manuf Technol, Volume 54, 2011, Pages 515–523.

[89] Ramesh A., *Prediction of process-Induced Microstructural Changes in Orthogonal Hard Machining*, Ph.D Thesis 2002, Mechanical Eng., Georgia Inst. of Technology.

[90] J Barry, G Byrne, *TEM study on the surface white layer in two turned hardened steels*, Materials Science and Engineering: A, Volume 325, Issues 1-2, 28 February 2002, Pages 356-364.

[91] Brinksmeir E, Brockhoff T., *White layers in machining steels*, 2nd Int. German and French Conf. on High Speed Machining Conf. Proc., 1999, Pages 7-13.

[92] A. Barbacki, M. Kawalec, *Structural alterations in the surface layer during hard machining*, Journal of Materials Processing Technology, Volume 64, Issues 1-3, February 1997, Pages 33-39.

[93] W. Österle, H. Rooch, A. Pyzalla, L. Wang, *Investigation of white etching layers on rails by optical microscopy, electron microscopy, X-ray and synchrotron X-ray diffraction*, Materials Science and Engineering: A, Volume 303, Issues 1-2, 15 May 2001, Pages 150-157.

[94] Qi B, He N, Li L, Zhao W., *Investigation on White Layer Formation in PCBN Hard Turning GCr15*, Key Eng Mater Volume 241, 2010, Pages 431-432.

[95] J.G. Li, M. Umemoto, Y. Todaka, K. Tsuchiya, *A microstructural investigation of the surface of a drilled hole in carbon steels*, Acta Materialia, Volume 55, Issue 4, February 2007, Pages 1397-1406.

[96] A.A. Torrance, A. Cameron, *Surface transformations in scuffing*, Wear, Volume 28, Issue 3, June 1974, Pages 299-311.

[97] A. Ramesh, J. Thiele, S. Melkote, *Residual Stress and Sub-surface Flow in Finish Hard Turned AISI 4340 and 52100 Steels: A Comparative Study*, ASME IMECE, Manufacturing Science & Engineering Conf. Proc., 1999, Pages 831-837.

[98] Shaw, M. and Vyas, A., *Heat-Affected Zones in Grinding Steel*, Ann. CIRP, Volume 43/1, 1993, Pages 279-282.

[99] Okusa, K., Takahashi H. and Nishizawa, M., *Behavior of White Layer during Cutting of Iron and Steels*, Bull. Japan Soc. Of Prec. Engg., 1978, Volume 12 No. 4, Pages 171-176.

[100] Kim, W. and Kwon, P., *Phase Transformation and Its Effect on Flank Wear in Machining Steels*, Journal of Manufacturing Science and Engineering, 2002, Volume 124, Pages 659-666.

[101] Y. Kevin Chou e Hui Song, *Thermal modeling for white layer predictions in finish hard turning*, International Journal of Machine Tools and Manufacture, Volume 45, Issues 4-5, April 2005, Pages 481-495.

[102] A.W. Warren, Y.B. Guo, M.L. Weaver, *The influence of machining induced residual stress and phasetransformation on the measurement of subsurface mechanical behavior using nanoindentation*, Surface & Coatings Technology, Volume 200, 2006, Pages 3459– 3467.

[103] Sangil Han, *Mechanism and modeling of white layer formation in orthogonal machining of steels*, PhD Thesis, Georgia Institute of Technology May 2006.

[104] Jing Shi, Jia-Yeh Wang, and C R Liu, *Modelling white layer thickness based on the cutting parameters of hard machining*, Proc. IMechE Volume 220 Part B: J. Engineering Manufacture, 2006, Pages 119-128.

[105] A. Attanasio, D. Umbrello, C. Cappellini, G. Rotella, R. M' Saoubi, *Tool wear effects on white and dark layer formation in hard turning of AISI 52100 steel*, Wear, In Press, Corrected Proof, Available online 7 July 2011.

[106] Dale W. Schwach, Y.B. Guo, *A fundamental study on the impact of surface integrity by hard turning on rolling contact fatigue*, International Journal of Fatigue Volume 28, 2006, Pages 1838–1844.

[107] A. Devillez, G. Le Coz, S. Dominiak, D. Dudzinski, *Dry machining of Inconel 718, workpiece surface integrity*, Journal of Materials Processing Technology, Volume 211, 2011, Pages 1590–1598.

[108] Leonardo Roberto da Silva, Eduardo Carlos Bianchi, Ronaldo Yoshinobu Fusse,

Rodrigo Eduardo Catai, Thiago Valle Franca, Paulo Roberto Aguiar, *Analysis of surface integrity for minimum quantity lubricant—MQL in grinding,* International Journal of Machine Tools & Manufacture, Volume 47, 2007, Pages 412–418.

[109] Z. Zurecki, R. Ghosh, J. H. Frey, *Investigation of white layers formed in conventional and cryogenic hard turning of steels,* Proceedings of IMECE03.

[110] Sandro E. Dutra Xavier, Sergio Delijaicov, Adalto de Farias, Marco Stipkovic Filho and Gilmar Ferreira Batalha, *Investigation on the surface integrity and tool wear in cryogenic machining,* International conference on advances in materials and processing technologies, AMPT 2010.

[111] M. Field, J.F. Kahles, *Review of surface integrity of machined components,* Ann. CIRP, Volume 20 (1), 1971, Pages 153–163.

[112] J.A. Bailey, S. Jeelani, S.E. Becker, *Surface integrity in machining AISI 4340 steel,* J. Eng. Ind., Volume 98 (3), 1976, Pages 999–1007.

[113] Y. Matsumoto, M.M. Barash, C.R. Liu, *Effect of hardness on the surface integrity of AISI 4340 steel,* J. Eng. Ind., Volume 108, 1986, Pages 169–175.

[114] W. Konig, A. Berktold, K.F. Koch, *Turning versus grinding – a comparison of surface integrity aspects and attainable accuracies,* Ann. CIRP, Volume 42 (1), 1993, Pages 39–43.

[115] A.M. Abrao, D.K. Aspinwall, *The surface integrity of turned and ground hardened bearing steel,* Wear, Volume 96, 1996, Pages 279–284.

[116] S.O. Swain, *Doctoral Thesis,* Purdue University,West Lafayette, IN, 1996.

[117] Y.K. Chou, C.J. Evans, Trans. NAMRI/SME XXVI (1998) 117–122.

[118] J. D. Thiele, S. N. Melkote, R. A. Peascoe and T. R. Watkins, *Effect of cutting-edge geometry and workpiece hardness on surface residual stresses in finish hard turning of AISI 52100 steel,* J. Manuf. Sci. Eng.- Trans. ASME, Volume 122, 2000, Pages 642-649.

[119] Schreiber E., Schlicht H., *Residual stresses after turning of hardened components,* In: Proceedings of the international conference on residual stresses, 1986; 853–60.

[120] Guo Y.B., Schwach D.W., *An experimental investigation of white layer on rolling contact fatigue using acoustic emission technique*, Int. J. Fatigue, Volume 27, 2005, Pages 1051–1061.

[121] Field M, Koster WP, Kohls JB, Snider RE, Maranchik J Jr., *Machining of high strength steels with emphasis on surface integrity*, Technical Report AFMDC 70-1, Metcut Research Associates Inc.; 1970.

[122] Snoeys R, Leuven K, Maris M, Peters J., *Thermally induced damage in grinding*, Ann CIRP, Volume 27, 1978; Pages 571–581.

[123] S.R. Agha, C.R. Liu, *Experimental study on the performance of superfinish hard turned surfaces in rolling contact*, Wear, Volume 244, Issues 1-2, 20 August 2000, Pages 52-59.

[124] Stephen Smith, Shreyes N. Melkote, Edgar Lara-Curzio, Thomas R. Watkins, Larry Allard, Laura Riester, *Effect of surface integrity of hard turned AISI 52100 steel on fatigue performance*, Materials Science and Engineering: A, Volume 459, Issues 1-2, 25 June 2007, Pages 337-346.

[125] Kalpakjian, S., Schmid, S., Manufacturing Engineering and Technology, 4th Edition, Prentice Hall Inc, 2001.

[126] Diniz, A.E., Oliveira, A.J., *Hard turning of interrupted surfaces using CBN tools*, Journal of Materials Processing Technology, Volume 195, 2008, Pages 275–281.

[127] Ko, T.J., Him, H.S., *Surface integrity and machinability in intermittent hard turning*, The International Journal of Advanced Manufacturing Technology, Volume 18, 2001, Pages 168–175.

[128] N. Narutaki, Y. Yamane, Ann. CIRP 28/1, 1979, Pages 23–28.

[129] T. Ohtani, H. Yokogawa, Bull. Jpn. Soc. Prec. Eng. 22 (3), 1988, Pages 229–231.

[130] G. Chryssolouris, J. Appl. Metalworking 2 (2) 1982.

[131] M.A. Davies, Y. Chou, C.J. Evans, Ann. CIRP 45/1, 1996, Pages 77–82.

[132] Juvinall, R.C., Marshek, K.M., *Fundamentals of Machine Component Design*, third ed. John Wiley & Sons, Hoboken, 1999.

[133] Ibrahim A. A., *PhD thesis: Finite element modeling of hard turning*, the Ohio state University, 2007.

[134] D. Umbrello, J. Hua, R. Shivpuri, *Hardness-based flow stress and fracture models for numerical simulation of hard machining AISI 52100 bearing steel*, Materials Science and Engineering, Volume A 374, 2004, Pages 90–100.

[135] Guo, Y. and Liu, C., *3D FEA Modeling of Hard Turning*, Journal of Manufacturing Science and Engineering, Volume 124, 2002, No. 2, Pages 189-199.

[136] American Society for Testing and Materials International - ASTM E975-00 (2003) Standard Practice for X-Ray Determination of Retained Austenite in Steel with Near Random Crystallographic Orientation. 03.01, W. Conshohocken, PA.

[137] Pappas N., *Calculating Retained Austenite in Steel Post Magnetic Processing Using X-Ray Diffraction*, B.S. Undergraduate Mathematics Exchange, Volume 4(1), 2006, Pages 9-14.

[138] J. C. Outeiro, *PhD thesis: Determinação experimental das tensões residuais por difracção de raios-X.*

[139] Taylor, F. W., *On the art of cutting metals*, Transactions of the ASME, Volume 28, 1906, Pages 31-350.

[140] Komanduri, R., *Machining and grinding: A historical review of the classical papers*, Applied Mechanics Review, Volume 46/3, 1993, Pages 80-132.

[141] Komanduri, R., Hou, Z. B., *A review of the experimental techniques for the measurement of heat and temperatures generated in some manufacturing processes and tribology*, Tribology International, Volume 34, 2001, Pages 653-682.

[142] M.A. Davies, T. Ueda, R. M' Saoubi, B. Mullany, A.L. Cooke, *On the measurement of temperature in material removal processes*, CIRP Annals - Manufacturing Technology, Volume 56, Issue 2, 2007, Pages 581-604.

[143] Joint Committee on Powder Diffraction Standards (JCPDS): Powder Diffraction File, Inorganic Volume Sets 6-10, 1980, Page 150.

[144] Joint Committee on Powder Diffraction Standards (JCPDS): Powder Diffraction File, Inorganic Volume Sets 31-32, 1988, Page 209.

[145] Joint Committee on Powder Diffraction Standards (JCPDS): Powder Diffraction File, Inorganic Volume Sets 35-36, 1990, Pages 283.

[146] Badeshia HKDH. Progress in Mater Sci, Volume 57, 2012, Page 268.

[147] Hengerer F, Brockmüller U, Sörström PO., *Through-hardening or case-hardening for tapered roller bearings*, In: Hoo JJC (Eds.) Creative use of bearing steels. Philadelphia (USA): ASTM, Volume 21, 1993.

[148] Zaccone MA, Krauss G., Metall Mater Trans A Volume 24, 1993, Page 2263.

[149] Geijselaers HJM, Perdahciouglu ES., Scripta Mater, Volume 60, 2009, Page 29.

[150] Hartnett MJ, Palazotto AN. Tribol Trans, Volume 19, 1976, Page 115.

[151] Umbrello D., *Influence of material micristructure changes on surface integrity in hard machining of AISI 52100 steel,* Int. J. Adv. Manuf. Technol., Volume 54/9, 2011, Pages 887-898.

[152] Akcan, N.S.; Shah, S.; Moylan, S.P.; Chhabra, P.N., Chandrasekar, S.; Farris, T.N., *Characteristics of white layers formed in steels by machining*, Proc. ASME MED, Volume 10, 1999, Pages 789-795.

[153] Ramesh, A.; Melkote, S.N., *Modeling of white layer formation under thermally dominant conditions in orthogonal machining of hardened AISI 52100 steel*, Int. J. Mach. Tools & Manuf., Volume 48, 2008, Pages 402-414.

[154] Fischer, C.E.; Bandar, A.R., *Finite element simulation of surface microstructure effects in metal cutting,* CIRP Workshop on High Performance Cutting, Dublin (Ireland), (2008).

[155] Bariani, P.F.; Dal Negro, T.; Bruschi, S., *Testing and Modelling of Material Response to Deformation in Bulk Metal Forming*, CIRP Annals - Manufacturing Technology, Volume 53(2), 2004, Pages 573-596.

[156] Habak, M.; Lebrun, J.L.; Morel, A., *A study of the influence of the metallurgical state on shear band and white layer generation in 100Cr6 steel: application to machining,* 10th ESAFORM Conference on Material Forming, Zaragoza (Spain), 2007.

[157] Arimoto, K.; Li, G.; Arvind, A.; Wu, W.T., The modeling of heat treating processes, ASM 18th Heat Treating Conference, Oct 12-15, 1998, Chicago, IL.

[158] Deform. (2008), Deform 2D V9.1 User Manual, Scientific Forming Technologies Corporation Ed., Columbus, OH.

[159] ASM International., *Heat Treating of Steels and Surface Hardening of Steel*, ASM Handbook, Heat Treating, Volume 4, 1991.

[160] Ramesh, A., *Prediction of process-induced microstructural changes in orthogonal hard machining*, Ph.D Thesis, Mechanical Eng., Georgia Inst. of Technology, 2002 (Atlanta, USA).

[161] Brozzo P, De Luca B, Rendina R, *A new method for the prediction of formability limit of metal sheet*, Proceedings of the 7th Biennial Conference of the International Deep Drawing Research Group, 1972.

[162] Umbrello D, Jawahir IS, *Numerical modeling of the influence of process parameters and workpiece hardness on white layer formation in AISI 52100 steel*, Int J Adv Manuf Technol Volume 44, 2009, Pages 955–968.

[163] Outeiro JC, Ee KC, Dillon Jr OW, Wanigarathne PC, Jawahir IS, *Some observations on comparing the modelled and measured residual stresses on the machined surface Induced by orthogonal cutting of AISI 316 L steel*, Proceedings of the 9th CIRP International Workshop on Modeling of Machining Operations. Bled, Slovenia, 11–12 May, 2006, Pages 475–481.

[164] Guo, Y.B.; Sahni, J., *A comparative study of hard turned and cylindrically ground white layers*, Int. J. Mach. Tools Manuf., Volume 44(2), 2004, Pages 135-145.